

NASA Contractor Report 4031

Application of Higher Harmonic Blade Feathering on the OH-6A Helicopter for Vibration Reduction

F. K. Straub and E. V. Byrns, Jr.

CONTRACT NAS1-16266
DECEMBER 1986

(NASA-CR-4031) APPLICATION OF HIGHER
HARMONIC BLADE FEATHERING ON THE OH-6A
HELICOPTER FOR VIBRATION REDUCTION Final
Report (McDonnell-Douglas Helicopter Co.)
190 p

87-15175

Unclass
40301

CSCL 01A H1/02

The NASA logo, consisting of the word "NASA" in a bold, sans-serif font.

NASA Contractor Report 4031

Application of Higher Harmonic Blade Feathering on the OH-6A Helicopter for Vibration Reduction

F. K. Straub and E. V. Byrns, Jr.

*McDonnell Douglas Helicopter Company
Mesa, Arizona*

Prepared for
Langley Research Center
under Contract NAS1-16266



National Aeronautics
and Space Administration

**Scientific and Technical
Information Branch**

1986

TABLE OF CONTENTS

Acknowledgments.....	v
List Of Figures.....	vii
List Of Tables.....	xi
I. SUMMARY.....	1
II. INTRODUCTION AND PROGRAM HISTORY.....	2
A. Introduction.....	2
B. Program History.....	3
1. Background.....	3
1.1. General.....	3
1.2. Wind Tunnel Testing.....	4
1.3. Major Milestones In Flight Program.....	5
III. DESIGN OBJECTIVES.....	8
A. Location Of Actuators In The Stationary System.....	8
B. System Designed For One Goal.....	8
C. HHC Independence.....	9
D. 4P Signal Isolation By Analog Methods.....	9
E. Two Rotor Revolution Update.....	10
IV. THE HIGHER HARMONIC CONTROL SYSTEM.....	11
A. General HHC System.....	11
B. Baseline OH-6A Design.....	12
C. HHC System As Implemented On The OH-6A.....	14
1. Flight Control System Modifications.....	14
1.1. Primary Flight Control System.....	14
1.2. HHC Actuators.....	16
2. HHC Hydraulic System.....	17
2.1. HHC Hydraulic Pump.....	17
2.2. Pump Drive System.....	18
2.3. Manifold/Reservoir Assembly.....	19
2.4. Distribution System.....	19
3. HHC Electronic System.....	20
3.1 The Electronic Control Unit.....	21
3.1.1. ECU Overview.....	21
3.1.2. Sine/Cosine Generator.....	22
3.1.3. Gray Code Counter.....	22
3.1.4. Filter Section.....	23
3.1.5. Frequency To Voltage Converter.....	24
3.1.6. Correlator Section.....	24

3.1.7.	Actuator Driver Section.....	25
3.1.8.	Actuator LVDT Demodulator.....	25
3.1.9.	ECU Failure Indicators.....	25
3.1.10.	ECU Power Supply.....	26
3.1.11.	ECU Self Test Function.....	26
3.2.	Microcomputer Hardware.....	26
4.	Instrumentation.....	27
4.1.	Airborne Data Acquisition System.....	27
4.2.	Measurement Locations.....	28
D.	Weight And Power Requirements.....	29
E.	Flight Operation and Safety Features.....	30
1.	Open Loop Operation.....	30
1.1.	Manual Controller Description.....	30
1.2.	Flight Procedure.....	31
1.2.1.	Pre Take-Off Procedure.....	31
1.2.2.	HHC System Engagement.....	31
1.2.3.	HHC System Shutdown -- Non-Emergency Disengagement.....	31
1.2.4.	Post Landing Procedure.....	31
2.	Closed Loop Operation.....	32
2.1.	General Description.....	32
2.2.	Flight Procedure.....	32
2.2.1.	Pre Take-Off Procedure.....	33
2.2.2.	HHC System Engagement.....	33
2.2.3.	HHC System Shutdown -- Non-Emergency Disengagement.....	33
2.2.4.	Post Landing Procedure.....	33
3.	Safety Features Of The HHC System.....	33
3.1.	General Disengagement.....	33
3.2.	Self Test Caution Lights.....	34
3.2.1.	ECU Caution Light.....	34
3.2.2.	Cmptr Caution Light.....	35
3.2.3.	Hydro Caution Light.....	35
3.2.4.	Disc Caution Light.....	36
3.3.	ECU And Panel Assembly Circuit Breaker.....	36
3.4.	Malfunction Not Detected Or Controlled By The Self Test.....	36
3.4.1.	Servo - Actuator Hardover.....	36
3.4.2.	Uncontrolled Servo - Actuator Oscillations.....	36
3.4.3.	Hydraulic Leaks.....	37
3.4.4.	Jammed Controls.....	37
V.	ALGORITHM AND SOFTWARE DEVELOPMENT.....	38
A.	Mathematical Description Of The Algorithm.....	38
1.	Introduction.....	38
2.	Optimal Controller Sequence.....	39
3.	Kalman Filtering.....	40
4.	The Autocal Process.....	42
B.	Laboratory Role In Software Development.....	44

1.	Purpose Of The Simulation Laboratory.....	44
2.	Description Of The Simulation Laboratory Hardware.....	45
3.	Description of the Available Software.....	46
3.1.	Stand Alone Simulation - HHCSIM.....	46
3.2.	Closed Loop Simulation - HDRIVR.....	47
3.3.	Autocal Analysis - MXAUTO.....	47
4.	Conclusions Drawn From The Simulation Laboratory.....	49
VI.	FLIGHT TEST PROGRAM.....	52
A.	Program Overview.....	52
B.	Open Loop Flight Test Program.....	53
1.	Introduction.....	53
2.	Vibration Results.....	54
3.	HHC Effect On Blade Loads.....	56
C.	Closed Loop Flight Test.....	58
1.	Introduction.....	58
2.	1983 Closed Loop Vibration Results.....	59
3.	1984 Closed Loop Vibration Results.....	62
3.1.	Introduction.....	62
3.2.	Vibration Results For Level Flight.....	63
3.3.	Rotor Mast Bending For Level Flight.....	65
3.4.	Blade Angles For Level Flight.....	66
3.5.	HHC Actuator Positions And Loads For Level Flight.....	66
3.6.	HHC Effect On Blade Loads For Level Flight....	67
3.7.	HHC Effect On Pitch Link Loads For Level Flight.....	68
3.8.	Tail Boom Bending For Level Flight.....	68
3.9.	Vibration Results For Transient Flight Regimes.....	69
3.10.	Effect Of HHC On Aircraft Performance.....	71
VII.	CONCLUSIONS AND RECOMMENDATIONS.....	72
VIII.	REFERENCES.....	74
IX.	TABLES AND FIGURES.....	77
X.	APPENDICIES	
Appendix A:	Tail Rotor Control System Stress Analysis.....	A-1
Appendix B:	Control System Load Deflection Test.....	B-1
1.	Introduction.....	B-1
2.	Force Equilibrium Of The Control Mixer Assembly.....	B-1
3.	Load Deflection Curves.....	B-1
4.	Added Weight Effect On Primary Boost Stability.....	B-1
4.1.	Lateral Bellcrank.....	B-1
4.2.	Collective Bellcrank.....	B-1
4.3.	Total Penalty.....	B-2
5.	Free-Play Measurement Results.....	B-2

6.	Stiffness Breakdown For Mixer Assembly.....	B-2
7.	Summary Of Data.....	B-2
	7.1. Lost Motion In System At HHC Actuator.....	B-2
8.	Tables And Figures.....	B-5
Appendix C: OH-6A Characteristics.....		C-1

ACKNOWLEDGMENTS

This report documents the Higher Harmonic Control flight test program at MDHC. The work performed under NASA contract NAS1-16266 was funded jointly by the U.S. Army and by NASA, and it extended from 1980 to 1986. As with any project of this scope, numerous people contributed significantly to its success. The technical monitors, C. E. Hammond and J. H. Cline provided valuable support. Moreover, except for reduction of 1984 flight data, the authors are indebted to the following engineers for this report.

Dr. E. Roberts Wood, former MDHC Aeromechanics Manager, deserves a large amount of credit. While at MDHC, Dr. Wood was involved with all phases of the HHC program. In 1976, he drafted the original HHC preliminary design proposal and he followed the HHC program through the 1984 flights.

Richard W. Powers, former MDHC Senior Dynamics Engineer, was the project engineer during the predesign and design phases and through portions of fabrication and flight testing. Next, Dr. Brad P. Gupta directed the project from the system fabrication to completion of the flight test program.

In the design and testing of the system, several people must be mentioned. Ronald Rabin, former MDHC Control Systems Chief, developed the electronic control unit. Gene Munson, while Flight Test Engineer, oversaw the flight test phase of the program and operated the manual controller. Finally, Mark Ford and Doug Kokawa, former MDHC Aeromechanics Engineers, and John Graves made notable contributions.

John Molusis, of the University of Connecticut, was for the development of the closed loop algorithm. Jim Rivers and Zack Martin, while employed at MDHC, integrated the 1983 and 1984 software into the system.

The authors would like to recognize the special contributions of MDHC test pilots, Bob Ferry, Gary Lettrich and Robert Merrill. Mr. Ferry flew the aircraft on its first flight and continued as chief test pilot through the open-loop program. Mr. Lettrich pioneered the closed loop flight test program and Mr. Merrill piloted the 1983 and 1984 tests of the new software.

Finally, a special note of thanks is due Ruby House, MDHC Aeromechanics Secretary, for typing this report.

LIST OF FIGURES

<u>Figure Number</u>	<u>Title</u>
1	Trend of Helicopter Vibration Levels since 1955.
2	NASA/ARMY Aeroelastic Rotor Experimental System (ARES).
3	Typical Results from Open Loop Wind Tunnel Tests.
4	First Flight of HHC Equipped on OH-6A, on August 25, 1982.
5	Primary Elements of the HHC System.
6	HHC Electronics Block Diagram.
7	HHC Actuator Installation Schematic.
8	HHC Right Lateral Actuator Installation.
9	OH-6A Sperry SAS Flight Control System.
10	Schematic of the Convair Hydropac.
11	Control System Stiffness and Freeplay.
12	HHC Actuator Schematic.
13	HHC Actuator.
14	HHC Hydraulic Pump.
15	HHC Hydraulic Pump Installation.
16	HHC Hydraulic Schematic.
17	Electronic Control Unit Block Diagram.
18	Sine/Cosine Generator Block Diagram.
19	Two-Bit Gray Code Counter.
20	Two-Bit Gray Code Counter Timing Diagram.
21	4 Pole Butterworth and 2 Pole RC Band Pass Filter -- Pass Band is 26 to 38 Hz.
22	Simulated Bandpass Filter -- Input Frequency is 32 Hz.
23	Simulated Bandpass Filter Gain.
24	Simulated Bandpass Filter Phase Shift.
25	Simulated Bandpass Filter Distortion.
26	Typical Frequency to Voltage Converter.
27	ECU Correlator Block Diagram.
28	Actuator Driver Block Diagram.
29	LVDT Demodulator - One Channel.
30	Self Test Block Diagram.
31	Sperry SDP-175 Digital Computer.
32	Airborne Data Acquisition System (ADAS) Installation.
33	Open Loop Controller Schematic.
34	Open Loop Controller.
35	Open Loop Controller Command Generation - One Channel.
36	HHC Cockpit Control Panel.
37	Process Noise Gain Pot Setting.
38	Measurement Noise Gain Pot Setting.
39	Time Delay Gain Pot Setting.
40	Schematic of the Controller Operation.
41	Schematic of the Controller Initialization.
42	MDHC Higher Harmonic Control Simulation Laboratory.
43	Block Diagram of the HHC Sim Lab.
44	Variation of 4P Vibration with Input Phase at 60 KIAS.
45	Variation of 4P Vibration with Input Phase at 70 KIAS.
46	Variation of 4P Vibration with Input Phase at 80 KIAS.
47	Variation of 4P Vibration with Input Phase at 90 KIAS.
48	Variation of 4P Vibration with Input Phase at 100 KIAS.
49	The Effect of HHC on 3P, 4P and 5P Flapwise Blade Bending -- At $r/R = 15\%$.

<u>Figure Number</u>	<u>Title</u>
50	The Effect of HHC on 3P, 4P and 5P Chordwise Blade Bending -- At $r/R = 17\%$.
51	The Effect of HHC on 3P, 4P and 5P Blade Torsion -- At $r/R = 17\%$.
52	60 Knots Closed Loop HHC Engagement.
53	1983 Closed Loop HHC -- 4P Vertical Pilot Seat Accelerations versus Airspeed.
54	1983 Closed Loop HHC -- 4P Lateral Pilot Seat Vibrations versus Airspeed.
55	1983 Closed Loop HHC -- 4P Longitudinal Pilot Seat Vibrations versus Airspeed.
56	1983 Closed Loop HHC -- 3P, 4P and 5P Optimal Blade Feathering Angle versus Airspeed.
57	Software Execution Speed Comparison
58	1984 Closed Loop HHC -- 4P Vertical Pilot Seat Vibrations versus Airspeed.
59	1984 Closed Loop HHC -- 4P Lateral Pilot Seat Vibrations versus Airspeed.
60	1984 Closed Loop HHC -- 4P Longitudinal Pilot Seat Vibrations versus Airspeed.
61	1984 Closed Loop HHC -- 4P Vertical Pilot Seat Vibrations versus Airspeed -- Expanded Scale.
62	1984 Closed Loop HHC -- 4P Lateral Pilot Seat Vibrations versus Airspeed -- Expanded Scale.
63	1984 Closed Loop HHC -- 4P Longitudinal Pilot Seat Vibrations versus Airspeed -- Expanded Scale.
64	1984 Closed Loop Results -- 4P Vertical Pilot Seat Vibrations Frequency Spectrum at 100 Knots
65	1984 Closed Loop HHC -- 3P Vertical Pilot Seat Vibrations versus Airspeed.
66	1984 Closed Loop HHC -- 3P Lateral Pilot Seat Vibrations versus Airspeed.
67	1984 Closed Loop HHC -- 3P Longitudinal Pilot Seat Vibrations versus Airspeed.
68	1984 Closed Loop HHC -- 5P Vertical Pilot Seat Vibrations versus Airspeed.
69	1984 Closed Loop HHC -- 5P Lateral Pilot Seat Vibrations versus Airspeed.
70	1984 Closed Loop HHC -- 5P Longitudinal Pilot Seat Vibrations versus Airspeed.
71	1984 Closed Loop HHC -- 4P Vertical Aircraft C.G. Vibrations versus Airspeed.
72	1984 Closed Loop HHC -- 4P Lateral Aircraft C.G. Vibrations versus Airspeed.
73	1984 Closed Loop HHC -- 4P Longitudinal Aircraft C.G. Vibrations versus Airspeed.
74	1984 Closed Loop HHC -- Main Rotor Mast 4P Lateral Bending versus Airspeed.
75	1984 Closed Loop HHC -- Main Rotor Mast 4P Longitudinal Bending versus Airspeed.
76	1984 Closed Loop HHC -- 3P Blade Feathering Angle versus Airspeed.
77	1984 Closed Loop HHC -- 4P Blade Feathering Angle versus Airspeed.

<u>Figure Number</u>	<u>Title</u>
78	1984 Closed Loop HHC -- 5P Blade Feathering Angle versus Airspeed.
79	1984 Closed Loop HHC -- 3P Blade Flapping Angle versus Airspeed.
80	1984 Closed Loop HHC -- 4P Blade Flapping Angle versus Airspeed.
81	1984 Closed Loop HHC -- 5P Blade Flapping Angle versus Airspeed.
82	1984 Closed Loop HHC -- 4P Left Lateral Actuator Stroke versus Airspeed.
83	1984 Closed Loop HHC -- 4P Right Lateral Actuator Stroke versus Airspeed.
84	1984 Closed Loop HHC -- 4P Longitudinal Actuator Stroke versus Airspeed.
85	1984 Closed Loop HHC -- 4P Left Lateral Actuator Load versus Airspeed.
86	1984 Closed Loop HHC -- 4P Right Lateral Actuator Load versus Airspeed.
87	1984 Closed Loop HHC -- 4P Longitudinal Actuator Load versus Airspeed.
88	1984 Closed Loop HHC -- 3P Chordwise Blade Bending Moment versus Airspeed -- At $r/R = 17\%$.
89	1984 Closed Loop HHC -- 4P Chordwise Blade Bending Moment versus Airspeed -- At $r/R = 17\%$.
90	1984 Closed Loop HHC -- 5P Chordwise Blade Bending Moment versus Airspeed -- At $r/R = 17\%$.
91	1984 Closed Loop HHC -- 3P Flapwise Blade Bending Moment versus Airspeed -- At $r/R = 15\%$.
92	1984 Closed Loop HHC -- 4P Flapwise Blade Bending Moment versus Airspeed -- At $r/R = 15\%$.
93	1984 Closed Loop HHC -- 5P Flapwise Blade Bending Moment versus Airspeed -- At $r/R = 15\%$.
94	1984 Closed Loop HHC -- 3P Torsional Blade Bending Moment versus Airspeed -- At $r/R = 30\%$.
95	1984 Closed Loop HHC -- 4P Torsional Blade Bending Moment versus Airspeed -- At $r/R = 30\%$.
96	1984 Closed Loop HHC -- 5P Torsional Blade Bending Moment versus Airspeed -- At $r/R = 30\%$.
97	1984 Closed Loop HHC -- 1/2 Peak to Peak Chordwise Blade Bending Moment versus Airspeed -- At $r/R = 17\%$.
98	1984 Closed Loop HHC -- 1/2 Peak to Peak Flapwise Blade Bending Moment versus Airspeed -- At $r/R = 15\%$.
99	1984 Closed Loop HHC -- 1/2 Peak to Peak Torsional Blade Bending Moment versus Airspeed -- At $r/R = 30\%$.
100	1984 Closed Loop HHC -- 3P Pitch Link Load versus Airspeed.
101	1984 Closed Loop HHC -- 4P Pitch Link Load versus Airspeed.
102	1984 Closed Loop HHC -- 5P Pitch Link Load versus Airspeed.
103	1984 Closed Loop HHC -- 1/2 Peak to Peak Pitch Link Load versus Airspeed.
104	1984 Closed Loop HHC -- 4P Lateral Tail Boom Bending versus Airspeed.
105	1984 Closed Loop HHC -- 4P Vertical Tail Boom Bending versus Airspeed.

<u>Figure Number</u>	<u>Title</u>
106	1984 Closed Loop HHC -- 4P Torsional Tail Boom Bending versus Airspeed.
107	1984 Closed Loop Results -- 4P Vertical Pilot Seat Vibrations During 80 Knot Pullups
108	1984 Closed Loop Results -- 4P Lateral Pilot Seat Vibrations During 80 Knot Pullups
109	1984 Closed Loop Results -- 4P Longitudinal Pilot Seat Vibrations During 80 Knot Pullups
110	1984 Closed Loop Results -- 4P Vertical Pilot Seat Vibrations During 80 Knot 30 Degree Bank Turns
111	1984 Closed Loop Results -- 4P Lateral Pilot Seat Vibrations During 80 Knot 30 Degree Bank Turns
112	1984 Closed Loop Results -- 4P Longitudinal Pilot Seat Vibrations During 80 Knot 30 Degree Bank Turns
113	1984 Closed Loop Results -- 4P Vertical Pilot Seat Vibrations During 40 - 100 Knot Accelerations and Decelerations
114	1984 Closed Loop Results -- 4P Lateral Pilot Seat Vibrations During 40 - 100 Knot Accelerations and Decelerations
115	1984 Closed Loop Results -- 4P Longitudinal Pilot Seat Vibrations During 40 - 100 Knot Accelerations and Decelerations
116	1984 Closed Loop Results -- 4P Vertical Pilot Seat Vibrations During 40 - 100 Knot Speed Sweep Acceleration
B-1	Collective System Loads.
B-2	Lateral System Loads.
B-3	Longitudinal System Loads.
B-4	Exploded View of the Control Mixer Assembly.
B-5	Deflection Curve for Collective Loading.
B-6	Deflection Curve for Lateral Loading.
B-7	Deflection Curve for Longitudinal Loading.
B-8	Spring Rates for Collective Loading Outside the Freeplay Region.
B-9	Spring Rates for Later Loading Outside the Freeplay Region.
B-10	Spring Rates for Longitudinal Loading Outside the Freeplay Region.

LIST OF TABLES

<u>Table Number</u>	<u>Title</u>
1	HHC Actuator Design Characteristics
2	HHC Hydraulic Pump Design Criteria
3	PDP-11/B and SDP-175 Controller Characteristics
4	Master Instrumentation List
5	Weight of HHC System Components
6	Weight of HHC Flight Test Instrumentation
7	Blade Feathering Angles Resulting from Actuator Inputs
8	HHC Software Version Summary
9	HHC Controller Comparison
B-1	Free Play Summary
B-2	Summary of Stiffness Test Results

I. SUMMARY

This report presents the McDonnell Douglas Helicopter Company (MDHC) flight test program of higher harmonic blade feathering for vibration control. The contract, NAS1-16266, extended from 1980 to 1986 with funding from the U. S. Army and the National Aeronautics and Space Administration (NASA), in addition to substantial flight test support by MDHC.

The higher harmonic control (HHC) system superimposes fourth harmonic inputs upon the stationary swashplate. These inputs are transformed into 3P, 4P and 5P blade feathering angles in the rotating system. The vibrations are then altered at the pilot seat, where feedback accelerometers are located.

The program consisted of three distinct phases. First, the MDHC OH-6A helicopter (Army 67-17230) underwent numerous changes to incorporate the HHC system. Then, the open loop, or manual controlled, flight tests were performed, and finally, the closed loop, or computer controlled, system was tested. In 1983, one portion of the closed loop testing was performed, and in 1984, additional closed loop tests were conducted with improved software.

With the HHC system engaged, the 4P pilot seat vibration levels were significantly lower than the baseline OH-6A levels. Moreover, the system did not adversely affect blade loads or helicopter performance. In conclusion, this successful proof of concept project indicates HHC as a viable vibration suppression mechanism.

II. INTRODUCTION AND PROGRAM HISTORY

A. INTRODUCTION

The trend in helicopter crew station vibration levels over the past 30 years, Figure 1, indicates that the helicopter industry has reached an asymptote in vibration reduction employing currently known methods. As further confirmation of this fact, Figure 1 shows that the U.S. Army had to increase the specified vibration levels for the AAH/UTTAS procurement from the early 1970's target. The mid 1970's values better indicated realistic design goals which were consistent with the state-of-the-art in helicopter vibration control. The actual vibration levels achieved with present technology far exceed the desired value of 0.02 g's recommended by NASA Research and Technology Advisory Council Subpanel on Helicopter Technology, Washington, D.C., May 24, 1976. Although it has achieved a significant vibration reduction over the past 25 years, the helicopter industry will not reach the desired goal without a quantum advance in vibration control technology.

In contrast to the conventional passive means of vibration control, such as vibration absorbers and vibration isolators, higher harmonic control (HHC) is an active control concept. A passive device treats the vibratory loads after they have been generated, whereas the HHC system alters aerodynamic loads on the rotor to reduce the forces and moments which cause airframe vibrations. As an electronic, computer controlled system, HHC senses and cancels helicopter airframe vibrations by high frequency feathering of rotor blades. With the rapid evolution of lightweight microcomputers, coupled with advances in servo-actuator technology, the quantum advance in vibration control technology is within reach.

For the present program, an Army OH-6A (S/N 67-17230) was modified to incorporate higher harmonic blade pitch control by superimposing 4/rev swashplate motion upon the primary control inputs. Perturbing the stationary swashplate at 4/rev in the collective and cyclic controls, third, fourth and fifth harmonic blade feathering results in the rotating system. Main rotor rotational speed for the OH-6A is 483 rpm or 8 Hz. Pitch, roll, and collective motion of the stationary swashplate is provided by three electro-hydraulic high frequency servo-actuators. The three actuators are installed in the stationary system where they replace conventional rod-end links between the control mixer and the stationary swashplate. An onboard computer processes airframe vibration measurements and determines the optimal actuator motions for vibration reduction.

Following a brief history of the HHC concept, the design objectives and then the HHC system, as installed on the OH-6A, are described. Next, the control algorithm and its development are discussed. Finally, the open and closed loop flight test results are presented.

B. PROGRAM HISTORY

1. BACKGROUND

1.1 GENERAL

Prior to the OH-6A HHC flights, only one other HHC equipped helicopter was tested and that was over twenty years ago. The aircraft, a UH-1A helicopter with a two-bladed teetering rotor, was modified to incorporate a mechanical device by which amplitude and phase of second harmonic feathering were manually adjustable. In 1963, Drees and Wernicke [32], while reporting the program results concluded that, "even though the mechanism accomplished the anticipated changes in air load 2/rev thrust pulsations, the beneficial

effects on vibration and on load reduction were small." Most likely, these researchers were somewhat limited by a two-bladed rotor, since second harmonic feathering strongly couples with both first and third harmonics. The first harmonic airloads are also generated by the cyclic pitch needed for primary helicopter control.

Following the work of Drees and Wernicke, a number of theoretical and experimental studies further explored higher harmonic control and produced particularly promising results, References 10 through 20. These studies indicated that successful suppression of vibration required small blade oscillation amplitudes, in general less than 0.5 degrees. The small blade angles required were further confirmed in the MDHC flight test program.

1.2 WIND TUNNEL TESTING

To establish the feasibility of the higher harmonic control concept, wind tunnel tests were first conducted on an aeroelastically scaled model rotor system. As the predecessor to the MDHC flight test program, wind tunnel tests of the HHC concept were conducted in the 5 m (16 ft) NASA Langley Transonic Dynamics Tunnel (TDT), shown in Figure 2. Three different, fully articulated rotor models were used for these tests over the period 1976 - 1981. The models were all aeroelastically scaled and were 2.7 - 2.9 m (9 - 9.5 ft) in diameter. The rotors were tested at full scale tip Mach numbers in a Freon-12 atmosphere. The main goal of the wind tunnel test program was to validate open loop HHC. Acceptable levels of blade pitch had to significantly modify rotor vibratory forces and moments.

These tests were conducted by oscillating the swashplate at a frequency of 4 cycles/revolution in collective, longitudinal tilt, and lateral tilt. The input phase angles were varied at constant amplitude to

establish relationships between the inputs and the rotor hub force and moment response. Once an optimum phase was found, the amplitude was adjusted to minimize one vibratory hub load. These results, Hammond [10], were very encouraging and led to the HHC Predesign Contract. Typical of the test results, the fourth harmonic of vertical acceleration is shown with HHC "on" and with HHC "off", Figure 3. Later, additional wind tunnel results proved closed loop computer control of the HHC process was possible; see References 11-20.

2. MAJOR MILESTONES IN FLIGHT PROGRAM

In 1976 McDonnell Douglas Helicopter Company teamed with the U.S. Army and with NASA to systematically develop a flightworthy HHC system for the OH-6A. After investigating numerous concepts, a candidate HHC configuration was identified. The system chosen, along with the necessary modifications to the OH-6A, is presented in Section IV. Powers [9] presents all the considered HHC systems.

After the preliminary design contract the full flight test go ahead was announced in September 1980. The contract objective was to install and to fly an HHC system both in the open loop and closed loop mode. The flight test program was structured to duplicate the wind tunnel results. During the flight tests significantly reduced vibrations were recorded when comparing HHC to baseline OH-6A data, thus yielding an extremely successful proof of concept project.

The OH-6A underwent numerous preparatory changes. Most importantly, the primary control system had to be stiffened. Test results, Appendix B, indicated large flexibility and freeplay in the system which would reduce, if not eliminate, any HHC blade feathering. After a detailed analysis of the primary flight controls, the questionable parts were replaced resulting in a system suitable for HHC.

In addition to stiffening the primary flight controls, many other parts of the OH-6A were replaced or removed. The contract sponsors required two studies for the safety review before the first flight. First, since the tail rotor control system was completely replaced, a stress analysis of the new configuration was performed; see Appendix A. Secondly, a loads test of the primary control system was conducted; see Appendix B. With the approval of these analyses, the HHC equipped OH-6A was released for flight in August 1982.

On August 25, 1982, the first two open loop flights, each 15 minutes long at hover, were conducted at the MDHC test facility located at the U.S. Army's Proving Ground in Yuma, Arizona. The first flight is pictured in Figure 4. Following these early flights, the flight envelope was expanded to include forward speeds of up to 100 knots. Before the initial open loop flight testing had been completed, the HHC system had also been shown to reduce vibrations in flares and in wind-up turns.

The open loop, or manual control, flight test program involved 15 flight hours with the HHC system operational. Prior to the first flight, there were 20 hours of ground running with HHC engaged. The open loop flight test results demonstrated the potential for marked improvement in helicopter passenger comfort as well as for increased stability in precision weapon delivery.

After successful open loop flights, the closed loop flight testing was subsequently conducted. During this flight test program, computer controlled HHC successfully reduced airframe vibration levels automatically in both steady-state and transient flight conditions. Although the original algorithms suffered reduced performance at higher speeds, they did indicate the feasibility of closed loop HHC. Later, as refined algorithms were

developed based on lessons from flight tests results, HHC consistently reduced vibrations throughout the flight envelope.

The closed loop flight tests began in January, 1983, and ended in November, 1984. In all, over 26 hours were flown with HHC operational, using six different software versions of the same basic algorithm. Two more versions were developed and coded, however, the flight test program was terminated before they could be demonstrated.

III. DESIGN OBJECTIVES

In order to implement an HHC system on the OH-6A, specific design objectives were established. To ensure a successful flight test program, several decisions were made to define the system configuration. For further background, see Powers [9].

A. LOCATION OF ACTUATORS IN THE STATIONARY SYSTEM

A primary design decision was to accomplish both vibration sensing and corrective blade feathering in the stationary system. If the actuators were placed in the rotating system, multiple frequencies, specifically 3P, 4P and 5P would have to be generated. With the actuators installed beneath the stationary swashplate, any combination of blade 3P, 4P, and 5P feathering can be obtained by proper phasing of 4P stationary swashplate pitch, roll, and vertical motion. Also, a rotating hydraulic manifold and slip-ring assembly are thus avoided, and actuators and tube assemblies do not operate in a centrifugal force field.

B. SYSTEM DESIGNED FOR ONE GOAL

In addition to vibration reduction, other benefits may be realized from higher harmonic control application. HHC can be beneficial for blade stress reduction, McCloud [18], for improved performance by delaying the onset of retreating blade stall, Wernicke, et al. [32], and for gust load alleviation, Ham, et al. [21]. Ground resonance elimination, Straub, et al. [22], and rotor blade deicing, Lemont, et al. [23] are

also feasible. Although all are worthwhile goals to pursue, active vibrations control must first be successfully demonstrated. By initially investigating several objectives simultaneously, this project could become counterproductive. Therefore, this program is focused upon minimizing 4P vibration of the fuselage.

C. HHC INDEPENDENCE

The HHC signals are superimposed on the primary rotor controls which offers many advantages for the prototype system. First, the HHC system is independent of the primary control system, thereby reducing any unwanted effects on rotor trim. Second, with an HHC failure or malfunction, the helicopter control system returns to its original configuration. Third, the HHC and the primary control actuators need not be located in the same aircraft vicinity; the HHC actuators, therefore, are placed in near optimal installations. Aside from high reaction impedance, the selected location must provide minimal lost motion due to control system flexibility and freeplay. Finally, with this design, separate hydraulic supplies, tailored to the specific requirements of each, can be used for both the primary and the HHC actuator systems.

D. 4P SIGNAL ISOLATION BY ANALOG METHODS

Inherent in the design, the HHC system is required to repeatedly isolate the 4P component of the load or of the accelerometer electronic signal. Since modern microcomputers rapidly execute Fast Fourier Transforms

(FFTs), these methods initially appear desirable. However, a problem exists with FFT procedures in a real time application, such as HHC. The transforms are limited not by calculation time, but by required record length, which directly impacts the sampling time. For the OH-6A HHC system, an electronic analog technique is applied that precludes the need for FFT methods and provides essentially continuous sensor output sampling.

E. TWO ROTOR REVOLUTION UPDATE

An early objective was to complete both the data sampling and the computer updating within two rotor revolutions. For the OH-6A, where the rotor speed is 483 rpm, this limit becomes 0.25 seconds. With the original software, the closed loop system slightly exceeds this bound since the update rate is 0.267 seconds. The latest software version, with a cycle time of 0.162 seconds, far surpasses the goal. This rate should permit rapid updating of the HHC controls in transient flight regimes.

IV. THE HIGHER HARMONIC CONTROL SYSTEM

A. GENERAL HHC SYSTEM

Referring to Figure 5, the primary elements of the active vibration suppression system are:

1. Acceleration transducers that sense the vibratory response;
2. A higher harmonic blade pitch actuator system;
3. A flightworthy microcomputer, which incorporates the algorithm for reducing vibrations;
4. A signal conditioning system which interfaces between the sensors, the microcomputer and the HHC actuators.

Operation of the system, illustrated in the block diagram of Figure 6, is as follows. Triaxial accelerometers, mounted beneath the pilot's seat, sense the vertical, the lateral and the longitudinal vibrations which are then passed to the Electronic Control Unit (ECU). The ECU extracts the 4P sine and cosine components, and converts these vibration signals to DC signals suitable as input to the flight computer. These six feedback quantities serve two purposes in the control algorithm. First, these six signals help construct a mathematical model of the helicopter. Second, this data is the vector to be minimized using modern control theory. The flight computer calculates six actuator 4P motions, which are sent via the ECU as analog signals to drive the swashplate. The actuators replace existing links in the stationary system, Figures 7 and 8. The 4P signals transform to 3P, 4P and 5P blade motion, which corresponds to 24, 32 and 40 HZ for the OH-6A. This loop is updated approximately every 160 milliseconds for the latest software. With this integrated

system, the fuselage vibrations are reduced throughout the entire flight envelope.

B. BASELINE OH-6A DESIGN

The OH-6A (S/N 68-17230) selected for this program is unique in the Army inventory. The standard OH-6A incorporates a mechanical, or non-boosted, control system. This aircraft would be unsuitable for HHC applications because it would permit actuator feedback to the pilot's controls. As a result, the blade higher harmonic pitching motion would be significantly deteriorated. To preclude this, a specially modified OH-6A incorporating a Sperry stability augmentation system (SAS) for the primary controls, Figure 9, was bailed to MDHC for flight tests. The electromechanical SAS actuators are removed, however, the 1500 psi boost system is retained except in the yaw channel; see Appendix A.

A Stratopower pump, driven by 28 DC volts of aircraft power, provides the hydraulic boost which is completely separate from the HHC hydraulic system. A Convair Hydropac, which is an integrated reservoir, filter and valve package, supplies 0.7 gallons/minute of hydraulic fluid at operating pressure, Figure 10. In the event of a failure, the boosted system design provides a backup mechanical system. Before the HHC project, this control system was successfully flown for over 200 hours.

For the SAS controls configuration, the following parts are removed from the stock OH-6A:

1. Collective Bungee: Male Brg. Assembly
Retainer
Spring
Female Brg. Assembly

2. Lower Tunnel Area: Longitudinal Idler Bellcrank
Uni-Lock
Lateral Idler Bellcrank
T/R Bellcrank
3. Mixer Area: Lateral Bellcrank
Collective Bellcrank
Longitudinal Idler
T/R Bellcrank
Bracket
4. Tunnel Area: T/R Control Rod
Lateral Control Rod
Longitudinal Control Rod
Collective Control Rod

The following items are then added to the aircraft:

1. Control Position Transducers:
Lateral Cyclic
Longitudinal Cyclic
Directional Control
2. Lower Tunnel Area, to accommodate the SAS servos:
T/R Bellcrank
Lateral Bellcrank
Longitudinal Bellcrank
3. Mixer Area: Lateral Bellcrank
Collective Bellcrank
Longitudinal Idler
T/R Bellcrank
Bracket
Collective Compensator Assembly

Note: Installation of the SAS servos necessitated removal of the collective bungee, leaving the pilot with unassisted collective controls under the loss of boost hydraulic pressure. The bleed air powered collective compensator remedied this problem.

4. Tunnel Area: T/R Control Rod
Lateral Control Rod
Longitudinal Control Rod
Collective Control Rod
(2) Longitudinal and Lateral SAS Servos
T/R SAS Servo
Upper Tunnel Support
Boost Actuators

Note: The lateral, the longitudinal and the tail rotor control rods are shortened once to allow for the upper boost actuators and again for the lower SAS servos. The collective control rod was shortened only to allow for the boost actuator. The upper tunnel support provides mounting for the lower end of the four boost actuators.

Aside from the SAS electronics, boost hydraulic power system and assorted panel instruments, this summarizes the state of the baseline flight control system.

The only OH-6A rotor modifications are the removal of 3P and 5P blade pendulum vibration absorbers. These passive devices reduce vertical blade root shears and the 4P vibration levels. Since the development flights of the OH-6A did not contain the absorbers, their removal did not present a safety issue.

C. HHC SYSTEM AS IMPLEMENTED ON THE OH-6A

1. FLIGHT CONTROL SYSTEM MODIFICATIONS

Modifying an existing OH-6A to incorporate the HHC actuation system established challenging design requirements:

1. The primary flight control system had to be upgraded to permit high fidelity blade feathering.
2. High bandwidth servo-actuators had to be developed.
3. The existing flight control system presented numerous physical and kinematic constraints.

Working within the constraints of an existing flight control system, many issues arose that would not exist if HHC were to be integrated during aircraft development. The current program thus should be viewed as a "proof of principle" HHC evaluation and not as retrofit application study.

A discussion of the upgraded primary controls and of the actuation system follows. Additional details can be found in Wood, et. al. [3].

1.1. PRIMARY FLIGHT CONTROL SYSTEM

It was determined early in the HHC actuator checkout that the existing mechanical flight control system was incapable of transmitting high frequency feathering motion to the main rotor blades. A test program was designed to isolate the principle sources of lost motion. It revealed considerable freeplay in all three axes; see Appendix B. This control slop is typical of unboosted control systems rather than due to service life wear.

"True" freeplay, or zero stiffness, contributed less to lost motion, than did local bearing liner, bolt, bushing and bellcrank flexibilities. Careful modifications were performed to minimize lost motion and local flexibilities in the primary controls. Through the use of precision tolerance roller bearings, bolts, bushings, metal-to-metal rod end bearings and redesigned mixer components, a 75 percent reduction in freeplay and up to a 90 percent increase in end-to-end control system stiffness was achieved.

Referring to Figure 11, the initial system freeplay, ± 0.040 inches, was larger than the actuator stroke needed for vibration reduction, approximately ± 0.033 inches. After the new components were installed, the control system dead zone was decreased to ± 0.010 inches which was sufficient for HHC applications. Also showed the control system stiffness increased from $K = 2000$ lbs./in. to $K = 5000$ lbs./in., outside the freeplay region. Without the new primary controls system, the OH-6A could not demonstrate HHC effectiveness.

The primary control system changes are summarized below.

Lower Tunnel Area:

1. The longitudinal idler bellcrank was removed and replaced with the original part.

2. The lateral idler bellcrank was removed and replaced with the original part.
3. The T/R bellcrank was removed and replaced with the original part.

Tunnel Area:

1. The collective control rod was instrumented with strain gauges.
2. The lateral and the longitudinal SAS servos were removed and replaced with a new dummy machined fitting.
3. The tail rotor SAS servo was removed, as was the tail rotor boost actuator. The tail rotor control rod also was removed and all three components were replaced by the original tail rotor rod.
4. The upper tunnel support was machined to provide clearance for the T/R rod.

Mixer Area:

1. The anti-torque link and the 5/16 inch bolts were removed and replaced by an HHC actuator, an anti-torque frame and an anti-torque idler arm.
2. These new parts were secured to the stationary swashplate in the following fashion. The bushing at the longitudinal corner of the stationary swashplate was reamed from 0.3125 in. to 0.3750 in. I.D. A 0.375 inch bolt was then used to secure the actuator and the idler arm. The original spacer bushing was used to secure the actuator and the anti-torque frame to the longitudinal bellcrank.
3. The remaining two rod-end links were removed and replaced by HHC actuators. The mounting hardware remained unchanged.
4. The T/R bellcrank was removed and replaced. The bellcrank design was modified to provide greater clearances for the HHC actuator. A new flush head bolt was used to secure the tail rotor control rod to the new bellcrank.
5. The longitudinal link was instrumented with strain gauges.
6. The collective and lateral cyclic were changed from magnesium to machined 4130 steel.
7. The magnesium rotor hub was replaced by a new aluminium hub.

1.2. HHC ACTUATORS

The HHC actuator design was primarily driven by high system frequency response requirements. Piston area, drill passage diameter, seal friction and electro-hydraulic (EH) servo-valve characteristics enhance the installed response, which results in a usable range of approximately 90 Hz at command amplitudes of one degree pitch angle. The

HHC servo-actuators, Figures 12 and 13, have a total collective blade angle authority of two degrees, or roughly 11 percent of the total OH-6A collective pitch range. This translates into a total stroke for each actuator of ± 0.20 inches. Developed by MOOG Western Development Center, the actuators were designed for operation at 3000 psi.

The actuators replace existing links in the primary control system, located between the mixer and the stationary swashplate assembly, Figures 7 and 8. A center-driving lockout device sets the equipment to neutral position in the event of an hydraulic pressure loss or of an HHC disengagement. The design characteristics are summarized in Table 1.

Actuator control is derived from a MOOG servo-valve and an internally mounted linear variable differential transducer (LVDT). The transducer carrier frequency and the demodulation network design is tailored to improve system frequency response. All position loop closures and all compensation networks are mechanized in the ECU. A differential pressure transducer, manifold mounted beneath the EH valve, permits monitoring of the actuator loads. Lastly, although advances have been made in self-lubricating bearings with composite liners containing interwoven Teflon and glass fibers, metal-to-metal rod end bearings were selected for enhanced life and for minimal lost motion. With composite lined bearings, surface roughness grows when the amplitude of oscillation is reduced. Tending to increase liner wear, this phenomena precluded their application for the actuators.

2. HHC HYDRAULIC SYSTEM

2.1. HHC HYDRAULIC PUMP

A Sperry-Vickers axial piston, variable displacement pump, model PV3-075-15, provides hydraulic power. Although capable of absorbing 20 horsepower, the pump typically required three to four horsepower during closed loop testing.

Currently used on the F-16 primary flight control system, the pump was acceptance tested under General Dynamics Test Procedure prior to delivery to MDHC. The remaining pump design criteria are listed in Table 2.

2.2. PUMP DRIVE SYSTEM

Running at 2800 RPM, the pump is driven by an intermediate gearbox assembly attached to the engine spare power take-off pad. The nominal pad speed is 6016 RPM, with clockwise rotation looking at the pad. As the Allison turbine engine was derated from 400 SHP to 250 SHP, the sum of the front and the rear output torque did not exceed the maximum continuous engine rating of 4416 in.-lbs.

For the purposes of HHC, the six-bolt internal spline engine pad mates with a Soloy Conversions 660-2410 Gearcase Assembly. The gearcase assembly has been qualified for commercial applications on the MDHC Model 500D under FAA STC. This installation is shown in Figures 14 and 15.

The gearcase is rated for 20 HP maximum continuous power and it incorporates a drive shaft shear section design at 1036 in.-lbs. Straight cut gears in the unit yield a 2.3:1 reduction, at the nominal 2700 RPM output shaft speed. A shaft external to the gearcase permits the drive spline to be engaged or disengaged. Lubrication is provided by the Vickers pump case drain flow. Even with the 53 degree from vertical mounting angle of the engine assembly, the overhung moment of the pump/adaptor unit is within the 100 in.-lbs. design limit of the engine manufacturer.

2.3. MANIFOLD/RESERVOIR ASSEMBLY

A Berteau integrated manifold/reservoir is combined with the distribution network to filter, cool, accumulate and route the actuator hydraulic fluid. This assembly is bailed from the AAH - Apache program where it is the primary system reservoir for Phase I aircraft. The reservoir provides the following functions.

1. It manifolds for pump pressure, for flight controls, for ground service pressure and return, for pump suction and for flight controls return connections.
2. It is a 30 cu. in. fluid reservoir with level indicator. The reservoir is pressurized with turbine compressor bleed air to meet pump inlet requirements.
3. It is a high pressure switch, which is open above 3450 psi and closed below 1500 psi. The ECU senses this switch for a drop in the system pressure, thereby disabling the servo-valve commands.
4. As a check valve, it prevents the accumulator from motoring the hydraulic pump once the system is shut down. The cracking pressure is 2 - 8 psi.
5. As a high pressure relief valve, modified by Berteau under the contract, it increases to full flow of 8 gpm at 4200 psi. The cracking pressure is 3650 psi.
6. The internal fluid filter is removed in this application. A 15 micron absolute cartridge-type filter is present upstream of the manifold.

2.4. DISTRIBUTION SYSTEM

The pump pressure and the suction lines are routed to bulkhead fittings at the fuselage station 124.0 via flex hoses. The lines used on all return and all suction paths yield fluid velocities sufficiently close to the 15 fps design objective which precludes pump cavitation. Pump case drain oil, approximately 1 gpm, is routed to the inlet side of the Soloy gearcase and returns to the manifold/reservoir. Pump and gearcase vents are open to the atmosphere using short lengths of tubing. The hydraulic fluid is passed through the 15 micron filter, and then into the manifold. Two quick disconnect nipples are provided for the pressure and for the manifold/reservoir return lines.

A pressure line exits the manifold, travels forward along the cargo floor and is then secured to the canted control tunnel at fuselage station 78.22. A Sterer 28 volt solenoid valve is installed near the top of the tunnel and is activated by the pilot or by the ECU to disable the hydraulic system.

Emerging through the upper bulkhead fittings, the line travels aft along the roof of the cargo section where it connects to the distribution manifold. The HHC actuator pressure and return flex hoses are routed to and from the manifold. A return line then retraces the pressure line route across the fuselage roof and down the canted control tunnel at fuselage station 78.22. Near the top of the canted bulkhead, a divider circuit is installed to route approximately 50% of the flow into the heat exchanger. A fiberglass duct channels cooling air from the transmission oil cooler to the heat exchanger. The return line then continues along the cargo floor, terminating at the reservoir/manifold. The entire HHC hydraulic system is schematically shown in Figure 16.

A probe at the bulkhead pressure circuit "T" fitting monitors the hydraulic temperature, which is digitally displayed on the pilot's instrument panel. Finally, the crew and the cargo compartment are hydraulically isolated by 0.25 in. plexiglass panels, as required per MIL-E-38453.

3. HHC ELECTRONIC SYSTEM

The electronic components of the system generate HHC actuator drive commands, provide cockpit control interface, and perform self testing, Figure 6. The electronic control unit and the airborne digital controller are described below. Wood, et.al. [3] also provides a description of the HHC electronic system.

3.1. THE ELECTRONIC CONTROL UNIT

3.1.1. ECU OVERVIEW

The ECU provides an analog interface between the HHC actuators, feedback sensor package, airborne digital processor and cockpit control subsystems. Developed by MDHC using printed circuit board construction, the ECU performs a hardware analog of a discrete Fourier transform (DFT) to isolate the sine and cosine 4P components of three airframe accelerations. The six feedback components are transmitted to the digital controller in DC format. Actuator drive commands are constructed from computer-generated DC commands and the same 4P reference required for the hardware DFT. The DC commands are proportional to the optimal sine and cosine amplitudes of collective, lateral cyclic and longitudinal cyclic 4P swashplate motion. The ECU additionally provides the HHC actuator outer loop position closures and inner loop compensation needed to achieve the installed frequency response. Lastly, the ECU provides extensive self-test and failure mode protection including command limiting, rate limiting, hardover detection and protection, loss of power supplies, and loss of controller update to name a few.

The ECU, Figure 17, receives a 16P square wave and a 4P signal, both synchronized with the main rotor rotation. A 16 pole commutator is mounted atop the main rotor to generate these signals. With the reference signals, the ECU correlator section derives DC analog signals of the 4P vertical, longitudinal and lateral accelerations. To both simplify interface circuitry and to eliminate AC drive signals, all data provided to and generated by the flight computer is in DC form. The ECU performs all AC to DC and DC to AC conversions.

Two signals are derived from each acceleration transducer. One signal is directly proportional to the in-phase component of the measured 4P acceleration and the other is proportional to the quadrature component. The ECU also provides a DC analog signal of rotor rpm to the computer. The ECU generates two other DC signals, proportional to the magnitude of the sine and of the cosine 4P references. The remaining signal furnished by the ECU is a self-test which indicates the presence or the absence of any internally detected failure.

The computer provides DC analog signals to the ECU to control phase and magnitude of collective, lateral cyclic and longitudinal cyclic 4P swashplate motion. The computer similarly returns a "keep alive" signal to the ECU, indicating that the processor is operating in a normal manner.

In summary, the HHC ECU performs the following functions:

1. It extracts the 4P sine and cosine components of measured accelerations and it passes them to the computer in DC analog form.
2. Upon receipt of DC analog 4P control inputs from the computer, the ECU constructs the appropriate 4P AC servo-valve drive signals.
3. The ECU accomplishes servo-valve feedback compensation.
4. The ECU monitors the system for internal failures.
5. The ECU provides hardover protection.

3.1.2. SINE/COSINE GENERATOR

The sine/cosine generator contains a two-bit gray code counter, two identical Butterworth filter sections, two identical voltmeter sections and a frequency to voltage converter, Figure 18.

3.1.3. GRAY CODE COUNTER

The gray code counter block diagram is shown in Figure 19. The 16P reference signal clocks two D-type flip flops; whereas, the 4P sync reference presets the exact state of the flip flops at each quarter revolution. The resultant wave shapes are illustrated in Figure 20.

Output of the first flip flop becomes a 4P sine-phase wave, while the second output is a cosine-phased 4P square wave. These references are used for further processing.

3.1.4. FILTER SECTION

The two 4P reference signals, created by the gray code counter, are each passed through a filter section, consisting of a four-pole Butterworth low pass filter and two single-pole RC high pass filters, Figure 21. The combination provides a band width of 26 to 38 Hz, accommodating a ± 20 percent variation in main rotor RPM.

Figures 22 through 25 present computer simulation results of the filter section. The input/output signal wave shapes at the nominal mid-band frequency of 32 Hz are plotted in Figure 21. The output signal is nearly sinusoidal and has approximately 1.2 percent third, or 12P with respect to the main rotor RPM, harmonic distortion. There is no second, or 8P, harmonic distortion since a square wave contains only odd harmonic multiples. Roughly a 100 degrees phase shift exists between the input and the output signals, Figure 22. Moreover, peak output amplitude is very nearly equal to peak input amplitude, Figure 22. Figures 23 and 24, respectively, depict the gain and the phase shift as a function of frequency. As frequency increases, filter gain varies from near unity to 0.8, while the phase varies almost linearly from 60 degrees to 140 degrees. The third harmonic distortion with frequency migrates from 2.4 percent at 26 Hz to less than 1 percent at 38 Hz, Figure 25. Thus, the reference signals are very nearly pure sinusoids. Since the phase shift and the amplitude gain exhibit known relationships with frequency, the computer can be programmed to compensate for these trends. The frequency converter section generates an analog signal proportional to rotor RPM so

that computer compensation is present over the entire helicopter RPM operational band.

3.1.5. FREQUENCY TO VOLTAGE CONVERTER

A commercially available frequency to voltage converter develops analog output signal directly proportional to rotor RPM. A typical frequency to voltage converter is schematically shown in Figure 26.

3.1.6. CORRELATOR SECTION

The correlator consists of a bandpass filter, which is identical in design to the reference generator filter, two multipliers and two integrators, Figure 27. By using this filter in the vibration signal path, the phase shift between the square wave reference signal and the sinusoidal reference signal is equal to the phase shift in the feedback transducer signal. Therefore, when the 4P vibration component is multiplied by the sine and by the cosine reference signals, the effect of the filter generated phase shift is nullified. Specifically, let the 4P sine reference with Butterworth filter phase shift be represented by

$$e_s = E_s \sin(4\Omega t + \phi) \quad (\text{IV-1})$$

Similarly, let the 4P component of the vertical acceleration be written as

$$e_v = E_v \sin(4\Omega t + \alpha) \quad (\text{IV-2})$$

where α is an arbitrary phase. Butterworth filtering of e_v induces an amplitude gain K and a phase shift .

$$e'_v = KE_v \sin(4\Omega t + \phi + \alpha) \quad (\text{IV-3})$$

Multiplying (IV-1) by (IV-3), and invoking trigonometric identities yields

$$e_s \cdot e'_v = \frac{KE_s E_v}{2} [\cos(\alpha) - \cos(8\Omega t + 2\phi + \alpha)] \quad (\text{IV-4})$$

By integrating the multiplier output, the double frequency, or 8P term, is removed while the DC term is passed. Optimal solution update rates are achieved with correlator integration time constants approaching 1/1P, or around 125 milliseconds.

3.1.7. ACTUATOR DRIVER SECTION

One actuator driver consists of two multipliers, a summing junction and an output current, Figure 28. The function of the actuator drivers is as follows.

1. The ECU converts the optimal 4P feathering to gain and phase, K and ϕ .
2. Two DC signals are generated by the ECU for each actuator driver.

$$DC_1 = \frac{E_v K_1}{E_s} \cos(\beta_1 - \phi) \quad (IV-5)$$

$$DC_2 = \frac{E_v K_1}{E_c} \sin(\beta_1 - \phi) \quad (IV-6)$$

3. The actuator driver multiplies DC_1 by the sine reference and DC_2 is multiplied by the cosine reference. The results are summed to yield

$$DC_1 \cdot e_s + DC_2 \cdot e_c = E_v K_1 \sin(4\Omega t + \beta_1) \quad (IV-7)$$

In this manner, the computer generated optimal 4P feathering is converted into an appropriate sinusoidal driving current for each actuator.

3.1.8. ACTUATOR LVDT DEMODULATOR

The LVDT demodulators, Figure 29, are required for position feedback information.

3.1.9. ECU FAILURE INDICATORS

Eight magnetic failure indicators are mounted on the ECU box and they are labelled with the following nomenclature.

1. 4P Ref Fail
2. Hardover
3. Hydro Fail
4. Comp Fail
5. ECU Set Fail
6. Discs
7. Power Supply
8. 15 KC Ref Fail

The switches, being magnetic, retain their current state under loss of system power, thereby recording the failure mode(s). As installed, white signifies normal and black signifies a self-test malfunction. These indicators are intended for post flight troubleshooting, and not for pilot reference.

3.1.10. ECU POWER SUPPLY

The ECU power is obtained from the 28 DC volts ship power via an 18 gage wire connected to a junction box on the data acquisition system. The ECU peak power requirement is approximately 3 AMPS.

Five wiring harnesses make the following connections.

1. ECU to feedback accelerometers underneath pilot's seat.
2. ECU to magnetic interrupts, which are mounted on the non-rotating swashplate to generate a 4P reference.
3. ECU to hydraulic shut-off valve.
4. ECU to low pressure switch on the manifold.
5. ECU to the HHC servo-valves and the differential pressure transducers.
6. ECU to the control panel and the pilot stick switch.
7. ECU to the flight computer.

3.1.11. ECU SELF TEST FUNCTION

The ECU monitors the system for many different internal failures, Figure 30. The malfunctions, along with the system and the operator response, are described in Section IV.E.3.

3.2. MICROCOMPUTER HARDWARE

Although an analog approach offers advantages in size, weight, reliability and speed, a digital processor excels in flexibility, programming ease and array handling abilities.

The computer hardware utilized for this purpose is a Sperry Flight Systems Multiplex Remote Terminal Unit (MRTU) Type IIIA, pictured in Figure 31. The MRTU is a mil-spec airborne processor currently in use on

the AH-64A Apache as a backup MIL-STD-1553A data bus controller. The MRTU is comprised of an SDP-175 16 bit processor using 2901 bit slice architecture, a 1553 bus interface and an extensive A/D, D/A and discrete I/O capability. The flight computer characteristics are summarized in Table 3. The data bus interface serves as a communication link between the A/D front-end and the random access memory (RAM) in the SDP-175. Using direct memory access (DMA), digitized data is placed in RAM and it is refreshed autonomously every 20 milliseconds. The servicing of the data bus interrupts and of the keep alive timing is controlled by an I/O executive routine which also calls the HHC algorithm.

4. INSTRUMENTATION

4.1. AIRBORNE DATA ACQUISITION SYSTEM

The HHC flight test data is obtained using the Airborne Data Acquisition System (ADAS), which is mounted to a flat plate above the cargo floor, Figure 32. The ADAS accepts up to 72 channels of analog, digital and audio signals, although HHC flight tests utilized only 52 channels. It also conditions the data for recording and real time telemetering to a ground station. One hour of continuous inflight data can be recorded on the airborne analog tape. With this system, the data can range from DC to 2000 Hz signals. The ADAS provides standard pulse code modulation (PCM) for frequencies up to 250 Hz, and it provides high response PCM for frequencies up to 2000 Hz. The airborne PCM telemetry link is accomplished with a 5 watt transmitter and one L-band antenna, yielding over 75 statute miles of a direct line of sight coherent signal range. The electrical requirements of the ADAS are 28 volts DC for proper operation. A button type circuit breaker located on the main power bus

provides 50 AMP protection for a peak current of approximately 27 AMPs when recording data. Conveniently, the ADAS electrical requirements are satisfied by the existing aircraft generator.

4.2. MEASUREMENT LOCATIONS

To analyze the aircraft response, numerous instruments are installed for data collection. Aside from the necessary accelerometers, the majority of the readings are for rotor and fuselage loads. Furthermore, several performance indicators are tracked, and general flight data is recorded. The master instrumentation list is presented in Table 4.

On the main rotor, an MDHC standard instrumented blade is employed to measure, flapwise bending, chordwise bending and torsion moments. Other measurements include the blade feathering angle, pitch link loads and the actuator LVDT positions.

On the fuselage, both load and vibration sensors are installed. Two groups of triaxial accelerometers are located underneath the pilot seat. One set only measures the cockpit vibration levels, while the other is used as feedback signals to the ECU. The feedback set is comprised of three Sunstrand Model 2180 Mini-Pal accelerometers which have a flat frequency response to 50 HZ. After a proximity indicator determines the force balanced pendulum displacement, an error signal then supplies current to a torque coil, which restores the pendulum equilibrium. The coil current becomes the measure of vibrations. In addition to the cockpit, the aircraft c.g. vibrations are monitored by a third group of accelerometers. As for fuselage loads, several instruments are used. The tail boom has strain gauges bridges, at stations 211 and 270, which monitor the vertical bending, lateral bending, and torsional moments.

Also, the main rotor mast is instrumented to record lateral and longitudinal bending moments.

The test aircraft is further equipped to monitor basic performance data. To measure main rotor RPM, the stationary swashplate is equipped with a magnetic coil which is energized by a rotating ferrous probe. In addition, the main rotor shaft has a torsional strain gauge bridge which monitors the shaft torque. An engine torque pressure transducer determines the engine output power. Between these sensors, the power required can be compared with the power available, yielding an overall indicator of the helicopter performance.

Finally, some overall flight parameters are recorded. Airspeed, angle of attack, sideslip angle, and pitch, roll and yaw rates are all sensed so that the exact flight conditions are known. The cyclic collective and directional controls are instrumented with potentiometers to determine their respective positions.

D. WEIGHT AND POWER REQUIREMENTS

The HHC system weight accounts for the added components and changes due to the stiffened flight controls. The primary hydraulic boost system weight is not included in the total, since it is considered part of the basic aircraft configuration. The last actual weighing of the helicopter with the HHC components and flight test instrumentation installed was August 28, 1984. The aircraft basic weight was 1904.8 lbs., with the horizontal center of gravity at 106.1 inches.

The HHC system total weight was 158.2 lbs. The individual contributions to this total are listed in Table 5. The flight test instrumentation, listed in Table 6, weighed 290.0 lbs. Therefore, the OH-6A basic weight was increased 348.2 lbs. for the HHC test program.

The HHC hydraulic pump can absorb 20 horsepower. However, the flight tests show power consumption to be 3 to 4 horsepower. If a conservative estimate of one horsepower is allowed for the electrical power requirements, the total power absorbed is typically 5 horsepower. As proven with the above data, the HHC system requirements fall within the OH-6A limits.

E. FLIGHT OPERATION AND SAFETY FEATURES

1. OPEN LOOP OPERATION

1.1 MANUAL CONTROLLER DESCRIPTION

For the first portion of the program, the manual, or open loop, controller was used to verify the system operation and to understand HHC input effects. In later flights, the open loop system was used to confirm system operation.

The controller permits selection of the 4P input magnitude and phase in the lateral, longitudinal and collective channels, Figures 33 and 34. By turning the toggle switch, the requested input channel is enabled. The gain knob is set to the desired value, where 0 to 100% gain corresponds to 0.0 to ± 0.10 inches of actuator stroke. By using Table 7, the total blade feathering angle can be determined for any actuator input. The command phase is set from 0 to 360 degrees, with respect to the cosine signal.

The controller outputs are DC voltages which the ECU converts to 32 Hz actuator servovalve current. The gain and the phase signal generation for one channel is shown schematically in Figure 35. The phase input varies the relative amount of sine and cosine commands, whereas the gain setting adjusts both signals simultaneously.

The open loop controller contains three Simpson Model 1212 volt meters, which display the 4P component of the seat accelerations. With this visual vibration feedback, a crew member can optimize the system.

1.2 FLIGHT PROCEDURE

Flight operation of the open loop controller follows.

1.2.1 PRE TAKE-OFF PROCEDURE

1. Start engine per normal procedures.
2. Stabilize idle at 62 - 65% N1.
3. Generator switch - ON.
4. Flight control hydraulic pump switch - ON (Low pressure light - OUT).
5. Cyclic stick bypass switch - ON (up).
6. Inverter switch - 1 or 1 and 2.
7. Increase N2 to 101%.

1.2.2 HHC SYSTEM ENGAGEMENT

1. ECU yellow caution light - Verify extinguished.
2. HHC panel switch - ENABLE.
3. HHC cyclic switch - FORWARD HOLD.
4. HHC caution lights - OUT.
5. HHC cyclic switch - RELEASE.
6. Open loop controller toggle switch - ON for desired channel.
7. Open loop controller gain knob - SET to desired value.
8. Open loop controller phase knob - SET to desired value.

1.2.3 HHC SYSTEM SHUTDOWN -- NON-EMERGENCY DISENGAGEMENT

1. Open loop controller phase knob - DECREASE to zero setting for desired channel.
2. Open loop controller gain knob - DECREASE to zero setting for desired channel.
3. Open loop controller toggle switch - OFF for desired channel.

1.2.4 POST LANDING PROCEDURE

1. Hydraulic bypass switch - OFF (down).
2. Hydraulic pump - OFF.
3. HHC panel switch - DISABLE.

4. Shutdown engine per normal procedures.

2. CLOSED LOOP OPERATION

2.1 GENERAL DESCRIPTION

Later in the HHC program, a closed loop system was installed on the OH-6A aircraft. In this configuration, no operator intervention is necessary; the flight computer determines the actuator gain and phase. The ECU conditions the pilot seat vibration signals and sends the DC voltages to the computer. With the 4P sine and cosine inputs, the algorithm calculates the optimal feathering angle required. The complete mathematical description is presented in Section V.A. A cockpit control panel was provided for the crew in order to regulate the system, Figure 36. Aside from the enable/disable switch, a reset button is available to restart the computer program. However, with this function no new system initialization occurs the software parameters are frozen at their previous values. Only the enable/disable switch affects the transfer matrix and the baseline vibration vector calibration.

Finally, the control panel has three rotary potentiometers, or gain pots, which allow modification of certain computational parameters. Originally, the gain pots were intended to enhance the vibration reduction in one direction by changing the vibration weighting factors in the optimal controller cost function. More recently, the gain pots fine tune the Kalman filter by adjusting the process noise and the measurement noise factors. Also, for the latest software, the time delay between HHC updates is determined by the third gain pot. These setting values are shown graphically in Figures 37, 38 and 39.

2.2. FLIGHT PROCEDURE

Flight operation of the closed loop controller follows.

2.2.1 PRE TAKE-OFF PROCEDURE

1. Start engine per normal procedures.
2. Stabilize idle at 62 - 65% N1.
3. Generator switch - ON.
4. Flight control hydraulic pump switch - ON (Low pressure light - OUT).
5. Cyclic stick bypass switch - ON (up).
6. Inverter switch - 1 or 1 and 2.
7. Increase N2 to 101%.

2.2.2 HHC SYSTEM ENGAGEMENT

1. ECU yellow caution light - Verify extinguished.
2. Gain pots - SET as desired.
3. HHC panel switch - ENABLE.
4. HHC cyclic switch - FORWARD HOLD.
5. HHC caution lights - OUT.
6. HHC cyclic switch - RELEASE.
7. Aircraft response - Autocal for approximately six seconds, followed by closed loop operation.

2.2.3 HHC SYSTEM SHUTDOWN -- NON EMERGENCY DISENGAGEMENT

1. Reverse of HHC System Engagement.

2.2.4 POST LANDING PROCEDURE

1. Hydraulic bypass switch - OFF (down).
2. Hydraulic pump - OFF.
3. HHC panel switch - DISABLE.
4. Shutdown engine per normal procedures.

3. SAFETY FEATURES OF THE HHC SYSTEM

3.1 GENERAL DISENGAGEMENT

HHC servo actuator motion is inhibited either by disabling the servo valve drive current or by shutting off hydraulic power to the actuators. Aside from manual initiation by the pilot cyclic stick switch or by the panel toggle switch, the electronic control unit will disengage the system if any self test function has failed.

The 3-position, spring-loaded-to-center cyclic stick switch provides pilot on/off control of the ECU, which can be engaged after rotor RPM has reached 100%. The ECU self-test shutdowns are inhibited by

holding the switch forward. The normal engagement procedure is to push the switch forward until all of the HHC panel caution lights are extinguished, then the switch may be released. The HHC system is normally disconnected by moving the switch to the aft position and then releasing. This action disables the servo-valve drive current and the hydraulics, while commanding the computer to resume initialization and to wait looping.

The panel toggle switch allows the pilot to shut down the hydraulic system independently of the ECU.

3.2 SELF-TEST CAUTION LIGHTS

The ECU design incorporates extensive self test features to prevent propagation of spurious command signals. For single channel systems using in-line monitoring, the generally accepted failure rate is 0.001/flight hour. Thus, hardover signals are within the realm of possibility for this test program. For the actuator built-in authority, however, the test pilot indicated that the aircraft reactions would not pose a controllability problem.

Four panel caution lights inform the pilot of ECU self-test shutdown of the system. The lights are:

1. ECU caution
2. Cmptr caution
3. Hydro caution
4. Disc caution

3.2.1 ECU Caution Light

The electronic control unit (ECU) caution light is illuminated when the self-test detects any one of the following failures.

1. Loss of drive mounted commutator reference pulse.
2. Loss of rotor RPM or rotor RPM signal.
3. Loss of keep-alive signal from the computer.
4. Loss of sine/cosine reference.
5. Loss of servo command comparison.
6. Loss of valve current rate comparison.

7. Loss of power supply.
8. Loss of linear LVDT.

All eight failure modes above disable the servo-valve drive current.

In addition, the last four modes, those generally associated with a hardover, lead to disabling hydraulics. Due to flight safety threat from hardovers, the pilot should not attempt to restart an ECU failure condition.

If the ECU yellow caution light is ON, then:

- HHC cyclic stick switch - AFT
- HHC panel toggle - DISABLE

3.2.2 CMPTR CAUTION LIGHT

The compute fail caution light (CMPTR) indicates:

1. Loss of digital versus analog drive comparison.
2. Loss of keep-alive signal.

Both failure modes lead to disabling of the servo drive current.

If CMPTR yellow caution light is ON, then:

- A restart may be attempted by advancing the HHC cyclic stick switch until all caution lights have cleared.
- Otherwise,
- HHC cyclic stick switch - AFT
 - HHC panel toggle - DISABLE

3.2.3 HYDRO CAUTION LIGHT

If manifold/reservoir pressure drops below 2450 psi, the hydro fail caution (HYDRO) light is lit. This failure mode has no direct effect on the ECU drive signal. However, once hydraulic pressure falls, the servo command will not compare with the LVDT output and an ECU fail caution will result, leading to shutdown of the servo drive current.

If Hydro yellow caution light is ON, then:

- A restart may be attempted by advancing the HHC cyclic stick switch until all caution lights have cleared.
- Otherwise,
- HHC cyclic stick switch - AFT
 - HHC panel toggle - DISABLE

3.2.4 DISC CAUTION LIGHT

The disconnect caution light (DISC) will illuminate if the cyclic switch is cycled OFF, if hydraulic pressure is lost at the manifold/reservoir or if any other caution light is illuminated or was momentarily illuminated.

If Disc caution light is ON then:

- A restart may be attempted by advancing the HHC cyclic stick switch until all caution lights have cleared.

Otherwise,

- HHC cyclic stick switch - AFT
- HHC panel toggle - DISABLE

3.3 ECU AND PANEL ASSEMBLY CIRCUIT BREAKER

The circuit breaker protects the control panel and the electronics of the HHC system. Spurious signals, leading to servo oscillations and/or hardovers, may be generated by resetting the system with the panel-mounted 5 Amp breaker.

3.4 MALFUNCTIONS NOT DETECTED OR CONTROLLED BY THE SELF-TEST

Given the limited reliability of single channel in-line monitored systems, the following failure modes are conceivable:

1. Servo-actuator hardover
2. Uncontrolled servo-actuator oscillations
3. Hydraulic leaks
4. Jammed Controls

3.4.1 SERVO-ACTUATOR HARDOVER

An HHC actuator hardover will produce a sudden, but limited authority, trim change in any or all of the main rotor control axes.

If sensed, then:

- Cyclic stick switch - AFT
- HHC panel toggle - DISABLE

3.4.2 UNCONTROLLED SERVO-ACTUATOR OSCILLATIONS

If uncontrolled oscillations are sensed, then:

- Cyclic stick switch - AFT
- HHC panel toggle - DISABLE

3.4.3 HYDRAULIC LEAKS

If hydraulic leaks are detected, then:

- Cyclic stick switch - AFT
- HHC panel toggle - DISABLE

An immediate landing is recommended due to the possibility of fire.

3.4.4 JAMMED CONTROLS

Excessive control forces experienced during flight may indicate frozen bearings and/or control system interferences. Caution must be exercised when attempting to free jammed controls using the boosted primary controls. The primary boost actuator force capability exceeds limit load levels for some components.

V. ALGORITHM AND SOFTWARE DEVELOPMENT

A. MATHEMATICAL DESCRIPTION OF THE HIGHER HARMONIC CONTROL ALGORITHM

1. INTRODUCTION

The HHC system is based on a real time, self adaptive controller. Using Kalman filtering, various parameters are estimated to identify a system model at each time step. The control inputs are based on an optimal control solution of the model. Through this approach, the algorithm operates without a priori knowledge of the system. As a beneficial result, this controller is readily transportable from one helicopter to another. It does not require extensive flight testing to develop control derivatives and control gains as functions of flight condition and aircraft configuration. A schematic of the controller operation is shown in Figure 40.

The selected control algorithm was derived from one of several developed by John A. Molusis [8] of the University of Connecticut, under sponsorship of the Army Structures Laboratory and NASA Langley Research Center. This "cautious controller," based on Eqs. (12) - (15) of Ref. 8 demonstrated superior performance during computer simulations and during wind tunnel testing, Hammond [10]. The caution terms preclude large changes in the control inputs from one iteration to the next. In addition, the controller operates smoothly during changing test conditions.

We assume the HHC system is described as follows.

$$\underline{z} = \underline{z}_0 + T \Theta \quad (V-1)$$

where \underline{z} = 6x1 vector of measured vibrations (g's).
 \underline{z}_0 = 6x1 vector of baseline vibrations (g's).
 T = 6x6 transfer matrix relating actuator controls to vibration changes (g's/inch or g's/decavolt;

Conversion: 1 inch = 0.05 volts).
 $\underline{\theta} = 6 \times 1$ vector of actuator controls (decavolt).

The overall HHC objective is to reduce the helicopter vibrations, \underline{z} . First, estimates of \underline{z}_0 and T , denoted $\hat{\underline{z}}_0$ and \hat{T} respectively, are calculated and then controls, $\underline{\theta}$, are computed. Below, the optimal control routines, the Kalman filtering techniques and the initial estimation of $\hat{\underline{z}}_0$ and \hat{T} are described.

2. OPTIMAL CONTROLLER SEQUENCE

The HHC system employs a cautious minimum variance controller for computing the optimal control inputs. The penalty function to consider is

$$J = E [\underline{z}^T W_z \underline{z} + \underline{\theta}^T W_\theta \underline{\theta}] \quad (V-2)$$

where $E[\dots]$ = expected value.
 $W_z = 6 \times 6$ diagonal vibration weighting matrix.
 $W_\theta = 6 \times 6$ diagonal control weighting matrix.

Partitioning the system equation (V-1) by rows,

$$\underline{z}_j = \hat{\underline{z}}_{0j} + \hat{T}_j \underline{\theta} \quad (V-3)$$

where $j =$ the j -th row

and substituting into equation (V-2), the penalty function becomes

$$J = E [\sum_{j=1}^6 W_{z_{jj}} (\hat{\underline{z}}_{0j} + \hat{T}_j \underline{\theta})^2 + \underline{\theta}^T W_\theta \underline{\theta}] \quad (V-4)$$

Computing the expected value of equation (V-4), and then equating the partial derivatives $\frac{\partial J}{\partial \underline{\theta}}$ to zero, the optimal controls, $\underline{\theta}^*$, are

$$\underline{\theta}^* = -(\hat{T}^T W_z \hat{T} + W_\theta + \sum_{j=1}^6 W_{z_{jj}} P_{\hat{f}})^{-1} (\hat{T}^T W_z \hat{\underline{z}}_0 + \sum_{j=1}^6 W_{z_{jj}} P_{\hat{z}_0}^T) \quad (V-5)$$

where $P_{\hat{f}}$ = the covariance matrix for \hat{T} , calculated by Kalman filtering techniques.

$P_{\hat{z}_0}$ = the covariance matrix for \hat{z}_0 , calculated by the Kalman filtering techniques.

To complete the HHC loop, Kalman filtering updates estimates of both \hat{z}_0 and \hat{T} .

3. KALMAN FILTERING

The Kalman filter routine provides real time identification of the system transfer matrix, \hat{T} , and the baseline vibrations, \hat{z}_0 , and it recomputes both covariance matrices, $P_{\hat{T}}$ and $P_{\hat{z}_0}$. Properly implemented, the Kalman filter reduces the uncertainty in the system model.

First of all, the system is redefined for the i-th and the i+1-th interval.

$$\underline{z}_{i+1} = \underline{\Theta}^T \hat{T}^T + \underline{z}_i \quad (V-6)$$

Now, a new state variable, \underline{h} , is defined such that

$$\underline{h}_{j\hat{i}} = (\tau_j^T | \underline{z}_{0j})_{\hat{i}}^T \quad (V-7)$$

where \underline{z}_{0j} = the j-th element of the response vibrations at the i-th iteration.
 τ_j = the j-th column of T at the i-th iteration.

Rewriting equation (V-6) using the new state variable, we obtain

$$\underline{z}_{i+1} = (\underline{\Theta}^T | 1) \underline{h}_{\hat{i}} \quad (V-8)$$

Letting

$$\underline{x} = (\underline{\Theta}^T | 1) \quad (V-9)$$

the state equation may be written as

$$\underline{z}_{i+1} = \underline{x}_i \underline{h} + \underline{\eta} \quad (V-10)$$

where $\underline{\eta}$ = zero mean white gaussian measurement noise.

To solve equation (V-10), the state vector, \underline{h} , must be tracked for each iteration which is represented by

$$\underline{h}_{j,i+1} = \underline{h}_{j,i} + \underline{w}_{j,i} \quad j = 1, 2, \dots, 6 \quad (V-11)$$

where \underline{w}_j = a discrete white random noise sequence.
 \underline{h}_j = j-th column of the state variable.

The \underline{w} vector is the system state time variation due to changes in flight condition, gross weight, etc. This quantity is labelled the state process noise.

Equations (V-10) and (V-11) present a well defined filtering problem. The solution, including the covariance matrix update, is given below.

$$\underline{K}_{i+1} = \underline{P}_i \underline{x}_i^T (R + \underline{x}_i \underline{P}_i \underline{x}_i^T)^{-1} \quad (V-12)$$

$$\underline{P}_{i+1} = (\underline{I} - \underline{K}_{i+1} \underline{x}_i) \underline{P}_i + \underline{Q} \quad (V-13)$$

$$\underline{h}_{j,i+1} = \underline{h}_{j,i} + \underline{K}_{i+1} (\underline{z}_{j,i+1} - \underline{x}_i \underline{h}_{j,i}) \quad (V-14)$$

where \underline{I} = the identity matrix.
 \underline{P} = i-th estimate of the state covariance matrix.
 \underline{Q} = process noise covariance matrix.
 \underline{R} = measurement noise covariance matrix.

The system covariance matrix, \underline{P} , is a combination of the baseline vibration covariance, $\underline{P}_{\underline{\hat{x}}_0}$, and of the transfer matrix covariance, $\underline{P}_{\underline{\hat{r}}}$. Referring to the optimal controller expression, equation (V-5), the following definitions hold.

$P_{\hat{z}_0}$ = the upper left diagonal element of the P matrix.
 $P_{\hat{f}}$ = the lower right 36 elements of the P matrix composing a 6 x 6 matrix.

Initially, the off diagonal elements of P are all zero.

The measurement noise covariance, R, is actually a scalar. if \underline{x} were to be expanded to a diagonal matrix, R would also be a matrix. This would permit distinguishing between the noise values for each measurement.

Overall, the filter accuracy would improve, however, the coding difficulty and computational time would also increase.

Equations (V-12), (V-13) and (V-14) are a complete system for tracking the state variable, \underline{h} . Once the state is calculated, the new baseline vibrations, the transfer matrix and the covariance matrix, $\hat{\underline{z}}_0$, \hat{T} and P respectively, are substituted in the controller routine, equation (V-5).

3. THE AUTOCAL PROCESS

Before any closed loop optimization can occur, initial values of the baseline vibration vector and the transfer matrix, \underline{z}_0 and T respectively, must be determined. The estimates will be denoted $\hat{\underline{z}}_0$ and \hat{T} . The autocalibration procedure chosen for flight test implementation, shown schematically in Figure 41, consists of the following steps.

Step 1: With zero controls, measure the baseline vibrations, \underline{z}_0 .

Step 2: Probe the system with a known unit control vector,

$$\underline{\theta}_1^T = (1, 0, 0, 0, 0, 0) \quad (V-15)$$

and measure the resulting system vibrations, \underline{z} .

Now,

$$T \underline{\Theta}_1 = \underline{z} - \hat{\underline{z}}_0 \quad (V-16)$$

Multiplying T by $\underline{\Theta}_1$, the first column of the matrix is obtained, since both \underline{z} and $\hat{\underline{z}}_0$ are known.

Steps 3 - 7: Repeat step 2, except probing with a different unit vector. In other words,

$$\begin{aligned} \underline{\Theta}_2^T &= (0, 1, 0, 0, 0, 0) \\ \underline{\Theta}_3^T &= (0, 0, 1, 0, 0, 0) \\ &\vdots \\ \underline{\Theta}_6^T &= (0, 0, 0, 0, 0, 1) \end{aligned} \quad (V-17)$$

This yields the transfer matrix estimate, column by column. With $\hat{\underline{z}}_0$ and \hat{T} initialized, the HHC closed loop operation may begin.

The actual autocal procedure differs somewhat from the description above. Instead of unit control vectors, a one-eighth full scale pulse is used, where full scale is 10 decavolts. The reduced amplitude prevents hardovers of the actuators or drastic vibration increases during autocal. In reality, equations (V-15) and (V-16) are rewritten as

$$\underline{\Theta}_1^T = \left(\frac{1}{8}, 0, 0, 0, 0, 0 \right) \quad (V-18)$$

and

$$\hat{T}_{ACTUAL} \underline{\theta}^T = \theta (\underline{z} - \hat{\underline{z}}_0) \quad (V-19)$$

Finally, the control probes are not instantaneous. For non-averaging software, versions B36, B35 and earlier, the unit pulses last one second to allow the system to reach steady state prior to measuring. The settle down time is estimated to be approximately one second, however, this value has not been thoroughly investigated. For the averaging software, versions B55, B56 and B37, the pulse is approximately 1.3 seconds to enable additional data collection.

B. LABORATORY ROLE IN SOFTWARE DEVELOPMENT

1. PURPOSE OF THE SIMULATION LABORATORY

The higher harmonic control simulation laboratory (Sim Lab), Figure 42, has an integral function in the project development. Through proper applications, the sim lab investigates different hypotheses, and thereby reduces the need for costly flight tests. The sim lab develops and tests all of the flying HHC software. More recently, the lab also performs post flight data analysis.

"Stand alone" modelling programs are used to develop algorithms. These simulations can be performed on any digital computer. Even with a simple model of the helicopter dynamics which cannot reproduce the flight data faithfully, these simulations are an excellent software development tool. Different algorithms and their implementation can be compared, and the stand alone simulations can model various computational effects. The programs can analyze the effects of different arithmetic precision or even

the effects of varying word lengths. The precision sensitive portions of the algorithm can be determined.

Any simulation project must contain a closed loop check out phase which includes the flight computer and software in a real time environment. If the results of previous stand alone runs can be reproduced, the new flying proms are probably bug free. This step does not guarantee no software errors, but it does greatly reduce their probability.

The sim lab demonstrates the need for a more accurate helicopter model. With proper simulation during software development, the project cost is reduced during the flight test phase. Ideally, the simulation program should include a more realistic rotor-fuselage dynamic analysis.

2. DESCRIPTION OF THE SIMULATION LABORATORY HARDWARE

The HHC sim lab has been continuously expanded and upgraded during the project. The present status is depicted in Figure 43. A description of the components is given below.

The Andromeda/DEC PDP-11/B, operating under an RT-11 system, is the primary computer. Aside from a 20 megabyte hard disk, the Andromeda contains one double density single sided floppy drive and two single density single sided floppy drives. This computer supports 9 channels each of digital to analog and of analog to digital converters, which are used when communicating with the flight computer. The Andromeda employs an ADM 3A monitor and a Teletype Model 40 line printer. With this system, various algorithms can be developed and tested. In addition, the Andromeda simulates a simple model of the helicopter dynamics. The PDP-11/B characteristics are summarized in Table 3.

The Sperry SDP-175 flight computer and its software development station is another major hardware component of the laboratory. The flight software is coded and verified with this equipment. The development station is based upon the Intel MDS 8080 computer. This computer supports both a line printer and a monitor, and it can create assembly language programs for the SDP-175. Once a program is debugged, the software is transferred to the SDP-175, first by using the Sperry Memory Simulator, and later by physically installing the 4K proms on which the algorithm is burned into the flight computer memory board. The Andromeda then executes the helicopter model which tests the flight software. As long as no divergence occurs, the proms are then considered for flight.

An IBM personal computer is being interfaced into the simulation laboratory to handle output processing. The output can then be presented in concise graphical form on the Houston Instruments plotter.

3. DESCRIPTION OF THE AVAILABLE SOFTWARE

Three main FORTRAN programs are used for software development. HHCSIM is a "stand alone" simulation; it executes only within the Andromeda environment. HDRIVR controls the closed loop testing, which involves actual flying software. Finally, the third program, MXAUTO, processes flight data. This software is described in detail in the next three sections.

3.1. STAND ALONE SIMULATION - HHCSIM

HHCSIM, as the main program module is termed, is a laboratory tool which compares the results of various higher harmonic control algorithms. This code models both the HHC active control system and in a simple fashion the helicopter vibratory response. This software does not faithfully

reproduce actual flight data. Instead, in the early stages, HHCSIM determines whether a particular algorithm will converge. Convergence is defined as the reduction of vibration below baseline values with the abatement maintained for long runs. In later phases, HHCSIM compares alternative algorithms or various initial values. Different system parameters can have a significant impact on HHC performance. Applied properly, HHCSIM reveals the general tendencies and the relative merits of different options.

3.2 CLOSED LOOP SIMULATION - HDRIVR

The HDRIVR code controls the closed loop simulation which tests actual flying software. HDRIVR sends vibration levels to the flight computer and then reads the calculated HHC control inputs. In this fashion, an algorithm can be thoroughly tested before installation on the aircraft. HDRIVR only controls the flow of information between the flight computer and the Andromeda. No new algorithms are developed through this program.

The dynamic modelling of the helicopter in HDRIVR and HHCSIM, is based on a simple model. The helicopter vibration levels are calculated as random noise added to the baseline levels. Both the transfer matrix and the vibration levels randomly walk from their current values if a maneuver is simulated. However, since the sim lab purpose is to develop and to compare different flying algorithms, this model has proven adequate. General vibration trends are exposed although true vibration levels are not predicted. If true vibration levels are desired, then the sim lab code must be incorporated with a realistic coupled rotor and fuselage dynamics program.

3.3. AUTOCAL ANALYSIS - MXAUTO

MXAUTO is an utility program originally written to calculate a few HHC system transfer matrices from flight data recorded during the autocal procedures. At first, the intention was merely to use the resulting transfer matrices for more realistic Andromeda simulations. Later, the code was modified to investigate numerous other areas. For example, as the data base of matrices grows, MXAUTO allows more insight into the considerable controls coupling, which results in near singular, or ill-conditioned, matrices. The program, in conjunction with special flight software, can also evaluate the linearity of the HHC apparatus. Finally, the program uses a statistical analysis code to compute estimates of the measurement noise.

Aside from evaluating the autocal process, the MXAUTO code also analyzes the raw vibration data. Statistical analysis must compensate for the measurement noise since no filtering techniques exist in the autocal routine. Assuming a gaussian white noise, averaging with a check of the standard deviations reduces the sampling error.

For the raw data point collections, the standard deviation of the sample is calculated below.

$$\sigma_{SAMPLE}^2 = \frac{\sum [(z_i)^2 - (\frac{\bar{z}}{\sqrt{N}})^2]}{N-1} \quad (V-20)$$

where σ_{SAMPLE} = standard deviation of the sample.
 z_i = i-th measurement of the vibration.
 \bar{z} = mean of vibration measurements.
 N = sample size.

Moreover, the standard deviation of the means is shown below.

$$\bar{\sigma}_z^2 = \frac{\sigma_{SAMPLE}^2}{N} \quad (V-21)$$

where $\bar{\sigma}_z$ = standard deviation of the mean.

The standard deviation of the mean, equation (V-21), compares the spread of individual means. The standard deviation of the sample, equation (V-20), indicates the data point distribution of one sample.

Finally, the standard deviation of the transfer matrix elements, given below, is derived from the standard deviations of the means, equation (V-21).

$$\sigma_{t_{i,j}} = 8 (\bar{\sigma}_{z_i}^2 + \bar{\sigma}_{z_{0i}}^2)^{1/2} \quad (V-22)$$

where $\sigma_{t_{i,j}}$ = the standard deviation of the i,j-th element of the transfer matrix.
 $\bar{\sigma}_{z_i}$ = the standard deviation of the mean for the i - th element of z.
 $\bar{\sigma}_{z_{0i}}$ = the standard deviation of the mean for the baseline vibrations, z_0 .

The factor of 8 is a scaling parameter; see Section V.A.4.

By computing the norm of $\bar{\sigma}_z$, the measurement noise is estimated. With these routines, MXAUTO yields a measure of the data integrity. These results increase the qualitative understanding of the HHC system.

4. CONCLUSIONS DRAWN FROM THE SIMULATION LABORATORY

The sim lab is a valuable tool in the development of flight software. Some of the problems that were revealed and resolved by exercising the sim lab are described below.

First of all, any simulation run must extend over several hundred frames. Glitches and spikes sometimes occur after a long period of apparent convergence. For example, different initial values for the covariance matrix can have drastically different effects on convergence. The values $P_{i,j} =$

5.0 ($i = j$) and $P_{L,j} = 0$ ($i \neq j$) were selected after extensive testing. Although not necessarily an optimum, these values yield successful results. Moreover, almost any system value improperly chosen may lead to divergence. The sim lab can indicate which parameters are sensitive to divergence and aid in development of safe and effective software.

Many new insights become available as the simulation laboratory increases its post processing capabilities. Through the statistical analysis contained in MXAUTO, parameters previously estimated are determined from actual flight data. For example, the measurement noise in the Kalman filtering routines is calculated via MXAUTO. Currently, the measurement noise is in the range of 0.01 to 0.03. This allows for more realistic simulations and for better flying software.

Aside from the statistical analysis, MXAUTO has enabled the creation of a transfer matrix data base. As the number of available matrices increase, the data can be analyzed for any similarities or any patterns. If possible, the time consuming autocal process may be eliminated. By prestoring numerous matrices, the algorithm may select the proper transfer matrix as a function of flight condition. This sim lab application is an area of ongoing research at McDonnell Douglas Helicopters.

The HHC sim lab is constantly used to investigate new areas. MDHC is currently analyzing the HHC algorithm and the HHC flight data in order to fully develop this concept. The optimal time delay between HHC updates is tested. The applications of robust Kalman filtering and of ideal Kalman parameters are researched. By fine tuning the filter to the system, the overall performance should drastically increase. A major algorithm revision is being considered which should reduce the order of the system. By taking advantage of the closely coupled channels, i.e. the vertical and the lateral,

the overall vibration may still be reduced while increasing the condition of the transfer matrix.

VI. FLIGHT TEST PROGRAM

A. PROGRAM OVERVIEW

The HHC flight tests began on August 29, 1982, and were performed in two phases. First, the open loop HHC system was installed on the OH-6A. With the ability to independently vary gain and phase inputs, the manual controller allowed investigation of the HHC mechanics and it was used throughout the program as a benchmark to verify proper functioning of the HHC system.

During the second phase of flights, the closed loop, or computer controlled, system was tested. Various software versions were evaluated for their vibration reduction ability. The current HHC software has evolved over a long period of flight testing. Since early 1983 when the first software version (PROM3) flew, the algorithm implementation was constantly improved. Table 8 lists all software versions and gives a summary of their salient features.

The "PROM3" algorithm successfully reduced vibrations for steady state level flight. However, algorithm performance at high speeds and during maneuvers was not deemed satisfactory. After the HHC system was refurbished, the testing resumed in 1984. The first two attempts of improved algorithms, P3B30 and B34, both failed to reduce vibrations. These codes probably had improperly selected initial values for the covariance matrix diagonal elements.

The B35 prom performed well for level flight. The 4 per rev vibrations were substantially reduced at all speeds. Up to and including B35, the gain pots were programmed to allow tuning of the vibration weighting

matrix coefficients. To investigate the effects of the Kalman parameters, the next software version, B36, had provisions to tune the process noise covariance and the measurement noise covariance. This version produced the most successful results of the entire program. Not only were lower vibration levels maintained for level flight at all speeds, but the algorithm also reduced vibrations during maneuvers.

In an attempt to improve results in nonsteady flight conditions, version B55 was developed and flown. Although the level flight results were comparable with previous tests, the maneuver results diverged in various instances. Therefore, this version was less successful than B36.

Two software versions, B56 and B37, have been developed without undergoing flight tests. These versions have combined the vibration reduction performance of B36 with the improved autocal procedure of B55. Software B55 has an averaging autocal routine, whereas all previous software initialization was based upon one reading per unit control input. The averaging procedure should allow for a more consistent initialization procedure. However, without any flight test results for these codes, their performance is only speculation.

B. OPEN LOOP FLIGHT TEST PROGRAM

1. INTRODUCTION

The purpose of the open loop flight test program was to obtain a data base for subsequent closed loop HHC testing. The open loop level flight envelope consisted of recording HHC data at hover, 40, 50, 60, 70, 80, 90 and 100 knots. Because of the typical high summer ambient temperatures in Yuma, Arizona, when these flights were conducted, the OH-6A was flown with doors

off for the hover, 40 and 50 knot airspeed conditions and with doors on for airspeeds 60 knots and above. This helped to prevent overheating of either the electronic equipment in the aft compartment or the two hydraulic systems. In Figure 4, the aircraft doors off configuration is depicted. In addition level flight evaluation, the flight crew explored coordinated and wind-up turns, approaches, flares, accelerations and decelerations. For this phase of the program, data was taken during 15 hours of flying with the HHC system turned on and was backed up by 17 hours of ground testing with HHC engaged.

As noted earlier, the HHC manual controller can operate the 4P lateral cyclic, the 4P longitudinal cyclic, and the 4P collective either as individual commands or in any combination. For the flight test program, the inputs were tested independently at each airspeed. The HHC blade angle motion was set while a phase sweep was conducted in 30 degree increments. This test indicated the phase angle for maximum vibration reduction at that airspeed. For selected airspeeds, phase sweeps were performed at more than one HHC blade angle amplitude setting.

As designed and installed, the system had a maximum ± 2 degrees authority for collective blade angle movement. Preliminary tests showed that this was probably more blade angle authority than required. As a result, an electronic limit was established in the ECU which restricted maximum actuator stroke to roughly ± 0.10 inches. Most open loop flight data points were flown at about 50 percent of this amplitude, which, allowing for some lost motion between the actuators and the blades, yielded about ± 0.33 degree of collective blade angle motion.

2. VIBRATION RESULTS

Figures 44, 45, 46, 47 and 48 show open loop test results for lateral swashplate excitation equivalent to ± 0.33 degree of blade angle. Each plot represents an airspeed of 60, 70, 80, 90, and 100 knots respectively. Peak accelerations in g's as measured vertically and laterally by accelerometers mounted under the pilot's seat are plotted versus the 4P command phase. Note that the horizontal dashed lines indicate corresponding vertical and lateral baseline vibration levels with HHC off.

The five figures have certain characteristics in common, which will be discussed for 60 knots airspeed, Figure 44. A distinct change in vibration levels from baseline to HHC on is apparent at all phase angles. The zero phase condition is the first data point recorded during each run, followed by 30 degree increments to 360 degrees. Since a typical phase sweep test at a given airspeed takes ten to fifteen minutes to record, there is a corresponding time lapse between the 0 degree and 360 degree record. As one good indicator of the data fidelity and of the data scatter, the test points at zero degree phase should be compared with 360 degree phase. Ideally, they should be identical.

Referring again to Figure 44, the HHC system initially increases the aircraft vibrations, as phase is varied, reaching a maximum vertical vibration value of 0.38 g at a phase angle of 90 degrees. Referring to Figures 45, 46, 47 and 48, for 70, 80, 90 and 100 knots respectively, similar trends are noted. If the wrong phase angle is applied, HHC has the capability to significantly raise the vibration levels. For example, for 100 knots, a phase angle of about 150 degrees increases vertical levels from 0.37 g to 0.66 g, Figure 48. Therefore, a definite cause and effect relationship between HHC inputs and airframe vibration levels is established. Also note for 100 knots, the minimum vibration level occurs at 330 degree phase angle,

which is 180 degrees removed from the phase angle for which maximum vibration levels occur. The plots at the other airspeeds also follow this trend within approximately 30 degrees.

As shown for 60 knots, both vertical and lateral vibration levels reach their maximum and their minimum values at the same manual controller phase settings Figure 44. The maximum occurs at 90 degrees phase angle, while the minimum is at 300 degrees phase angle. Using only the lateral channel of the manual controller with an arbitrary blade angle input of ± 0.33 degree, vertical vibration levels are lowered from 0.25 g to 0.04 g and the lateral vibration levels are reduced from 0.12 g to 0.02 g. If further reduction is desired at this phase setting, the flight test engineer can change the amplitude gain setting.

One final point of interest is observed from the vibration data. For 60, 70 and 80 knots, Figures 44, 45 and 46, respectively, the maximum HHC induced vibration level remains essentially constant at about 0.40 g vertically and at 0.20 g laterally. However, at 90 knots, the maximum vertical level jumps to 0.51 g with the lateral increasing to 0.26 g, and likewise, levels at 100 knots continue to grow to 0.66 g vertically and 0.28 g laterally. At the higher airspeeds of 90 and 100 knots, the HHC induced vibrations are no longer attributed solely to main rotor forces. These higher levels are possibly due to vibratory wake impingement on the OH-6A empennage.

3. HHC EFFECT ON BLADE LOADS

The effect of HHC on the third, fourth and fifth harmonics of blade flapwise and chordwise bending moment is shown in Figures 49 and 50. The 70 knot level flight airspeed condition is presented with the manual controller

providing only lateral inputs. The most inboard blade strain gages are depicted with the flapwise gage at 15 percent blade radius and with the chordwise gage at 17 percent blade radius. Since the blade flapwise moment goes to zero at the offset hinge, the inboard bending gage is a direct indicator of 3P, of 4P and of 5P vertical shear at the hub. From the patterns shown, the chordwise bending bridge indicates the trend in rotating hub 3P, 4P and 5P inplane forces. However, the lead-lag damper which allows a chordwise moment at the blade root clouds this result.

Consider first Figure 49, where the effect of the HHC phase sweep on blade 3P, 4P and 5P flapwise moments near the root is plotted. The variation of all three blade bending moment harmonics follows the same trend as observed for pilot seat vibration levels. In other words, blade 3P, 4P and 5P flapwise bending moments, and corresponding blade root shears, are amplified in the first 180 degrees of phase sweep and they are attenuated from 180 to 360 degrees. For the data shown, the 3P values have a minimum at 270 degrees phase, the 4P at 330 degrees phase and the 5P at 240 degrees phase.

In Figure 50, the corresponding phase plots of blade chordwise bending are given. Using 300 degrees as the phase angle for minimum vibration, it is seen that the 3P and the 4P moment values are below the baseline level, while the 5P is above. However, the magnitude of the 4P component is the largest contributor at about twice the value of the 3P or 5P moments.

The third, fourth and fifth harmonics of blade torsion as a function of manual controller phase are plotted in Figure 51. Since HHC is driving the blade at 3P, 4P and 5P, it is not surprising to see that these components have increased above the corresponding baseline harmonics at most phase angles.

C. CLOSED LOOP FLIGHT TEST PROGRAM

1. INTRODUCTION

During the closed loop flight test program, the HHC controller performance is evaluated. Using fourth harmonic collective, lateral and longitudinal cyclic swashplate inputs, the HHC algorithm minimizes simultaneously the pilot seat 4P vertical, lateral, and longitudinal vibration levels. During these flights, baseline data and closed loop data was recorded for the following flight conditions: hover, 40 - 100 knot level flight in 10 knot increments, and various maneuvers.

To obtain the data, the aircraft is stabilized at the desired test condition. First, the baseline data is recorded. Then, after HHC is engaged and the system has settled, the closed loop data is taken. During the transient test condition, HHC is engaged and is allowed to stabilize prior to entering the maneuver. For example, during decelerations from 60 knots, HHC is engaged at 60 knots ten seconds before beginning the deceleration. For banked turns, the system is initialized and allowed to stabilize in level flight before entering the turn.

A typical engagement and controller operation is shown for 60 knots in Figure 52. The traces shown are the time histories of the three HHC actuator motions (LVDT) signals, and three of the six vibration components being minimized. The three vibration traces represent the fourth harmonic sine component of the longitudinal, the lateral and the vertical accelerations at the pilot's seat. The cosine components, not shown, represent the remaining three parameters which the controller reduces. In the figure, the time increases from right to left.

The initialization, or autocal, of HHC is seen in the actuator traces, where the trial inputs are readily apparent. Even though the actuators move at 4 cycles/revolution, these motions appear as a band on the traces because of the time scale. Due to the arrangement of the HHC actuators, all three actuators drive collective inputs, two actuators drive lateral inputs and only one is needed for longitudinal inputs, Figure 52 and Table 7.

Prior to flight test of the system, the initialization process was thought to be objectionable to the crews. Involving a rapid stepping through six different control inputs, autocal produces six different vibration levels. However, during flights, the crew hardly noticed the initialization, and thus, the process was satisfactory for continued use.

Once autocal is complete, the closed loop controller operation begins. Most evident from the longitudinal LVDT trace, the controller gradually increases the amplitude of the HHC inputs until the vibrations are minimized. Controller disengagement is readily apparent from the actuator traces. Interestingly, the vibration levels very quickly return to their baseline values once the system is off. The pilot commented that the effect of HHC is much more apparent at disengagement than at engagement due to the quick change in vibration levels. During engagement, the levels are reduced gradually, which is due to both the algorithm caution terms and to the controller update rate.

2. 1983 CLOSED LOOP VIBRATION RESULTS

In 1983, the first closed loop HHC flights were performed. With the early software version, PROM3, these tests proved the feasibility of HHC for vibration reduction. However, the system performance was degraded as speed increased. PROM3 results, detailed in Wood, et. al. [1], are summarized below.

In Figures 53, 54 and 55, the fourth harmonic of vertical, lateral and longitudinal pilot seat accelerations are plotted versus airspeed. All the points are for stabilized flight. As seen from these figures, HHC is successful in achieving significant vertical and lateral vibration reduction over the entire speed range. Longitudinal vibrations are reduced up to approximately 65 knots, but increases occur beyond this airspeed. Also, the vertical vibration reduction is not as dramatic at the higher airspeeds as at the lower airspeeds from Figure 53.

The blade higher harmonic feathering angles, corresponding to the data points shown in Figures 53, 54 and 55, are shown in Figure 56. The data is for the third, the fourth and the fifth harmonics since the feathering angle is measured in the rotating system. The HHC system applies only 4P motions to the stationary swashplate, which are converted into third, fourth and fifth harmonics in the rotating system. The feathering motions are predominantly 3P at 40 knots, but at 100 knots, an approximately equal mixture of third, fourth and fifth harmonics exists. In every case, all the HHC inputs are less than one-half degree.

In reference to the reduced effectiveness of HHC at the higher airspeeds, one might argue that the system reached the limit of its authority. Thus further reductions in vibration are not possible. Yet, the actuators never encountered the electronically set limits. The system is capable of almost two degrees of collective feathering angle, which is further restricted electronically to roughly $\pm 3/4$ degree of collective input. Since these bounds were not approached during flight, the authority argument is invalid.

Three other explanations come to mind concerning the behavior of the HHC system at the higher speeds. First of all, possible system nonlinearities may affect HHC results. Molusis [25] has shown through analytical simulation that system nonlinearity significantly influences the control algorithm. Nonlinearities in the vibration problem physics could cause the controller to achieve local minima as opposed to global minima. The controller performance under these conditions would be quite sensitive to its initialization. Unfortunately, the effect of actuator amplitude during initialization was never analyzed in flight tests.

As another possible cause, the relative strength of each input must be considered. The actuator motion time histories indicate predominantly longitudinal commands at the higher speeds, with only small amounts of lateral input. In contrast, the open loop results show lateral, not longitudinal, inputs to be most effective in achieving vibration reduction. Furthermore, the longitudinal control system is roughly only 50% as stiff as the lateral control system. One actuator drives in the longitudinal case, whereas two actuators drive in the lateral condition. All this indicates that the longitudinal system is less effective than the lateral system for vibration reduction. Yet, the controller persists in driving the longitudinal inputs, which may be due to equal control weighting in the algorithm. A series of tests were conducted with an updated software version, B35, to investigate this idea. Unlike earlier flights, these tests varied the vibration weighting via the three potentiometers on the HHC cockpit control panel. The varying of these matrix coefficients did not affect the vibration levels.

Finally, as the third explanation for high speed degradation, the Kalman filter must be considered. If improperly tuned, the filter will not correctly track a dynamic system. Basically, the measurement and the process noise parameters, denoted R and Q respectively in the Kalman equations, must reflect the actual system values. If not, the filter provides erroneous updates of the state vector. To pursue this idea, another software version, B36, was developed with the first two control panel potentiometers setting the filter parameters. These flights produced the most successful results of the entire project.

3. 1984 CLOSED LOOP TEST RESULTS

3.1 INTRODUCTION

Between the 1983 and the 1984 closed loop testing, the aircraft and the control system was completely refurbished. The actuators were returned to Moog Inc., torn down and all the worn bearings and seals were replaced. Afterwards, the wiring harness was rebuilt, followed by a wiring continuity and fidelity check. To confirm that no errors had been introduced, the open loop controller was installed and earlier open loop results were repeated.

From changes made to the flying software, the calculation time decreased from 162 ms to 58 ms, with a corresponding change in total update time from 267 ms to 163 ms, Figure 57. This reduction was largely attributed to two arithmetic changes. First, the Kalman gain vector in the PROM3 version was determined by an iterative method, whereas in later versions, it is determined directly. Also, for the 1983 software, calculations were done fixed point and in double precision. For the 1984 versions, scaling problems were avoided by using floating point arithmetic, and calculation time was reduced by operating in single precision.

Version B35 demonstrated improved high speed vibration reduction. However, the vibration weighting coefficient tuning did not significantly affect the vibration levels. In addition to high speed level flight, this software reduced vibrations during maneuvers. Since the gain pot setting 10-10-10 yields identical software for B35 and B36, the flight data at 10-10-10 is directly comparable to software B35 results. Therefore, only results for the Q and R tuning software B36 are presented below. The differences between PROM3 and B36 are summarized in Table 9.

For B36, the first gain pot adjusts the process noise parameter, Q, while the second pot varies the measurement noise coefficient, R. The actual values of these settings are depicted in Figures 37 and 38, for Q and R respectively. The two extremes associated with measurement noise are as follows. With low measurement noise the control system is responsive, but tends to go unstable while with high measurement noise the control system is less responsive and more stable. The two extremes associated with process noise are as follows. With low process noise the controller performs better but does not respond well to large changes in the process parameters. On the other hand with large process noise the performance is slightly degraded but controller can adapt to large process changes (e.g., maneuvers). As with B35, the third gain pot adjusts the longitudinal vibration weighting.

For the majority of the level flight plots, multiple points were available for each test condition. The graphs present the mean of all the test points for both the baseline and the HHC on data. The vertical bars represent \pm one standard deviation to indicate the data scatter.

3.2. VIBRATION RESULTS FOR LEVEL FLIGHT

In Figures 58, 59 and 60, the 4P vertical, lateral and longitudinal vibrations are plotted versus airspeed. Unlike the 1983 tests, the dramatic vibration reductions in the vertical direction are maintained throughout the speed sweep. In fact, even as the baseline vibrations climb exponentially, the HHC vertical vibrations appear relatively constant at 0.05 g. In the other two channels, lateral and longitudinal, the HHC reduction is not as dramatic. Yet, the vibration levels with HHC on are still consistently lower than the baseline values.

As for the effects of filter tuning, the different gain pot settings are more apparent in Figures 61 through 63. Here, the 4P vertical, the 4P lateral and the 4P longitudinal pilot seat vibrations are again presented but on an expanded scale. Only the mean point is plotted where multiple test points existed. Viewing the vertical plot, where the most dramatic effects are observed, a few tentative conclusions may be made. The filter tuning produced very little effect for level flight when compared with the overall HHC results. On these expanded scale plots, no one gain pot setting is superior or inferior. Therefore, the improved performance of the 1984 software resulted from numerous changes, Table 9, and not simply the tunable filter parameters.

As for harmonics other than 4P, the HHC performance is degraded. The pilot seat vertical vibration frequency spectrum for 100 knots is presented in Figure 64. The gain pot settings 10-10-10 and 5-5-10 are shown along with the baseline data. Aside from the 4P signal, the HHC system slightly degraded the vibration levels. This behavior was observed for all three directions.

For 3P and 5P pilot seat vibration levels, HHC consistently induces slightly higher vibrations in all three directions. Figures 65, 66 and 67 present the 3P vertical, lateral and longitudinal vibrations, whereas Figures 68 through 70 present similar plots for the fifth harmonic. Although the vibrations increase, this delta is not of the same magnitude as the 4P reduction. In the longitudinal direction, the 3P and the 5P vibration increases are roughly 0.005 g, whereas the 4P reduction is approximately 0.015 g. Likewise, the 3P and the 5P vertical vibration levels are raised by approximately 0.02 g, while the 4P levels dropped by nearly 0.25 g. Therefore, these slight increases are tolerable when compared with the fourth harmonic reduction.

Finally, before this evaluation is completed, the vibration levels throughout the ship must be analyzed. Unfortunately, only one other set of accelerometers, located at the aircraft c.g., are available for data. In Figures 71, 72 and 73 respectively, the c.g. 4P vertical, lateral and longitudinal vibrations, are plotted versus airspeed. Unlike the pilot seat data, HHC slightly increased the vertical and the lateral vibrations, Figures 71 and 72. On the other hand, the c.g. longitudinal vibrations are significantly less with HHC on, Figure 73, which differs from the pilot seat results, Figure 60. Without additional accelerometer locations, no conclusions may be made about the overall aircraft vibrations. However, these plots of the c.g. vibrations, especially Figures 71 and 72, demonstrate the possible negative effects from HHC.

3.3 ROTOR MAST BENDING FOR LEVEL FLIGHT

The OH-6A aircraft employs the MDHC stationary rotor mast, which is instrumented to determine the 4P oscillatory bending moments. These gages indicate the reduction of vibratory loads that are transferred to the

fuselage. With HHC, the 4P lateral and longitudinal mast bending moments are reduced over the entire speed range, Figures 74 and 75 respectively. Even though the HHC effect is reduced at higher speeds, the vibratory loads are still less than the baseline values.

3.4 BLADE ANGLES FOR LEVEL FLIGHT

The rotating system blade feathering angles versus airspeed are presented for the third, fourth and fifth harmonics, Figures 76, 77 and 78, respectively. Interestingly, at all airspeeds, the inputs are predominantly 3P and 5P. Very little 4P feathering occurs.

As for the blade flapping angles, a different trend arises. For the third harmonic, the angles are generally less with HHC as compared to the baseline, Figure 79. For the 4P component, the baseline and the HHC data is interspersed, Figure 80. At 80 and 90 knots only, the HHC data is above the baseline. In fact, at these speeds, the fourth harmonic of the baseline flapping angle approaches zero. Finally, for the fifth harmonic of flap angle, the HHC data generally is above the baseline values at all speeds, Figure 80.

3.5 HHC ACTUATOR STROKES AND LOADS FOR LEVEL FLIGHT

In Figures 82, 83 and 84, the 4P strokes of the left lateral, the right lateral and the longitudinal actuators as measured by the LVDTs are presented. Similar to earlier closed loop tests, the longitudinal input is the most dominant. Since the pilot seat vibrations are reduced at high speeds, it is concluded that the optimal controller operates adequately with equal vibration weighting.

Also, as one last point of interest from these figures, the HHC actuators never approach their electronically set stroke limit of ± 0.100 inches. The system is operating far from its authority limit.

To determine the actual work an actuator does, its load, in addition to its displacement, must be considered. In Figures 85, 86 and 87, the actuator loads corresponding to the above displacements are plotted. Unlike the displacements, the right lateral, and not the longitudinal, actuator experiences the greatest load, Figures 85 and 86 respectively. The left lateral actuator sees the least load, Figure 87. Under the greatest load, the right lateral actuator is probably the most significant HHC input. On the other hand, the longitudinal actuator has the biggest displacement due to the reduced stiffness in this control channel. Therefore, the open loop data is confirmed. The controller is using one of the more effective channels for vibration reduction.

3.6 HHC EFFECT ON BLADE LOADS FOR LEVEL FLIGHT

The influence of HHC on blade loads is presented for 3P, 4P and 5P. In Figures 88, 89 and 90, the chordwise bending moment at 17% radius is plotted versus airspeed, while Figures 91, 92 and 93, show the flapwise bending moment at 15% radius. Finally, the torsional moment at 30% radius is given in Figures 94, 95 and 96.

At the third and the fourth harmonics, the chordwise data scatter indicates almost no change to a slight increase in bending moment, with HHC engaged, Figures 88 and 89. At 5P, the chordwise moment is significantly increased over the entire speed sweep, Figure 90. In a similar fashion, the flapwise data shows a slight reduction at 3P and 4P, with a significant increase over baseline values at 5P, Figures 91, 92 and 93 respectively. Lastly, the torsional moments increased for these harmonics since HHC is driving the blade at these frequencies, Figures 94, 95 and 96.

The increases in some harmonics of blade loads with reductions in others might be expected. The wind tunnel test program, Hammond [10], had indicated that blade loads were likely to increase with HHC engaged. As a result, the blade loads were monitored closely during the flight test program. The increased loads are well within the design loads for the OH-6A blade.

The variation of oscillatory loads, or one-half peak to peak, with airspeed are presented for blade chordwise, flapwise and torsional moments in Figures 97, 98 and 99 respectively. These measurements are at the same blade radius location as presented for the harmonic data. Again, an increase with HHC on is apparent which is a trend similar to the wind tunnel testing, Hammond [10].

3.7 HHC EFFECT ON PITCH LINK LOADS FOR LEVEL FLIGHT

The pitch link loads versus airspeed are shown for the 3P, the 4P and the 5P frequency in Figures 100, 101 and 102. In addition, the cyclic oscillatory pitch link load is plotted versus airspeed in Figure 103. The increase in pitch link load with HHC engaged was totally expected since the HHC driving forces goes through the pitch link. Again, these loads are well within the design endurance limit for the pitch links.

3.8 TAIL BOOM BENDING FOR LEVEL FLIGHT

Aside from vibrations, the OH-6A is instrumented to record various fuselage moments. If vibrations at one location are reduced at the expense of another location, then HHC is not a viable solution. To demonstrate that HHC does not adversely affect the fuselage moments, the 4P tail boom bending, which is an indicator of vibration levels, is presented for the lateral, the longitudinal and the torsional moments, Figures 104, 105 and 106 respectively. For both the lateral and the vertical moments, the loads with

HHC engaged are generally lower than the baseline, Figures 104 and 105. The torsional moment data scatter, on the other hand, demonstrates neither a positive or a negative effect of HHC, Figure 106.

3.9 VIBRATION RESULTS FOR TRANSIENT FLIGHT REGIMES

With the improved 1984 software, the HHC controller performed quite well during transient flight conditions. Results similar to the level flight data were obtained during maneuvers. In the following section, the 4P pilot seat vibrations are presented for three different test conditions which are as follows.

1. Various g load pullups at 80 knots.
2. Right and Left 30 degree banked turns at 80 knots.
3. Accelerations and decelerations from 40 to 100 knots.

The blade and fuselage loads data showed very similar trends as during level flight. The HHC system did not produce undue strain on the OH-6A even during maneuvers.

For the maneuver bar graphs, Figures 107-115, the data was collected in the following fashion. For all maneuver conditions, the data was reduced at time of the peak vertical vibrations. This instant represents the largest demand on the HHC system. Then, the 4P vibrations were analyzed to determine the mean and the standard deviation for repeated maneuvers. The test point which was closest to the vibration means was then completely evaluated. Therefore, the plots roughly represent the mean results for the test condition.

The 4P pilot seat vibrations observed during 80 knot pullups are presented in Figures 107, 108 and 109 in the vertical, lateral and longitudinal directions respectively. The gain pot settings for these tests was 5-5-10. The HHC controller significantly reduced vibrations in the vertical and lateral directions for each g load presented. However,

in the longitudinal directions, HHC increased the vibrations. These longitudinal vibrations were approximately five times less than the vertical vibrations.

The 4P pilot seat vibrations are shown next for 30 degree right and left turns at 80 knots with various gain pot settings. With the gain pot setting 5-5-10, the vibrations were reduced in the vertical and lateral directions but raised in the longitudinal direction. On the other hand, all three vibrations were reduced when the gain pots were set to 10-5-10. Kalman filter tuning did affect the HHC performance during maneuvers.

The next type of maneuver, acceleration and deceleration, was evaluated in two distinct tests. First, the peak vibrations were reduced to investigate overall HHC performance. These 4P vibrations demonstrated the Kalman filter tuning capacity, Figures 113-115. For the vertical vibrations, the previous trends of HHC results were repeated, Figure 113. However, in the lateral and longitudinal directions, the vibrations were increased with the gains pots at 5-5-10, Figures 114 and 115. The gain pot setting 10-5-10 demonstrated somewhat improved results over 5-5-10, even though these vibrations were comparable to baseline levels.

The second type of acceleration test was designed to investigate the HHC system tracking capability. After initializing the controller at 40 knots, the aircraft was accelerated to 100 knots and data was recorded in 10 knot increments. In Figure 116, the 4P vertical pilot seat vibrations for this test, are superimposed on the baseline and HHC on mean level flight results. The HHC controller kept up with the rapidly changing flight condition. The same conclusion holds for the lateral and longitudinal vibrations. These results are not shown since, due to the gains being set at 5-5-10, vibrations were not reduced in these two directions.

3.10 EFFECT OF HHC ON AIRCRAFT PERFORMANCE

The overall aircraft performance is of interest because HHC is altering the aerodynamics of the rotor system. The flight test program was not a rigorous performance test program, but some instrumentation was included to measure performance. The basic performance indicators were main rotor shaft torque and engine torque pressure. These results proved statistically inconclusive. To determine if HHC has a positive performance effect, a more detailed performance test program would be required.

VII. CONCLUSIONS AND RECOMMENDATIONS

Overall, this program was extremely successful in meeting its goals. The higher harmonic control system, integrated into the OH-6A, significantly reduced pilot seat 4P vibrations. This system can have a tremendous impact on airframe vibrations for future helicopters. Conclusions from the present program and some thoughts and recommendations for future HHC work are presented below.

1. At the pilot seat, the fourth harmonic of vibrations were significantly reduced. Vibrations at other frequencies were increased only insignificantly. Vibrations were reduced at all flight speeds as well as during several maneuver conditions.
2. The HHC system did not induce undue loads on the helicopter. All the increased loads, both blade and fuselage, remained well within design tolerances. In addition, the HHC power requirements were small and were satisfied by existing aircraft systems.
3. The 1984 closed loop results demonstrated the effects of Kalman filter tuning. For level flight, the parameters have little effect on HHC performance. However, during maneuvers, the Kalman filter parameters greatly influence the HHC vibration reduction.

The improvements in the 1984 high speed data resulted from numerous changes. The decreased computation time was one significant factor.

4. Since the flight test program was concentrated on monitoring vibrations and loads, precise helicopter performance parameters are not available. Yet from the existing data, HHC did not adversely affect vehicle performance. For a firm quantitative analysis a true performance test program must be initiated.
5. Aside from the pilot seat, only the helicopter c.g. vibrations were recorded. Although the 4P levels slightly increase at this location, the vibrations do not necessarily follow this trend throughout the helicopter. In fact, the tail boom moments, which are an indicator of vibration levels, are reduced by HHC.

As an extension of the HHC concept, multiple locations of one vibration direction, such as the vertical, may be minimized throughout the aircraft. With the coupling between the three directions, the overall aircraft vibrations may reach even lower levels.

6. As with any flight test program of this magnitude, extensive data was recorded which could not be presented in this report. This additional data will serve as a valuable data base when developing an HHC system for larger and faster helicopters.
7. HHC is expected to be superior than any other method of vibration control. This is due to the fact that HHC attacks the source of vibrations, and that it adapts to changing flight conditions. Being an active vibration reducing device, the weight of an HHC system is estimated to be significantly lower than any number of passive devices such as bifilar absorbers, airframe vibration absorbers, etc.
8. The added complexity and the mechanical system wear associated with an HHC implementation can be minimized at a low cost by proper design. Future aircraft which will most likely be full fly-by-wire will have significantly reduced mechanical control paths, and therefore will require very little control modification to eliminate mechanical wear when HHC is included.
9. Although HHC implementations requires sensors and computers, the future helicopters are expected to contain considerable amounts of such resources in which case HHC is not likely to make large demands in terms of additional resources and complexity.

VIII. REFERENCES

1. Wood, E.R.; Powers, R.W.; Cline, J.H.; and Hammond, C.E.: "On Developing and Flight Testing a Higher Harmonic Control System." Proceedings of the 39th Annual Forum of the American Helicopter Society, St. Louis, MO, May 9 - 11, 1983. Also, Journal of the American Helicopter Society, Vol. 30, No. 1, January 1985, pp. 3-20.
2. Wood, E.R.; and Powers, R.W.: "Practical Design Considerations of a Flightworthy Higher Harmonic Control System." Proceedings of the 36th Annual Forum of the American Helicopter Society, Washington, D.C., May, 1980. Also, AIAA Paper No. 80-0688.
3. Wood, E.R.; Powers, R.W.; and Hammond, C.E.: "On Methods for Application of Higher Harmonic Control." Proceedings of the 4th European Rotorcraft and Powered-Lift Aircraft Forum, Stresa, Italy, September 13 - 15, 1978, Paper No. 22.
4. Gupta, B.P.; Logan, A.H.; and Wood, E.R.: "Higher Harmonic Control for Rotary Wing Aircraft." Proceedings of the AIAA/AHS/ASEE Aircraft Design Systems and Operations Meeting, San Diego, CA, October 31 - November 2, 1984.
6. Wood, E.R.; and Gupta, B.P.: "Higher Harmonic Control: Vibration Reduction for Reduced Weight." Proceedings of the 44th Annual Conference of the Society of Allied Weight Engineers, Arlington, Texas, May 20 - 22, 1985.
7. Wood, E.R.: "Higher Harmonic Control for the Jet Smooth Ride." Vertiflite, Vol. 29, No. 4, May/June, 1983.
8. Molusis, J.A.; Hammond, C.E.; and Cline, J.H.: "A Unified Approach to the Optimal Design of Adaptive and Gain Scheduled Controllers to Achieve Minimum Helicopter Rotor Vibration." Journal of the American Helicopter Society, April 1983, pp. 9 - 18.
9. Powers, R.W.: Preliminary Design Study of a Higher Harmonic Blade Feathering Control System. NASA CR-159327, June, 1980.
10. Hammond, C.E.: "Wind Tunnel Results Showing Rotor Vibratory Loads Reduction Using Higher Harmonic Control." Proceedings of the 36th Annual Forum of the American Helicopter Society, Washington, D.C., May, 1980.
11. Shaw, J.; Albion, N.; Hanker, E.J. Jr.; and Teal, R.S.: "Higher Harmonic Control: Wind Tunnel Demonstration of Fully Effective Vibratory Hub Force Suppression." Proceedings of the 41st Annual Forum of the American Helicopter Society, Fort Worth, Texas, May 15 - 17, 1985.
12. Lehmann, G.: "The Effect of HHC to a Four Bladed Hingelss Model Rotor." Proceedings of the 41st Annual Forum of the American Helicopter Society, Fort Worth, Texas, May 15 - 17, 1985.
13. Saito, S.: Application of an Adaptive Blade Control Algorithm to a Gust Alleviation System. NASA TM-85848, September, 1983.

14. Johnson, W.: Self-Tuning Regulators for Multicyclic Control of Helicopter Vibration. NASA TP-1996, March, 1982.
15. Ham, N.D.; and McKillip R.M., Jr.: "A Simple System for Helicopter Individual-Blade-Control and Its Application to Gust Alleviation." A Collection of Technical Papers, Part 1 - AIAA/ASME/ASCE/AAS 21st Structures, Structural Dynamics and Materials Conference, May 1980, pp. 57-68. (Available as AIAA-80-0666.)
16. Shaw, J.; and Albion, N.: "Active Control of the Helicopter Rotor for Vibration Reduction." Proceedings of the 36th Annual Forum of the American Helicopter Society, Washington, D.C. May 1980.
17. Brown, T.J.; and McCloud, J.L., III: "Multicyclic Control of a Helicopter Rotor Considering the Influence of Vibration, Loads and Control Motion." Proceedings of the 36th Annual Forum of the American Helicopter Society, Washington, D.C., May 1980.
18. McCloud, J.L., III: "Multicyclic Control for Helicopters: Research in Progress at Ames Research Center." Proceedings of the 36th Annual Forum of the American Helicopter Society, Washington, D.C., May 1980.
19. Taylor, R.B.; and Farrar, F.A.: "An Active Control System for Helicopter Vibration Reduction by Higher Harmonic Pitch." Proceedings of the 36th Annual Forum of the American Helicopter Society, Washington, D.C., May, 1980.
20. Yen, J.G.: "Vibration Reduction with Higher Harmonic Blade Feathering for Helicopters with Two Bladed Teetering and Four Bladed Hingless Rotors." Proceedings of the 36th Annual Forum of the American Helicopter Society, Washington, D.C., May, 1980.
21. Ham, N.D.; and Whitaker, H.P.: "A Wind Tunnel Investigation of Tilt Rotor Gust Alleviation Systems." Final Report, NASA CR-152264, January, 1978.
22. Straub, F.K.; and Warmbrodt, W.: "The Use of Active Controls to Augment Rotor/Fuselage Stability." Journal of the American Helicopter Society, Vol. 30, No. 3, July, 1985, pp. 13 - 22.
23. Lemont, H.E.; and Upton, H.: "Vibratory Ice Protection for Rotor Blades." Final Report, USAAMRDL-TR-77-29, Fort Eustis, VA, June, 1978.
24. Molusis, J.A.: Investigation of Unexplained Behavior and Nonlinearity Observed in Wind Tunnel Tests of Higher Harmonic Control. USAAVRADCOTR-83-D-8, August 1983.
25. Molusis, J.A.: "The Importance of Nonlinearity on the Higher Harmonic Control of Helicopter Vibration." Proceedings of the 39th Annual Forum of the American Helicopter Society, St. Louis, Missouri, May 9-11, 1983.
26. Davis, M.W.: "Development and Evaluation of a Generic Active Helicopter Vibration Controller." Proceedings of the 40th Annual Forum of the American Helicopter Society, Crystal City, VA, May 16 - 18, 1984.

27. Davis, M.W.: Refinement and Evaluation of Helicopter Real-Time-Self Adaptive Active Vibration Controller Algorithms. NASA CR-3821, August, 1984.
28. Bass, R.W.; and Zes, D.: "Robust Tuning of Kalman Filters." Proceedings of the American Control Conference, June 19 - 21, 1985, Paper No. WA6.
29. Scharf, L.L.; and Sigurdsson, S.: "Fixed Point Implementation of Fast Kalman Prediction." IEEE Transactions on Automatic Control, Vol. AC-29, No. 9, September 1984, pp. 850 - 852.
30. Kosut, R.L.; and Friedlander, B.: "Robust Adaptive Control: Conditions for Global Stability." IEEE Transactions on Automatic Control, Vol. AC-30, No. 7, July, 1985, pp. 610 - 624.
31. Van Wingerden, A.J.M.; and De Koning, W.L.: "The Influence of Finite Word Length on Digital Optimal Control." IEEE Transactions on Automatic Control, Vol. AC-29, No. 5, May, 1984, pp. 385 - 391.
32. Wernicke, R.K.; and Drees, J.M.: "Second Harmonic Control." Proceedings of the 19th Annual National Forum of the American Helicopter Society, Washington, D.C., May 1963.

IX. TABLES AND FIGURES

Length	6.25 \pm 0.003 in.
Stall Load	786 lbs.
Actuator locked below	1200 psi.
Actuator unlocked above	1600 psi.
Locking time:	
From full extend	170 ms.
From full retract	250 ms.
Limit load (zero inlet pressure)	\pm 750 lbs.

HHC ACTUATOR CHARACTERISTICS
Table 1

Fluid:	MIL-H-5606
Delivery:	0.75 cu. in/rev
Max. Continuous RPM:	7500 RPM
Typical Operating RPM:	2800 RPM
Min. Recommended Inlet Pressure:	10 psia
Recommended Nominal Operation Pressure:	3000 psi
Pressure At Which Displ. Will Begin To Reduce:	2850 psi
Pressure Rise As Displ. Is Reduced To Zero:	150 psi
Dry Weight:	8.9 lbs
Estimated Efficiency At 2700 RPM, Full Flow:	90 %
Input Horsepower At 2700 RPM, Full Flow:	17.5 HP
Rotation:	Counterclockwise, looking at shaft

HHC HYDRAULIC PUMP DESIGN CRITERIA
Table 2

	<u>11/B</u>	<u>SDP-175</u>	
Weight:	35 Kg, (78 pounds)	7 Kg, (15 pounds)	
Power Dissipation:	175 Watts	40 Watts	
Memory:	32K-words by 16 bit	24K ROM, 2K RAM by 16 bit Expandable to 64K	
Processor:	General purpose, 16 bit data and instructions	General Purpose, 16-bit data and instructions	
	Instruction times:	Instruction times:	
	3.5 μ sec add, subtract	0.5 μ sec add, subtract	
	30.0 μ sec multiply	5.5 μ sec multiply	
	78.0 μ sec divide	12.0 μ sec divide	
	3.5 μ sec test, set bit	0.75 μ sec test, set bit 800 KOPS for standard airborne mix	
Software:	Assembly, Basic, FORTRAN Real time operating system	Assembly, Floppy disk operating system	
I/O:	16 A/D Channels	<u>Input</u>	<u>Output</u>
	6 D/A Channels	4 AC	0 AC
		20 DC	20 DC
		16 28V Discrete	16 28V Discrete
		48 5V Discrete	56 5V Discrete
Functions:	Laboratory data acquisition	Airborne remote terminal bus, control avionics processing	

PDP-11/B AND SDP-175 CONTROLLER CHARACTERISTICS
Table 3

MEAS-NO.	DESCRIPTION (INCL LOCATION)	SYMBOL	RANGE	UNITS	ACCURACY	FREQUENCY RESPONSE
00003	AIRBORNE TAPE RECORDER SYNC LIGHT ON/OFF	A/B REC SYNC	0 OR 32	COUNTS		0 TO 6 HZ
00004	MUX FLIP BUFFER (ENCODER) 5 VDC POWER	MUX FF LOGIC	DISCRETE	DN/OFF		0 TO 2 HZ
00005	VERIFICATION OF MUX RECORDED DATA STREAM A	MUX DATAECA	STEADY	COUNTS		0 TO 6 HZ
00006	VERIFICATION OF MUX RECORDED DATA STREAM B	MUX DATAECB	STEADY	COUNTS		0 TO 6 HZ
00007	MUX BUS DATA RECORDING GOOD/BAD	MUX REC ON	0 TO 256	COUNTS		0 TO 6 HZ
01000	M.R. PITCH LINK LOAD B1	MR PIT LKLD1	-1000 TO 1000	LBS	+/-1%	0 TO 50 HZ
01001	M.R. BLADE FLAPWISE BENDING @ 15%	MR BL FWB 15	-6000 TO 6000	IN-LBS	+/-1%	0 TO 50 HZ
01002	M.R. BLADE FLAPWISE BENDING @ 50%	MR BL FWB 50	-4000 TO 4000	IN-LBS	+/-1%	0 TO 50 HZ
01003	M.R. BLADE CHORDWISE BENDING @ 17%	MR BL CWB 17	-12000 TO 12000	IN-LBS	+/-1%	0 TO 50 HZ
01004	M.R. MAST LONGITUDINAL BENDING @ W.L. 68.25	MAST LONGLWR	-75000 TO 75000	IN-LBS	+/-1%	0 TO 50 HZ
01005	M.R. MAST LATERAL BENDING @ W.L. 68.25	MAST LAT LWR	-45000 TO 45000	IN-LBS	+/-1%	0 TO 50 HZ
01006	LONGITUDINAL LOAD LINK	LONG LG LINK	-2400 TO 2400	LBS	+/-1%	0 TO 50 HZ
01007	M.R. MAST BASE LONGITUDINAL BENDING	MASTBASELONG	-75000 TO 75000	IN-LBS	+/-1	0 TO 50 HZ
01008	M.R. MAST BASE LATERAL BENDING	MASTBASELAT	-50000 TO 50000	IN-LBS	+/-1	0 TO 50 HZ
01009	M.R. MAST LONGITUDINAL BENDING @ W.L. 73.0	MAST LONG UP	-75000 TO 75000	IN-LBS	+/-1%	0 TO 50 HZ
01010	M.R. MAST LATERAL BENDING @ W.L. 73.0	MAST LAT UFR	-50000 TO 50000	IN-LBS	+/-1%	0 TO 50 HZ
01019	M.R. PITCH HOUSING FLAPWISE BENDING	MR PH FWB	-12000 TO 12000	IN-LBS	+/-1%	0 TO 50 HZ
01020	M.R. SHAFT TORQUE	MR SHAFT TOR	-10000 TO 57000	IN-LBS	+/-1%	0 TO 50 HZ
01021	M.R. DAMPER LOAD	MR DAMFER LD	-1200 TO 2000	LBS		0 TO 50 HZ
01022	M.R. BLADE CHORDWISE BENDING @ 50%	MR BL CWB 50	-7500 TO 7500	IN-LBS	+/-1%	0 TO 50 HZ
01023	M.R. BLADE CHORDWISE BENDING @ 75%	MR BL CWB 75	-7500 TO 7500	IN-LBS	+/-1%	0 TO 50 HZ
01024	M.R. BLADE FLAPWISE BENDING @ 20%	MR BL FWB 20	-4500 TO 4500	IN-LBS	+/-1%	0 TO 50 HZ
01025	M.R. BLADE FLAPWISE BENDING @ 30%	MR BL FWB 30	-4000 TO 4000	IN-LBS	+/-1%	0 TO 50 HZ
01026	M.R. BLADE FLAPWISE BENDING @ 70%	MR BL FWB 70	-3000 TO 3000	IN-LBS	+/-1%	0 TO 50 HZ
01027	M.R. BLADE TORSION @ 17%	MR BL TOR 17	-3000 TO 3000	IN-LBS	+/-1%	0 TO 50 HZ

MEAS-NO. DESCRIPTION (INCL LOCATION).

MEAS-NO.	DESCRIPTION (INCL LOCATION)	SYMBOL	RANGE	UNITS	ACCURACY	FREQUENCY RESPONSE
01028	M.R. BLADE TORSION @ 50%	MR BL TOR 50	-2000 TO 2000	IN-LBS	+1%	0 TO 50 HZ
01030	M.R. BLADE FLAPWISE BENDING @ 90%	MR BL FWB 90	-2500 TO 2500	IN-LBS	+1%	0 TO 50 HZ
01038	M.R. PITCH LINK LOAD B2	MR FIT LKLD2	-1000 TO 1000	LBS	+1	0 TO 50 HZ
01039	M.R. BLADE CHORDWISE BENDING @ 30%	MR BL CWB 30	-10K TO 10K	IN-LBS		0 TO 100 HZ
01040	M.R. BLADE TORSION @ 30%	MR BL TOR 30	-2500 TO 2500	IN-LBS		0 TO 100 HZ
01041	M.R. BLADE TORSION @ 70%	MR BL TOR 70	-1000 TO 1000	IN-LBS		0 TO 100 HZ
01103	TAILBOOM VERTICAL BENDING @ STA 211	TB VERT 211	-50000 TO 50000	IN-LBS	+1%	0 TO 50 HZ
01104	TAILBOOM LATERAL BENDING @ STA 211	TB LAT 211	-60000 TO 60000	IN-LBS	+1%	0 TO 50 HZ
01105	TAILBOOM TORSION @ STA. 211	TB TORS 211	-20000 TO 20000	IN-LBS	+1	0 TO 50 HZ
01106	TAILBOOM VERTICAL BENDING @ STA 270	TB VERT 270	-30000 TO 30000	IN-LBS	+1	0 TO 50 HZ
01107	TAILBOOM LATERAL BENDING @ STA 270	TB LAT 270	-40000 TO 40000	IN-LBS	+1	0 TO 50 HZ
01108	TAILBOOM TORSION @ STA 270	TB TORS 270	-15000 TO 15000	IN-LBS	+1	0 TO 50 HZ
01200	COLLECTIVE CONTROL ROD LOAD	COLCONTROLD	-120 TO 120	LBS	+1%	0 TO 50 HZ
01201	HHC LONGITUDINAL ACTUATOR LOAD NO. 3	HHCNGACTLD	-500 TO 500	LBS	+10%	0 TO 50 HZ
01202	HHC LEFT LATERAL ACTUATOR LOAD	HHCLLACTALD	-500 TO 500	LBS	+10%	0 TO 50 HZ
01203	HHC RIGHT LATERAL ACTUATOR LOAD	HHCRLACTALD	-500 TO 500	LBS	+10%	0 TO 50 HZ
02001	AIRSPEED SHIP SYSTEM	AIRSPEEDSHIP	0 TO 200	KNOTS	+1%	0 TO 6 HZ
02002	BOOM STATIC PRESSURE	PS BOOM	0 TO 20	PSIA	+-.2%	0 TO 6 HZ
02004	STATIC PRESSURE SHIP SYSTEM	PS SHIP	5 TO 20	PSIA		0 TO 75 HZ
02124	BOOM AIRSPEED SQUARED	AIRSPEED800M	0 TO 40000	KNOTS**2	+1	0 TO 6 HZ
02125	AIRSPEED SHIP SQUARED	AIRSPEEDSHIP	0 TO 40,000	KNS**2		0 TO 75 HZ
03001	TOTAL AIR TEMPERATURE	TOT AIR TEMP	-40 TO 62	DEG C	+-.1	0 TO 100 HZ
03002	EXHAUST GAS TEMPERATURE	EGT	0 TO 1000	DEG C	+1	0 TO 100 HZ
03004	HYDRAULIC TEMPERATURE BOOST SYSTEM	BOOST HYD T	0 TO 400	DEG F	+4%	0 TO 6 HZ
03005	HYDRAULIC TEMPERATURE HHC SYSTEM	HHC HYD T	0 TO 400	DEG F	+4%	0 TO 6 HZ

HH	1	TEST NO.	50	FLIGHT NO.	0	***** MASTER MEASUREMENT LIST *****	HHC	PAGE	3
MEAS-NO.	DESCRIPTION (INCL LOCATION)	SYMBOL	RANGE	UNITS	ACCURACY	FREQUENCY RESPONSE			
05008	VERTICAL ACCEL - RIGHT SEAT	VERTACL RSEAT	-1 TO 4	G'S	+-1%	0 TO 6 HZ			
05009	LATERAL ACCEL - RIGHT SEAT	LATACL RSEAT	-3 TO 3	G'S	+-1%	0 TO 6 HZ			
05010	LONGITUDINAL ACCEL - RIGHT SEAT	LONGACL RSEAT	-3 TO 3	G'S	+-1%	0 TO 6 HZ			
05052	HHC LONGITUDINAL FEEDBACK ACCELEROMETER	HHC LONG ACL	-2 TO 2	G'S	+-0.05	0 TO 50 HZ			
05053	HHC LATERAL FEEDBACK ACCELEROMETER	HHC LAT ACL	-2 TO 2	G'S	+-0.05	0 TO 50 HZ			
05054	HHC VERTICAL FEEDBACK ACCELEROMETER	HHC VERT ACL	-2 TO 2	G'S	+-0.05	0 TO 50 HZ			
06001	ROLL RATE	ROLL RATE	-100 TO 100	DEG/SEC		0 TO 250 HZ			
06002	PITCH RATE	PITCH RATE	-100 TO 100	DEG/SEC		0 TO 250 HZ			
06003	YAW RATE	YAW RATE	-100 TO 100	DEG/SEC		0 TO 250 HZ			
06007	C.G. VERTICAL ACCELERATION STA 100	CG VERT ACL	-1 TO 4	G'S	+-0.1%	0 TO 6 HZ			
06008	C.G. LATERAL ACCELERATION STA 100	CG LAT ACL	-1 TO 4	G'S	+-0.1%	0 TO 6 HZ			
06009	C.G. LONGITUDINAL ACCELERATION STA 100	CG LONG ACL	-1 TO 4	G'S	+-0.1%	0 TO 6 HZ			
06010	VERTICAL ACCELERATION AT C.G. HIGH FREQUENCY	CG VT ACL HF	-3.0 TO 3.0	G'S	+-0.05	0 TO 100 HZ			
06011	LATERAL ACCELERATION AT C.G. HIGH FREQUENCY	CG LT ACL HF	-3.0 TO 3.0	G'S	+-0.05	0 TO 100 HZ			
06012	LONGITUDINAL ACCELERATION AT C.G. HIGH FREQUENCY	CG LG ACL HF	-3.0 TO 3.0	G'S	+-0.05	0 TO 100 HZ			
07001	MAIN ROTOR RPM	RPM MR	0 TO 120	PERCENT	+-1%	0 TO 6 HZ			
07004	ENGINE TORQUE	ENG TORQUE	0 TO 100	PSIA	+-1%	0 TO 6 HZ			
07007	HHC ECU DC RPM OUTPUT	ECU DC RPM	0 TO 10	HERTZ	+-0.5%	0 TO 6 HZ			
07009	RPM MAIN ROTOR IN REV/MINUTE	RPM MR RPM	0 TO 520	RPM	+-1%	0 TO 6 HZ			
08000	GENERATOR CURRENT	GEN CURRENT	0 TO 150	AMPS	+-1	0 TO 60 HZ			
08002	HHC ECU SINE REFERENCE OUTPUT	HHC SIN REF	-10 TO 10	SINE	+-0.1%	0 TO 50 HZ			
08003	HHC ECU COSINE REFERENCE OUTPUT	HHC COS REF	-10 TO 10	COSINE	+-0.1%	0 TO 50 HZ			
08019	HHC VERTICAL VIBRATION (SIN)	Z VIB SIN	-2 TO 2	VOLTS	2%	0 TO 50 HZ			
08020	HHC LATERAL VIBRATION (SIN)	Y VIB SIN	-2 TO 2	VOLTS	2%	0 TO 50 HZ			
08021	HHC LONGITUDINAL VIBRATION (SIN)	X VIB SIN	-2 TO 2	VOLTS	2%	0 TO 50 HZ			

HH 1 TEST NO. 90 FLIGHT NO. 0

***** MASTER MEASUREMENT LIST *****

HHC

PAGE 4

MEAS-NO. DESCRIPTION (INCL LOCATION).

MEAS-NO.	DESCRIPTION (INCL LOCATION)	SYMBOL	RANGE	UNITS	ACCURACY	FREQUENCY RESPONSE
08022	HHC COLLECTIVE COMMAND (SIN)	COL CMD SIN	-2 TO 2	VOLTS	2%	0 TO 50 HZ
08023	HHC COLLECTIVE COMMAND (COS)	COL CMD COS	-2 TO 2	VOLTS	2%	0 TO 50 HZ
08024	HHC LATERAL COMMAND (SIN)	LAT CMD SIN	-3 TO 3	VOLTS	2%	0 TO 50 HZ
08025	HHC LATERAL COMMAND (COS)	LAT CMD COS	-3 TO 3	VOLTS	2%	0 TO 50 HZ
08026	HHC LONGITUDINAL COMMAND (SIN)	LNG CMD SIN	-3 TO 3	VOLTS	2%	0 TO 50 HZ
08027	HHC LONGITUDINAL COMMAND (COS)	LNG CMD COS	-3 TO 3	VOLTS	2%	0 TO 50 HZ
08028	HHC VERTICAL VIBRATION (COS)	Z VIB COS	-2 TO 2	VOLTS		50 TO 100 HZ
08029	HHC LATERAL VIBRATION (COS)	Y VIB COS	-2 TO 2	VOLTS		50 TO 100 HZ
08030	HHC LONGITUDINAL VIBRATION (COS)	X VIB COS	-2 TO 2	VOLTS		50 TO 100 HZ
08032	DETERMINANT (THAT) MANTISSA	DET(THAT)MAN	-10 TO 9.9951	VOLTS		0 TO 12 HZ
08033	DETERMINANT (THAT) EXPONENT	DET(THAT)EXP	-10 TO 9.8438	VOLTS		0 TO 12 HZ
08034	ZO HAT (1), EXPONENT	ZOHAT(1)HAT	-10 TO 9.8438	VOLTS		0 TO 12 HZ
08035	SINE REFERENCE	SIN REF	-10 TO 10	VOLTS		0 TO 75 HZ
08036	COSINE REFERENCE	COS REF	-10 TO 10	VOLTS		0 TO 75 HZ
09001	MAIN ROTOR FLAP ANGLE BLADE 1	FLAP ANG M1	-8 TO 25	DEG'S	+-1%	0 TO 50 HZ
09002	FEATHERING ANGLE M.R. 1	FEAT ANG M1	-10 TO 25	DEG'S	+-1	0 TO 100 HZ
09003	LEAD LAG ANGLE M.R. 1	LELAG ANG M1	0 TO 100	PERCENT	+-1	0 TO 100 HZ
09004	LONGITUDINAL CONTROL POSITION	LNG CONT POS	0 TO 100	PERCENT	+-1%	0 TO 6 HZ
09005	LATERAL CONTROL POSITION	LAT CONT POS	0 TO 100	PERCENT	+-1%	0 TO 6 HZ
09006	DIRECTIONAL CONTROL POSITION	DIR CONT POS	0 TO 100	PERCENT	+-1%	0 TO 6 HZ
09007	COLLECTIVE CONTROL POSITION	COL CONT POS	0 TO 100	PERCENT	+-1%	0 TO 6 HZ
09008	ANGLE OF ATTACK	ANG OF ATCK	-15 TO 15	DEG'S	+-1	0 TO 100 HZ
09009	SIDESLIP ANGLE	SIDESLIP ANG	-45 TO 45	DEG'S	+-1	0 TO 100 HZ
09010	ROLL ATTITUDE	ROLL ATT	-90 TO 90	DEG'S	+-1	0 TO 100 HZ
09011	PITCH ATTITUDE	PITCH ATT	-90 TO 90	DEG'S	+-1	0 TO 100 HZ

MASTER INSTRUMENTATION LIST (Continued)
Table 4

HH 1	TEST NO.	90	FLIGHT NO.	0	DESCRIPTION (INCL LOCATION).	SYMBOL	RANGE	UNITS	ACCURACY	FREQUENCY RESPONSE
09012	YAW ATTITUDE					YAW ATT	0 TO 360	DEG'S	+-.1	0 TO 100 HZ
09014	TAIL ROTOR TO TAILBOOM PROXIMITY INDICATOR					TR/TB PROX	0 TO 896	COUNTS		
09017	HHC LEFT LATERAL ACTUATOR POSITION					HHCLLTACTPOS	-.02 TO .02	INCHES	+-.1%	0 TO 50 HZ
09026	HHC RIGHT LATERAL ACTUATOR POSITION					HHCLRTACTPOS	-.02 TO .02	INCHES	+-.1%	0 TO 50 HZ
09027	M.R. AZIMUTH INDEX					MR AZIMUTH	0 TO 512	COUNTS	+-.1%	0 TO 6 HZ
09028	HHC LONGITUDINAL ACTUATOR POSITION					HHCLNGACTPOS	-.02 TO .02	INCHES	+-.1%	0 TO 50 HZ
09030	MAIN ROTOR FEATHER ANGLE BLADE 3					FEATH ANG M3	-20 TO 20	DEG'S	+-.5	0 TO 50 HZ
09032	MAIN ROTOR LEAD LAG ANGLE BLADE 3					LELAG ANG M3	-3.8 TO 8.2	DEG'S	+-.1%	0 TO 50 HZ
09033	MAIN ROTOR/TAIL BOOM PROXIMITY INDICATOR(STICKS)					MR/TB PROX	0 TO 896	COUNTS	+-.1%	0 TO 50 HZ

MASTER INSTRUMENTATION LIST (Continued)
Table 4

Stiffened Flight Control Components	
Removed - Aluminum Bellcranks, Links, etc.	-4.8 lbs.
Add - Steel Bellcranks, Links, etc.	25.0 lbs.
HHC Hydraulic Pump and Drive	27.0 lbs.
Three HHC Actuators	18.0 lbs.
Two Heat Exchangers	6.4 lbs.
Reservoir/Manifold and Accumulator	15.0 lbs.
Hydraulic Lines and Fluid	15.0 lbs.
Four Door Fans	6.0 lbs.
Associated wiring and Installation	30.0 lbs.
Electronic Control Unit	9.0 lbs.
Flight Computer	11.6 lbs.
Total	<u>153.2 lbs.</u>

WEIGHT OF HHC SYSTEM COMPONENTS

TABLE 5

Nose	5.2 lbs.
Cockpit	24.4 lbs.
ADAS Package (Wire Harnesses Included)	218.4 lbs.
Transducers	16.4 lbs.
Airspeed Boom	16.0 lbs.
Miscellaneous Brackets and Attachments	9.6 lbs.
Total	<u>290.0 lbs.</u>

WEIGHT OF HHC FLIGHT TEST INSTRUMENTATION

TABLE 6

C-2

HHC ACTUATOR MOTION			CONTROL ANGLES (1) (DEG'S)		
γ_1	γ_2	γ_3	A_1	B_1	θ_c
+0.20	+0.20	+0.20	0.0	0.0	+1.90
+0.20	+0.20	0.0	0.0	+2.65	+1.90
+0.20	+0.20	0.0	+2.65	0.0	0.0
+0.20	0.0	+0.20	+1.33	+1.33	+0.94
+0.20	0.0	+0.20	+1.33	+3.97	+0.94
0.0	+0.20	+0.20	+1.33	+1.33	+0.94
0.0	+0.20	+0.20	+1.33	+3.97	+0.94
+0.20	0.0	0.0	+1.33	+1.33	+0.94
0.0	+0.20	0.0	+1.33	+1.33	+0.94
0.0	0.0	+0.20	0.0	+2.65	0.0
+0.20	+0.20	+0.20	0.0	+5.30	+1.90
+0.20	+0.20	+0.20	+2.65	+2.65	0.0
+0.20	+0.20	+0.20	+2.65	+2.65	0.0

(1) CONTROL ANGLES - MEASURED AT BLADE - NO CONTROL FLEXIBILITY

A_1 LAT CYCLIC (+ ROLLING TO RIGHT)

B_1 LONG CYCLIC (+ DISK TILT BACK)

θ_c COLLECTIVE

BLADE FEATHERING ANGLES RESULTING FROM ACTUATOR INPUTS
Table 7

Proc Name	PROM3	P3B30	B34	B35	B36	B37	B55	B56
Assembly Date	1/28/83	2/8/84	2/28/84	3/17/84	3/23/84	1/15/85	9/15/84	1/21/85
First Flight	1/31/83	2/28/84	2/29/84	3/20/84	4/4/84	----	10/17/84	----
Convergence	yes	no	no	yes	yes	----	yes	----
Process Noise, Q	0.0050	0.0025	0.0025	0.0050	tunable	tunable	tunable	tunable
Meas. Noise, R	0.0100	0.0004	0.0004	0.0100	tunable	tunable	tunable	tunable
Time Delay, ms	105	105	105	105	105	tunable	tunable	tunable
Compute Time, ms	162	57	57	57	57	57	30	30
Update Rate, Hz	3.7	6.1	6.1	6.1	6.1	variable	variable	variable
Init. Covar. Diag.	5	2	2	5	5	5	3.5	5
Arithmetic Type	fixed(1)	float(2)	float	float	float	float	float	float
Autocal Method	non-avg.	non-avg.	non-avg.	non-avg.	non-avg.	averaging	averaging	averaging

(1) Double Precision Fixed Computing

(2) Single Precision Floating Computing

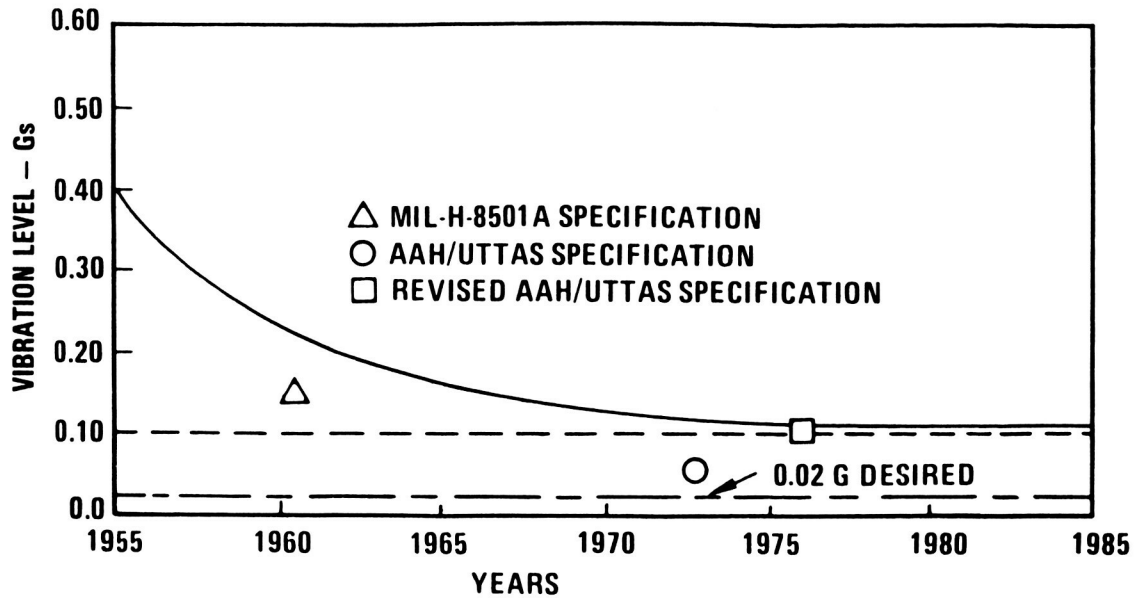
HHC SOFTWARE VERSION SUMMARY
Table 8

• SOFTWARE AND SIMULATION RESULTS

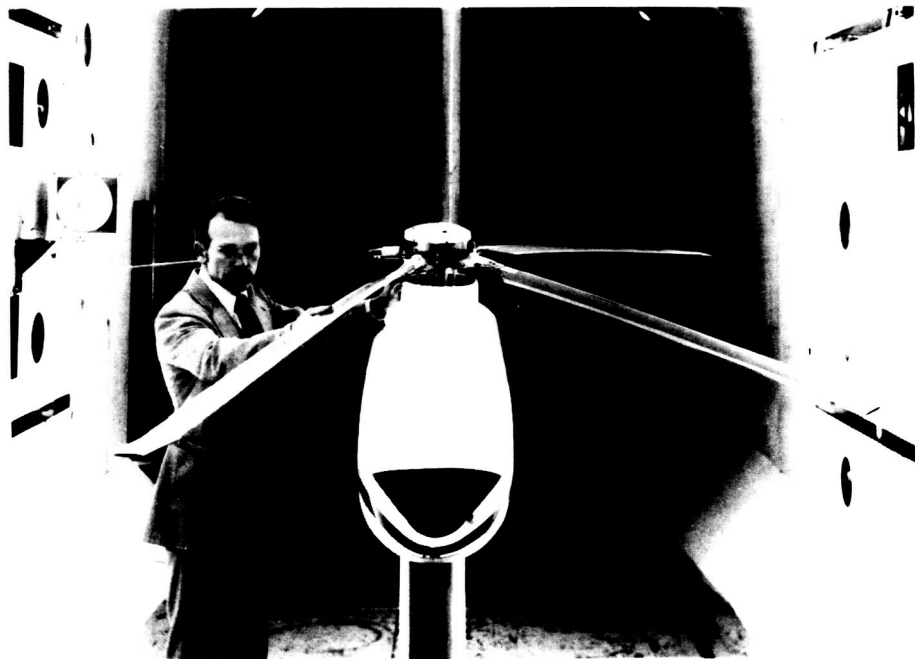
CONTROLLER COMPARISON		
	OLD JAN 1983	1984
R (MEAS. NOISE)	0.01	0.001 → 0.01
Q (PROCESS NOISE)	0.0050	0.0005 → 0.0050
KALMAN GAIN VECTOR	ITERATION	NO ITERATION
ARITHMATIC	DOUBLE PRECISION FIXED POINT	SINGLE PRECISION FLOATING POINT
CALCULATION TIME	162ms	58ms
UPDATE TIME	267ms	163ms

HHC CONTROLLER COMPARISON
Table 9

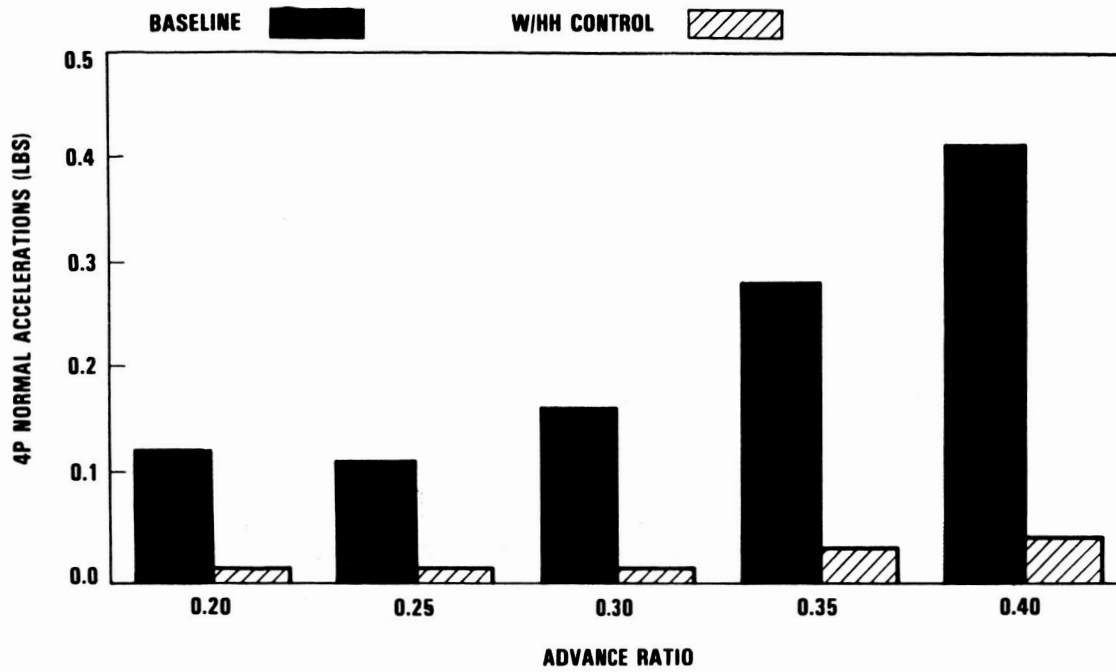
ORIGINAL PAGE IS
OF POOR QUALITY



TREND OF HELICOPTER VIBRATION LEVELS SINCE 1955
Figure 1



NASA/ARMY AEROELASTIC ROTOR EXPERIMENTAL SYSTEM (ARES)
Figure 2



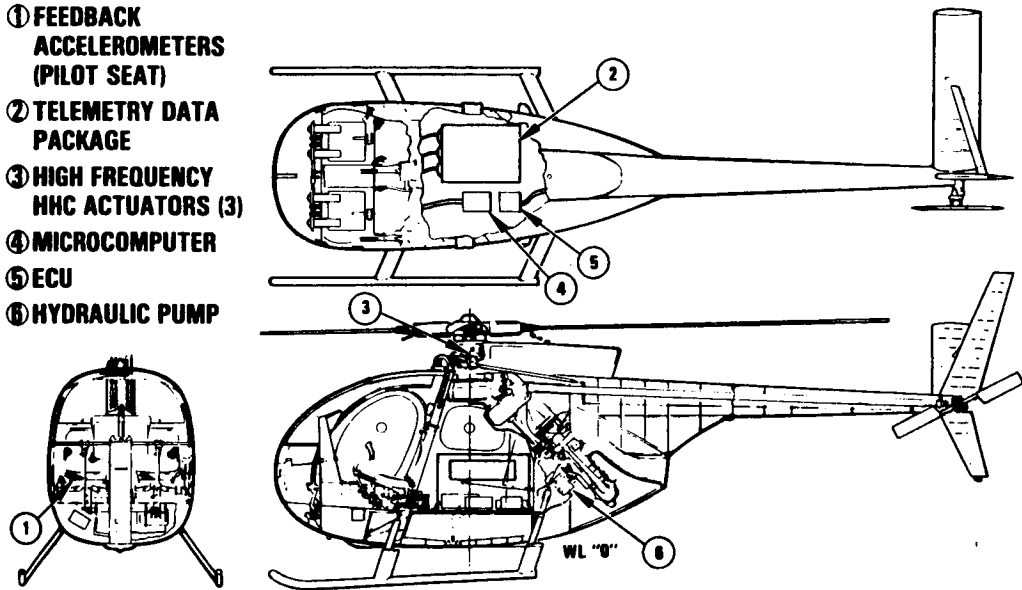
TYPICAL RESULTS FROM OPEN LOOP WIND TUNNEL TESTS
Figure 3

ORIGINAL PAGE IS
OF POOR QUALITY

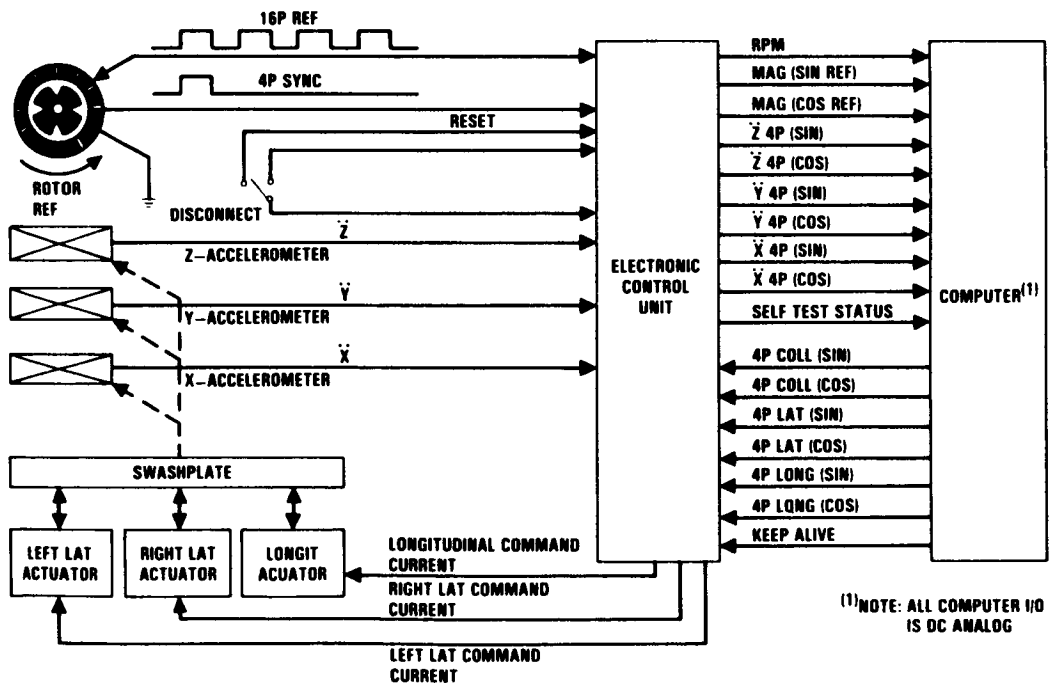


FIRST FLIGHT OF HHC EQUIPPED OH-6A, ON AUGUST 25, 1982
Figure 4

- ① FEEDBACK ACCELEROMETERS (PILOT SEAT)
- ② TELEMETRY DATA PACKAGE
- ③ HIGH FREQUENCY HHC ACTUATORS (3)
- ④ MICROCOMPUTER
- ⑤ ECU
- ⑥ HYDRAULIC PUMP

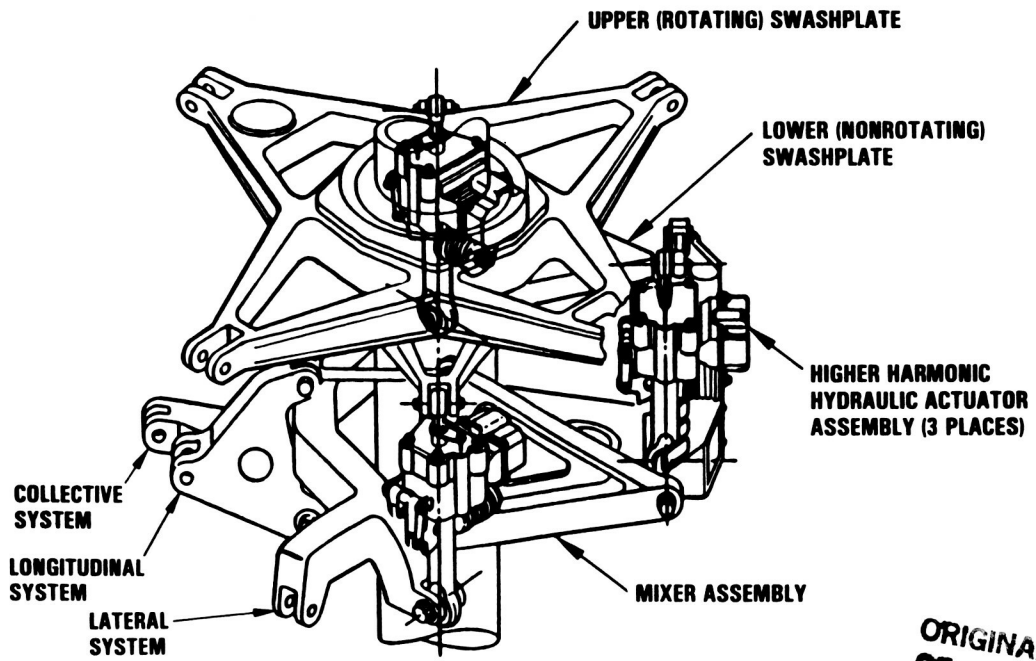


PRIMARY ELEMENTS OF THE HHC SYSTEM
Figure 5



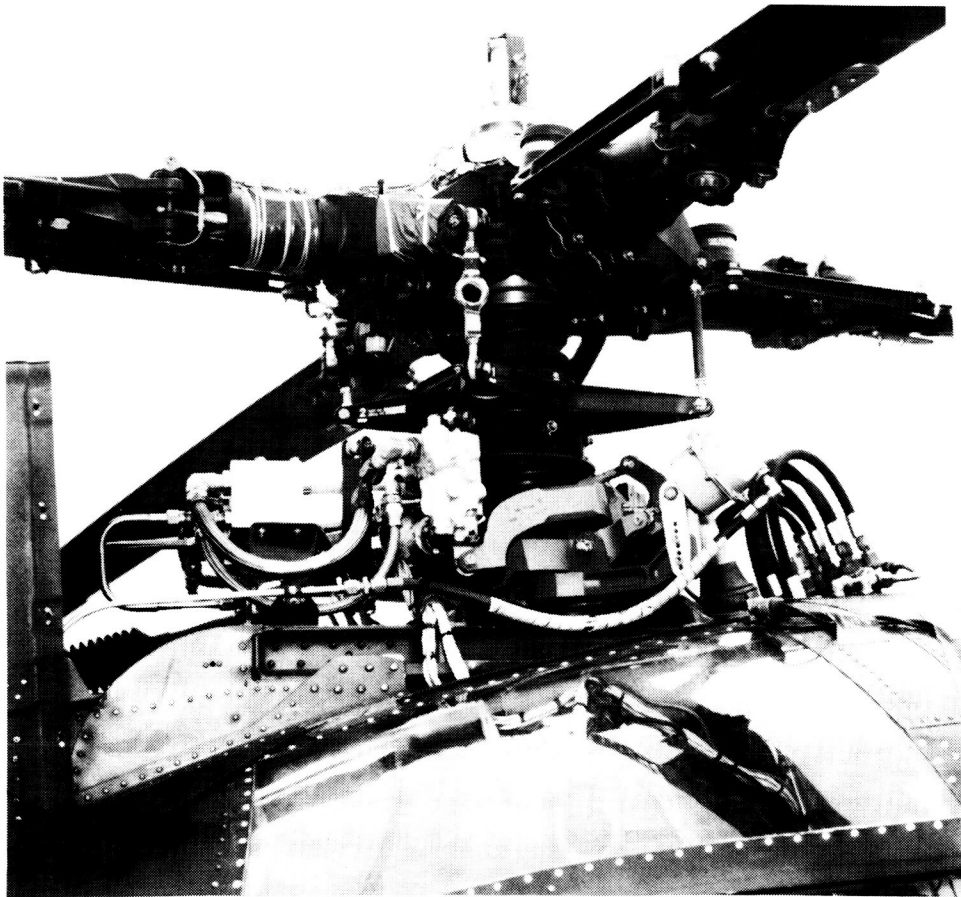
(1) NOTE: ALL COMPUTER I/O IS DC ANALOG

HHC ELECTRONICS BLOCK DIAGRAM
Figure 6

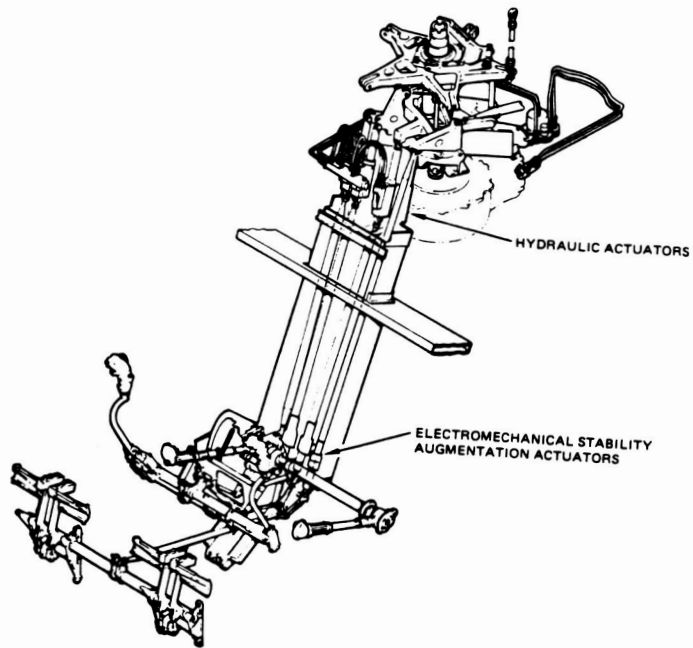


HHC ACTUATOR INSTALLATION SCHEMATIC
Figure 7

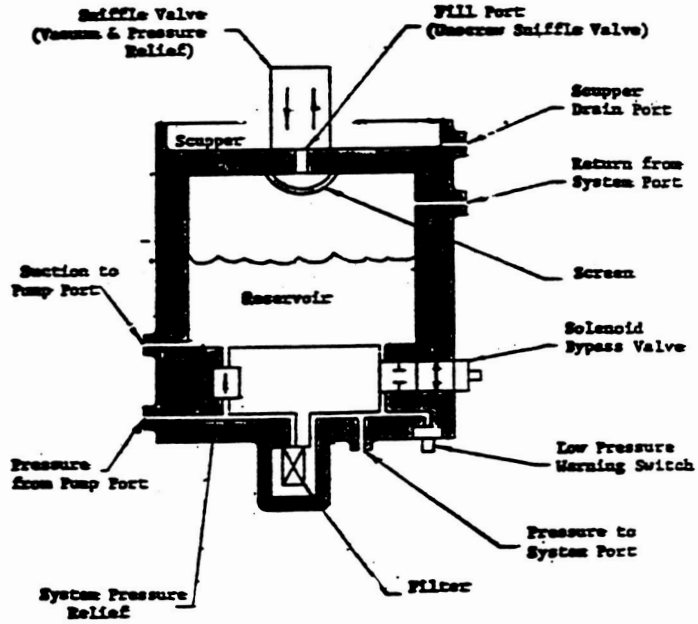
ORIGINAL PAGE IS
OF POOR QUALITY



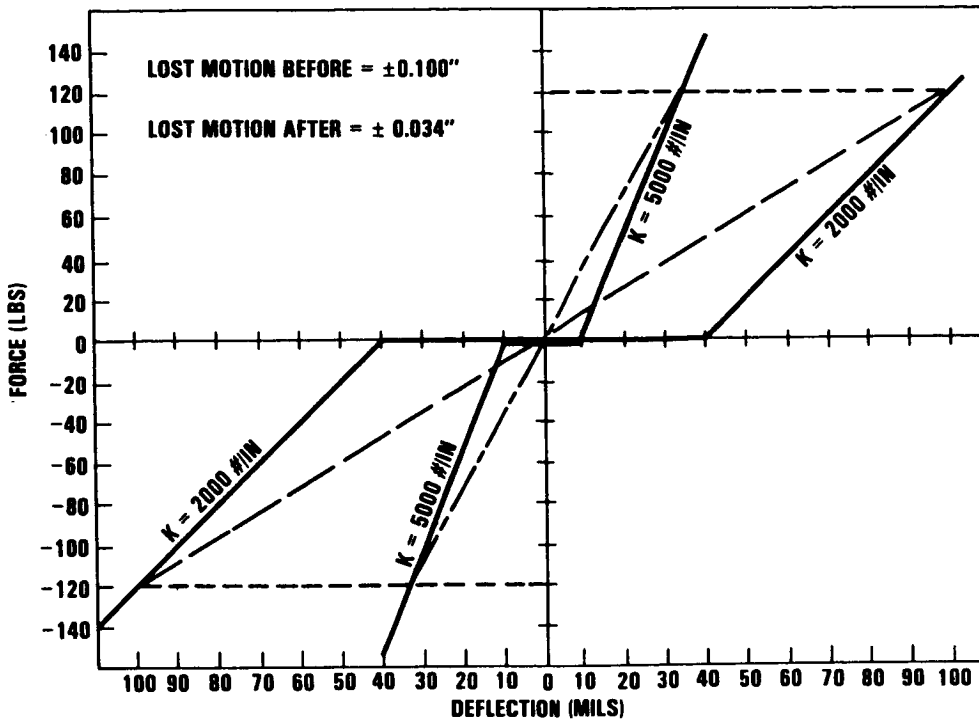
HHC RIGHT LATERAL ACTUATOR INSTALLATION
Figure 8



OH-6A SPERRY SAS FLIGHT CONTROL SYSTEM
Figure 9

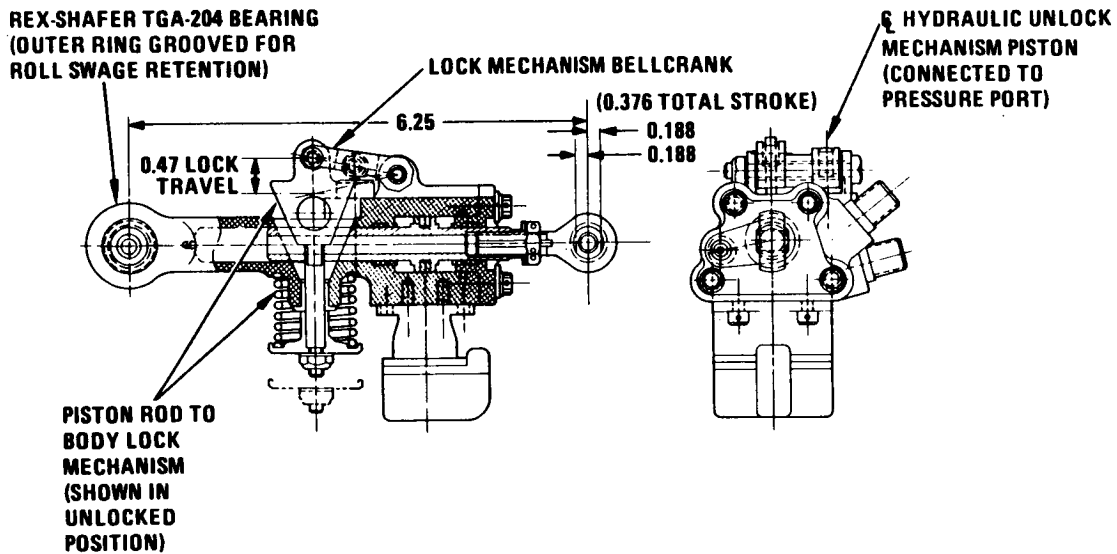


SCHEMATIC OF THE CONVAIRE HYRDOPAC
Figure 10

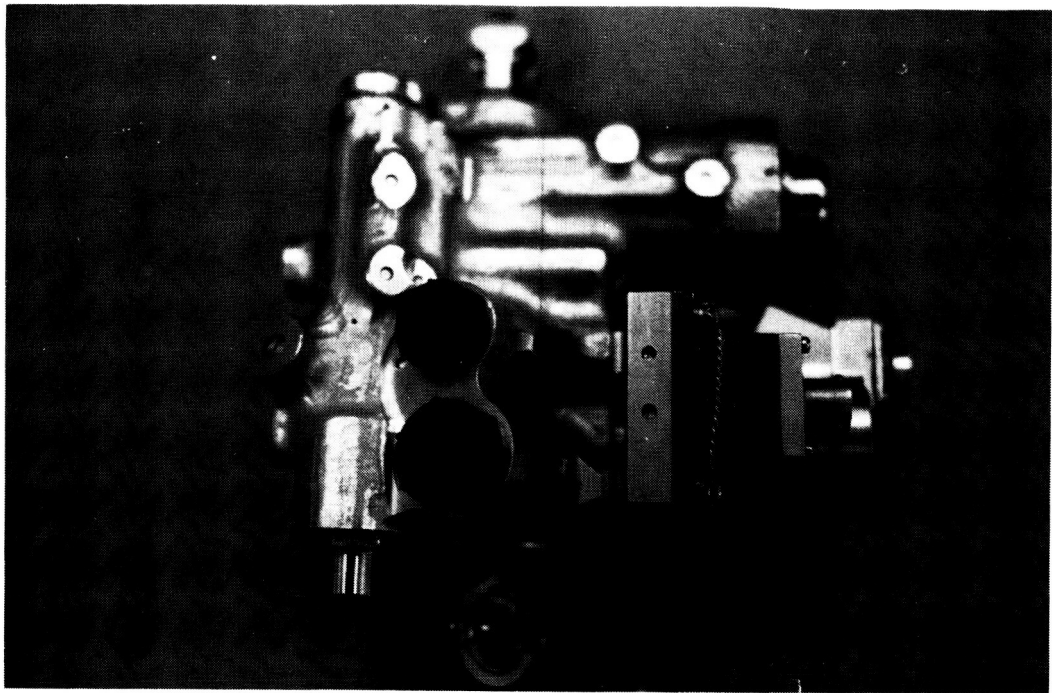


CONTROL SYSTEM STIFFNESS AND FREEPLAY
Figure 11

3045 JAMING
YTLAUD R009

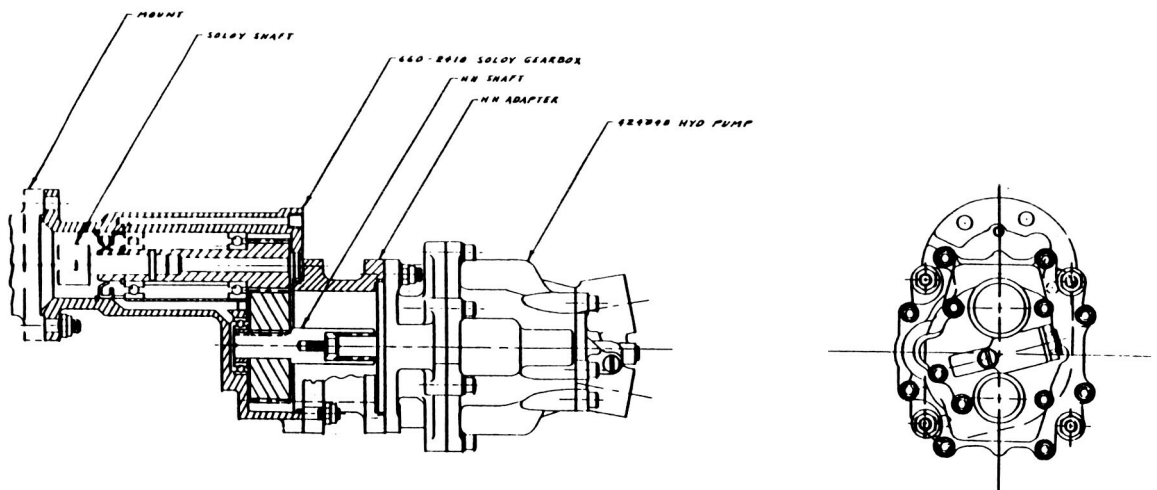


HHC ACTUATOR SCHEMATIC
Figure 12



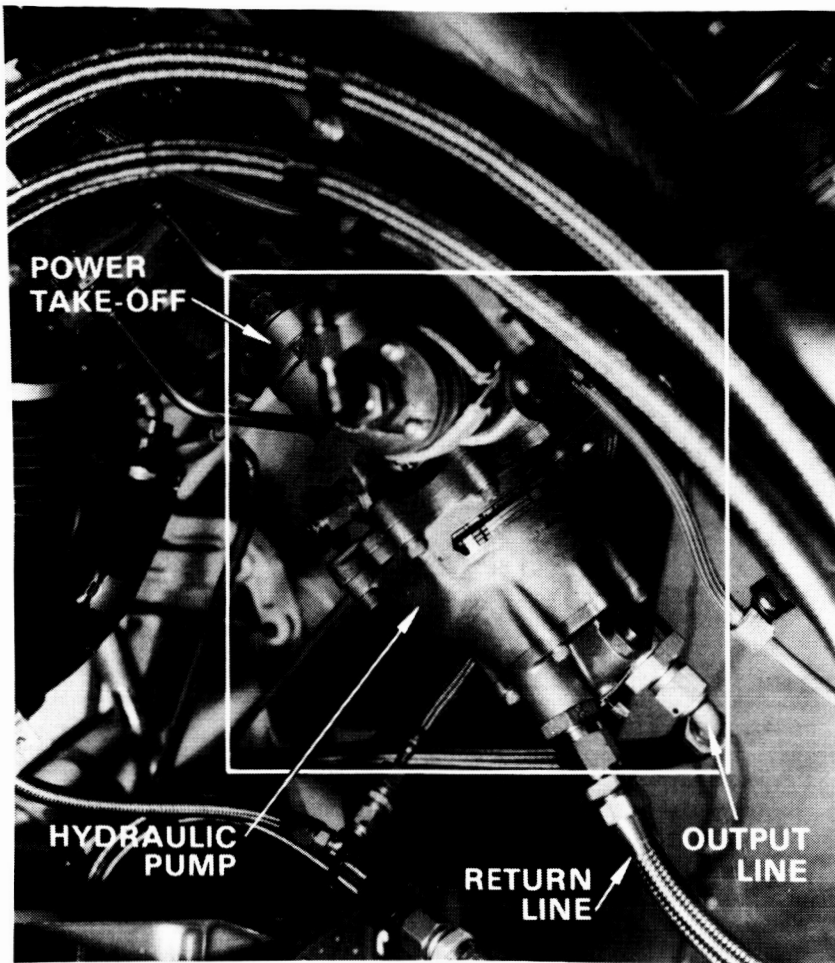
HHC ACTUATOR
Figure 13

**ORIGINAL PAGE IS
OF POOR QUALITY**

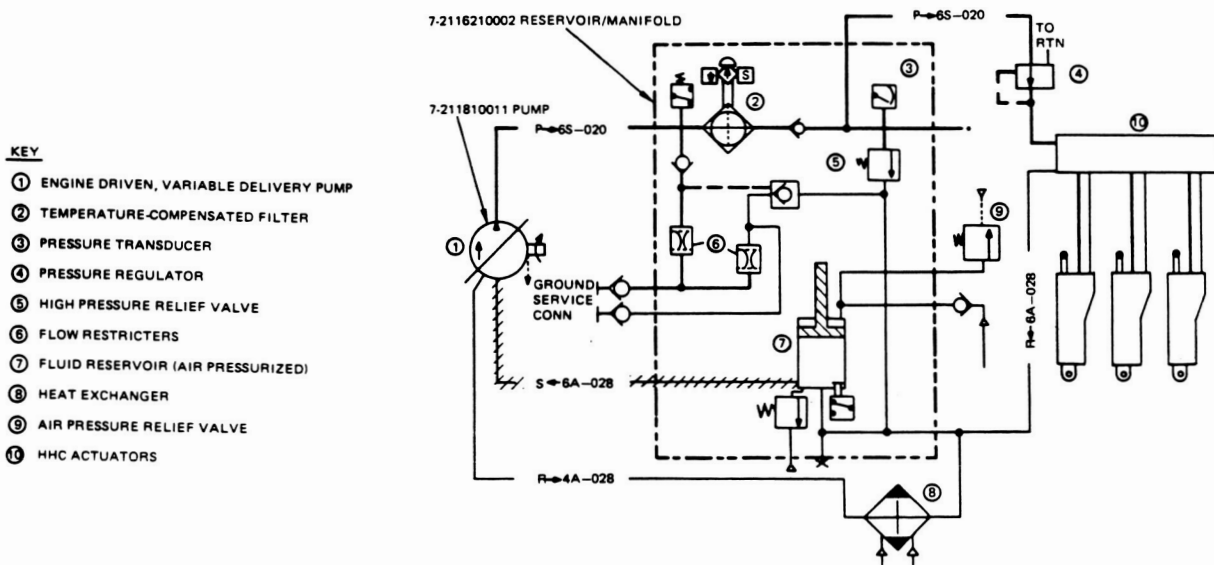


HHC HYDRAULIC PUMP
Figure 14

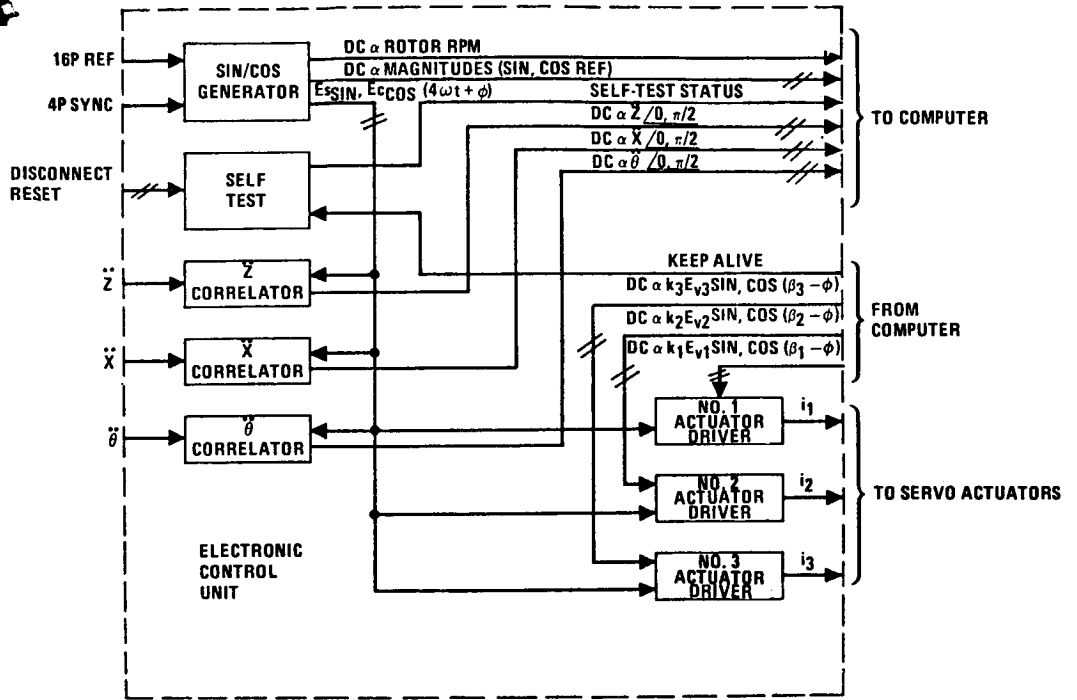
ORIGINAL PAGE IS
OF POOR QUALITY



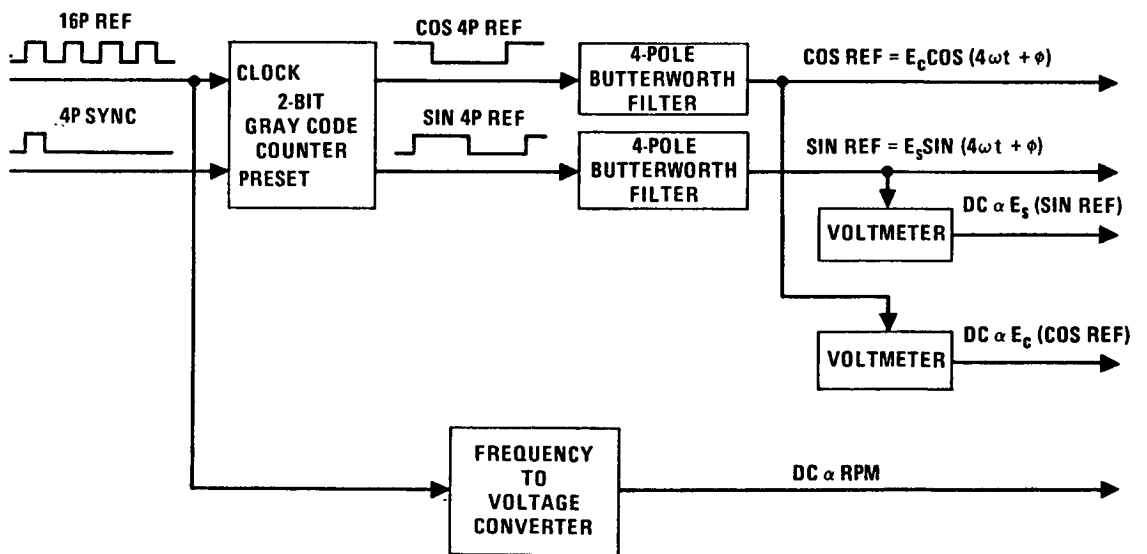
HHC HYDRAULIC PUMP INSTALLATION
Figure 15



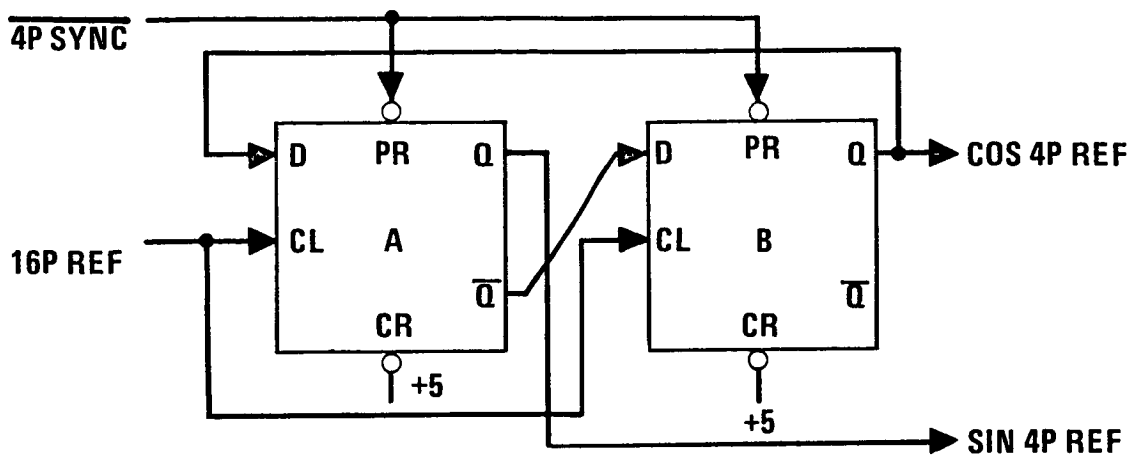
HHC HYDRAULIC SCHEMATIC
Figure 16



ELECTRONIC CONTROL UNIT BLOCK DIAGRAM
Figure 17



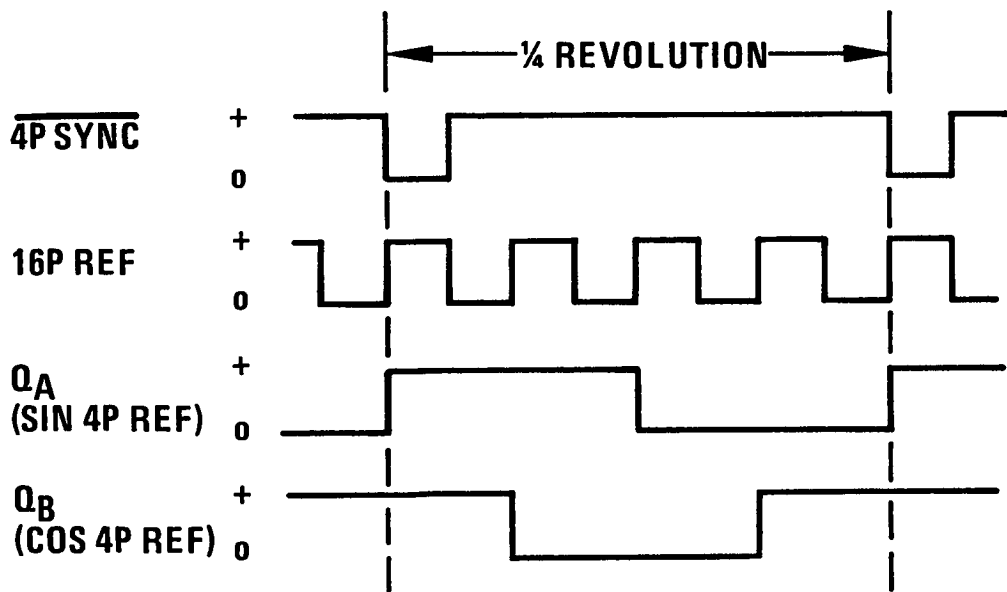
SINE/COSINE GENERATOR BLOCK DIAGRAM
Figure 18



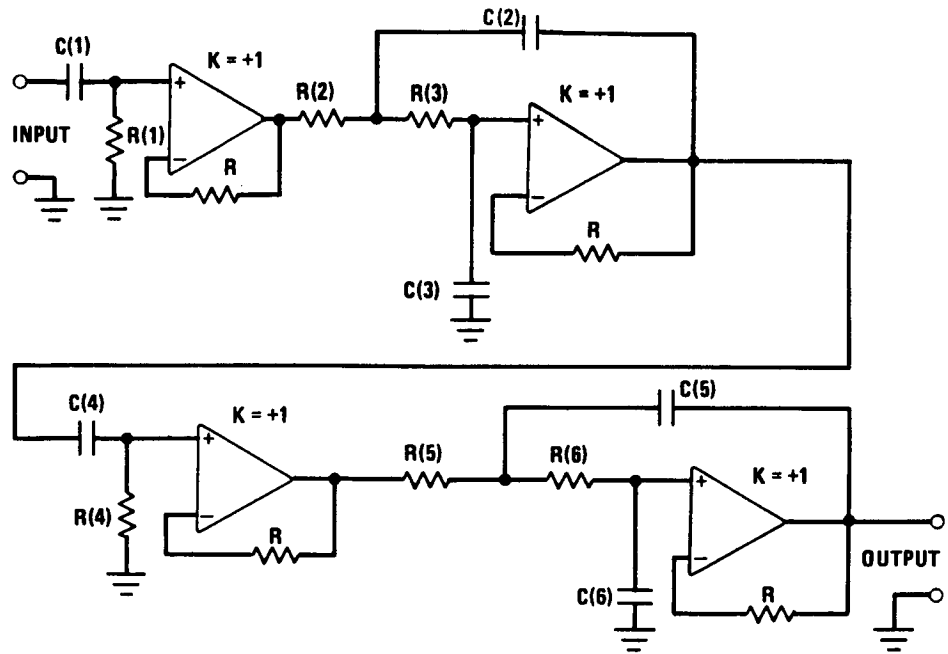
• D-FLIP/FLOP CHARACTERISTICS

- WHEN PR GOES LOW, Q LATCHES HIGH (TRUE)
- \bar{Q} = Q INVERTED
- ON THE RISING EDGE OF THE CL PULSE, Q COPIES D

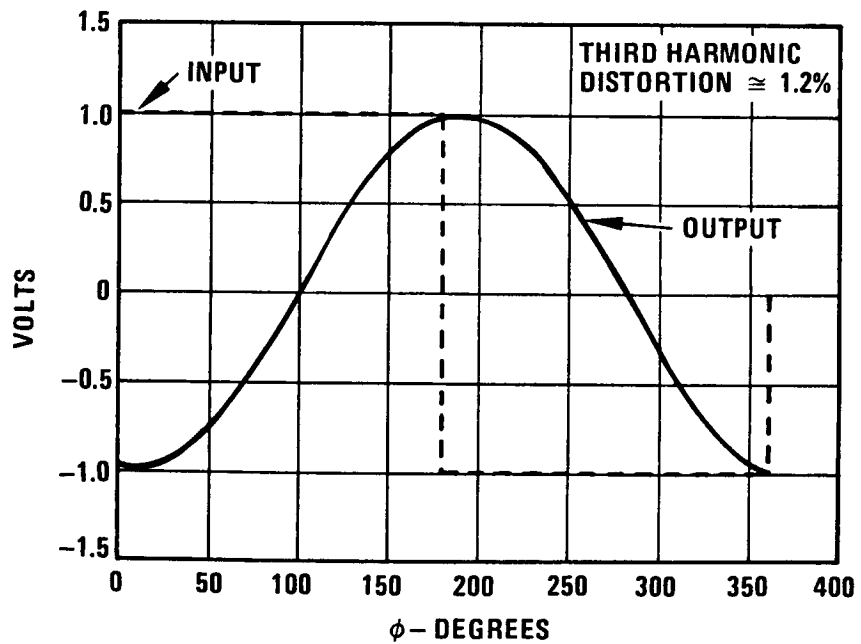
TWO-BIT GRAY CODE COUNTER
Figure 19



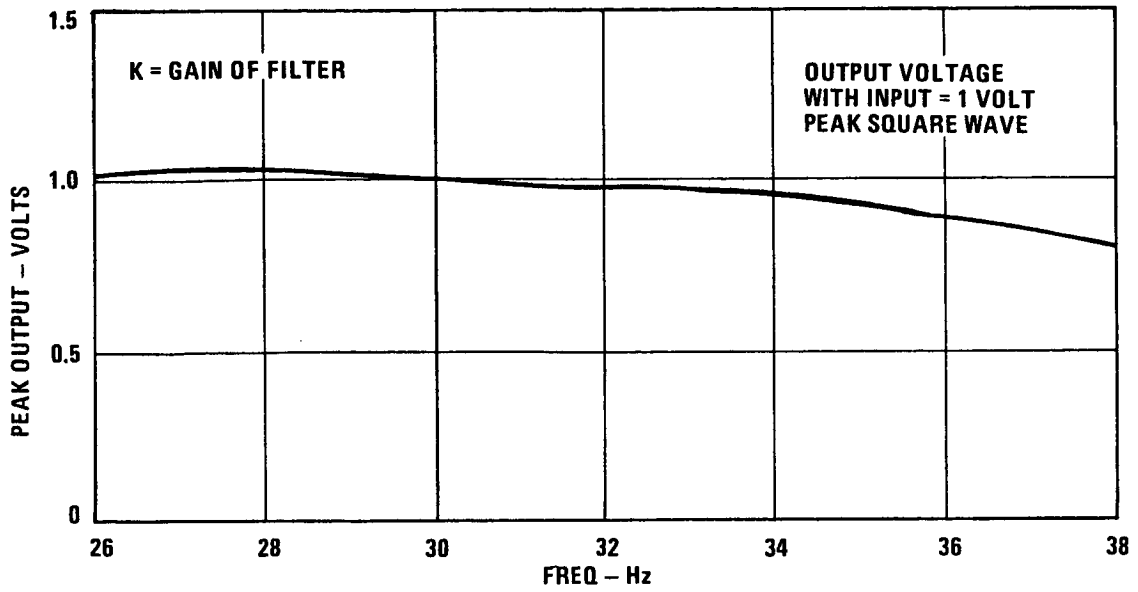
TWO-BIT GRAY CODE COUNTER TIMING DIAGRAM
Figure 20



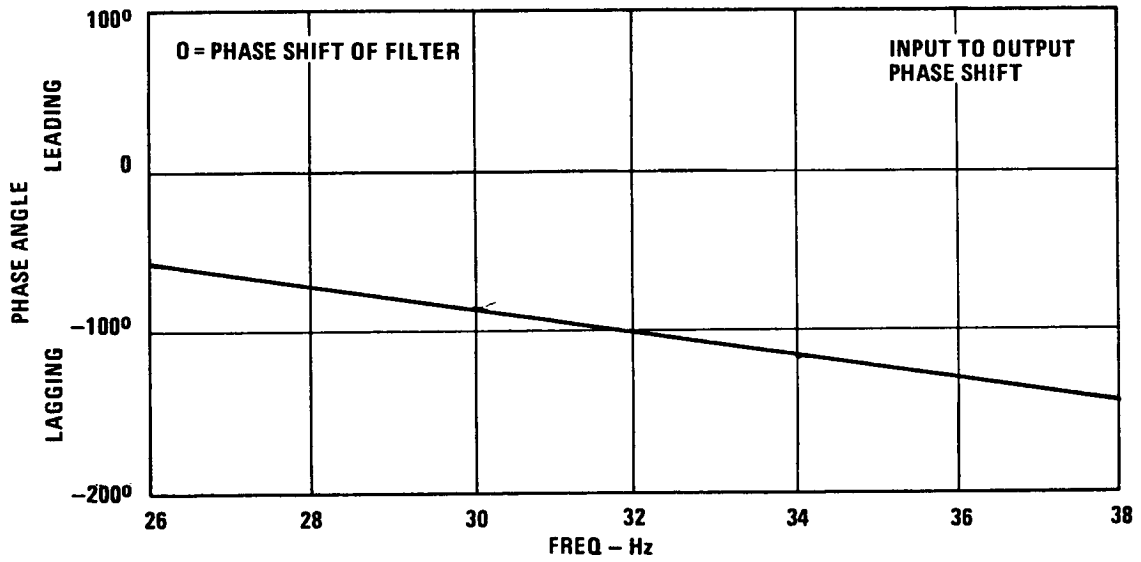
4 POLE BUTTERWORTH AND 2 POLE RC BAND PASS FILTER
 Pass Band is 26 to 38 Hz
 Figure 21



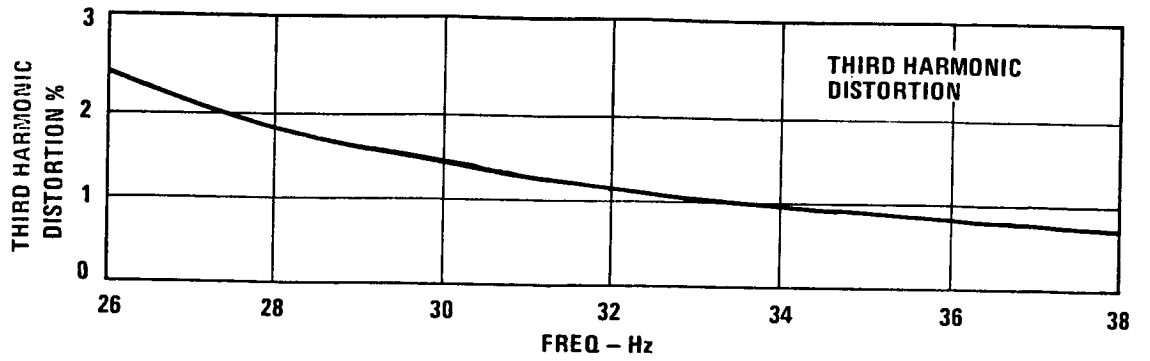
SIMULATED BANDPASS FILTER
 Input Frequency is 32 Hz
 Figure 22



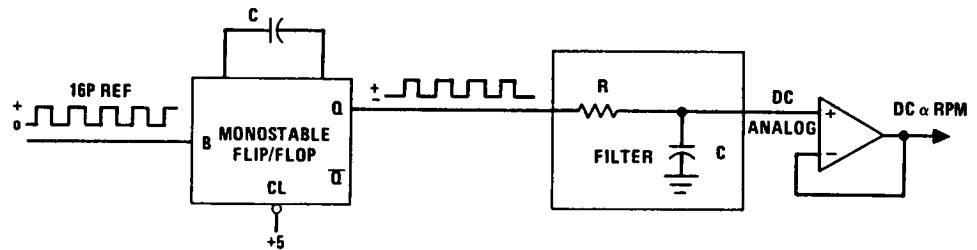
SIMULATED BANDPASS FILTER GAIN
Figure 23



SIMULATED BANDPASS FILTER PHASE SHIFT
Figure 24



SIMULATED BANDPASS FILTER DISTORTION
Figure 25



- MONOSTABLE FLIP/FLOP CHARACTERISTICS
 - EACH TIME THE INPUT TRANSITIONS FROM 0 TO +VOLTAGE, Q GOES TO A PLUS OUTPUT FOR A FIXED PERIOD OF TIME
 - THE EXTERNAL CAPACITOR, C, IS CHOSEN TO GIVE THE DESIRED DURATION OF THE Q OUTPUT PULSE
- FILTER CHARACTERISTICS
 - THE FILTER BLOCKS THE AC SIGNAL AND ALLOWS ONLY THE DC COMPONENT TO PASS THE AMPLIFIER
- TIMING

LOW RPM

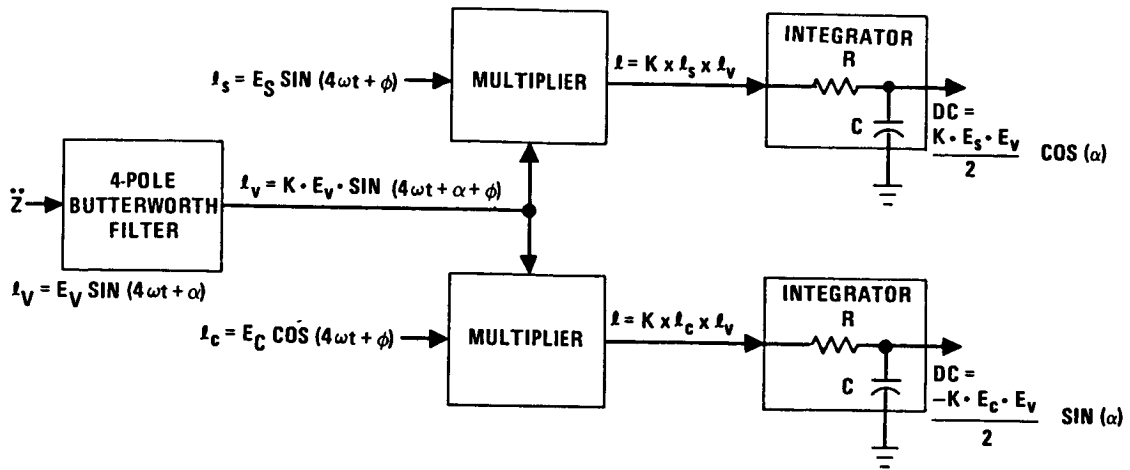
AVE (DC) IS LOW

HIGH RPM

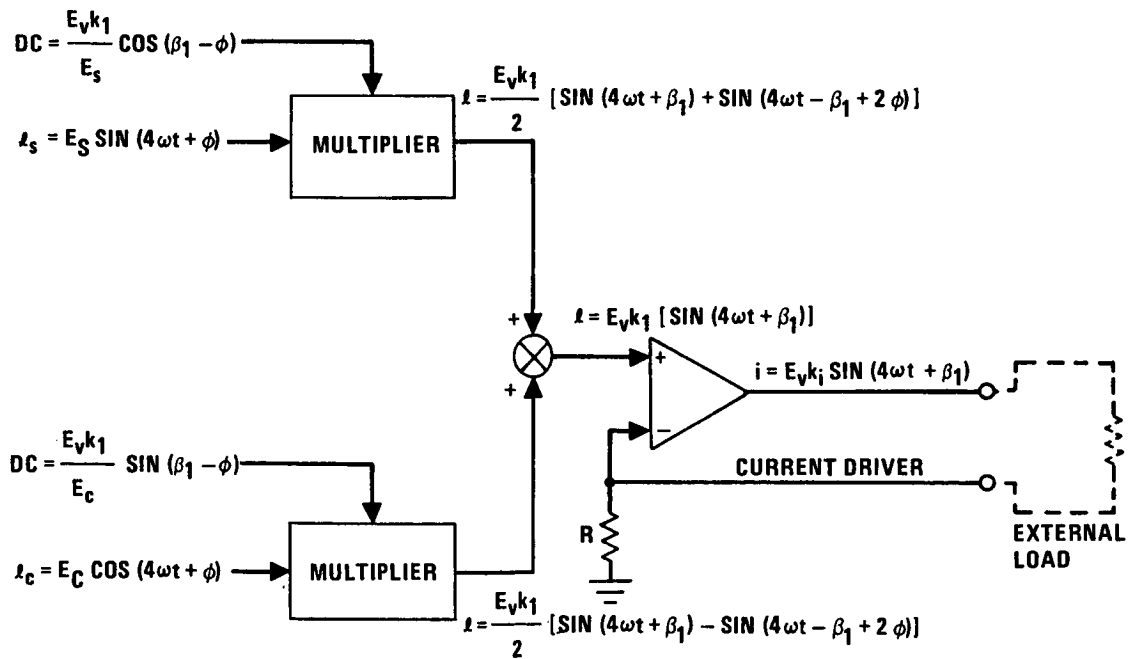
AVE (DC) IS HIGH

PULSE DURATION = CONSTANT
- DC OUTPUT IS DIRECTLY PROPORTIONAL TO FREQUENCY

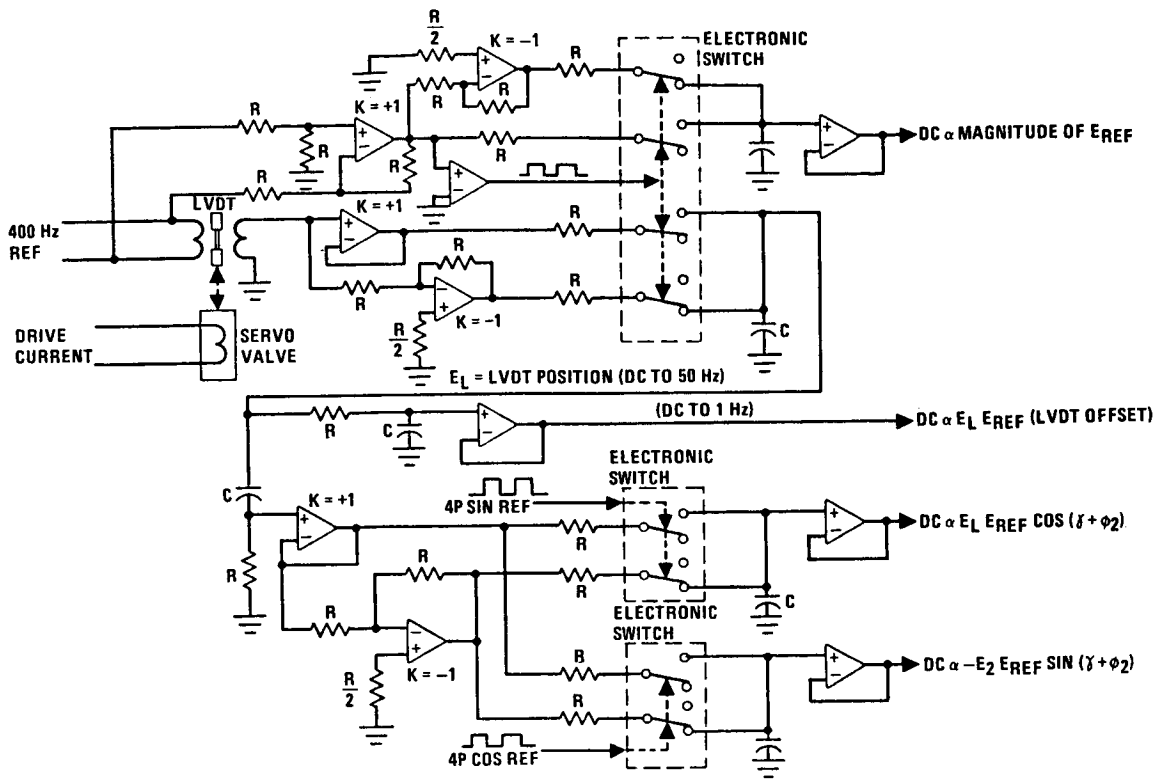
TYPICAL FREQUENCY TO VOLTAGE CONVERTER
Figure 26



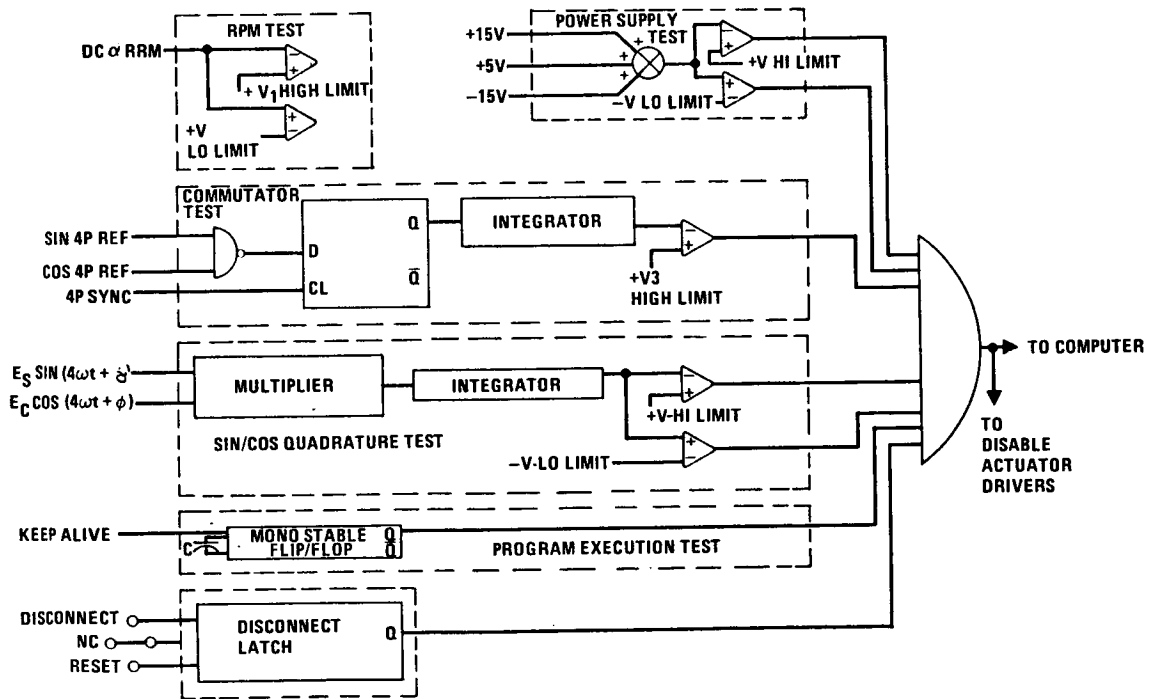
ECU CORRELATOR BLOCK DIAGRAM
Figure 27



ACTUATOR DRIVER BLOCK DIAGRAM
Figure 28

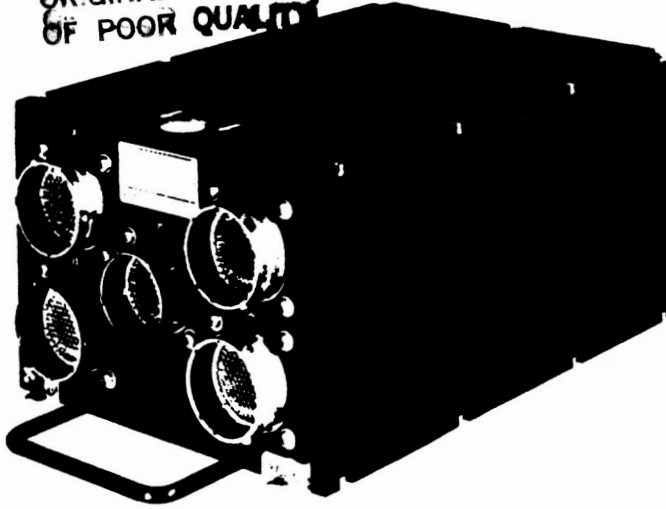


LVDT DEMODULATOR - One Channel
Figure 29

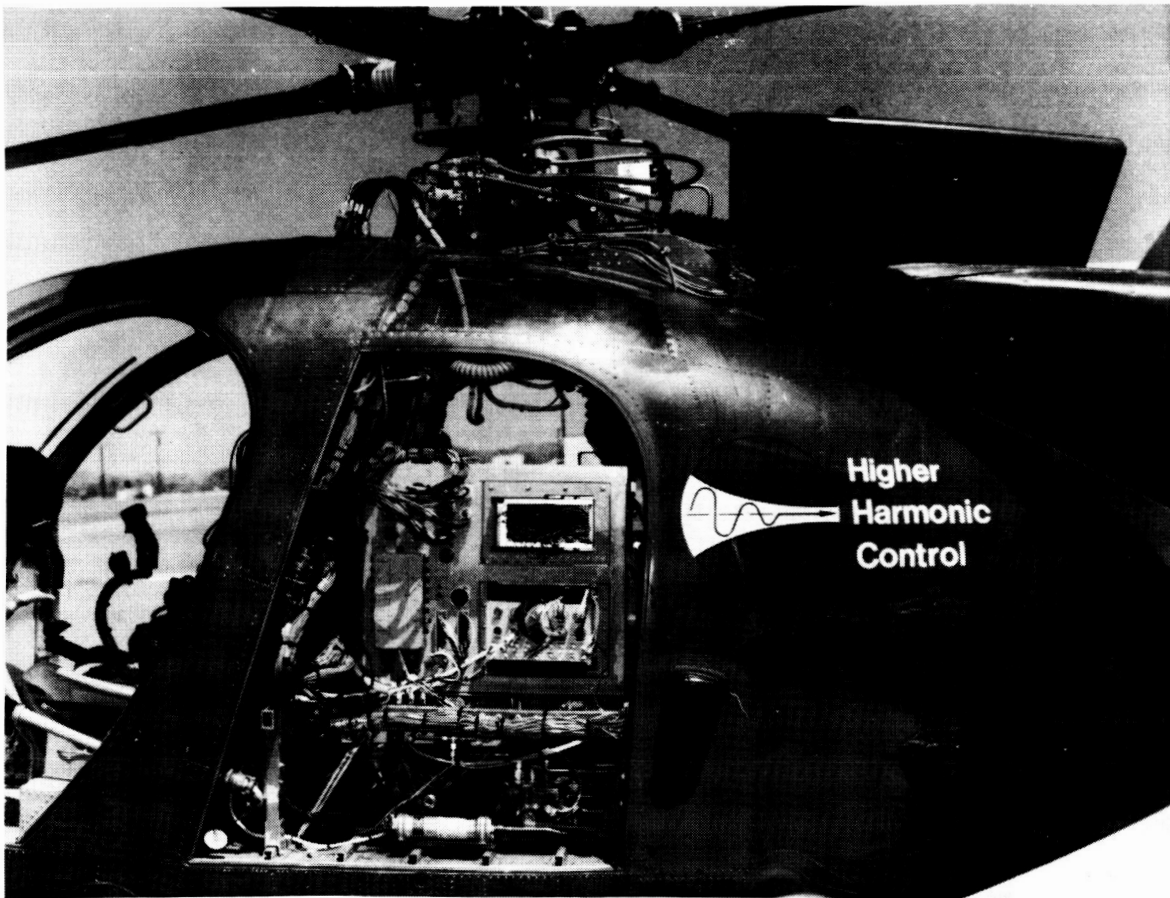


SELF TEST BLOCK DIAGRAM
Figure 30

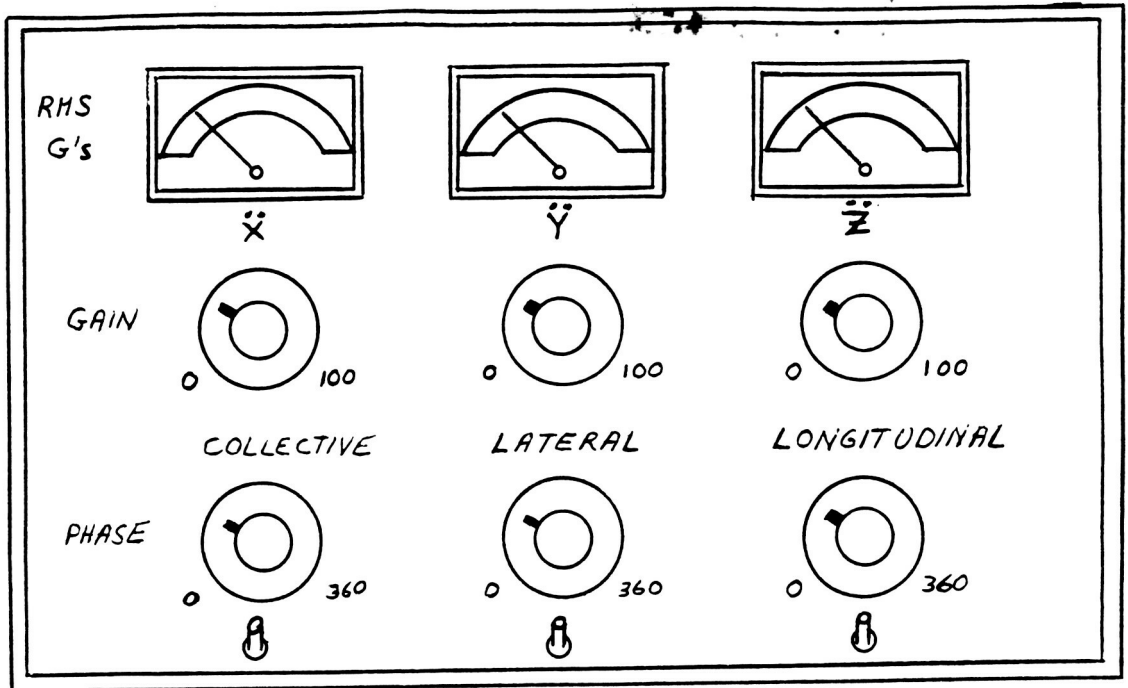
ORIGINAL PAGE IS
OF POOR QUALITY



SPERRY SDP-175 DIGITAL COMPUTER
Figure 31



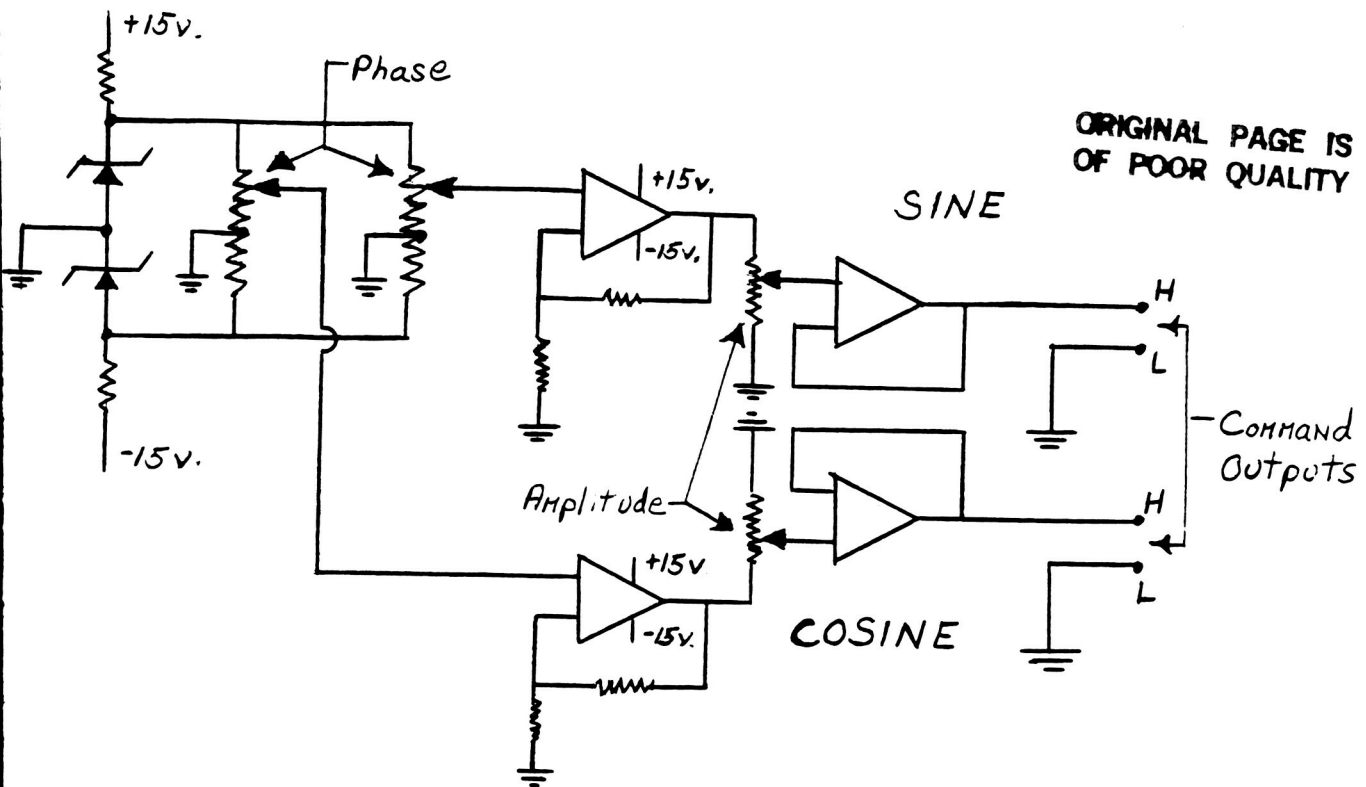
AIRBORNE DATA ACQUISITION SYSTEM (ADAS) INSTALLATION
Figure 32



OPEN LOOP CONTROLLER SCHEMATIC
Figure 33



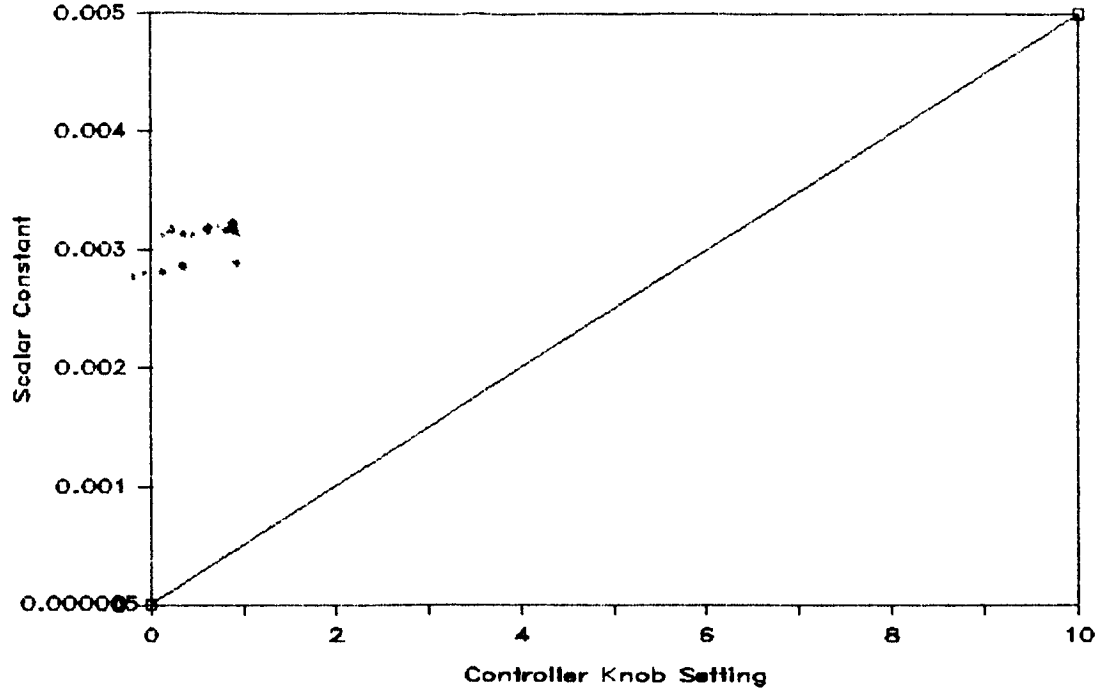
OPEN LOOP CONTROLLER
Figure 34



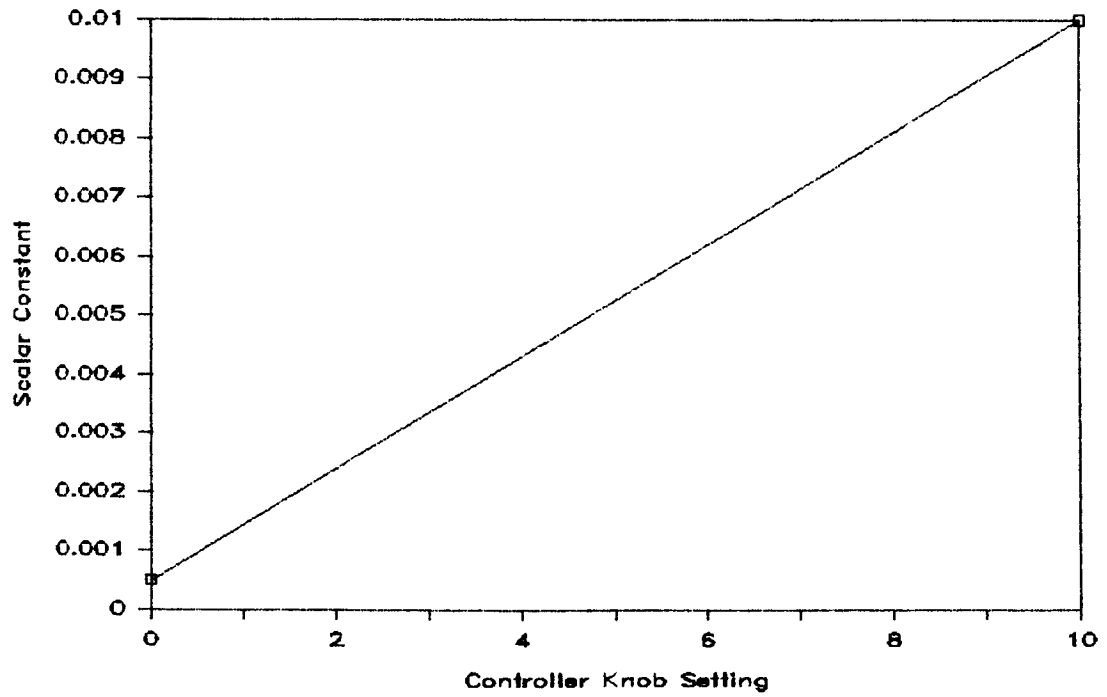
OPEN LOOP CONTROLLER COMMAND GENERATION - One Channel
Figure 35



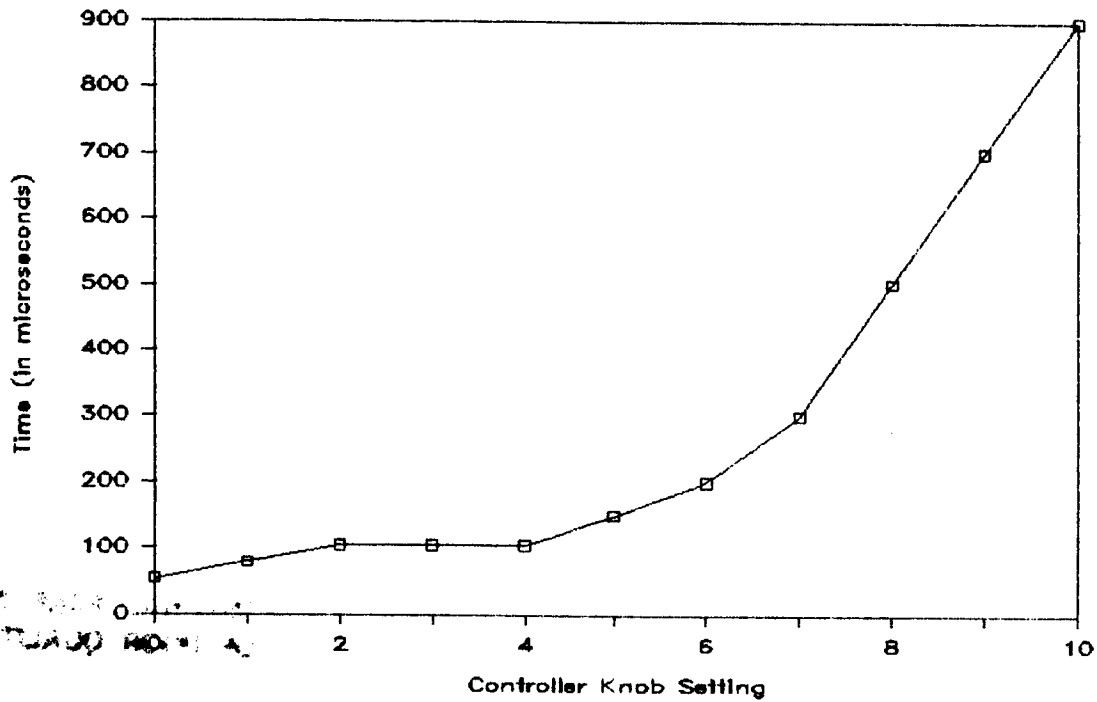
HHC COCKPIT CONTROL PANEL
Figure 36



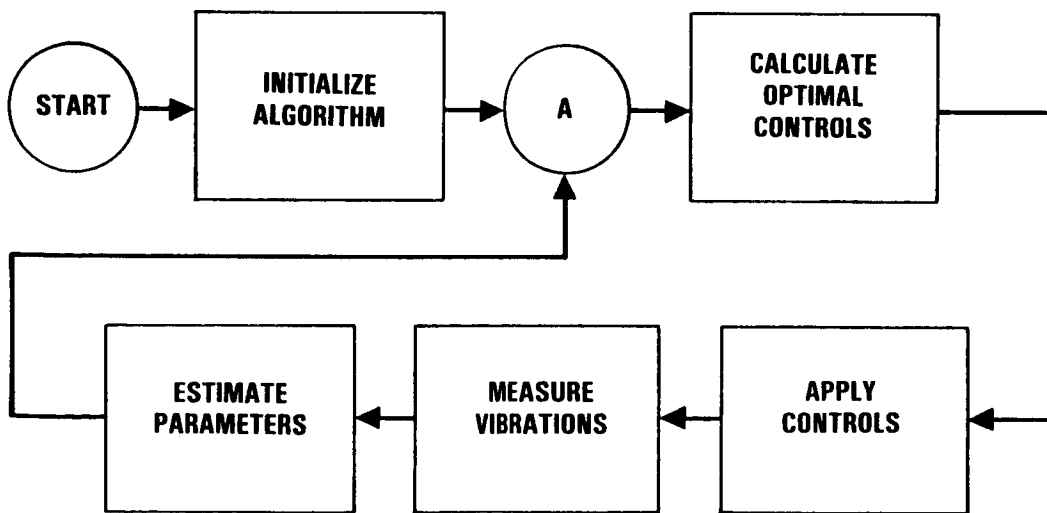
PROCESS NOISE GAIN POT SETTING
Figure 37



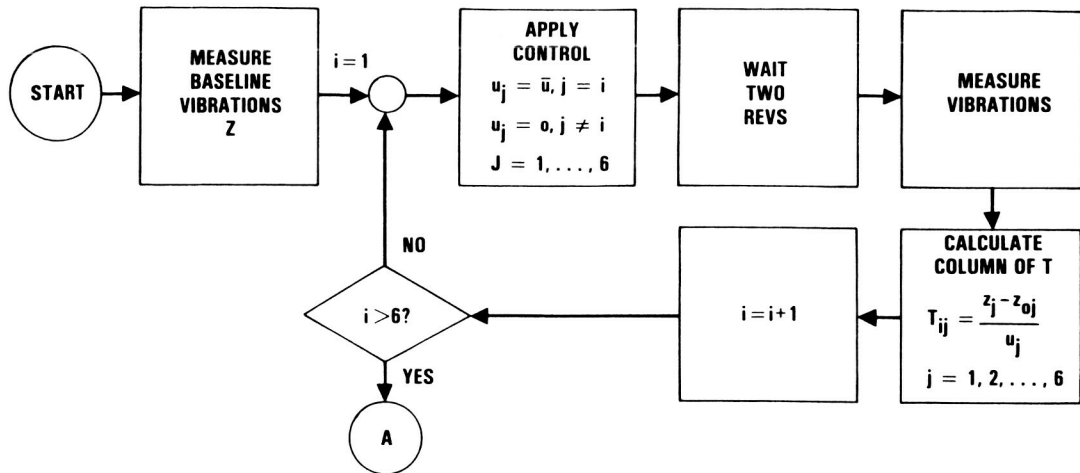
MEASUREMENT NOISE GAIN POT SETTING
Figure 38



TIME DELAY GAIN POT SETTING
Figure 39



SCHEMATIC OF THE CONTROLLER OPERATION
Figure 40

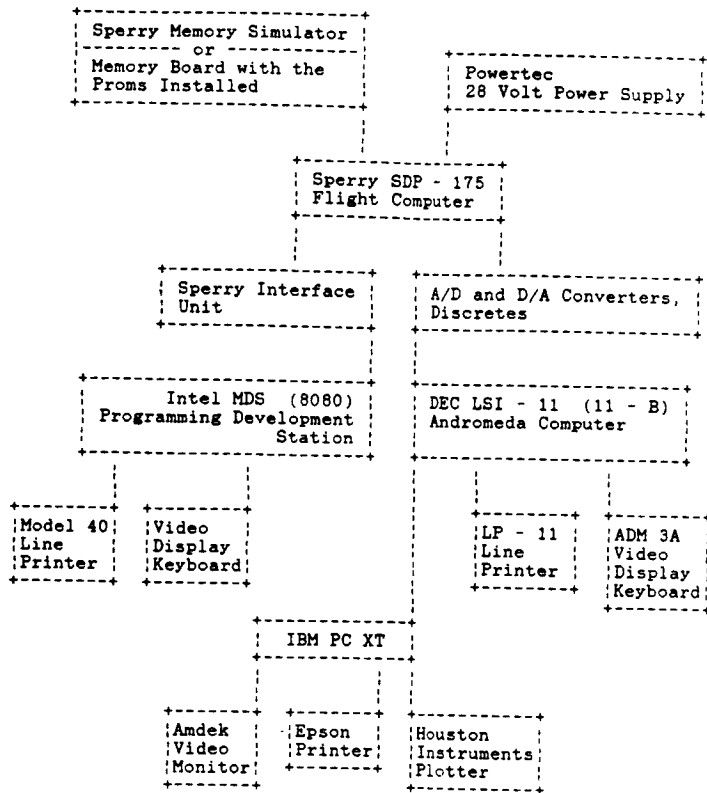


**ORIGINAL PAGE IS
OF POOR QUALITY**

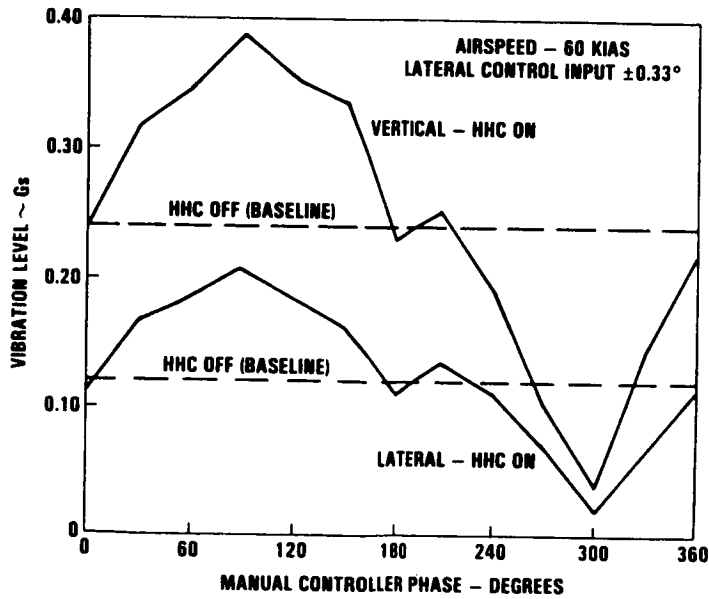
SCHEMATIC OF THE CONTROLLER INITIALIZATION
Figure 41



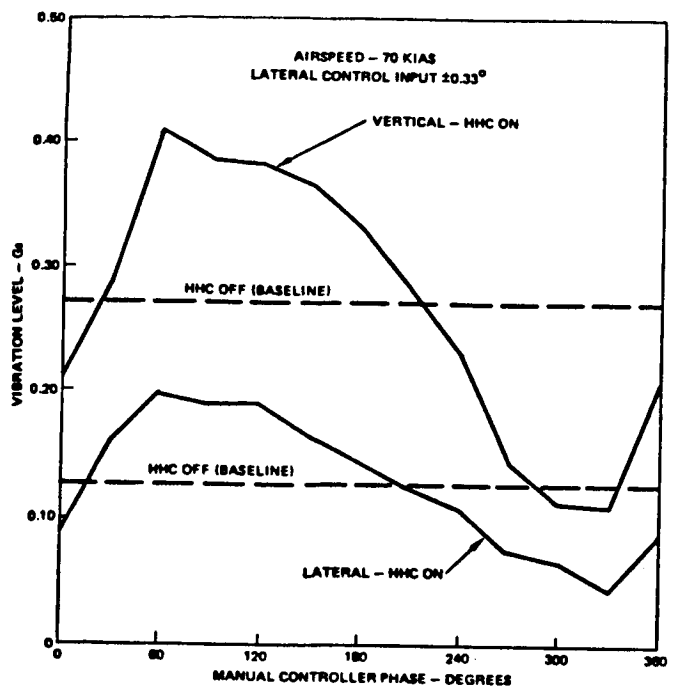
MDHC HIGHER HARMONIC CONTROL SIMULATION LABORATORY
Figure 42



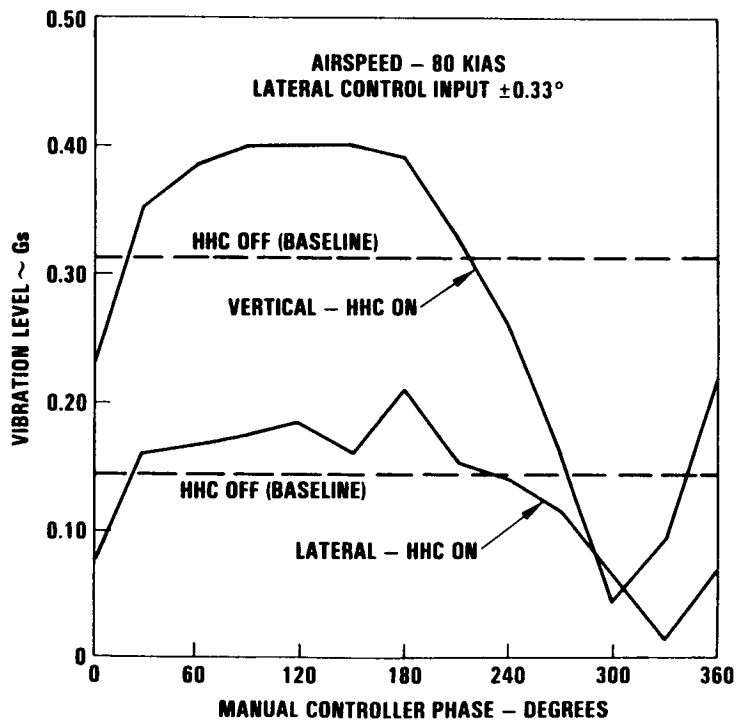
BLOCK DIAGRAM OF THE HHC SIM LAB
Figure 43



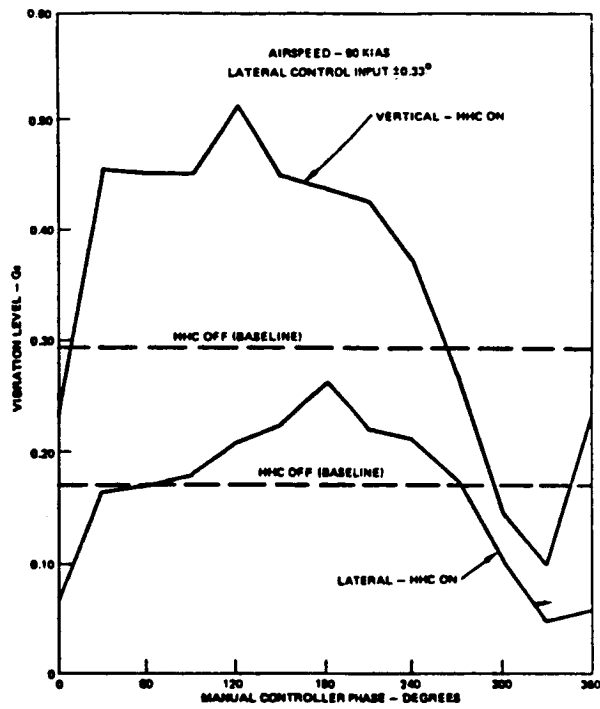
VARIATION OF 4P VIBRATION WITH INPUT PHASE AT 60 KNOTS
Figure 44



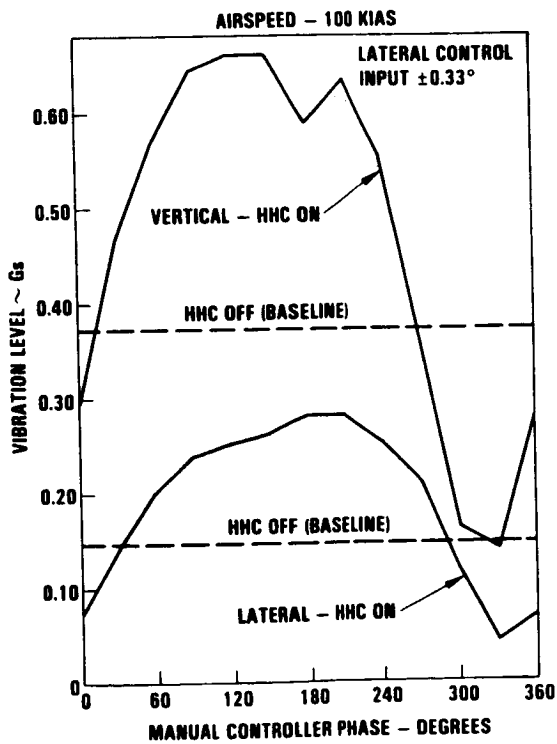
VARIATION OF 4P VIBRATION WITH INPUT PHASE AT 70 KNOTS
Figure 45



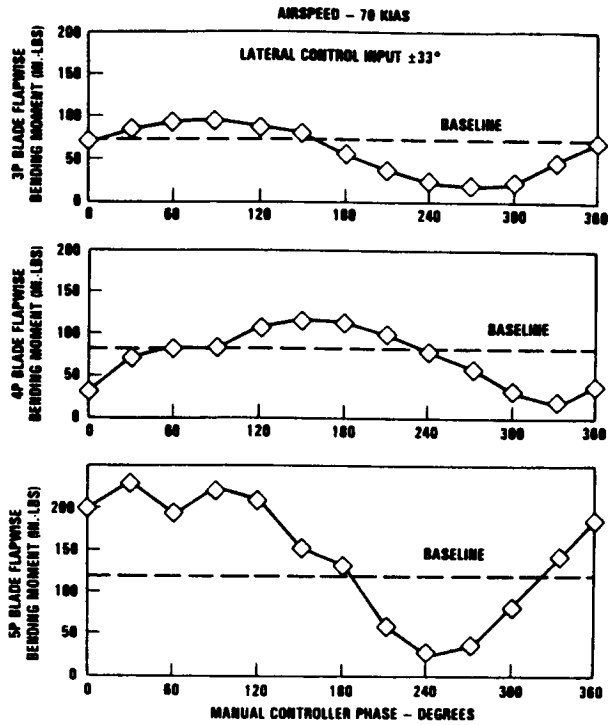
VARIATION OF 4P VIBRATION WITH INPUT PHASE AT 80 KNOTS
Figure 46



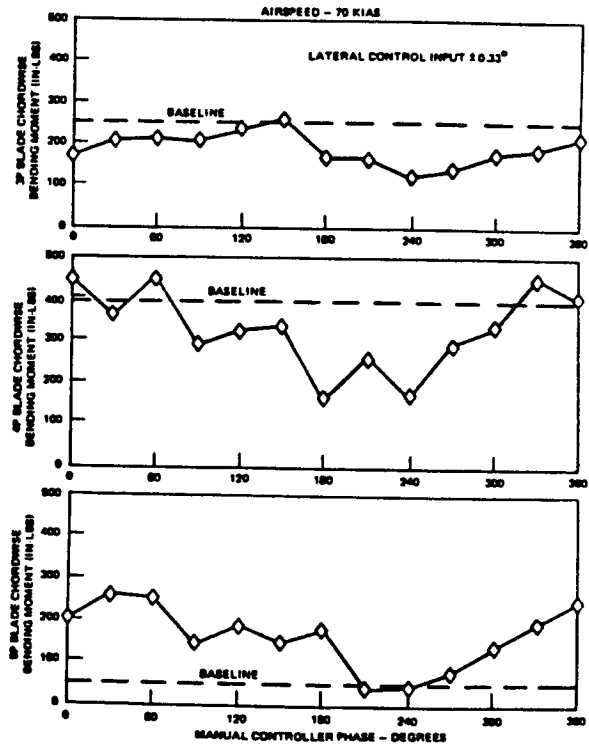
VARIATION OF 4P VIBRATION WITH INPUT PHASE AT 90 KNOTS
Figure 47



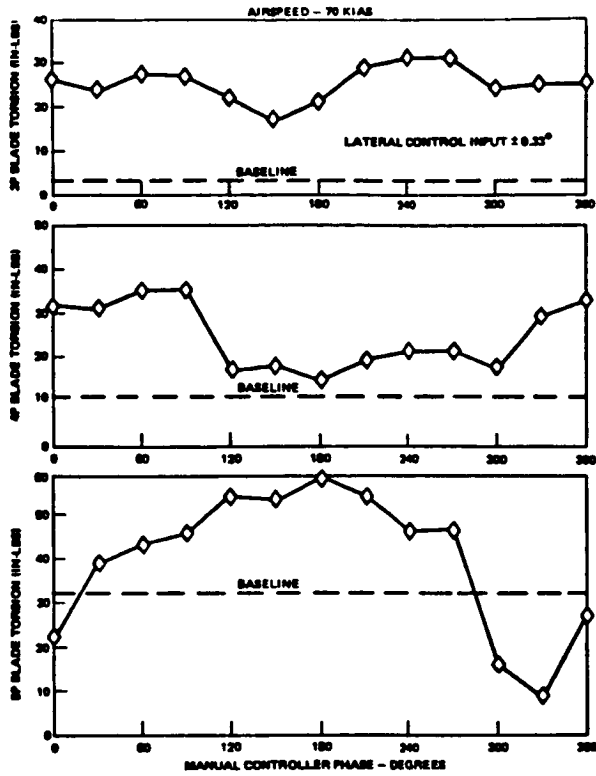
VARIATION OF 4P VIBRATION WITH INPUT PHASE AT 100 KNOTS
Figure 48



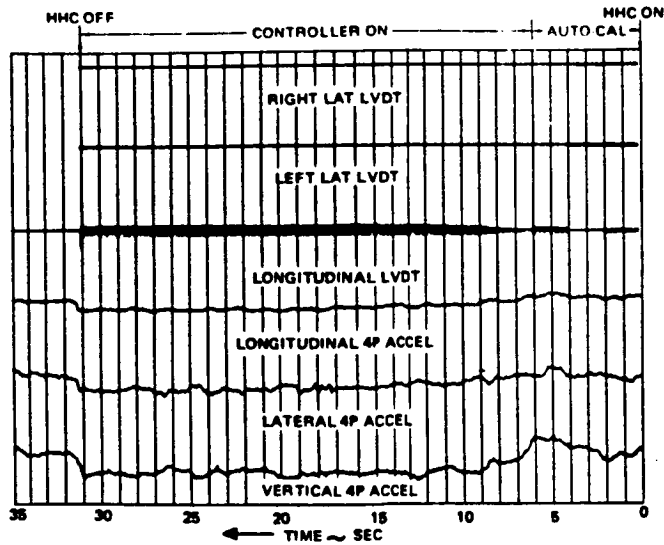
THE EFFECT OF HHC ON 3P, 4P AND 5P FLAPWISE BLADE BENDING
AT $r/R = 15\%$
Figure 49



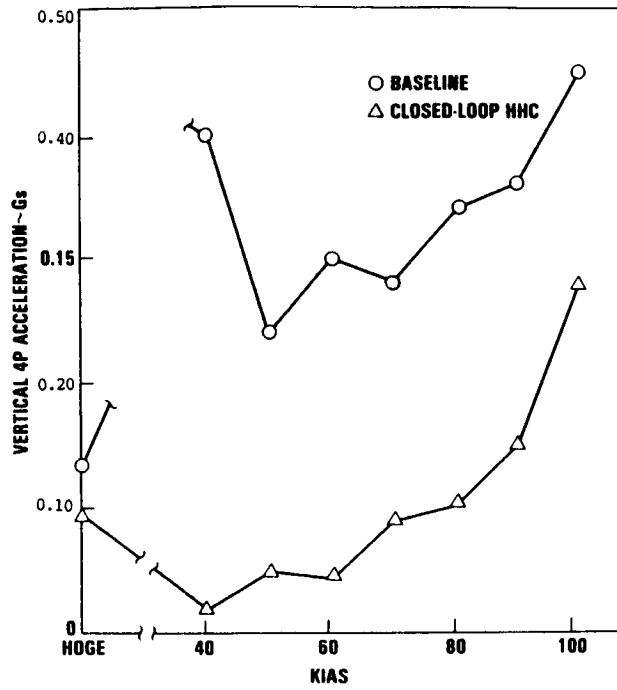
THE EFFECT OF HHC ON 3P, 4P AND 5P CHORDWISE BLADE BENDING
AT $r/R = 17\%$
Figure 50



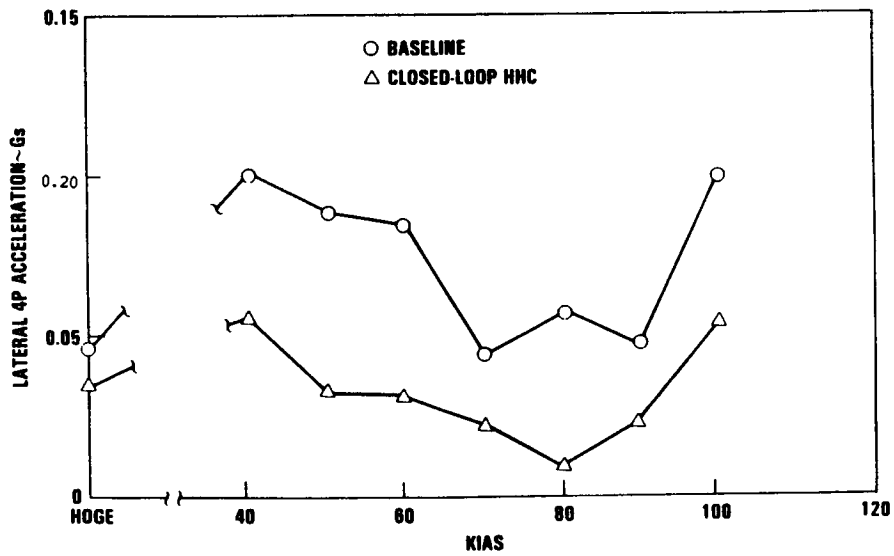
THE EFFECT OF HHC ON 3P, 4P AND 5P BLADE TORSION
 AT $r/R = 17\%$
 Figure 51



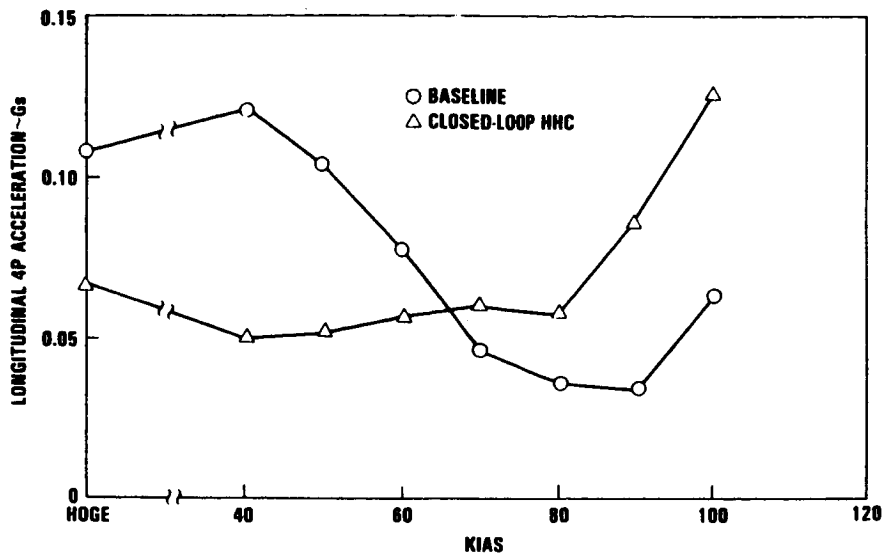
60 KNOTS CLOSED LOOP ENGAGEMENT
 Figure 52



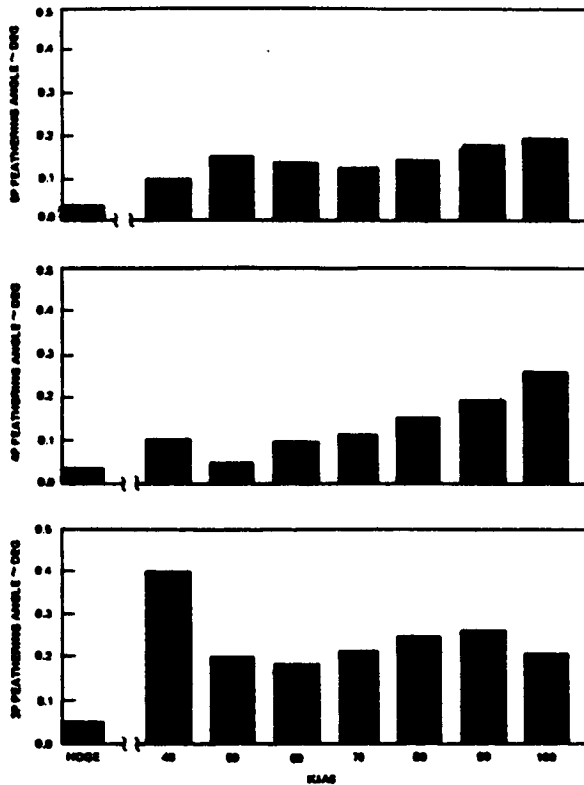
1983 CLOSED LOOP HHC
 4P VERTICAL PILOT ACCELERATIONS VERSUS AIRSPEED
 Figure 53



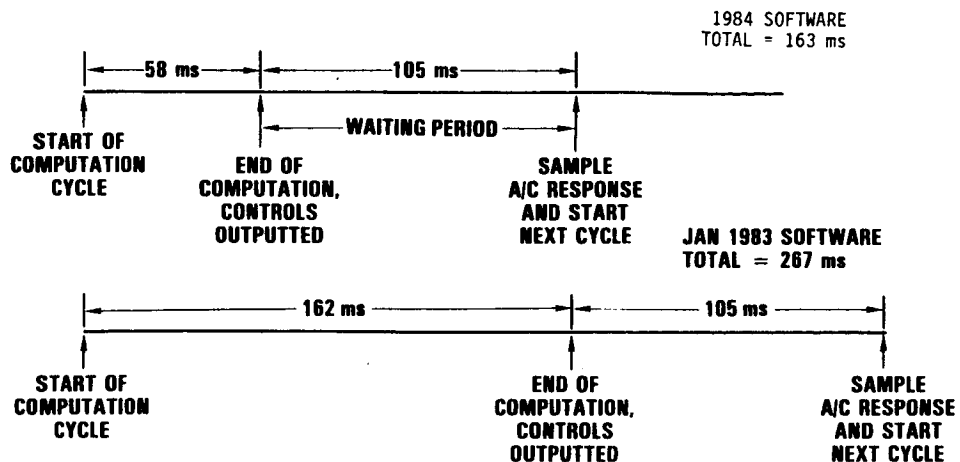
1983 CLOSED LOOP HHC
 4P LATERAL PILOT SEAT VIBRATIONS VERSUS AIRSPEED
 Figure 54



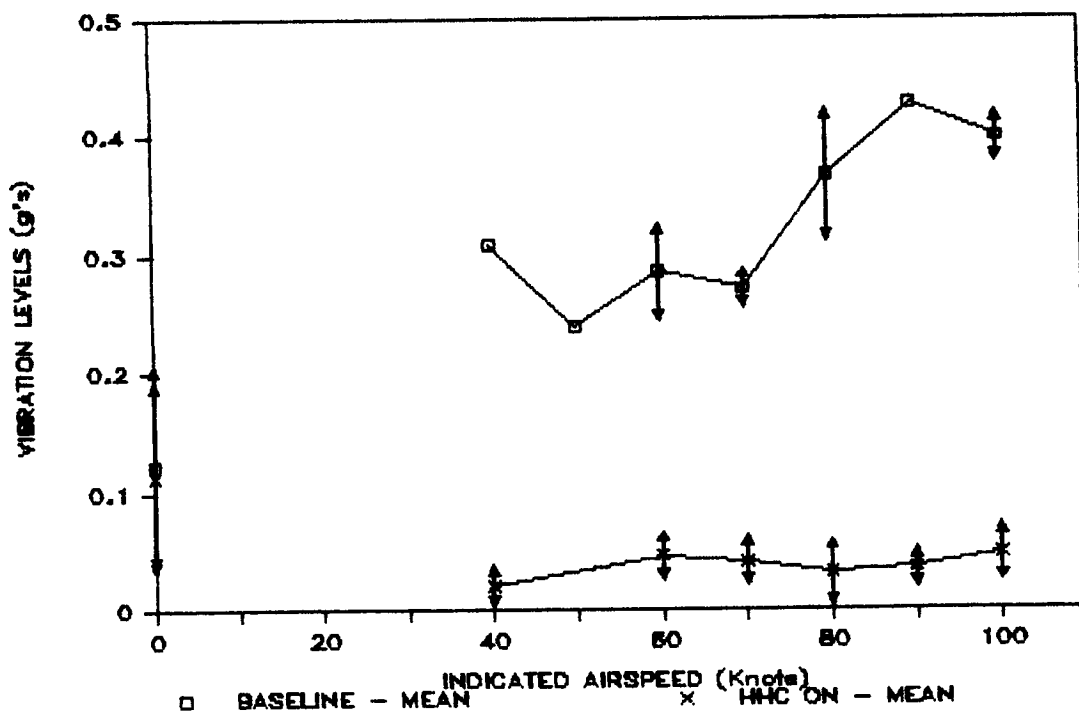
1983 CLOSED LOOP HHC
 4P LONGITUDINAL PILOT ACCELERATIONS VERSUS AIRSPEED
 Figure 55



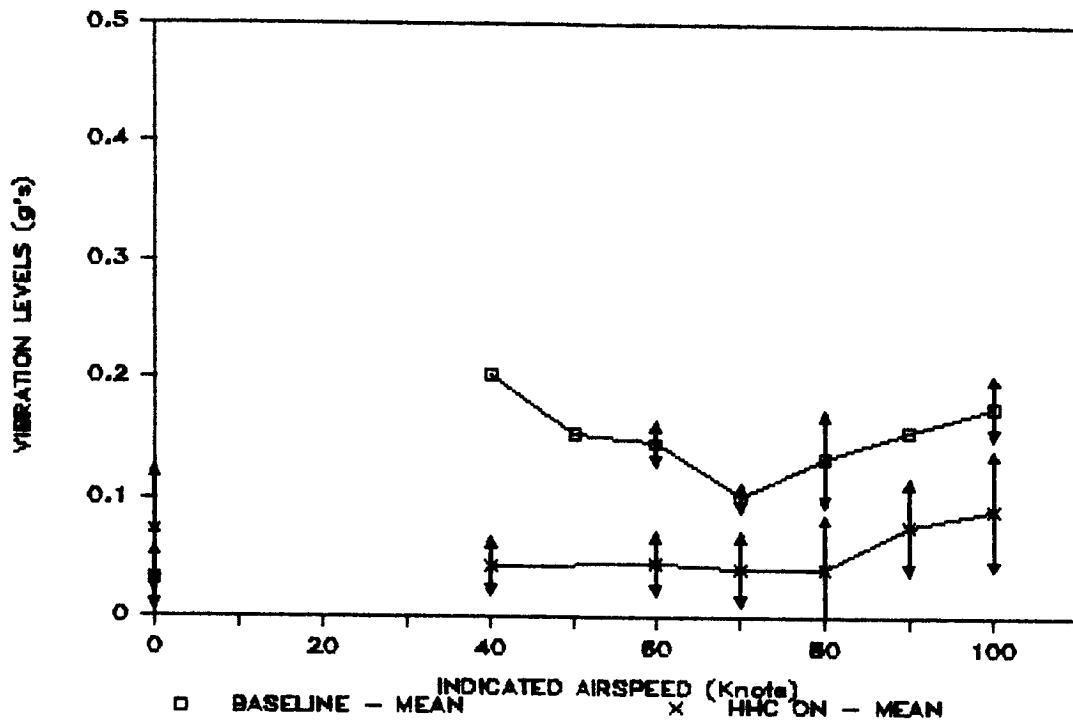
1983 CLOSED LOOP HHC
 3P, 4P AND 5P OPTIMAL BLADE FEATHERING ANGLE VERSUS AIRSPEED
 Figure 56



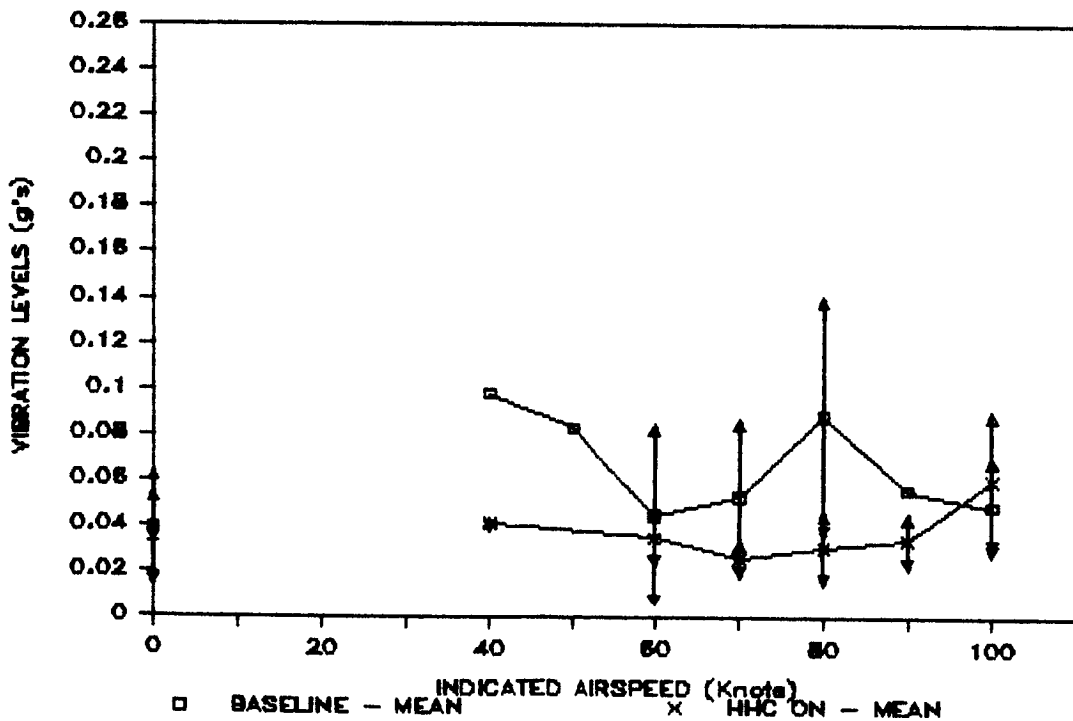
SOFTWARE EXECUTION SPEED COMPARISON
Figure 57



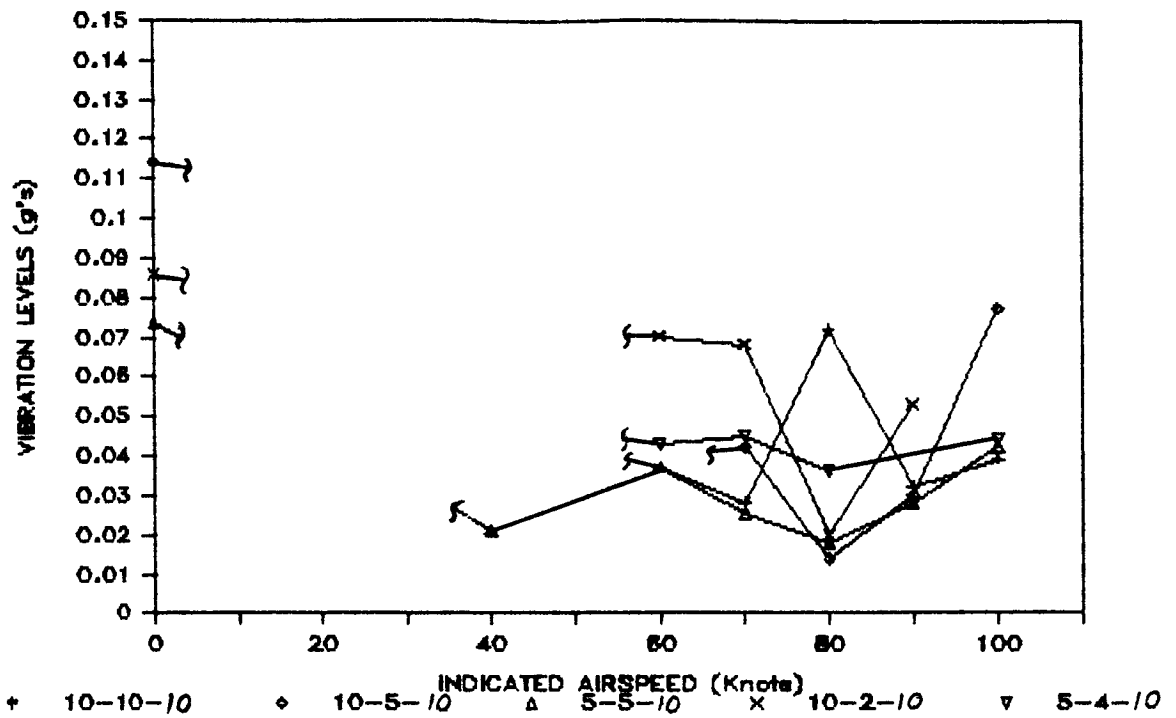
1984 CLOSED LOOP HHC
4P VERTICAL PILOT SEAT VIBRATIONS VERSUS AIRSPEED
Figure 58



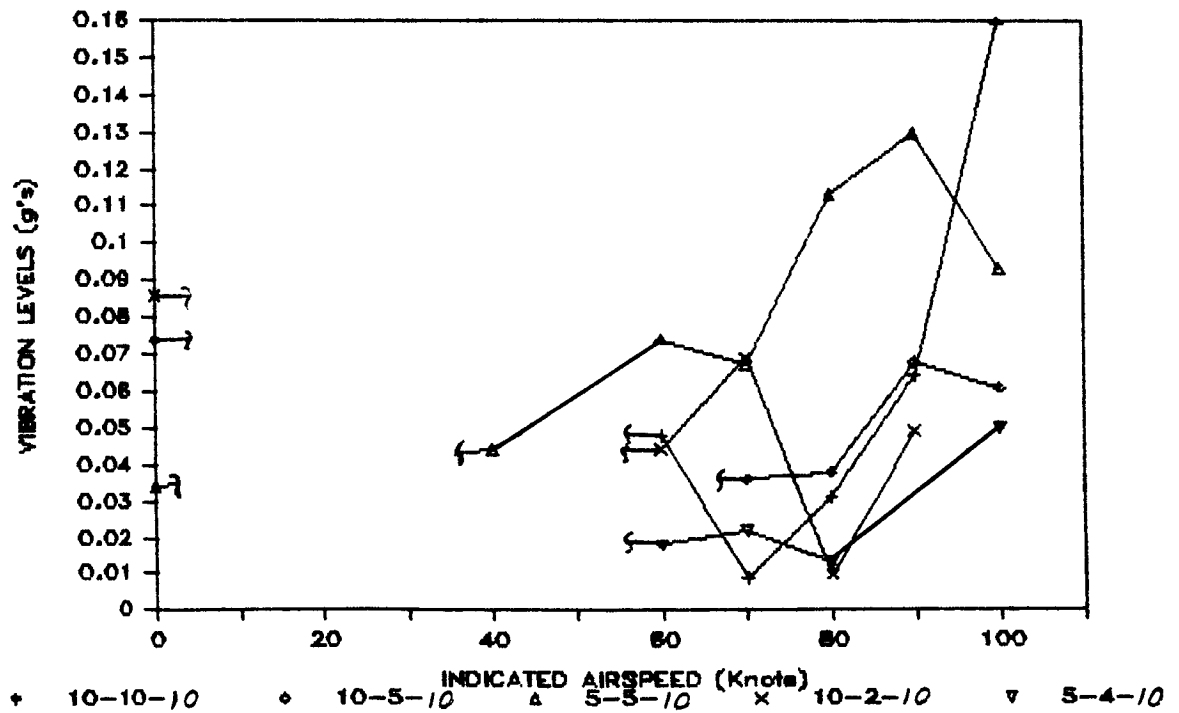
1984 CLOSED LOOP HHC
 4P LATERAL PILOT SEAT VIBRATIONS VERSUS AIRSPEED
 Figure 59



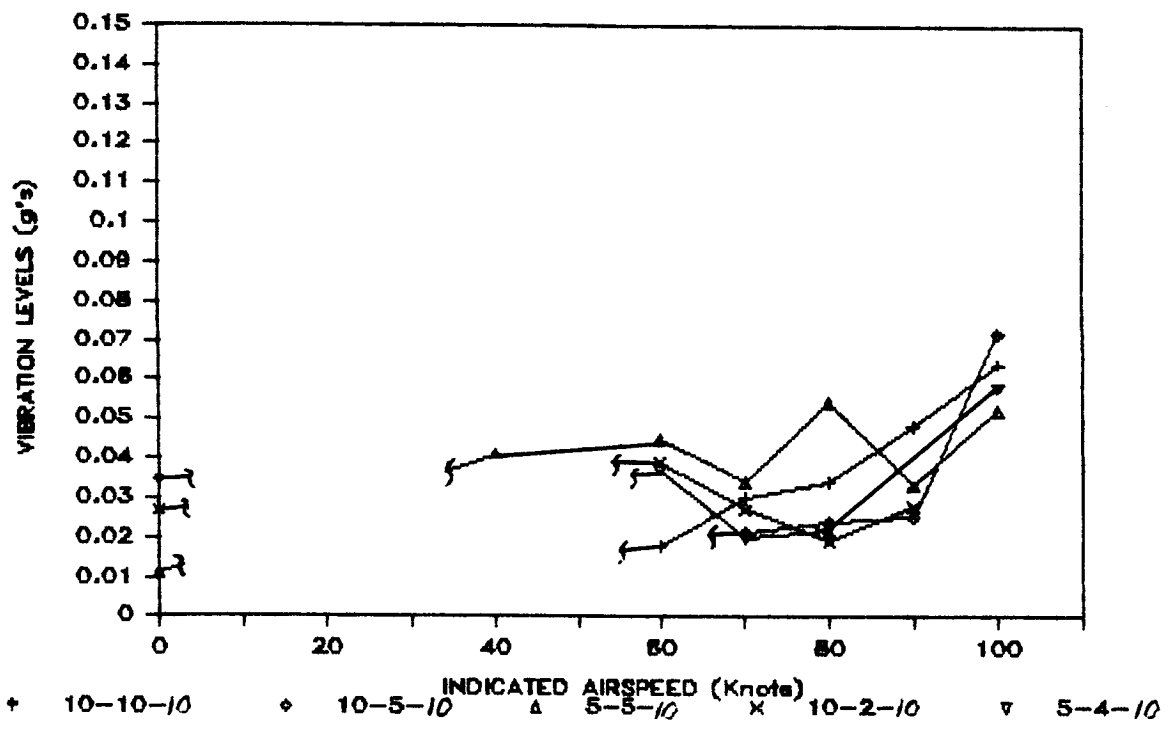
1984 CLOSED LOOP HHC
 4P LONGITUDINAL PILOT SEAT VIBRATIONS VERSUS AIRSPEED
 Figure 60



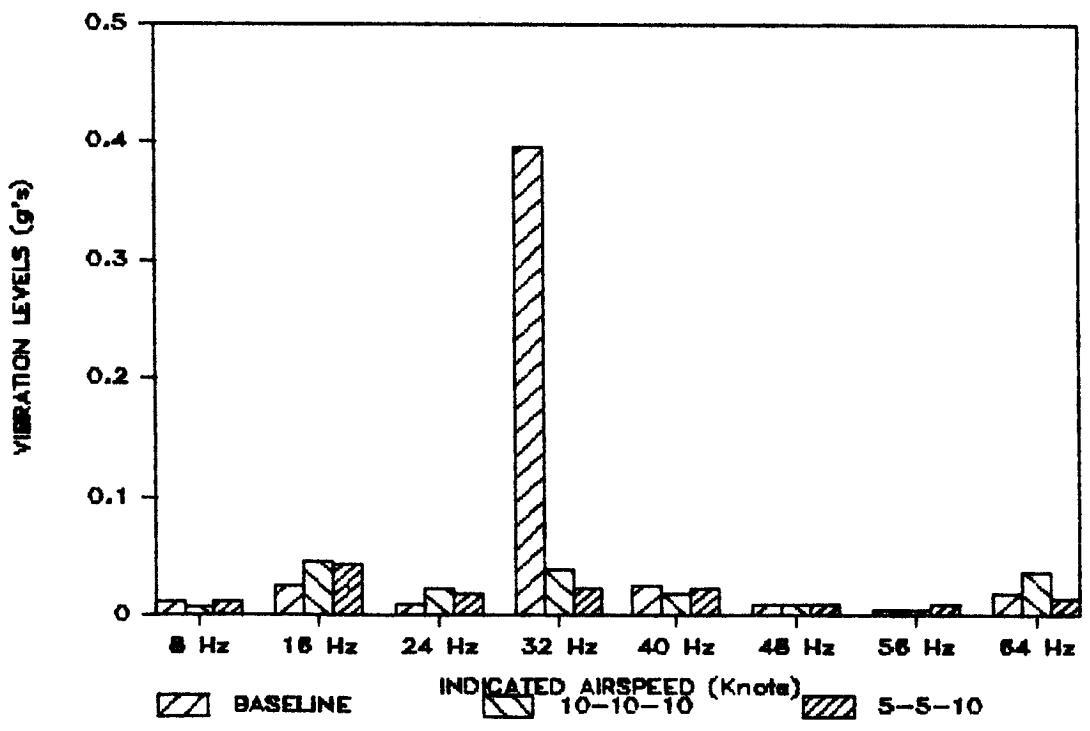
1984 CLOSED LOOP HHC
 4P VERTICAL PILOT SEAT VIBRATIONS VERSUS AIRSPEED
 EXPANDED SCALE
 Figure 61



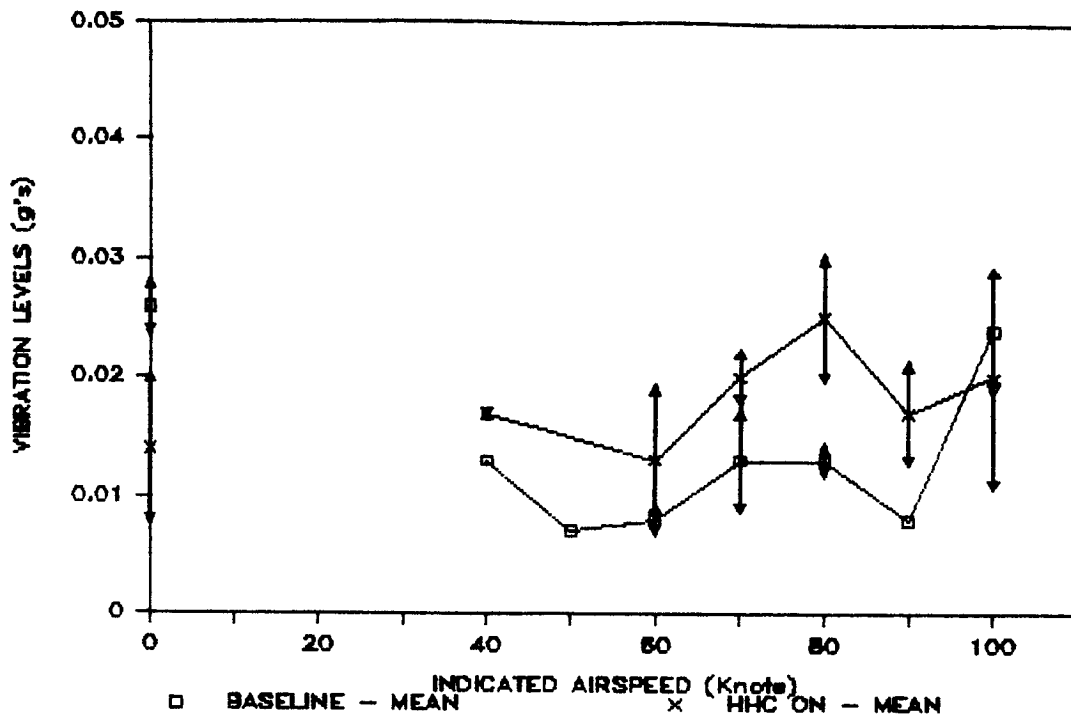
1984 CLOSED LOOP HHC
 4P LATERAL PILOT SEAT VIBRATIONS VERSUS AIRSPEED
 EXPANDED SCALE
 Figure 62



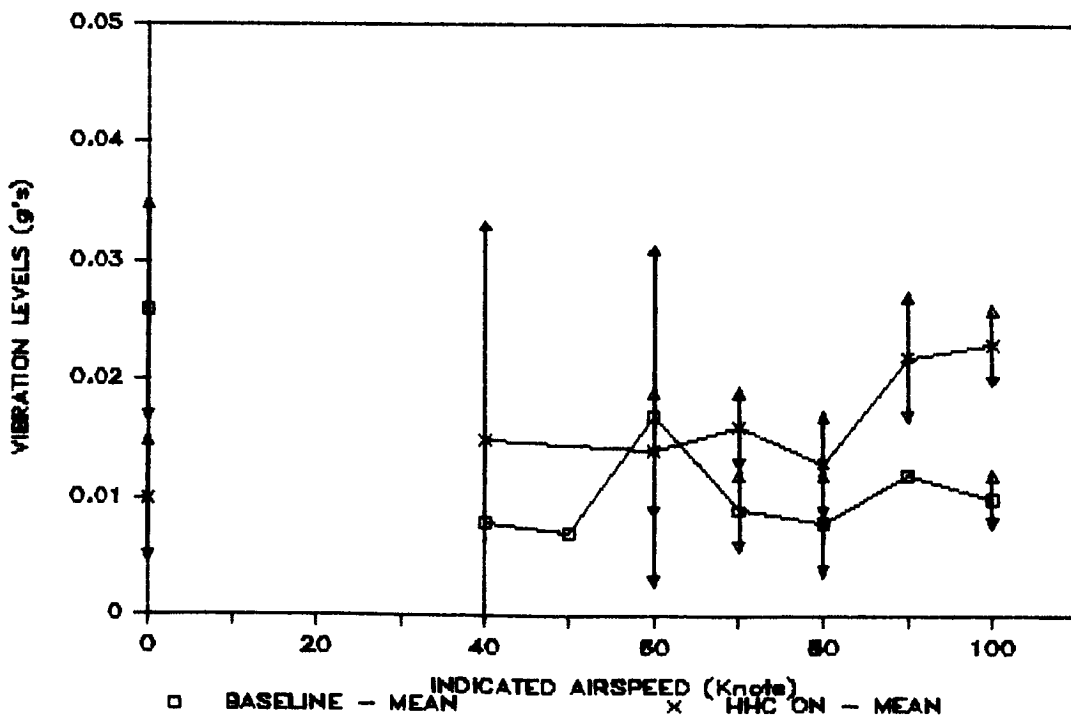
1984 CLOSED LOOP HHC
4P LONGITUDINAL PILOT SEAT VIBRATIONS VERSUS AIRSPEED
EXPANDED SCALE
Figure 63



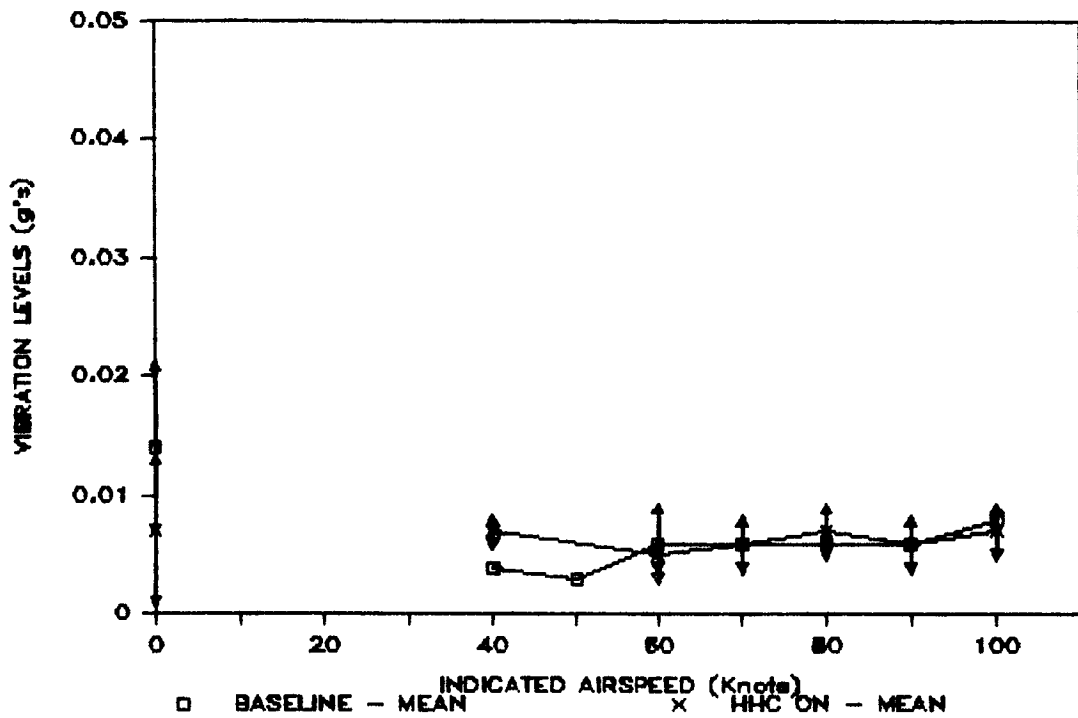
1984 CLOSED LOOP RESULTS
VERTICAL PILOT SEAT VIBRATIONS FREQUENCY SPECTRUM AT 100 KNOTS
Figure 64



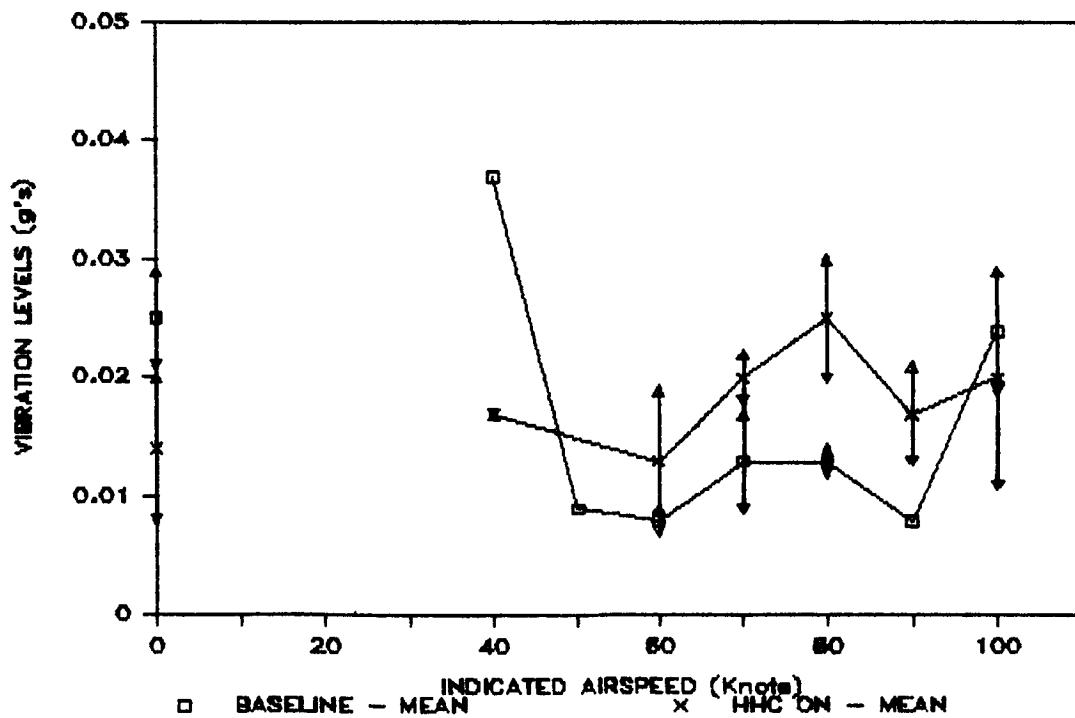
1984 CLOSED LOOP HHC
 3P VERTICAL PILOT SEAT VIBRATIONS VERSUS AIRSPEED
 Figure 65



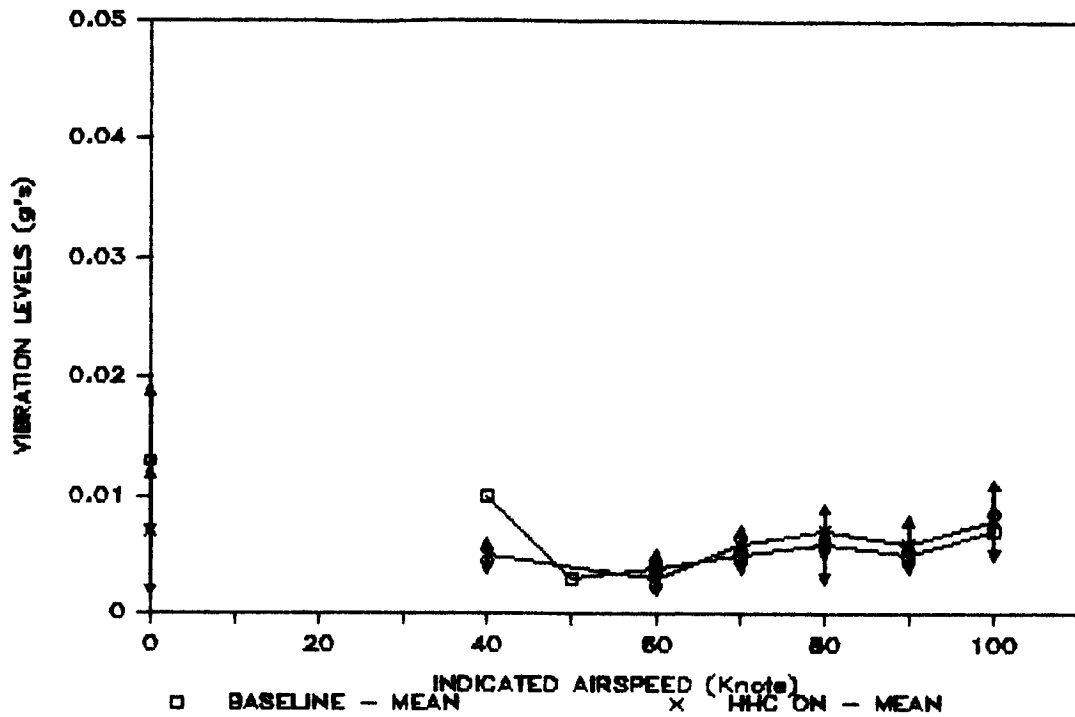
1984 CLOSED LOOP HHC
 3P LATERAL PILOT SEAT VIBRATIONS VERSUS AIRSPEED
 Figure 66



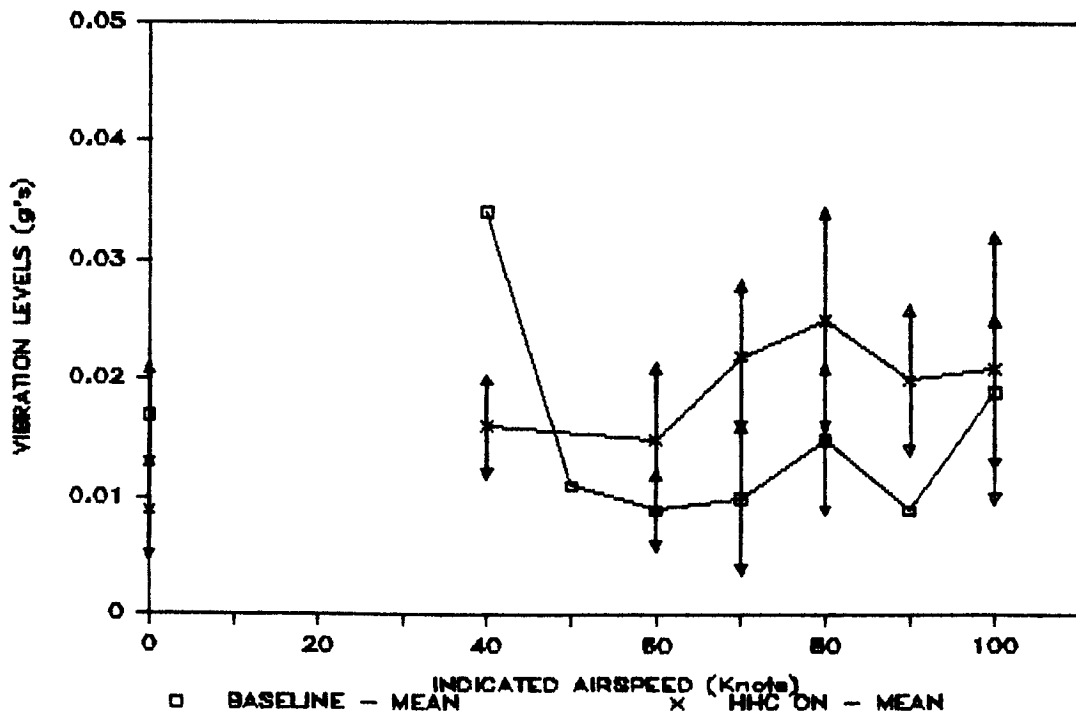
1984 CLOSED LOOP HHC
 3P LONGITUDINAL PILOT SEAT VIBRATIONS VERSUS AIRSPEED
 Figure 67



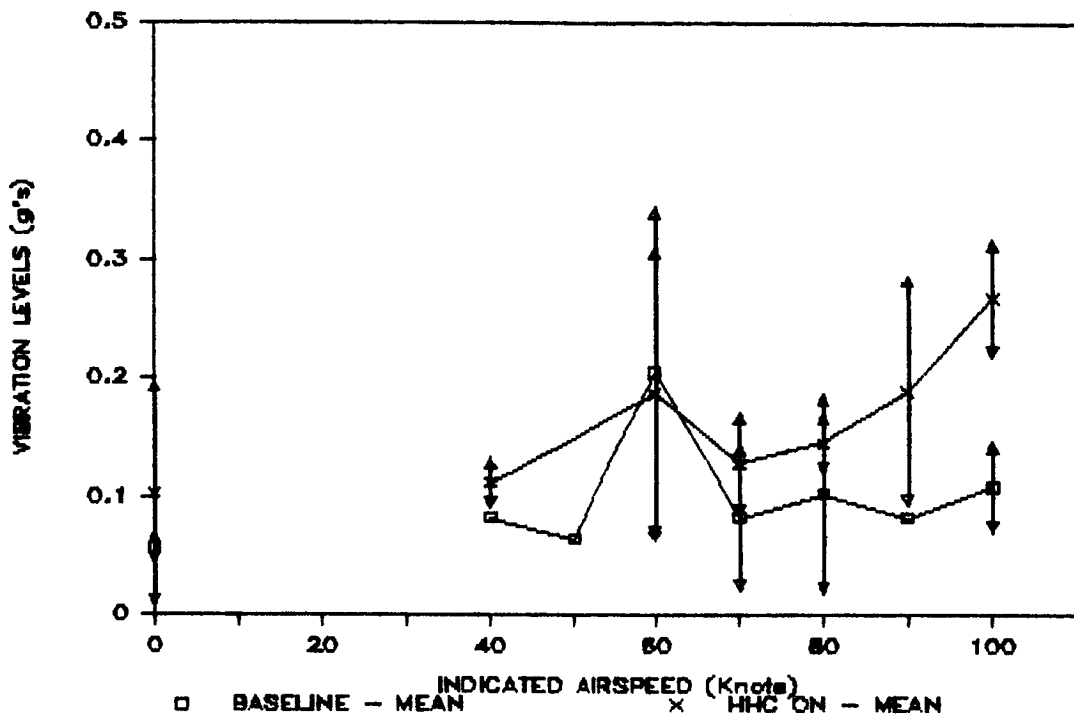
1984 CLOSED LOOP HHC
 5P VERTICAL PILOT SEAT VIBRATIONS VERSUS AIRSPEED
 Figure 68



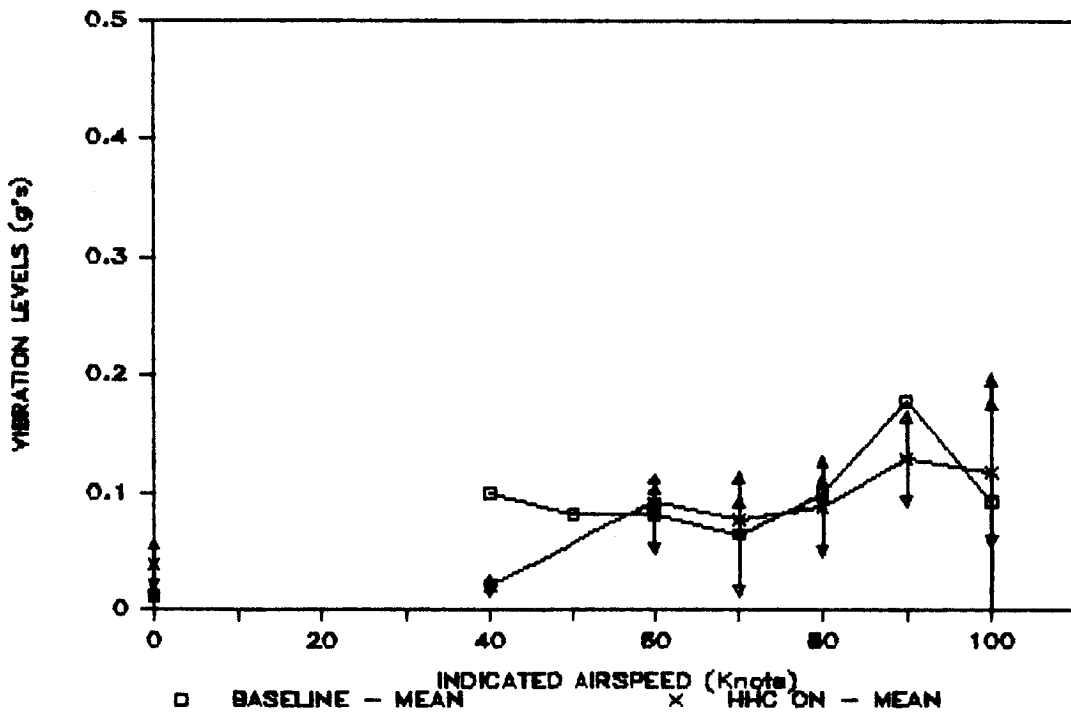
1984 CLOSED LOOP HHC
 5P LATERAL PILOT SEAT VIBRATIONS VERSUS AIRSPEED
 Figure 69



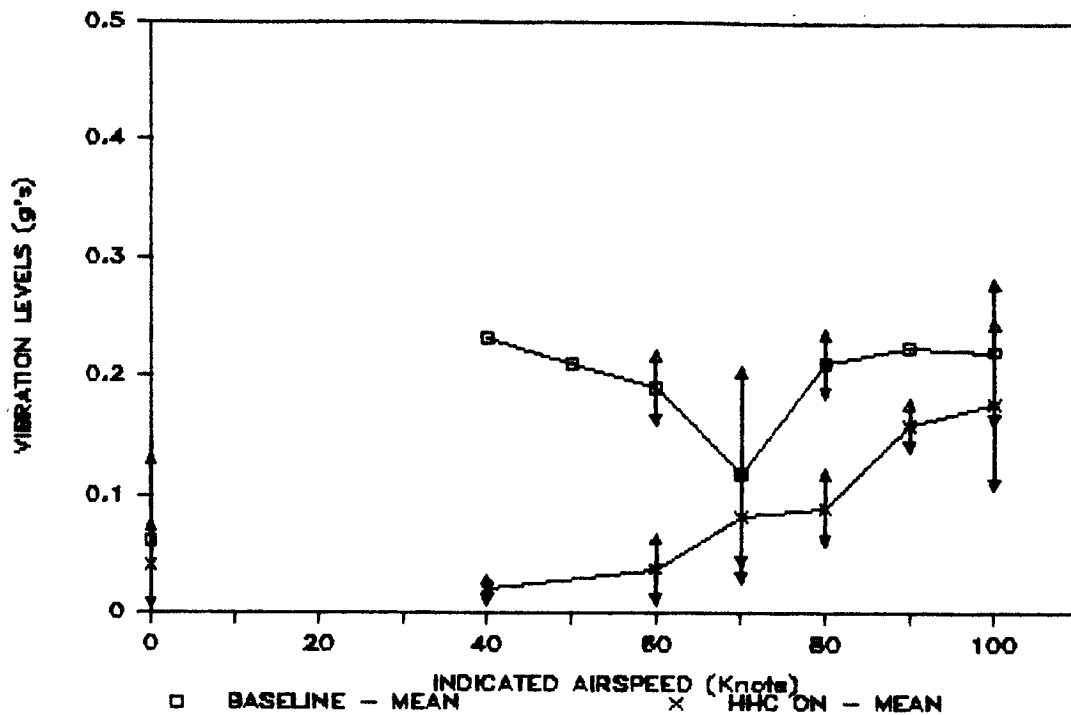
1984 CLOSED LOOP HHC
 5P LONGITUDINAL PILOT SEAT VIBRATIONS VERSUS AIRSPEED
 Figure 70



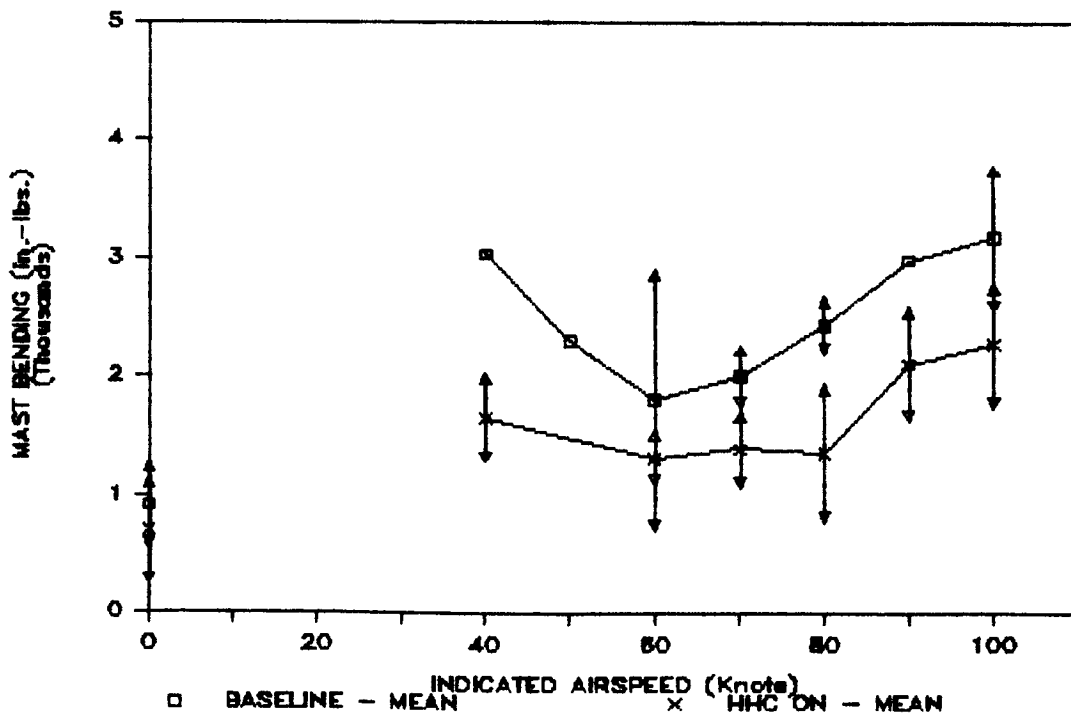
1984 CLOSED LOOP HHC
 4P VERTICAL AIRCRAFT C.G. VIBRATIONS VERSUS AIRSPEED
 Figure 71



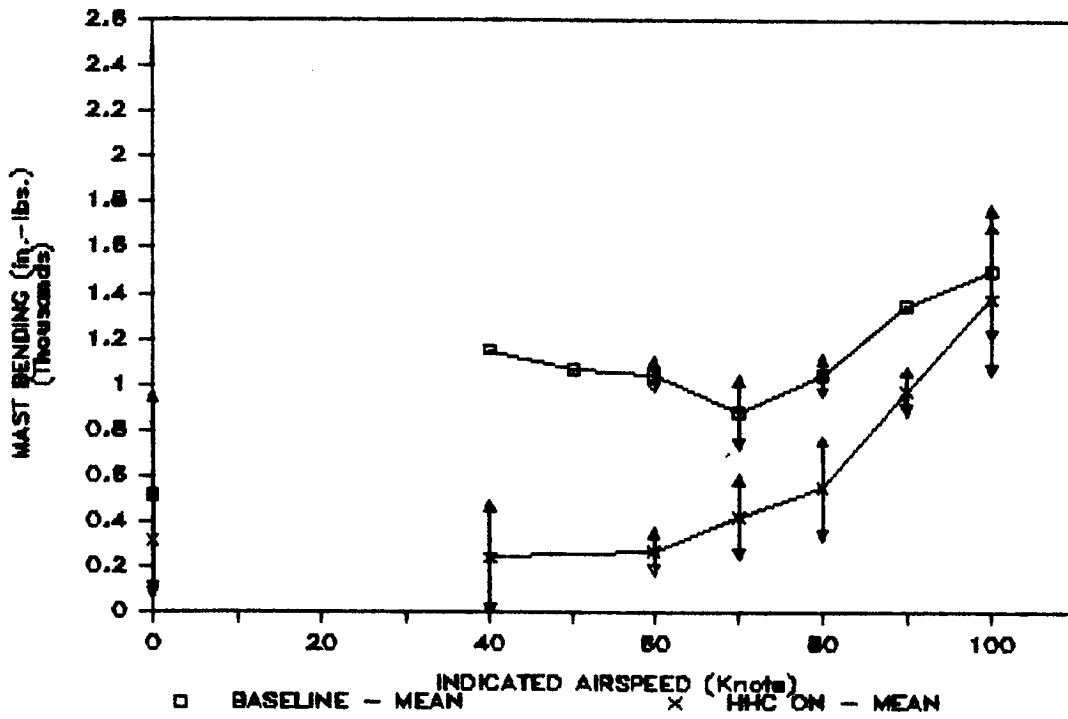
1984 CLOSED LOOP HHC
 4P LATERAL AIRCRAFT C.G. VIBRATIONS VERSUS AIRSPEED
 Figure 72



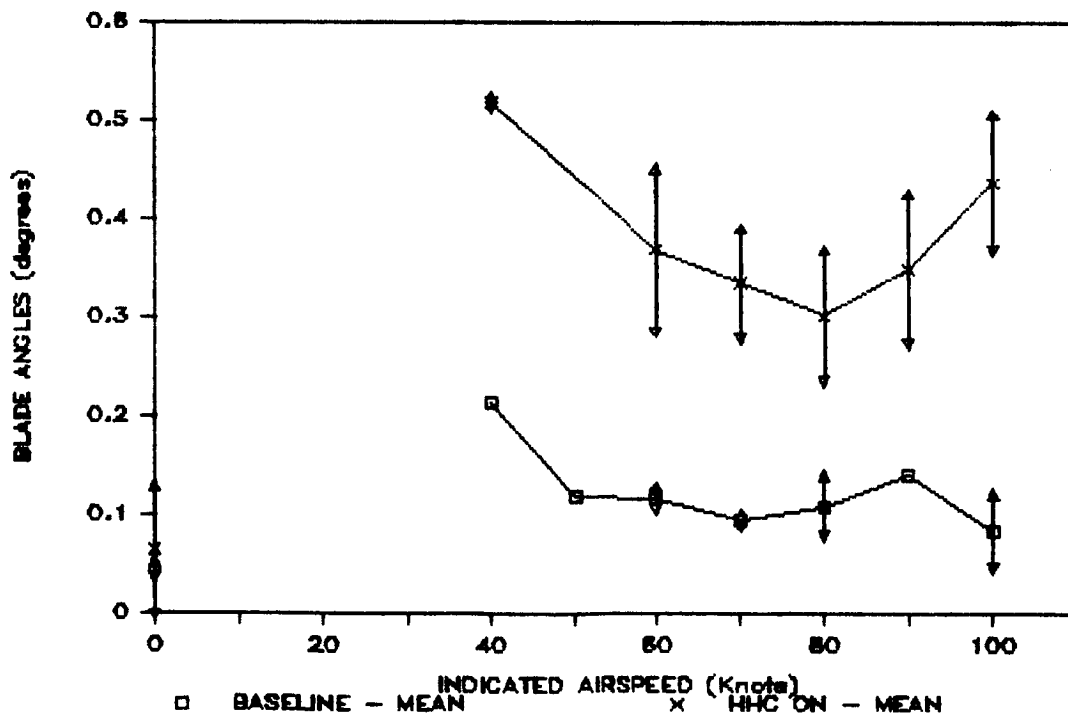
1984 CLOSED LOOP HHC
 4P LONGITUDINAL AIRCRAFT C.G. VIBRATIONS VERSUS AIRSPEED
 Figure 73



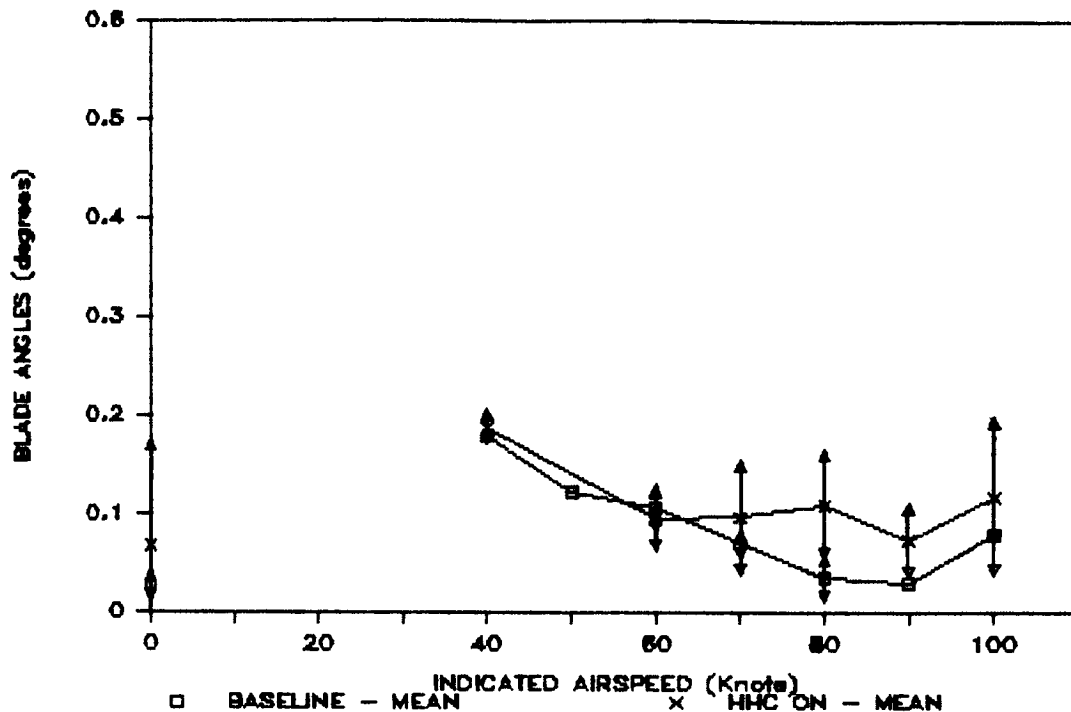
1984 CLOSED LOOP HHC
 MAIN ROTOR MAST 4P LATERAL BENDING VERSUS AIRSPEED
 Figure 74



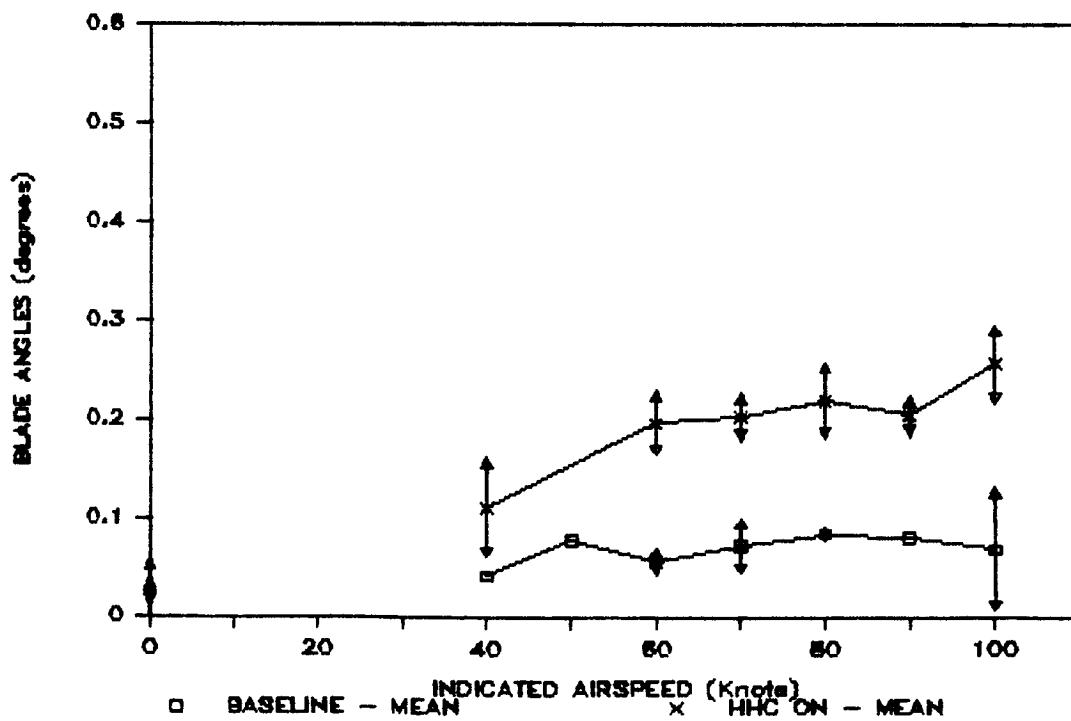
1984 CLOSED LOOP HHC
 MAIN ROTOR MAST 4P LONGITUDINAL BENDING VERSUS AIRSPEED
 Figure 75



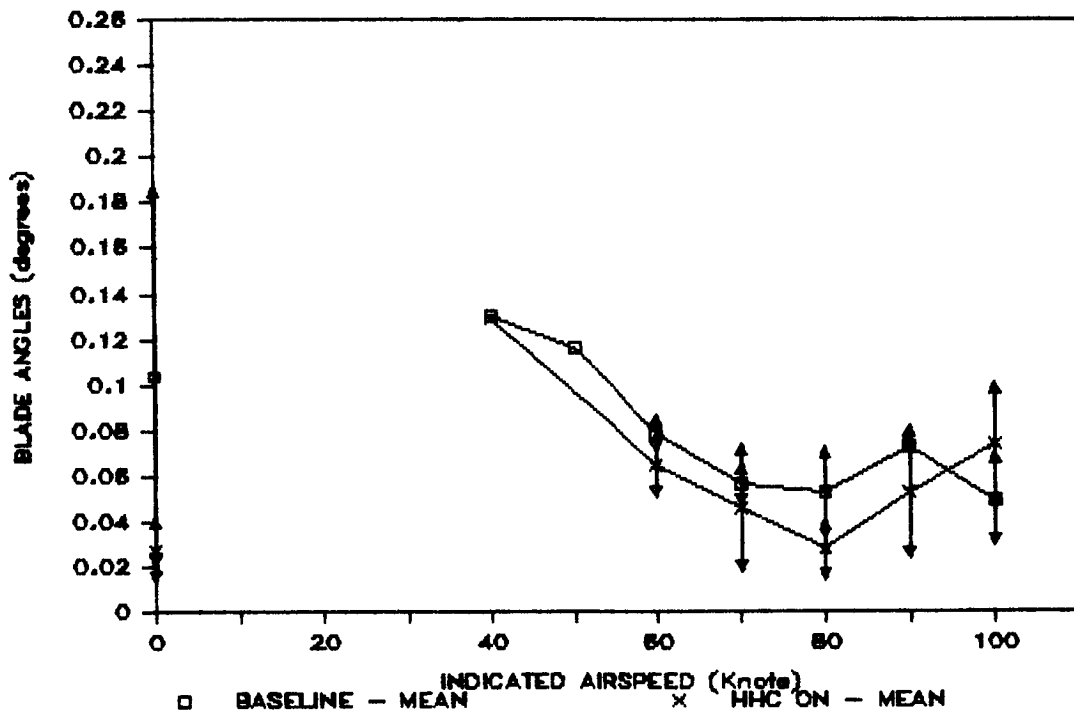
1984 CLOSED LOOP HHC
 3P BLADE FEATHERING ANGLE VERSUS AIRSPEED
 Figure 76



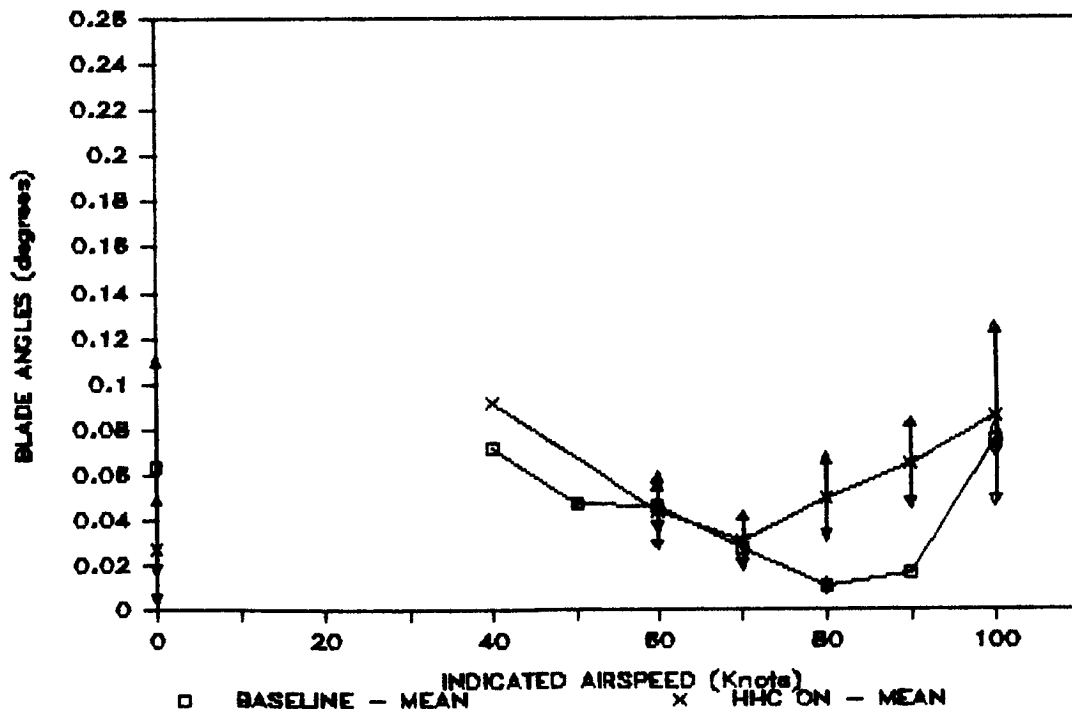
1984 CLOSED LOOP HHC
 4P BLADE FEATHERING ANGLE VERSUS AIRSPEED
 Figure 77



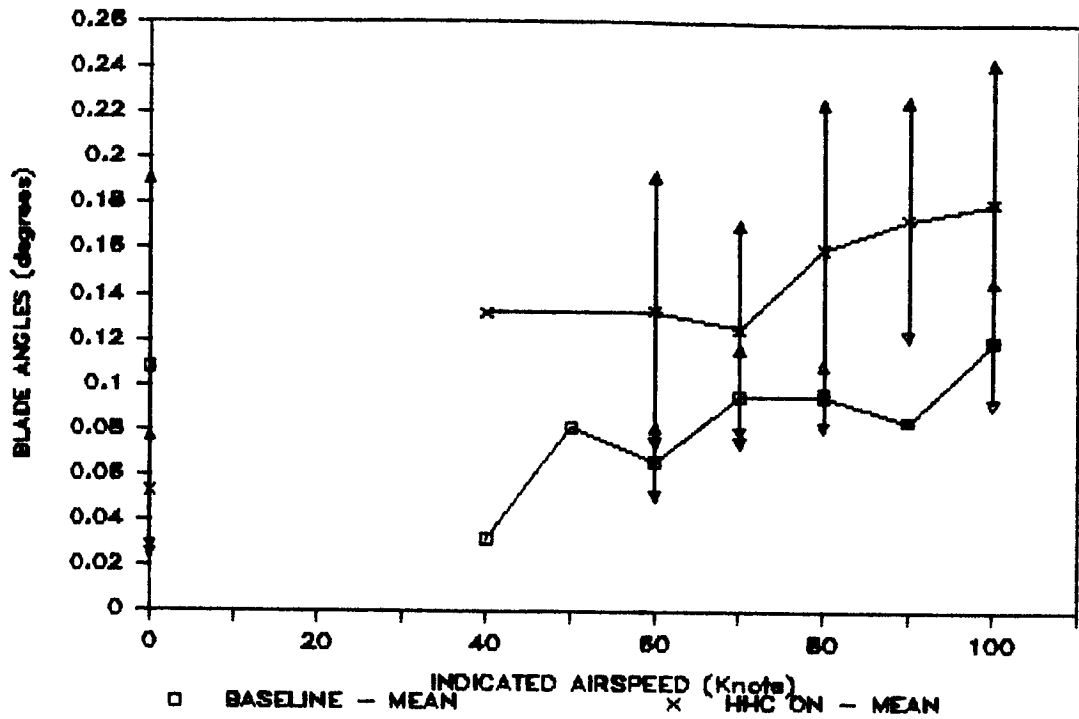
1984 CLOSED LOOP HHC
 5P BLADE FEATHERING ANGLE VERSUS AIRSPEED
 Figure 78



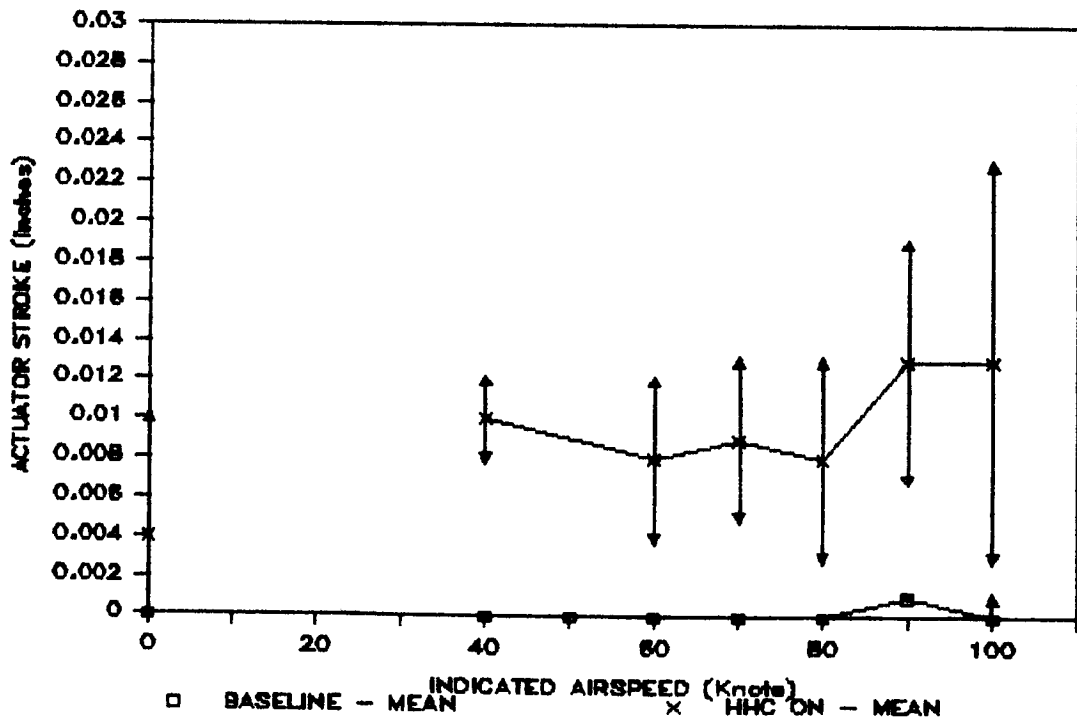
1984 CLOSED LOOP HHC
 3P BLADE FLAPPING ANGLE VERSUS AIRSPEED
 Figure 79



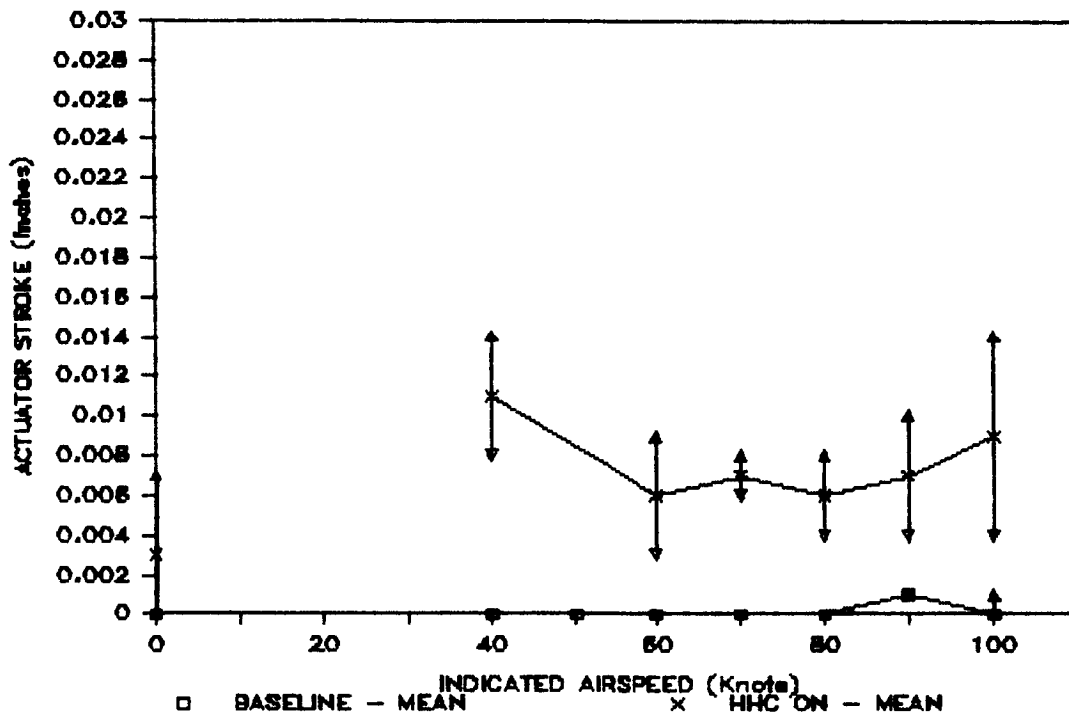
1984 CLOSED LOOP HHC
 4P BLADE FLAPPING ANGLE VERSUS AIRSPEED
 Figure 80



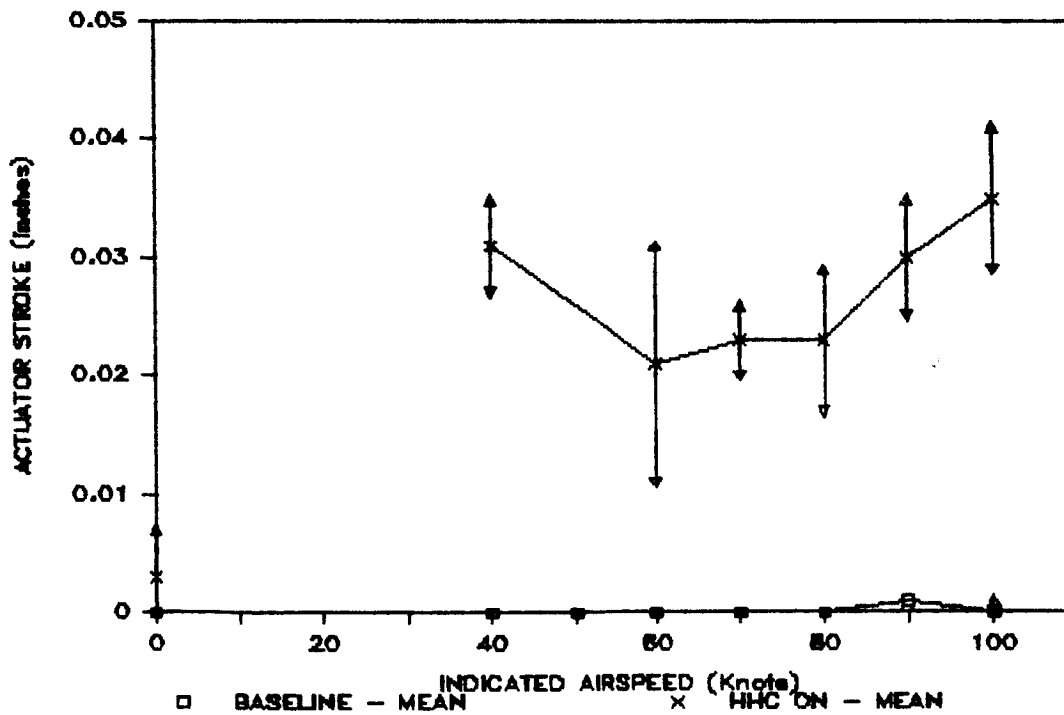
1984 CLOSED LOOP HHC
5P BLADE FLAPPING ANGLE VERSUS AIRSPEED
Figure 81



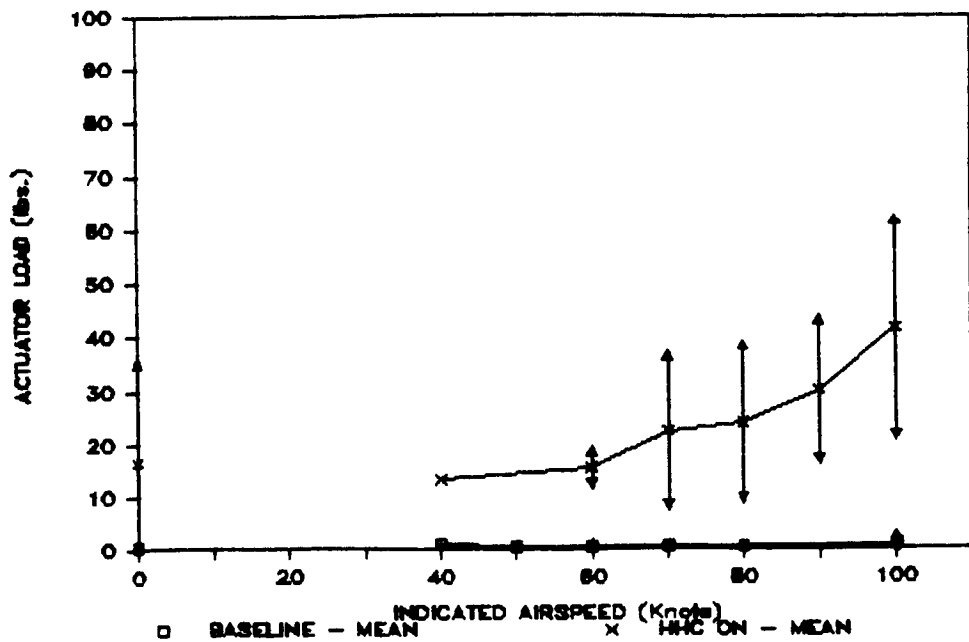
1984 CLOSED LOOP HHC
4P LEFT LATERAL ACTUATOR STROKE VERSUS AIRSPEED
Figure 82



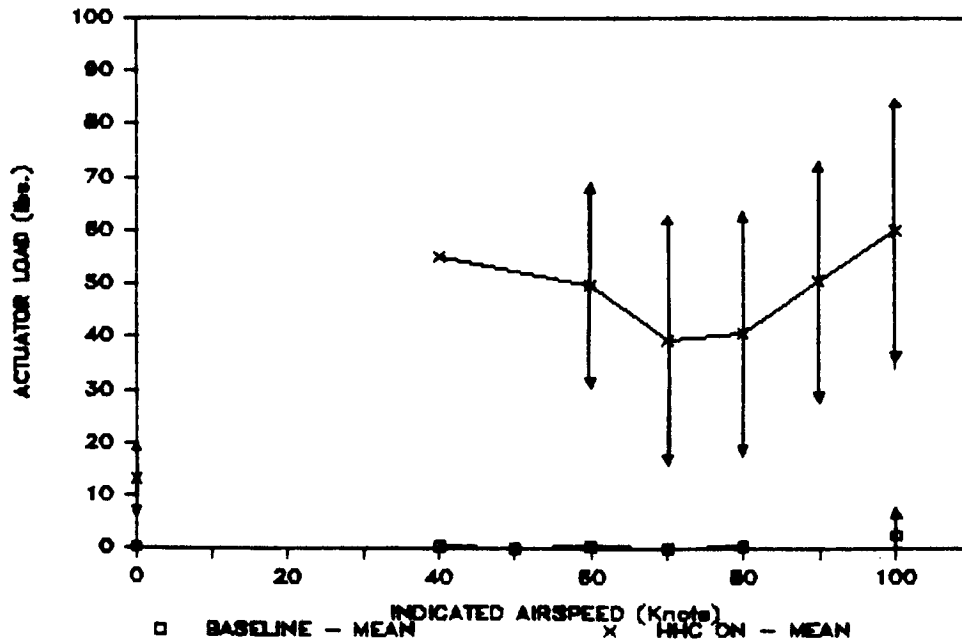
1984 CLOSED LOOP HHC
 4P RIGHT LATERAL ACTUATOR STROKE VERSUS AIRSPEED
 Figure 83



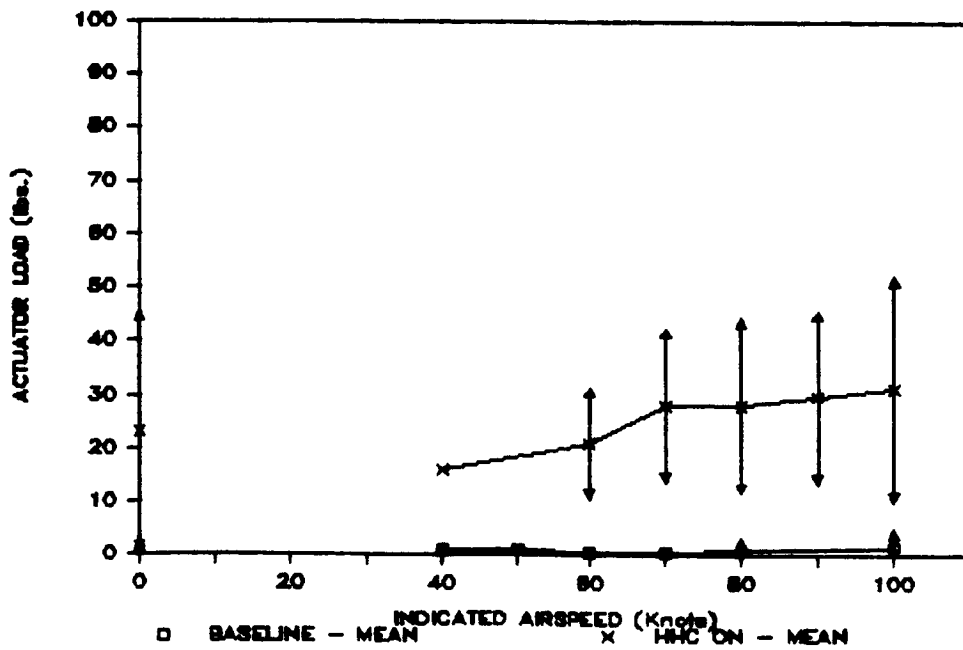
1984 CLOSED LOOP HHC
 4P LONGITUDINAL ACTUATOR STROKE VERSUS AIRSPEED
 Figure 84



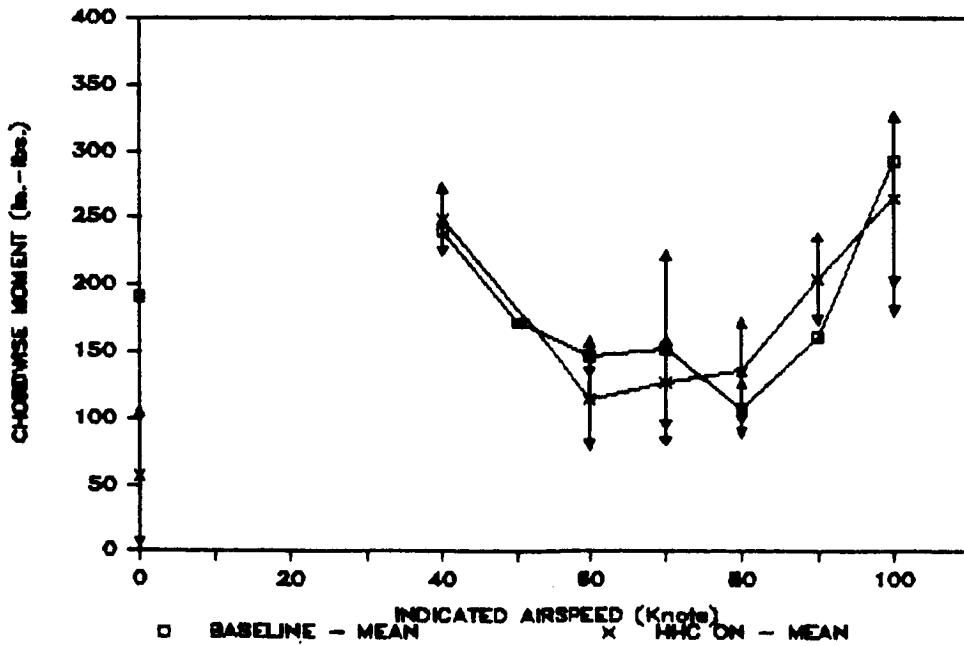
1984 CLOSED LOOP HHC
 4P LEFT LATERAL ACTUATOR LOAD VERSUS AIRSPEED
 Figure 85



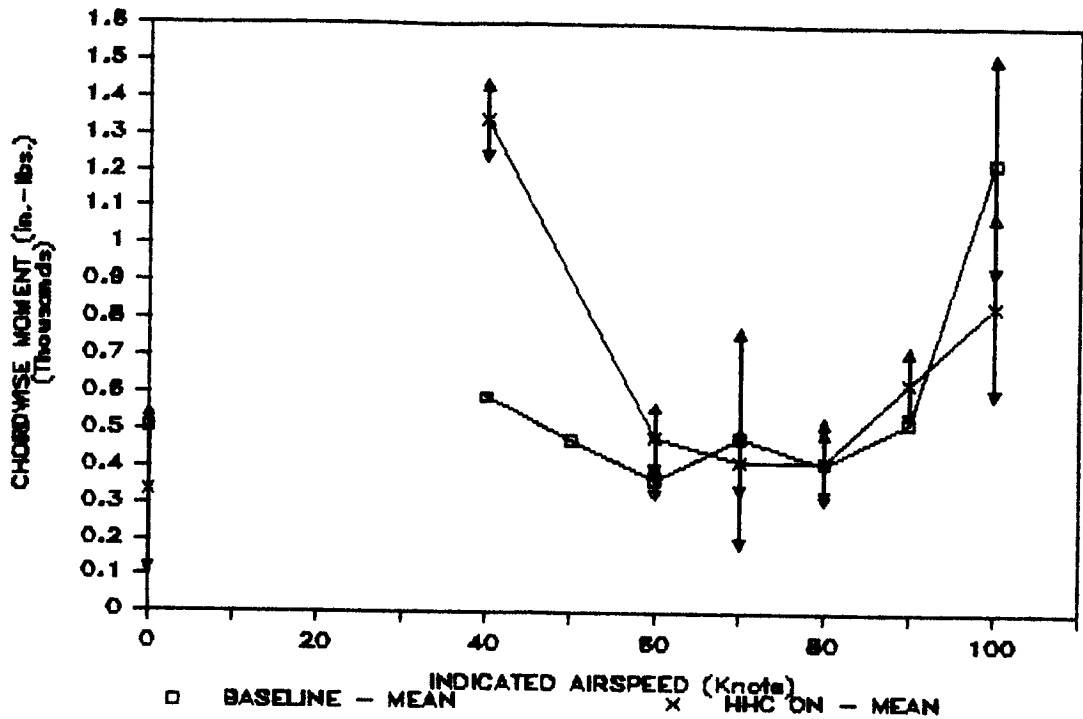
1984 CLOSED LOOP HHC
 4P RIGHT LATERAL ACTUATOR LOAD VERSUS AIRSPEED
 Figure 86



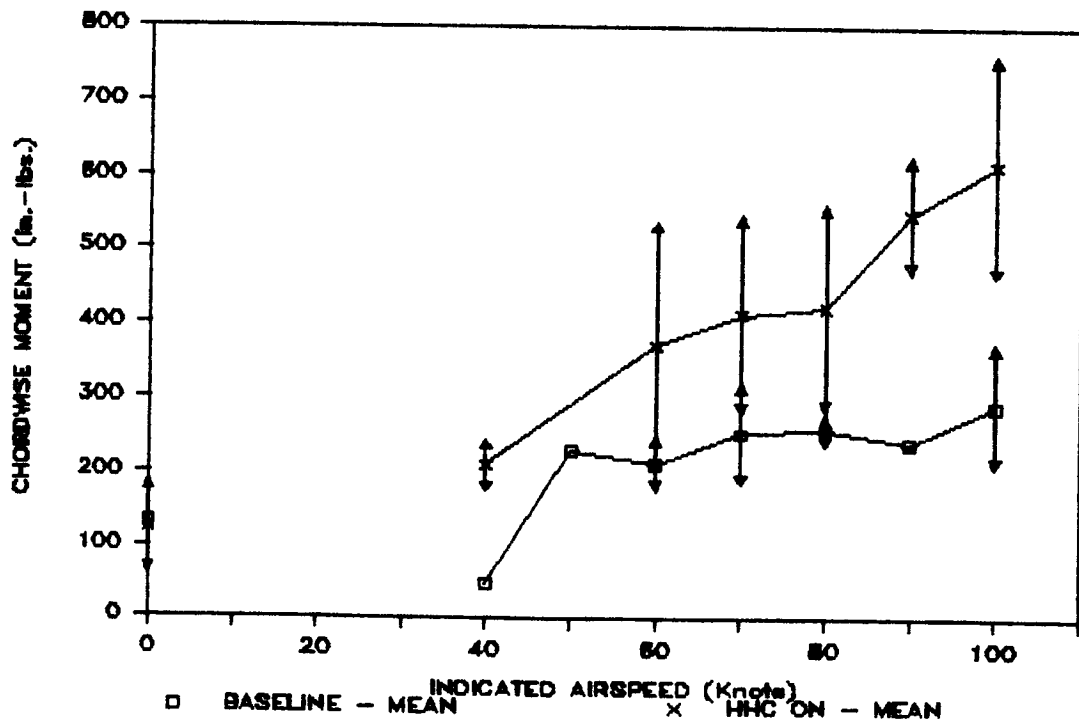
1984 CLOSED LOOP HHC
 4P LONGITUDINAL ACTUATOR LOAD VERSUS AIRSPEED
 Figure 87



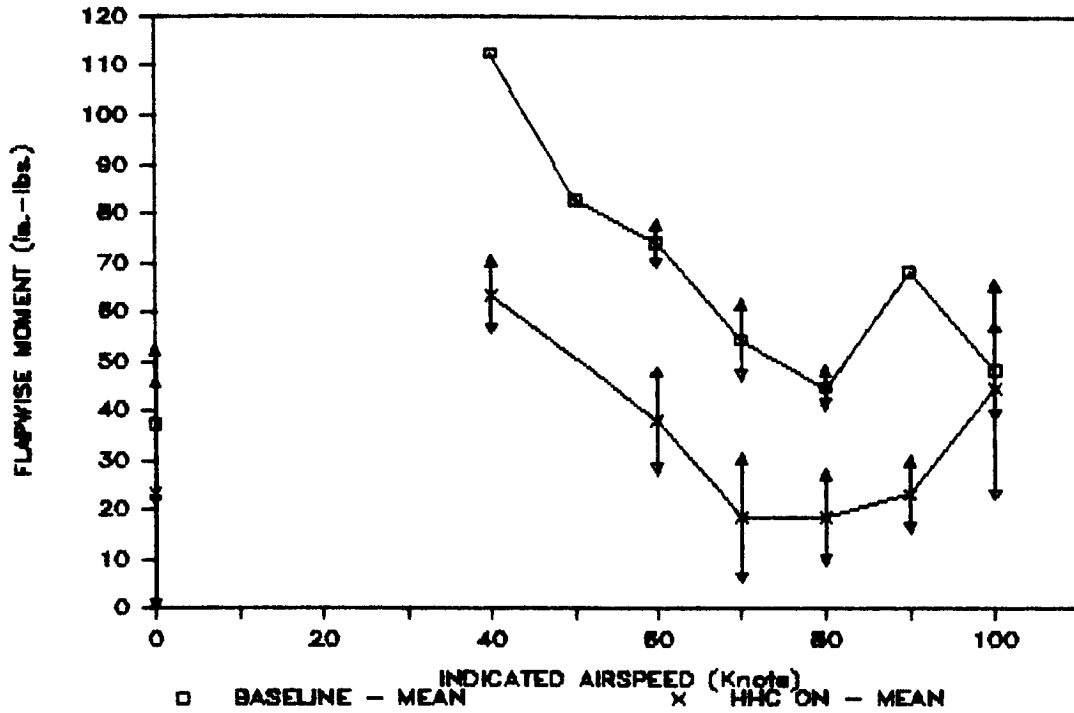
1984 CLOSED LOOP HHC
 3P CHORDWISE BLADE BENDING MOMENT VERSUS AIRSPEED
 AT $r/R = 17\%$
 Figure 88



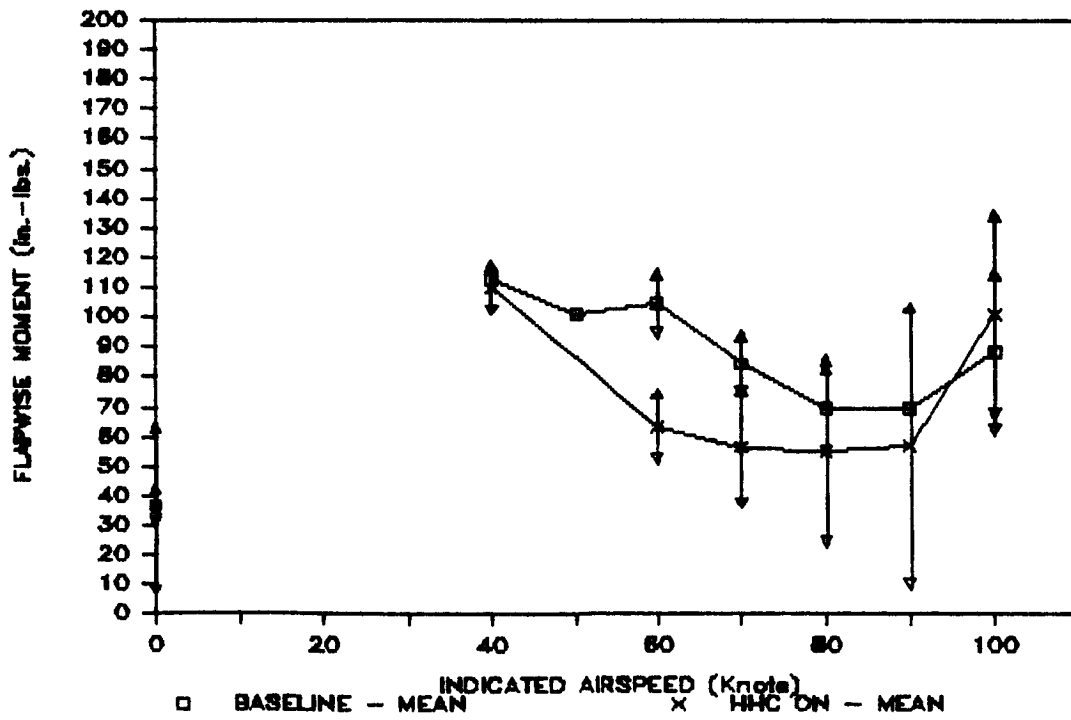
1984 CLOSED LOOP HHC
 4P CHORDWISE BLADE BENDING MOMENT VERSUS AIRSPEED
 AT $r/R = 17\%$
 Figure 89



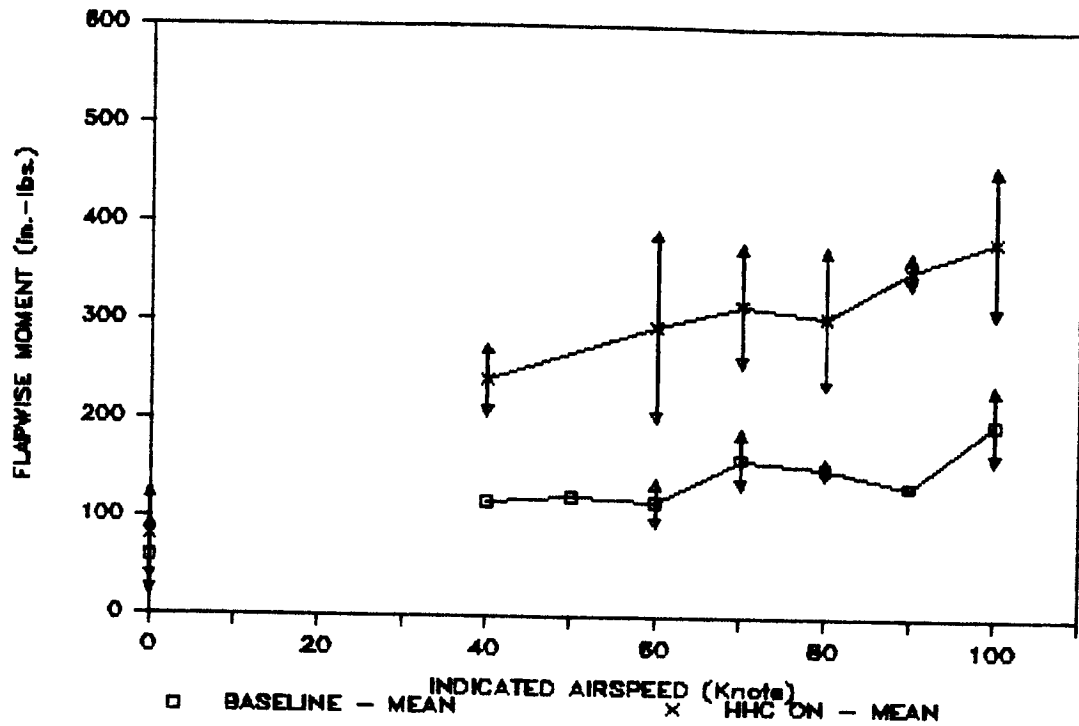
1984 CLOSED LOOP HHC
 5P CHORDWISE BLADE BENDING MOMENT VERSUS AIRSPEED
 AT $r/R = 17\%$
 Figure 90



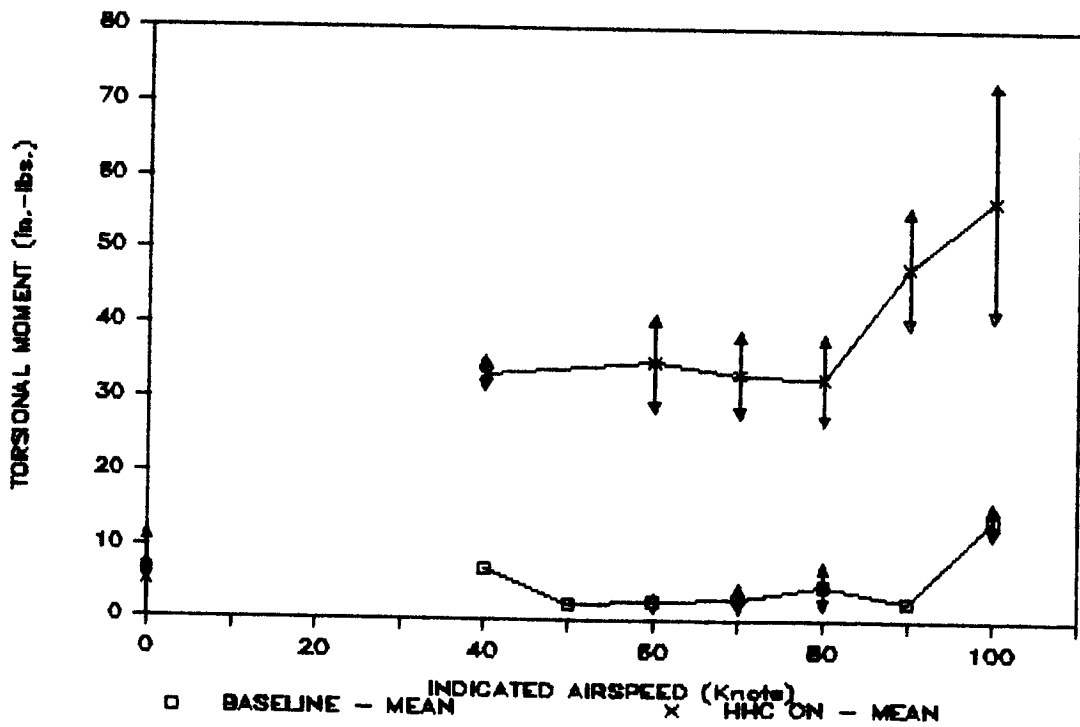
1984 CLOSED LOOP HHC
 3P FLAPWISE BLADE BENDING MOMENT VERSUS AIRSPEED
 AT r/R = 15%
 Figure 91



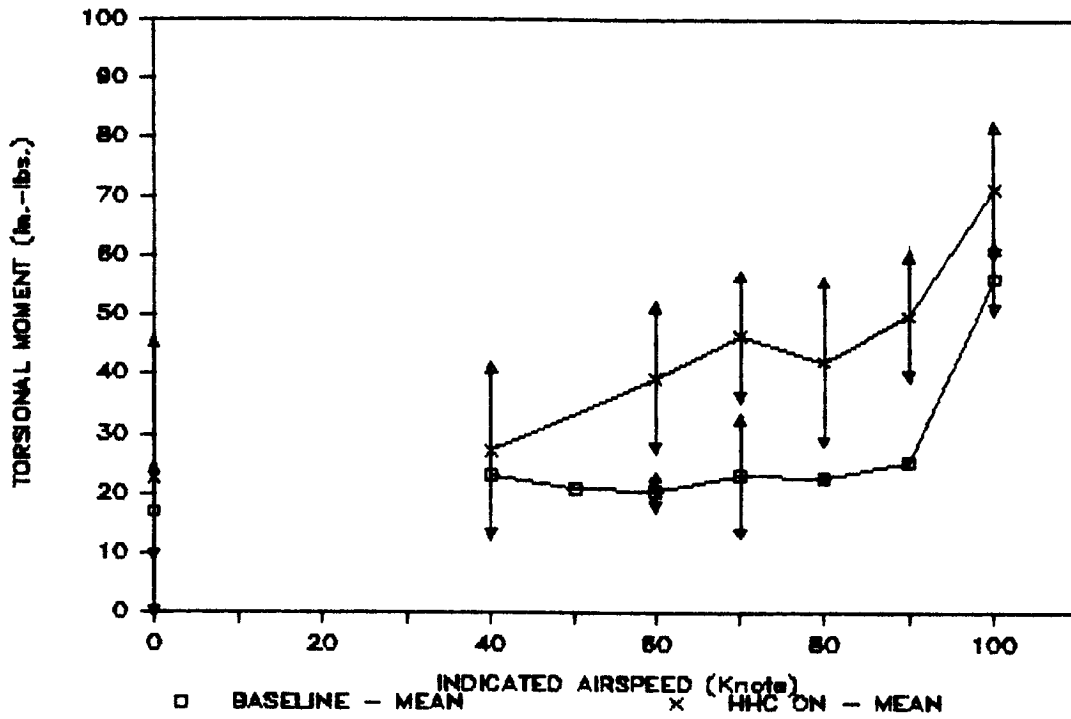
1984 CLOSED LOOP HHC
 4P FLAPWISE BLADE BENDING MOMENT VERSUS AIRSPEED
 AT r/R = 15%
 Figure 92



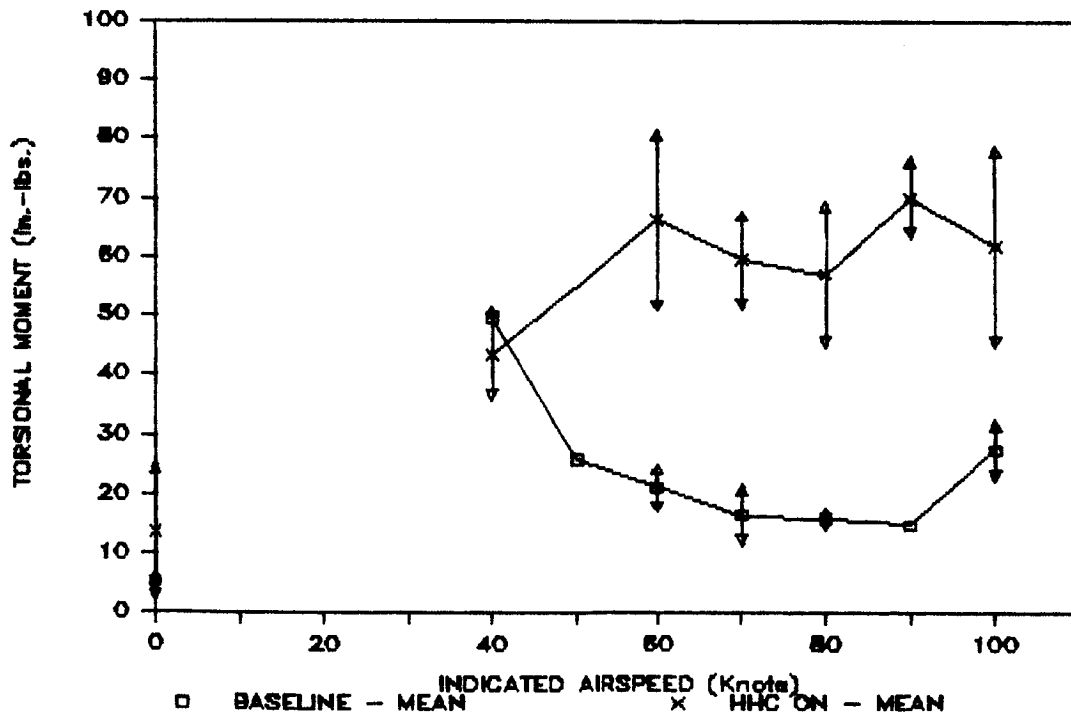
1984 CLOSED LOOP HHC
 5P FLAPWISE BLADE BENDING MOMENT VERSUS AIRSPEED
 AT $r/R = 15\%$
 Figure 93



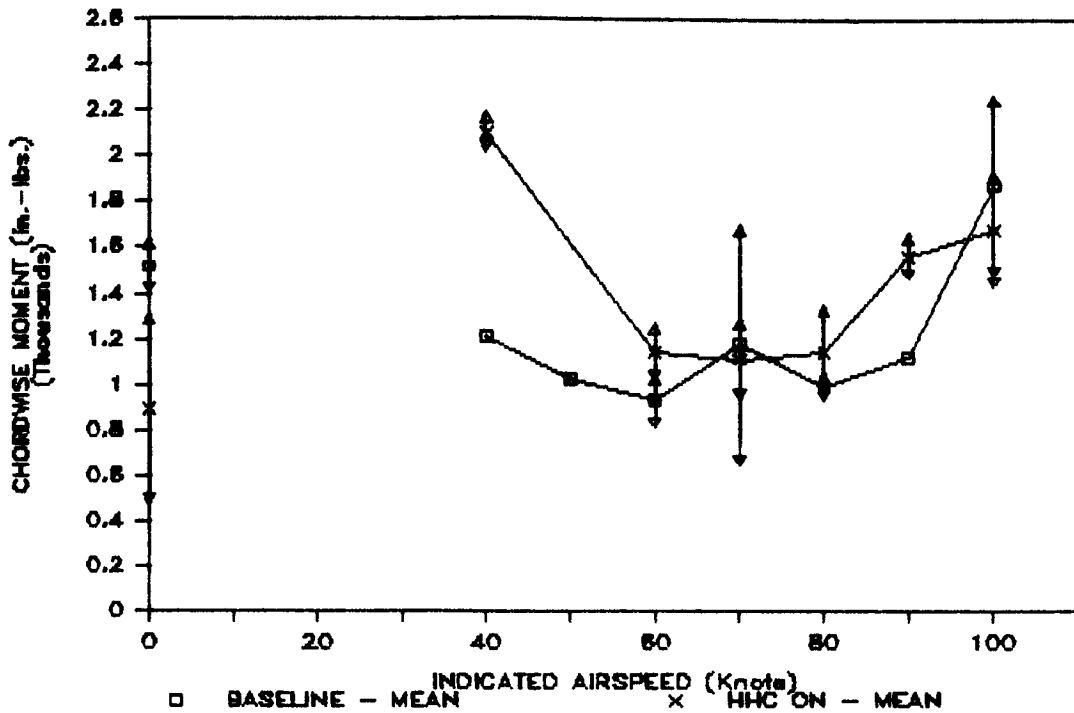
1984 CLOSED LOOP HHC
 3P TORSIONAL BLADE MOMENT VERSUS AIRSPEED
 AT $r/R = 30\%$
 Figure 94



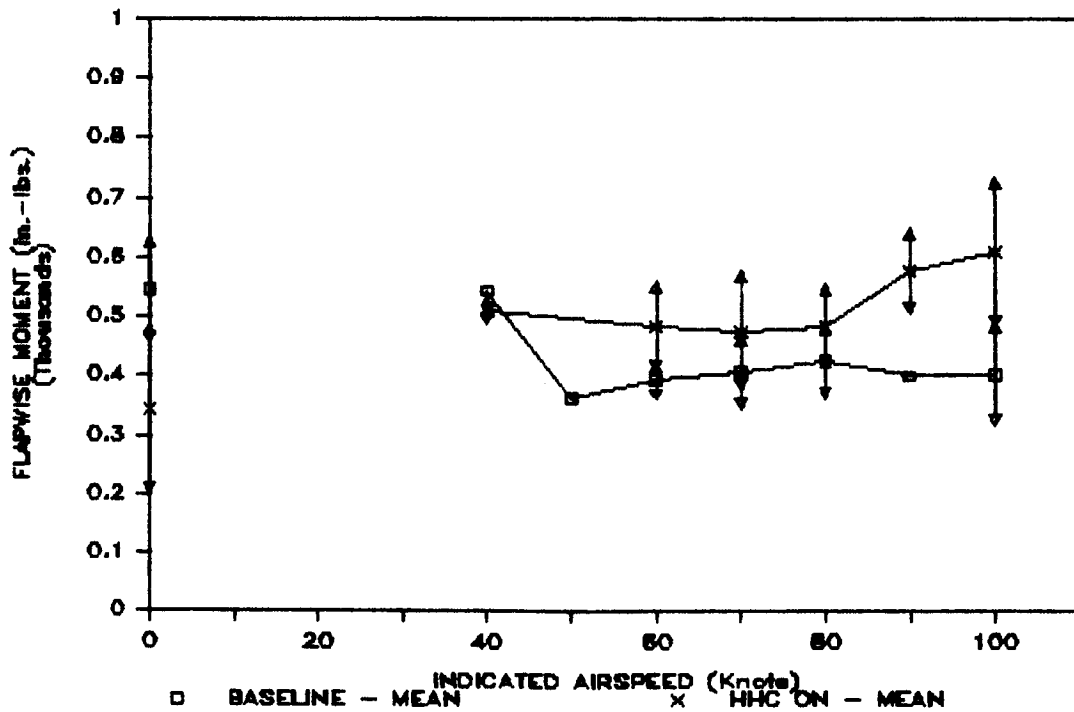
1984 CLOSED LOOP HHC
 4P TORSIONAL BLADE MOMENT VERSUS AIRSPEED
 AT $r/R = 30\%$
 Figure 95



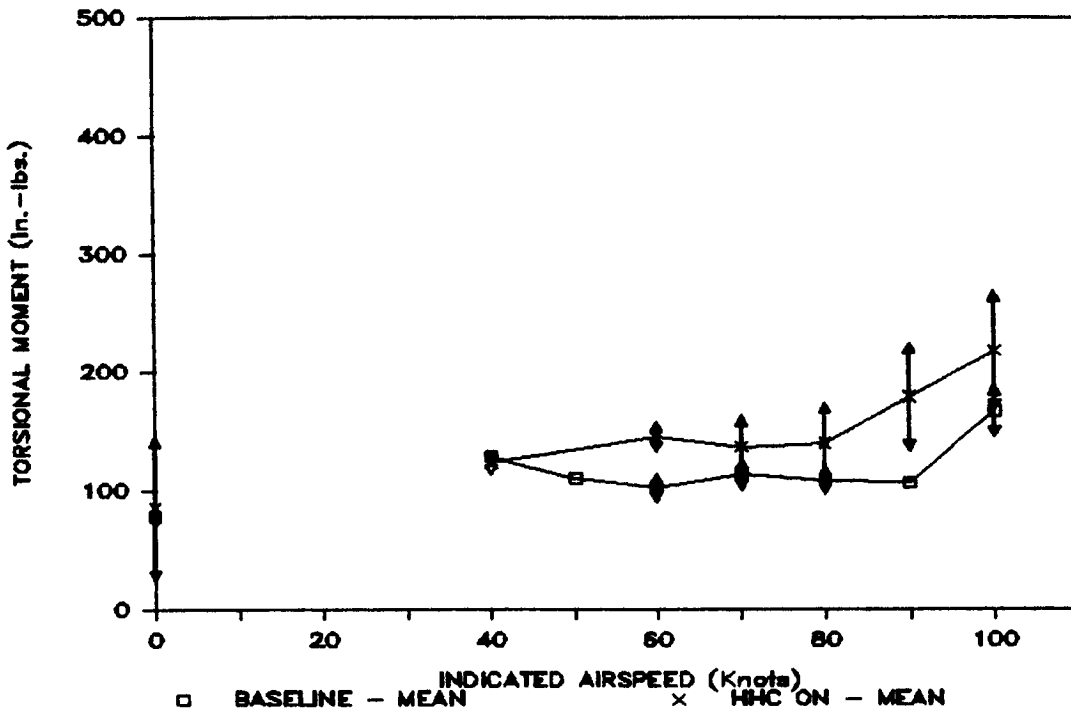
1984 CLOSED LOOP HHC
 5P TORSIONAL BLADE MOMENT VERSUS AIRSPEED
 AT $r/R = 30\%$
 Figure 96



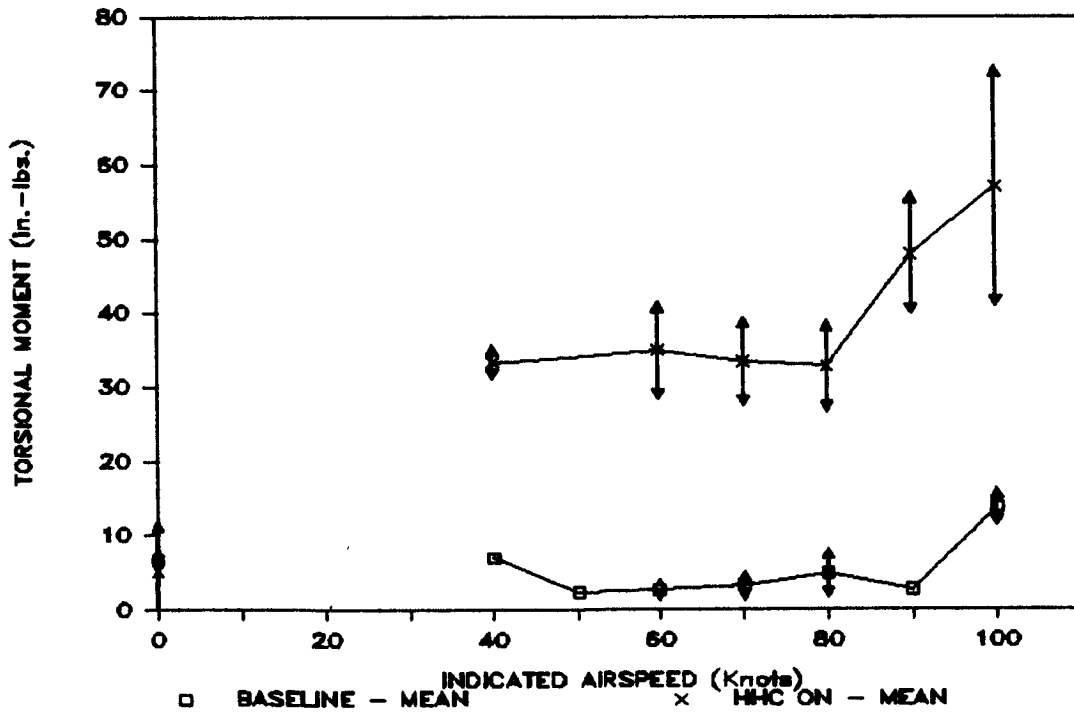
1984 CLOSED LOOP HHC
 1/2 PEAK TO PEAK CHORDWISE BLADE BENDING MOMENT VERSUS AIRSPEED
 AT r/R = 17%
 Figure 97



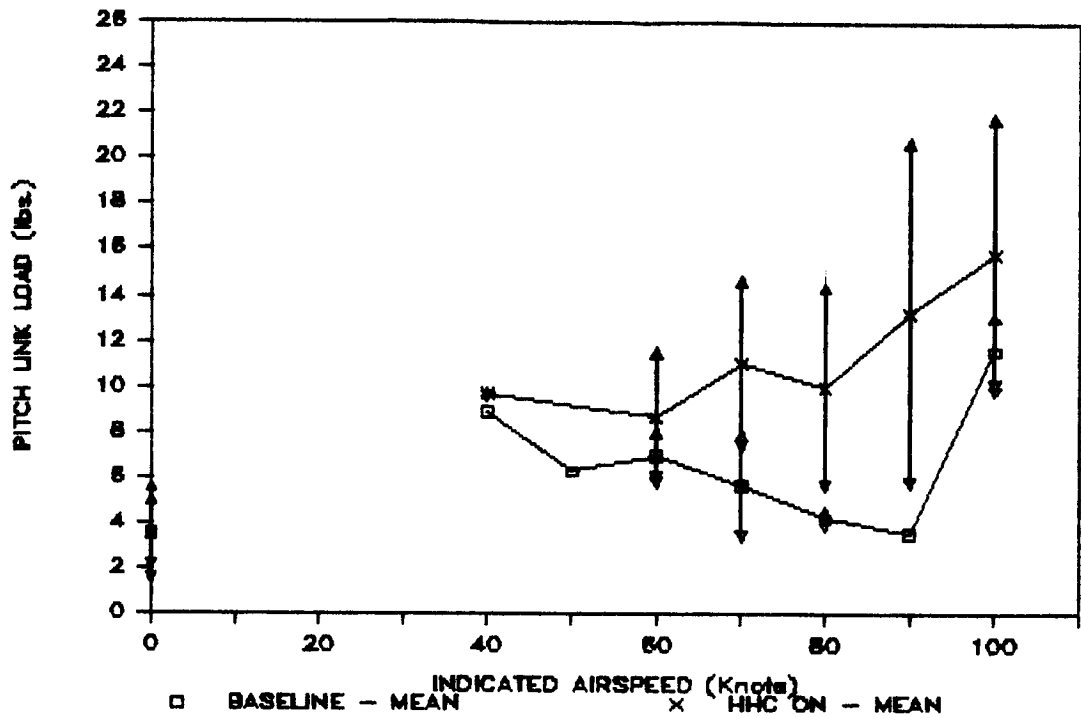
1984 CLOSED LOOP HHC
 1/2 PEAK TO PEAK FLAPWISE BLADE BENDING MOMENT VERSUS AIRSPEED
 AT r/R = 15%
 Figure 98



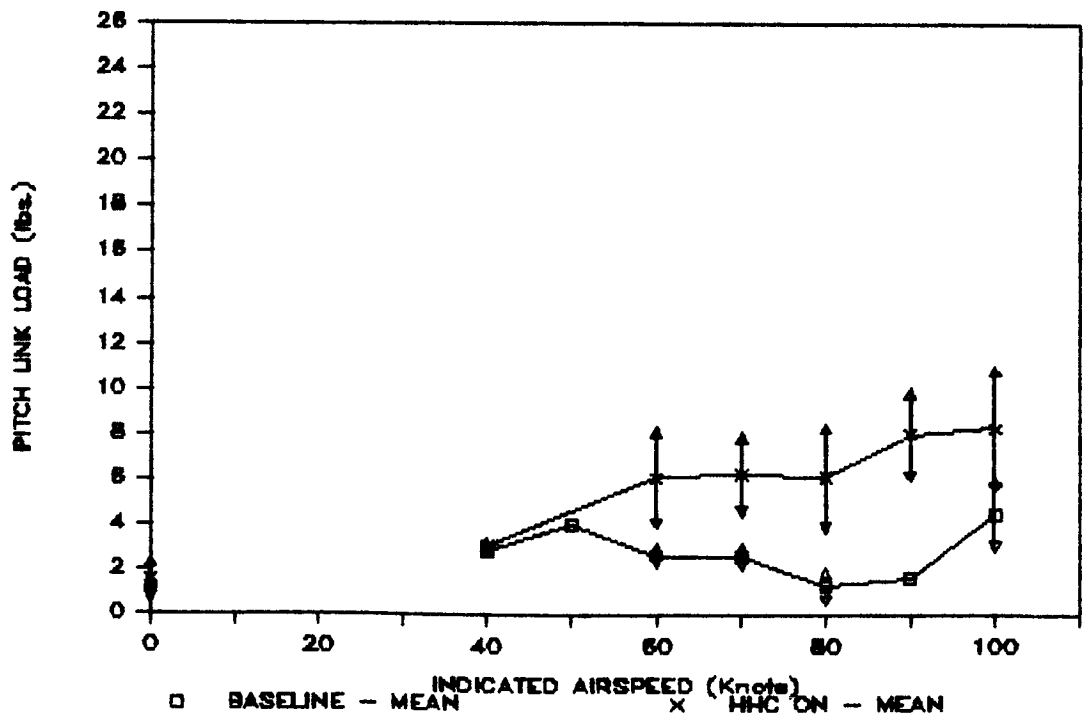
1984 CLOSED LOOP HHC
 1/2 PEAK TO PEAK TORSIONAL BLADE MOMENT VERSUS AIRSPEED
 AT r/R = 30%
 Figure 99



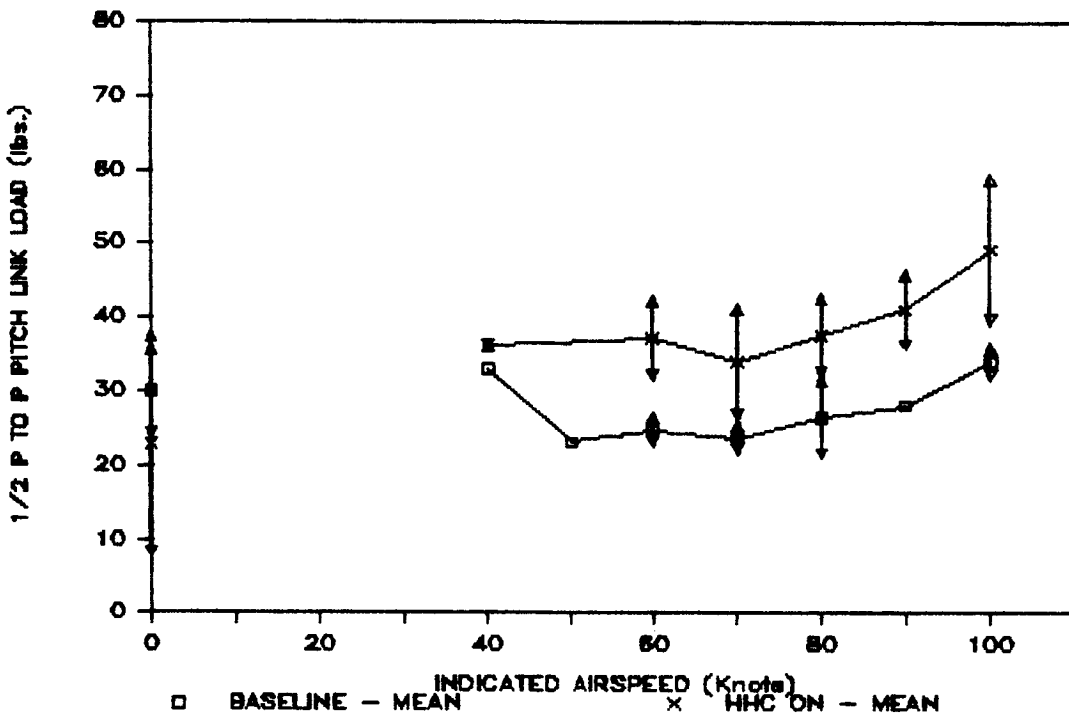
1984 CLOSED LOOP HHC
 3P PITCH LINK LOAD VERSUS AIRSPEED
 Figure 100



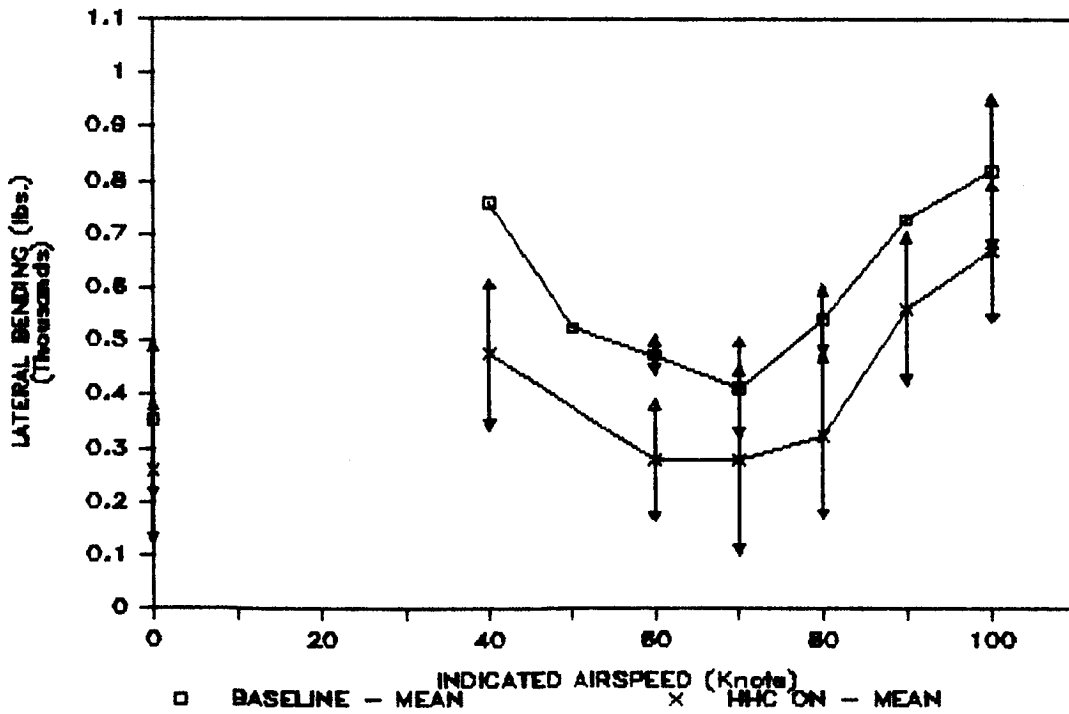
1984 CLOSED LOOP HHC
 4P PITCH LINK LOAD VERSUS AIRSPEED
 Figure 101



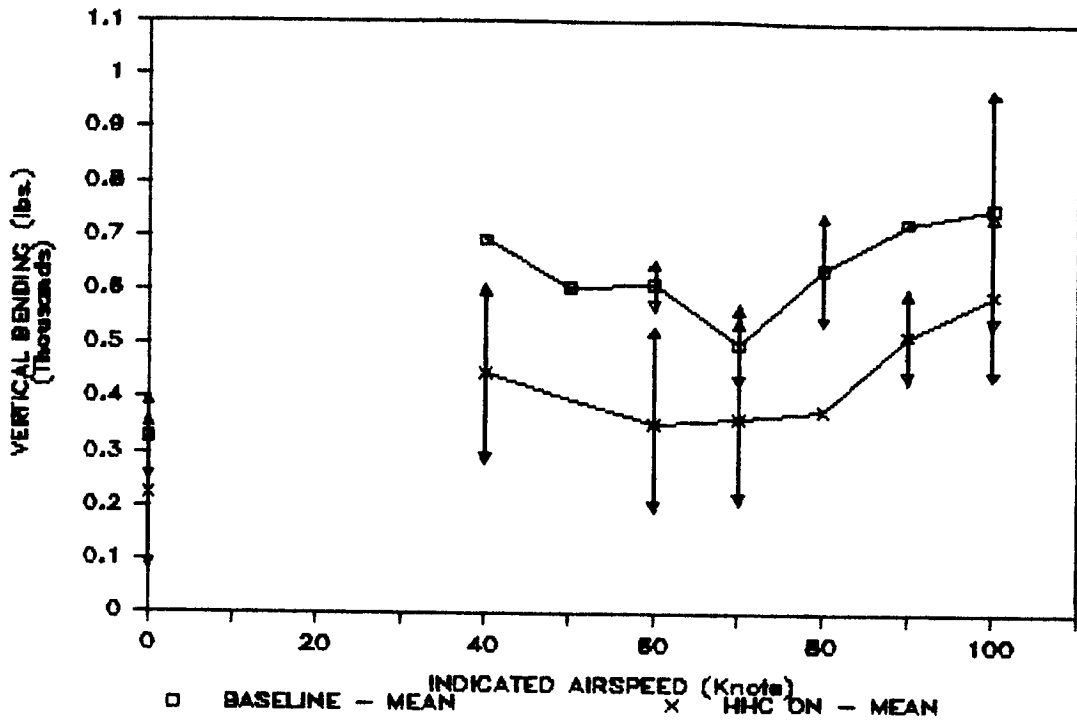
1984 CLOSED LOOP HHC
 5P PITCH LINK LOAD VERSUS AIRSPEED
 Figure 102



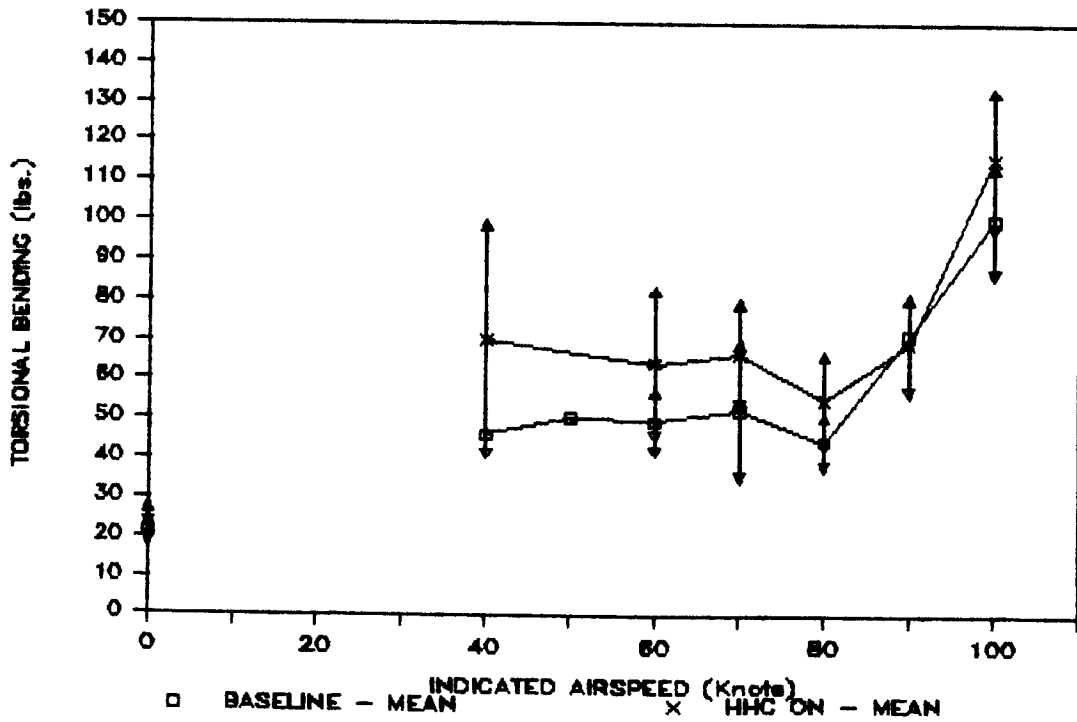
1984 CLOSED LOOP HHC
 1/2 PEAK TO PEAK PITCH LINK LOAD VERSUS AIRSPEED
 Figure 103



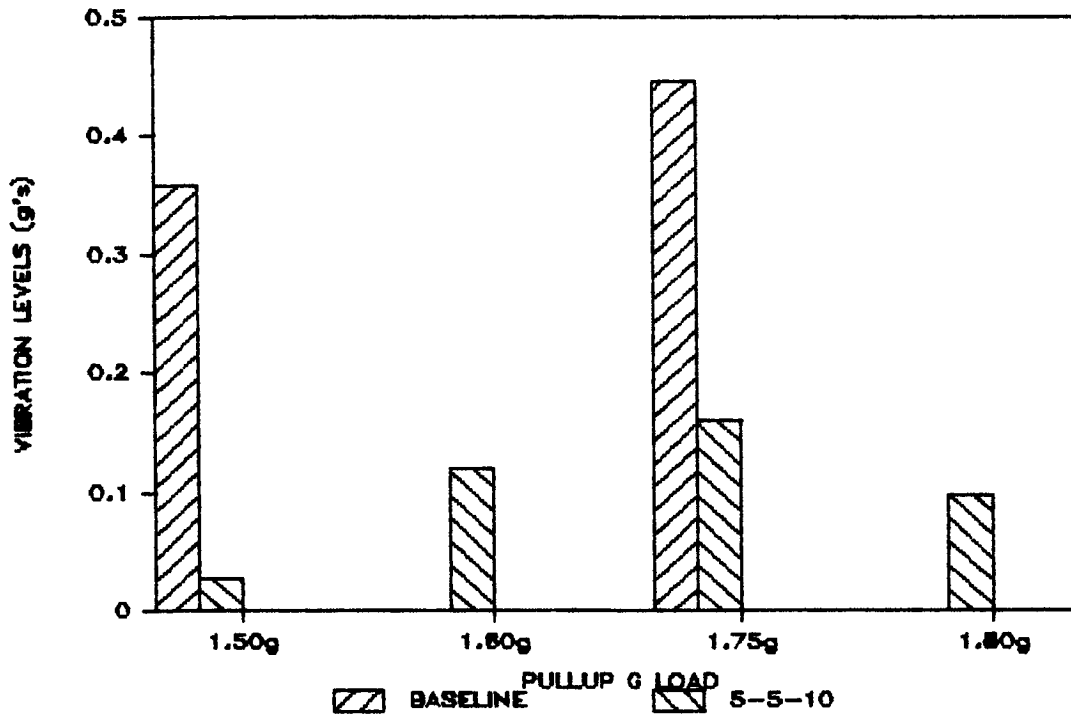
1984 CLOSED LOOP HHC
 4P LATERAL TAIL BOOM BENDING VERSUS AIRSPEED
 Figure 104



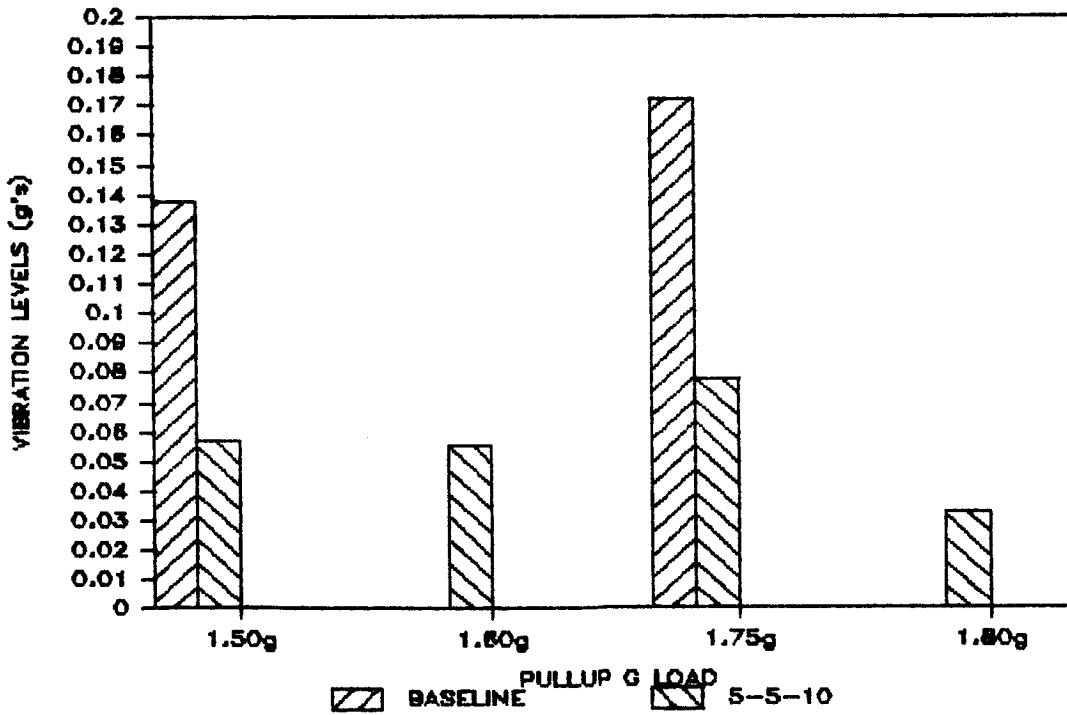
1984 CLOSED LOOP HHC
 4P VERTICAL TAIL BOOM BENDING VERSUS AIRSPEED
 Figure 105



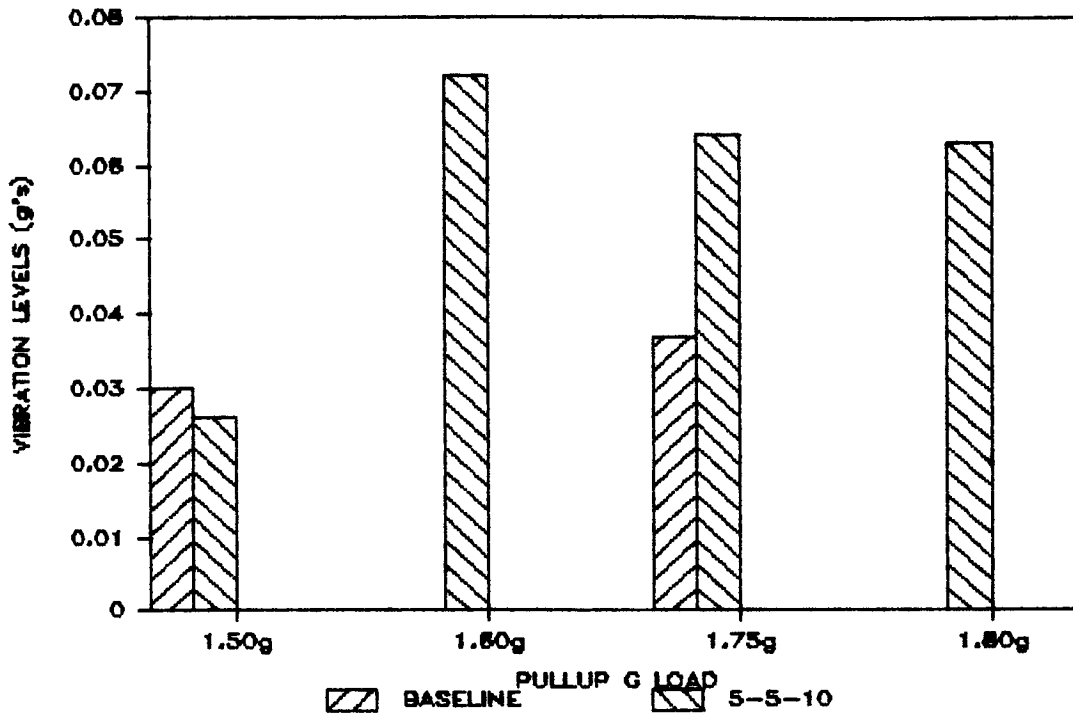
1984 CLOSED LOOP HHC
 4P TORSIONAL TAIL BOOM BENDING VERSUS AIRSPEED
 Figure 106



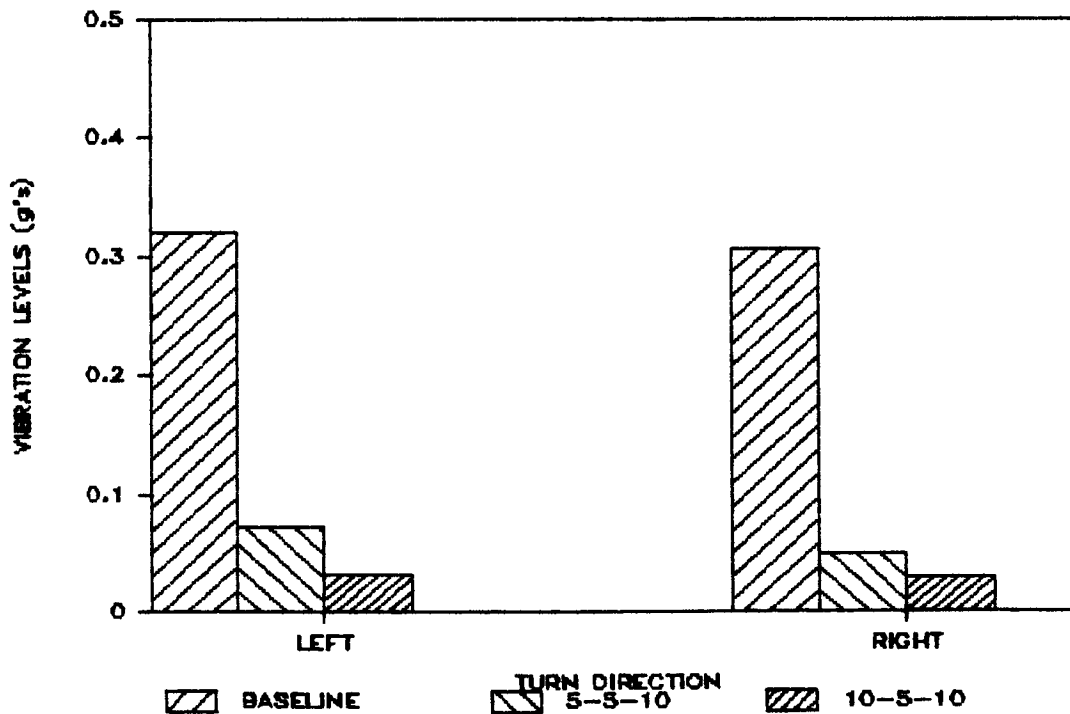
1984 CLOSED LOOP RESULTS
 4P VERTICAL PILOT SEAT VIBRATIONS DURING 80 KNOT PULLUPS
 Figure 107



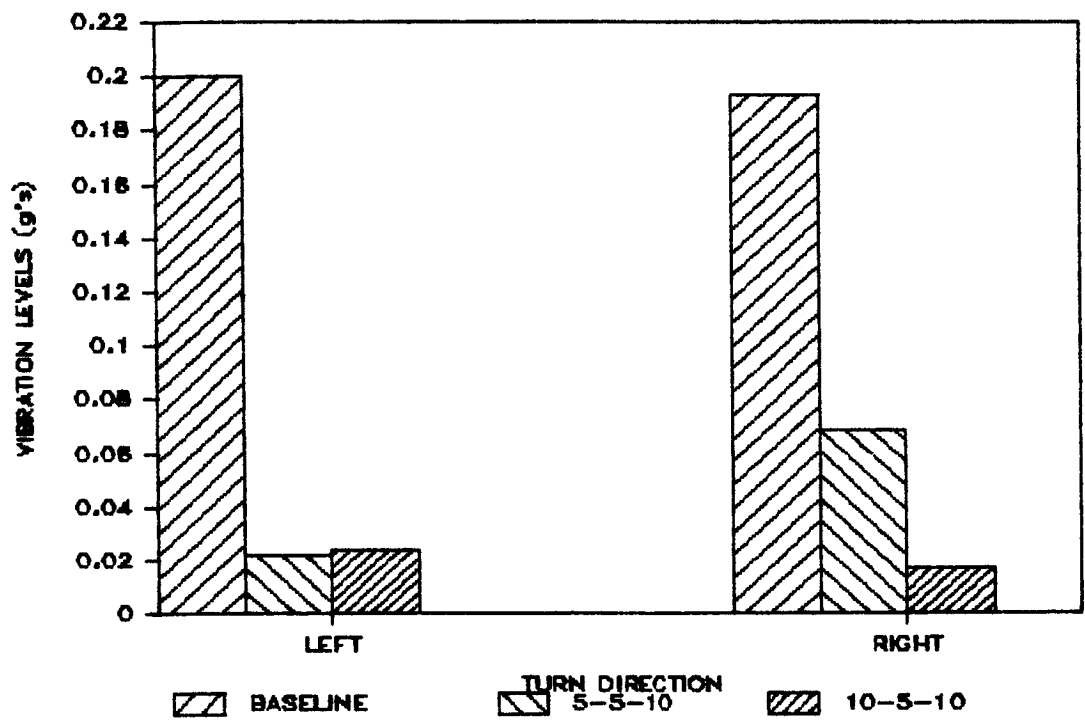
1984 CLOSED LOOP RESULTS
 4P LATERAL PILOT SEAT VIBRATIONS DURING 80 KNOT PULLUPS
 Figure 108



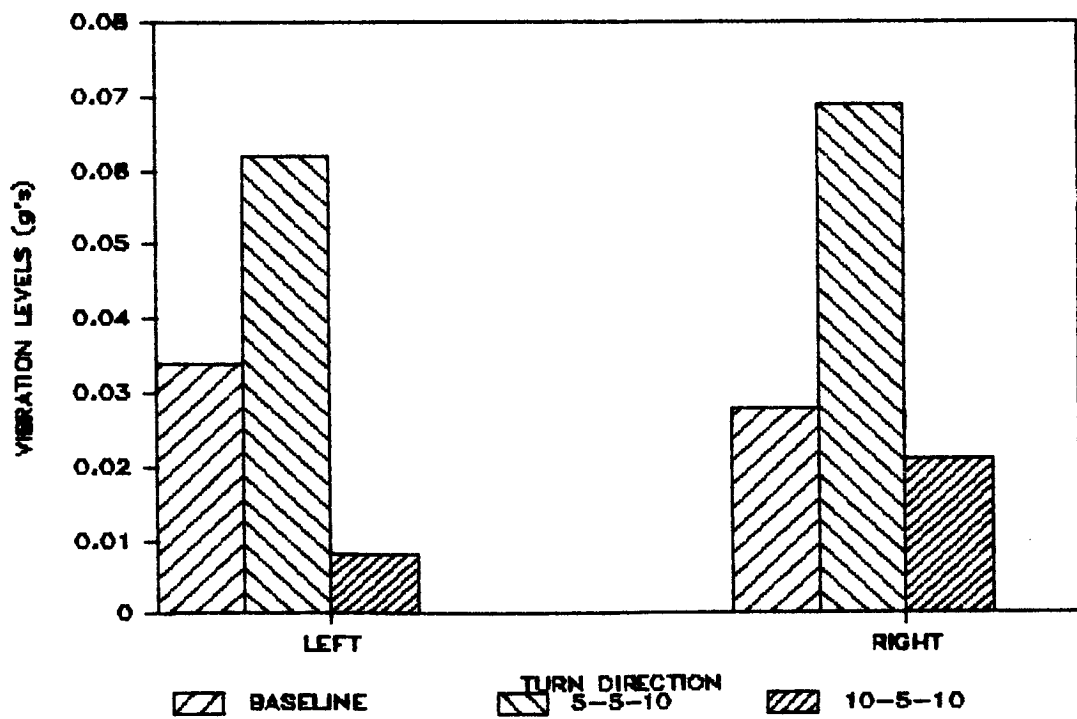
1984 CLOSED LOOP RESULTS
 4P LONGITUDINAL PILOT SEAT VIBRATIONS DURING 80 KNOT PULLUPS
 Figure 109



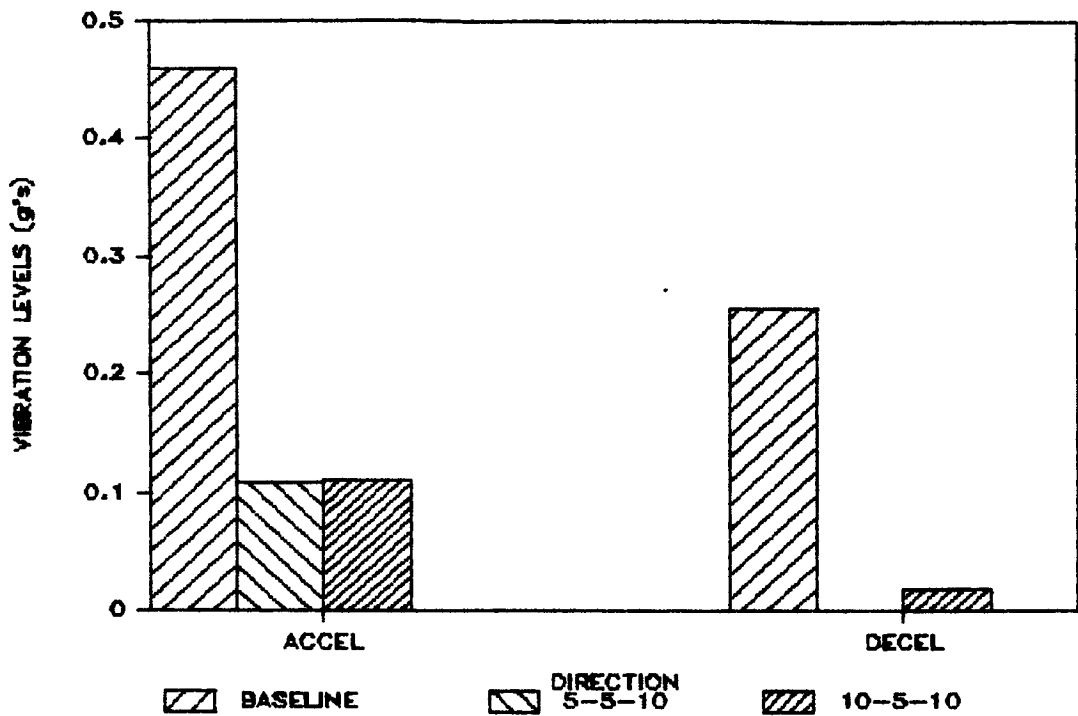
1984 CLOSED LOOP RESULTS
 4P VERTICAL PILOT SEAT VIBRATIONS DURING 80 KNOT 30 DEGREE BANK TURNS
 Figure 110



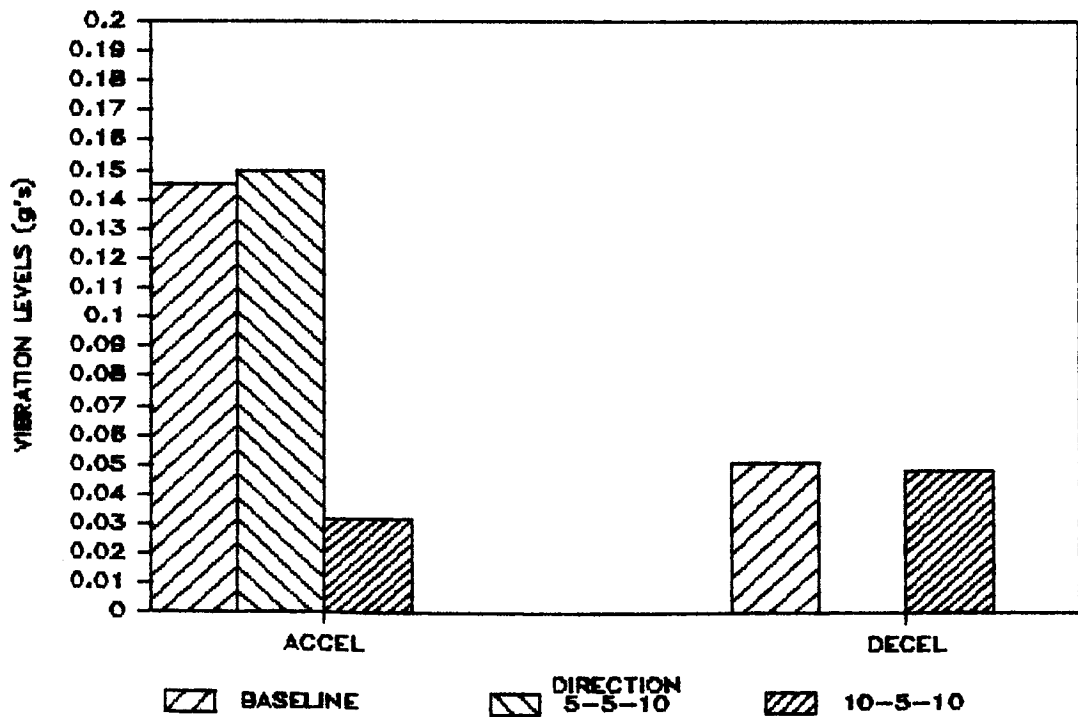
1984 CLOSED LOOP RESULTS
 4P LATERAL PILOT SEAT VIBRATIONS DURING 80 KNOT 30 DEGREE BANK TURNS
 Figure 111



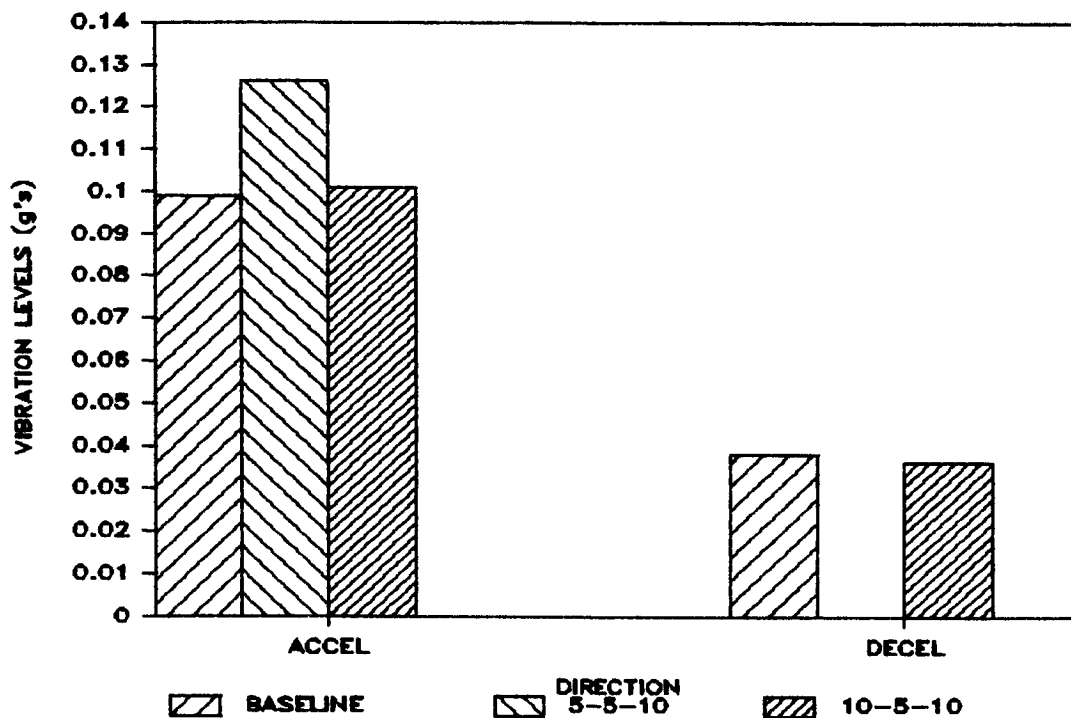
1984 CLOSED LOOP RESULTS
 4P LONGITUDINAL PILOT SEAT VIBRATIONS DURING 80 KNOT 30 DEGREE BANK TURNS
 Figure 112



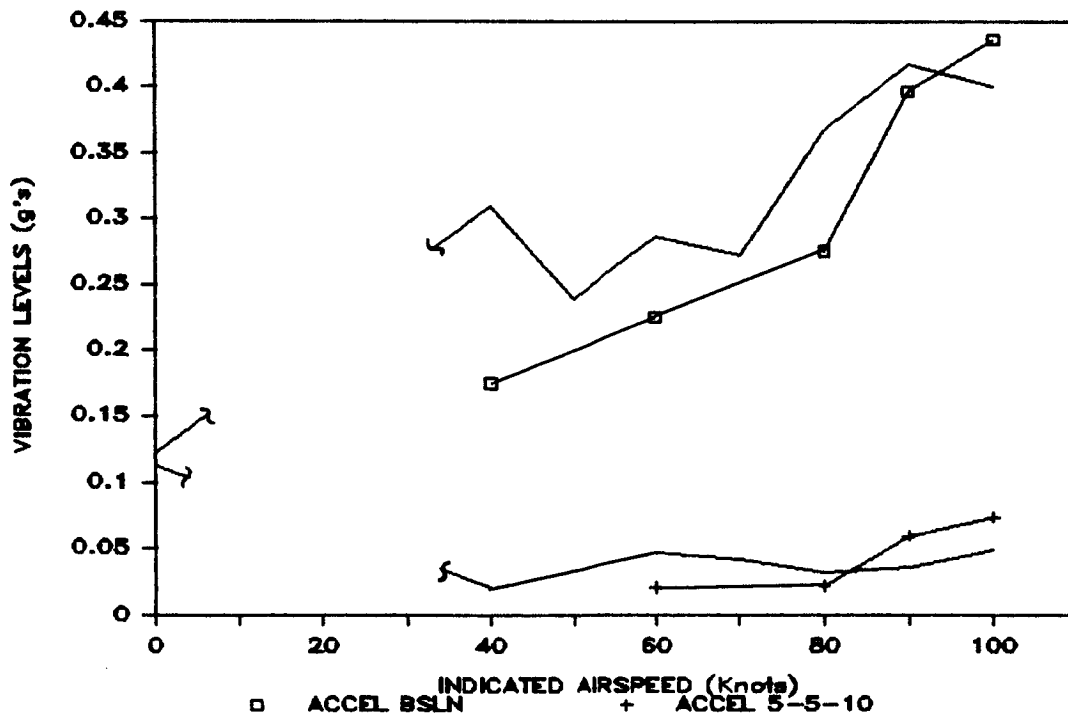
1984 CLOSED LOOP RESULTS
 4P VERTICAL PILOT SEAT VIBRATIONS DURING 40 - 100 KNOT
 ACCELERATIONS AND DECELERATIONS
 Figure 113



1984 CLOSED LOOP RESULTS
 4P LATERAL PILOT SEAT VIBRATIONS DURING 40 - 100 KNOT
 ACCELERATIONS AND DECELERATIONS
 Figure 114



1984 CLOSED LOOP RESULTS
 4P LONGITUDINAL PILOT SEAT VIBRATIONS DURING 40 - 100 KNOT
 ACCELERATIONS AND DECELERATIONS
 Figure 115



1984 CLOSED LOOP RESULTS
 4P VERTICAL PILOT SEAT VIBRATIONS DURING 40 - 100 KNOT
 SPEED SWEEP ACCELERATIONS
 Figure 116

X. APPENDICIES

APPENDIX A: TAIL ROTOR STRESS ANALYSIS

In the following pages, the tail rotor control system is analyzed. When the boost actuator was removed, the stock OH-6A parts were installed. Due to the numerous modifications to this OH-6A, the safety review board requested the stress analysis. With these results, the OH-6A control system was approved for flight testing.

TAIL ROTOR CONTROLS

PELLCRANK ASSEMBLY, TAIL ROTOR CONTROL

HHC STA 98750

LUG F-BEARING RETENSION

ORIGINAL PAGE IS
OF POOR QUALITY

R.H. BEARING LOADED AS SHOWN:

ASSUME INTERFACE PRESSURE VARIATION BETWEEN BALL BEARING OUTER RACE AND CYLINDRICAL WALL OF COUNTERBORE RESULTS IN VARIABLE INTENSITY OF FORCE PARALLEL TO

R_{FR} ACCORDING TO THE COSINE OF THE ANGLE DIA DIAMETRAL LOCATION, $.75 \text{ DIA} \pm \frac{\pi x}{2R}$.

AN EQUIVALENT RECTANGULAR DISTRIBUTION WITH CONSTANT RUNNING LOAD EQUAL TO THE MAXIMUM AT $x=0$ IS CONSIDERED TO BE SPREAD OVER A WIDTH $k\bar{D}$, WHERE $k = \int_0^{\alpha} \cos \frac{\pi x}{2R} dx = \frac{2}{\pi} \approx .64$

THE MEAN RADIUS OF FLANGE, $\bar{R} = \frac{1}{2} (.53 + \frac{.75}{2}) = .453 \text{ IN}$, SUBTENDING OVER ARC $2\alpha = 2 \sin^{-1} k = 2 (\sin^{-1} .64) \approx 80^\circ$ IS USED TO COMPUTE ASSUMED EQUIVALENT SHEAR AREA SECTOR,

$$A_s = \frac{80^\circ}{360^\circ} 2\pi \bar{R} d = (1.40) (.453) (.155) = .098 \text{ IN}^2$$

THE LOAD, R_{FR} , IS RESISTED BY SHEAR AND CANTILEVER BENDING OF THE FLANGE, PLUS CIRCUMFERENTIAL TENSION AND SHEAR IN THE RIM AT α , INTERACTING IN COMBINATION.

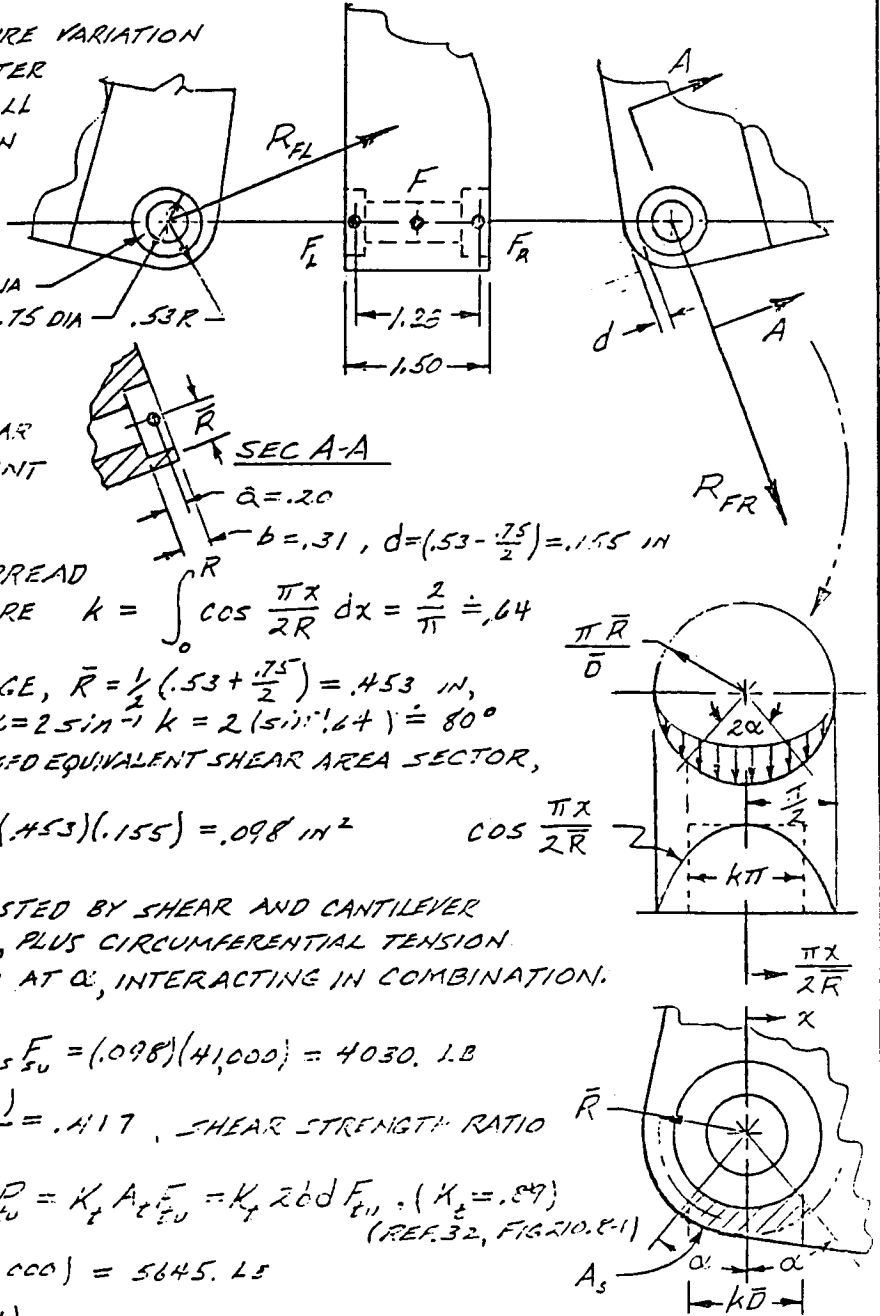
SHEAR STRENGTH, $F_{su} = A_s F_{su} = (.098)(41,000) = 4030 \text{ LB}$

$$R_s = \frac{1.5 R_{FR}}{F_{su}} = \frac{1.5(1121)}{4030} = .417, \text{ SHEAR STRENGTH RATIO}$$

RIM TENSILE STRENGTH, $P_{tu} = K_t A_t F_{tu} = K_t 2\alpha d F_{tu}$ ($K_t = .89$)
(REF. 32, FIG 210.8-1)

$$P_{tu} = (.89)(2 \times .31 \times .155)(66,000) = 5645 \text{ LB}$$

$$R_t = \frac{1.5 R_{FR}}{P_{tu}} = \frac{1.5(1121)}{5645} = .298, \text{ TENSILE STRENGTH RATIO}$$



TAIL ROTOR CONTROLS

BELLCRANK ASSEMBLY, TAIL ROTOR CONTROL

HHC STA 98150

LUG F (CONT'D)

RIM BENDING:

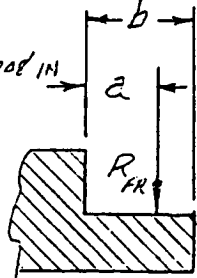
SCALE: 2/1

$$\bar{z}_o = \frac{\sin \alpha}{\alpha} \bar{R} \left(1 + \frac{1}{12} \frac{d^2}{\bar{R}^2}\right)$$

$$= (.9207)(.4525)(1.010) = .4208 \text{ IN}$$

$$A_s = 2\alpha \bar{R} d$$

$$= 1.3963(.4525)(.155) = .0979 \text{ IN}^2$$



$$I_{1-1} = \frac{1}{4} (\alpha + \sin \alpha \cos \alpha) (R_o^4 - R_i^4) \quad \text{SEC A-A}$$

$$= .29763 [(.530)^4 - (.375)^4] = .01760 \text{ IN}^4$$

$$I_{o-o} = I_{1-1} - A_s \bar{z}_o^2 = .01760 - .0979(.4208)^2 = .000265 \text{ IN}^4$$

$$z_c = R_o - \bar{z}_o = (.530 - .421) = .109 \text{ IN}$$

$$M = a R_{FR} = (.20)(1121) = 224.2 \text{ LB IN}$$

$$f_b = \frac{M z_c}{I_{o-o}} = \frac{(224.2)(.109)}{.000265} = 92,200 \text{ PSI}; F_{CU} \cong 60 \text{ KSI (ST)}$$

$$F_{bu} = f_m + f'_o (k-1) = [75 + 70(1.5-1)] \frac{60}{75} = 88 \text{ KSI (REF BRUHN, TABLE C3.2)}$$

BENDING STRENGTH RATIO; $R_b = \frac{1.5 f_b}{F_{bu}} = \frac{1.5(92,200)}{88,000} = 1.572$

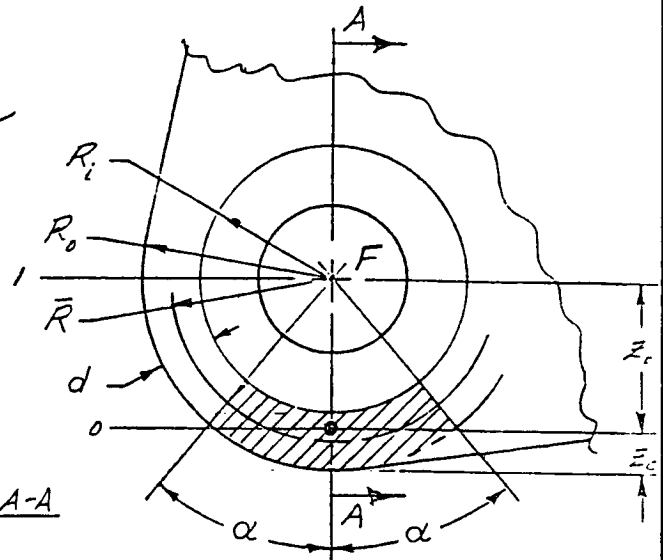
LUG FACTOR 1.15 IS APPLICABLE.

$$M.S. = \frac{1}{1.15} \left[\frac{1}{\sqrt{R_b^2 + R_s^2}} + \frac{1}{R_t} \right] - 1$$

$$M.S. = \frac{1}{1.15} \left[\frac{1}{\sqrt{(1.572)^2 + (.417)^2}} + \frac{1}{.298} \right] - 1$$

$$= \underline{\underline{+2.5 \text{ M.S.}}}$$

(BENDING, SHEAR AND LUG TENSION)



- $\alpha = 40^\circ (.6981 \text{ RAD})$
- $a = .200 \text{ IN}$
- $b = .310$
- $d = .155$
- $R_o = .530$
- $R_i = .375$
- $\bar{R} = .4525$

TAIL ROTOR CONTROLS

BELLCRANK ASSEMBLY, TAIL ROTOR CONTROL-

HHC STA 98.50

ORIGINAL PAGE IS
OF POOR QUALITY

LUG F - BOLT

NAS 1304-34 (REF DWG 369ASK3060 SHT 2 ZONE 16-F)

MATERIAL: ALLOY STEEL, 160-180 KSI F_{tu} (REF P.1066 HH STDS MANUAL)
DIAMETER (BEFORE CAD. PLATE), $D = .2484$ IN

UPON YIELDING, RADIAL CLEARANCE BETWEEN BUSHING (.375 DIA) AND HOLE (.406 DIA) IS ZERO AND BOLT INITIAL TENSION IS LOST. BENDING MOMENT REACTED BY BALL BEARING IS ASSUMED TO BE NEGLIGIBLE. ALSO, IT IS ASSUMED THAT SUPPORT LUG OF 369ASK3186 PROVIDES NEGLIGIBLE MOMENT REACTION.

$$P_{FR} = \sqrt{(P'_{FRX})^2 + (P'_{FRZ})^2} = \sqrt{(199)^2 + (801)^2} = 825 \text{ LB}$$

(REF ANALYSIS OF 369ASK3186)

$$e = \left(\frac{.217}{2} + .031 + .032 + \frac{.31}{2} \right) \doteq .327 \text{ IN}$$

$$M_{FR} = e P_{FR} = (.327)(825) = 270 \text{ LB IN}$$

ASSUME BEARING INNER RACE CONTRIBUTES NO HELP.

$$\frac{I}{C} = \frac{\pi D^3}{32} = \frac{\pi (.2484)^3}{32} = .00150 \text{ IN}^3$$

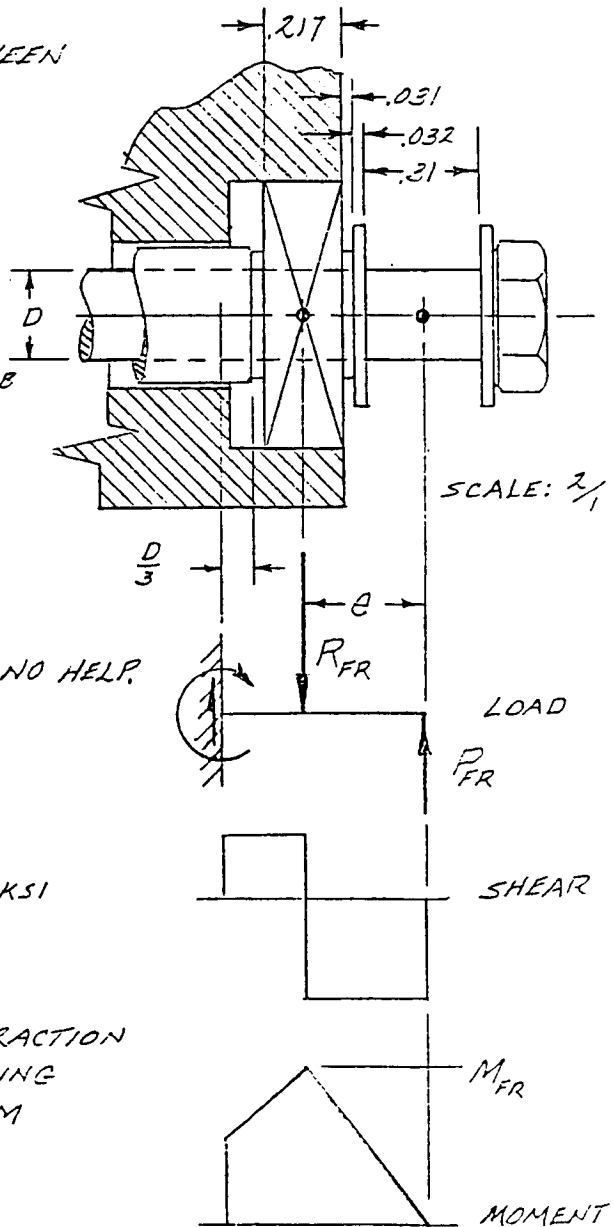
$$f_b = \frac{M_{FR}}{I/C} = \frac{270}{.00150} \doteq 179,400 \text{ PSI}$$

$$F_{bu} = f_m + f_b'(k-1) = 160 + 155(1.7-1) = 268 \text{ KSI}$$

(REF TABLE C3.2, BRJHN)

ASSUME NEGLIGIBLE SHEAR STRESS INTERACTION UNDER LINE OF ACTION OF BALL BEARING REACTION, R_{FR} , THE REGION OF MAXIMUM MOMENT, M_{FR} .

$$M.S. \text{ (BOLT BENDING)} = \frac{F_{bu}}{1.5 f_b} - 1 = \frac{268,000}{1.5(179,400)} - 1 = \boxed{0.00} \text{ M.S.}$$



SCALE: 2/1

TAIL ROTOR CONTROLS

PELLCRANK ASSEMBLY, TAIL ROTOR CONTROL

HHC STA. 98.50

ORIGINAL PAGE IS
OF POOR QUALITY

LUG F-BALL BEARING 369A7951-19 (MS27641-4)

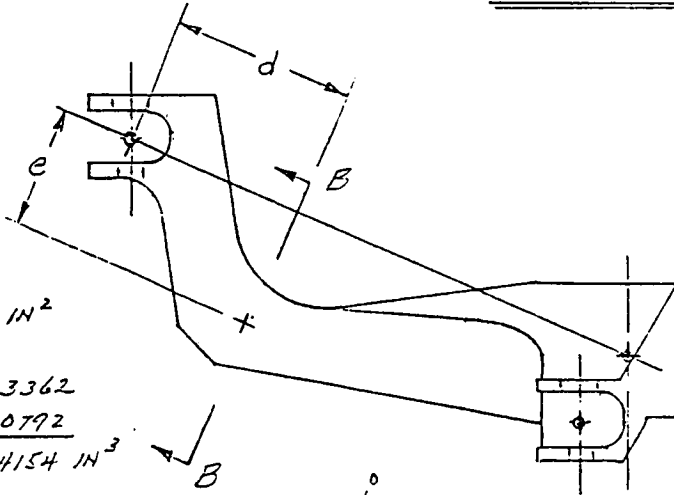
RADIAL LIMIT LOAD RATING = 1880. LBS (REF H.H. STANDARD MANUAL, P. 5500.2)

APPLIED LIMIT LOAD, $R_{FR} = 1121. LB$ (JAMMED CONTROL CONDITION)

$$M.S. = \frac{1880}{1121} - 1 = \underline{\underline{+.68 \text{ M.S.}}}$$

(BALL BEARING RADIAL LOAD)

SECTION E-E



A

$$\textcircled{1} A_1 = WA = (1.00)(.82) = .8200$$

$$\textcircled{2} A_2 = \frac{1}{2}Wb = \frac{1}{2}(1.00)(.18) = .0900$$

$$A = .9100 \text{ IN}^2$$

Q_{1-1}

$$\textcircled{1} Q_1 = A_1 \frac{a}{2} = (.82) \left(\frac{.82}{2} \right) = .3362$$

$$\textcircled{2} Q_2 = A_2 \left(a + \frac{b}{3} \right) = (.09) \left(.82 + \frac{.18}{3} \right) = .0792$$

$$Q_{1-1} = .4154 \text{ IN}^3$$

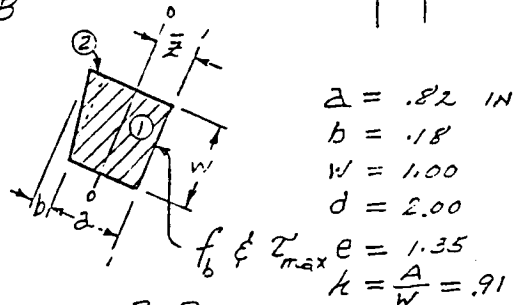
$$\bar{z} = \frac{Q_{1-1}}{A} = \frac{.4154}{.9100} = .4565 \text{ IN}; \quad I^2 = .2084 \text{ IN}^2$$

I_{1-1}

$$\textcircled{1} \begin{cases} Q_1 \frac{a}{2} = (.3362) \left(\frac{.82}{2} \right) = .1378 \\ \frac{WA^3}{12} = \frac{(1.00)(.82)^3}{12} = .0460 \end{cases}$$

$$\textcircled{2} \begin{cases} Q_2 \left(a + \frac{b}{3} \right) = (.0792) (.88) = .0697 \\ \frac{Wb^3}{36} = \frac{(1.00)(.18)^3}{36} = .0002 \end{cases}$$

$$I_{1-1} = .2537 \text{ IN}^4$$



SECTION B-B

SCALE: 1/2

$$I_{0-0} = I_{1-1} - A \bar{z}^2 = .2537 - .9100(.2084) = .0641 \text{ IN}^4$$

BENDING STRESS, $f_b = \frac{Mc}{I} = \frac{P_{DE} d \bar{z}}{I_{0-0}} = \frac{390(2.00)(.457)}{.0641} = 5560. \text{ PSI}$

TORSIONAL SHEAR STRESS, $\tau_{max} = K_1 \frac{P_{TE} e}{W k^2}$ $\frac{k}{W} = \frac{.91}{1.00} \Rightarrow K_1 = 4.62$ (REF. TABLE 21.2, P. 507, SHANLEY, STRENGTH OF MATERIALS)

$$\tau_{max} = (4.62) \frac{(390)(1.35)}{(1.00)(.91)^2} = 2940. \text{ PSI}$$

$$M.S. = \frac{1}{1.5 \sqrt{\left(\frac{f_b}{F_{bu}} \right)^2 + \left(\frac{\tau_{max}}{F_{su}} \right)^2}} - 1 = \frac{1}{1.5 \sqrt{\left(\frac{5560}{50000} \right)^2 + \left(\frac{2940}{41000} \right)^2}} - 1 = \underline{\underline{6.0 \text{ M.S.}}}$$

(BENDING & TORSION)

TAIL ROTOR CONTROLS

SUPPORT, BELLCRANK, TAIL ROTOR
 HHC STA 92.50

ORIGINAL PAGE IS
 OF POOR QUALITY

MATERIAL:

2024-T351 BAR
 QQ-A-225/6
 (2.50 x 5.00 x 5.25)

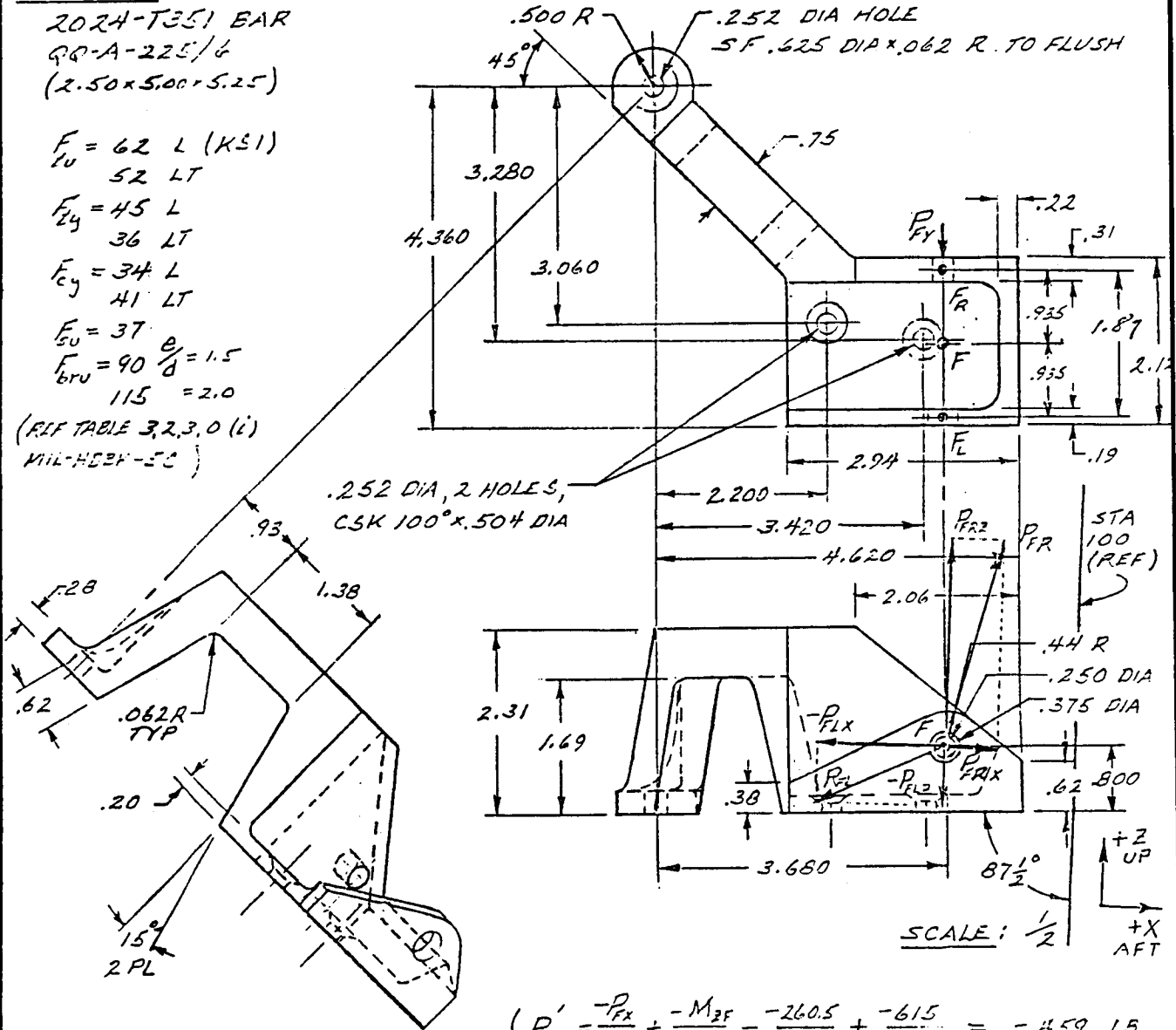
$F_u = 62 \text{ L (KSI)}$
 52 LT

$F_{24} = 45 \text{ L}$
 36 LT

$F_{cy} = 34 \text{ L}$
 41 LT

$F_{50} = 37$
 $F_{brv} = 90 \frac{b}{d} = 1.5$
 115 = 2.0

(REF TABLE 3.2.3.0 (i)
 MIL-HDBK-5C)



LOADS ON SUPPORT LUGS:
 (APPLIED ON LUGS BY BELLCRANK)

(REF STRESS ANALYSIS OF
 369ASK318'S BELLCRANK)

LOADS ARE REVERSIBLE AS A UNIT.

$$\begin{aligned} P'_{FLX} &= \frac{-P_{FX}}{2} + \frac{-M_{2F}}{1.87} = \frac{-260.5}{2} + \frac{-615}{1.87} = -459. \text{ LB} \\ P'_{FRX} &= \frac{-P_{FX}}{2} - \frac{-M_{2F}}{1.87} = \frac{-260.5}{2} - \frac{-615}{1.87} = +197. \text{ LB} \\ P'_{FL2} &= \frac{-P_{F2}}{2} - \frac{-M_{XF}}{1.87} = \frac{-454.4}{2} - \frac{+1073}{1.87} = -347. \text{ LB} \\ P'_{FR2} &= \frac{-P_{F2}}{2} + \frac{-M_{XF}}{1.87} = \frac{-454.4}{2} + \frac{+1073}{1.87} = +801. \text{ LB} \end{aligned}$$

(LIMIT)

TAIL ROTOR CONTROLS

SUPPORT, BELLCRANK, TAIL ROTOR

HHC STA 98.50

369 ASK 3186

FORCES: (APPLIED ON SUPPORT BY BELLCRANK)

ORTHOGONAL FORCE COMPONENTS ARE WITH REFERENCE TO THE X, Y PLANE OF THE BASE ($2\frac{1}{2}^\circ$ FROM THE AIRCRAFT X, Y PLANE).

$$P_{FL} = \sqrt{(-459)^2 + (-347)^2} = 575. \text{ LB}$$

$$P_{FR} = \sqrt{(+199)^2 + (+801)^2} = 825.$$

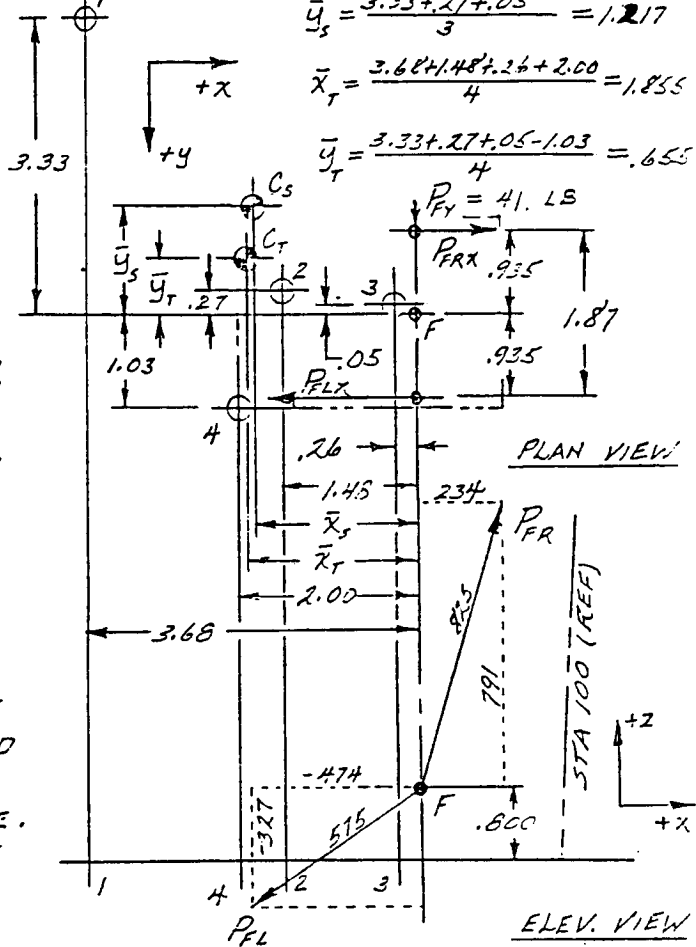
$$P_{FLX} = -575 \cos(\tan^{-1} \frac{-347}{-459} - 2\frac{1}{2}^\circ) = -474.$$

$$P_{FLZ} = -575 \sin(\tan^{-1} \frac{-347}{-459} - 2\frac{1}{2}^\circ) = -327.$$

$$P_{FRX} = 825 \sin(\tan^{-1} \frac{199}{801} + 2\frac{1}{2}^\circ) = +234.$$

$$P_{FRZ} = 825 \cos(\tan^{-1} \frac{199}{801} + 2\frac{1}{2}^\circ) = +791.$$

BELLCRANK SUPPORT IS ASSUMED TO BE RIGID. INTERSECTION OF THE EDGES OF THE BASE IS TREATED LIKE A CONNECTOR PROVIDED THE REACTION IS INTERFACE PRESSURE. SHEAR REACTIONS OCCUR ONLY AT THE THREE ACTUAL CONNECTORS.



$$\bar{x}_s = \frac{3.68 + 1.48 + 2.26}{3} = 1.80711$$

$$\bar{y}_s = \frac{3.33 + .27 + .05}{3} = 1.217$$

$$\bar{x}_T = \frac{3.68 + 1.48 + 2.26 + 2.00}{4} = 1.855$$

$$\bar{y}_T = \frac{3.33 + .27 + .05 - 1.03}{4} = .655$$

MOMENTS (TRANSMITTED FROM BELLCRANK)

$$M_{x_{C_T}} = .800 P_{Fy} - (\bar{y}_T + .935) P_{FLZ} + (.935 - \bar{y}_T) P_{FRZ} \quad \text{PER R.H. RULE}$$

$$= .800(+41) - (.655 + .935)(-327) + (.935 - .655)(+791) = +774. \text{ LB IN}$$

$$M_{y_{C_T}} = -.800 (P_{FLX} + P_{FRX}) + \bar{x}_T (P_{FLZ} + P_{FRZ}) \quad \text{PER R.H. RULE}$$

$$= -.800 [(-474) + (+234)] + (1.855) [(-327) + (+791)] = +1053.$$

$$M_{z_{C_s}} = -\bar{x}_s P_{Fy} + (\bar{y}_s - .935) P_{FRX} + (\bar{y}_s + .935) P_{FLX} \quad \text{PER R.H. RULE}$$

$$= -(1.807)(+41) + (1.217 - .935)(+234) + (1.217 + .935)(-474) = -1028.$$

TAIL ROTOR CONTROLS

SUPPORT, BELLCRANK, TAIL ROTOR
H H C, STA 98.50

COMBINED TENSION AND BENDING AT THREAD ROOT

$$\text{BENDING MOMENT, } M = m P_{33} = (.20)(207) = 41.4 \text{ LB. IN.}$$

$$\text{AT THREAD ROOT, } \frac{I}{c} = \frac{\pi}{32} d^3 = \frac{\pi}{32} (.2062)^3 = .000861 \text{ IN}^3$$

$$f_b = \frac{M}{I/c} = \frac{41.4}{.000861} = 48,100 \text{ PSI}$$

$$R_b = \frac{1.5 f_b}{F_u} = \frac{1.5(48,100)}{160,000} = .451$$

$$\text{AT THREAD ROOT, } A_t = \frac{\pi}{4} d^2 = \frac{\pi}{4} (.2062)^2 = .0334 \text{ IN}^2$$

$$f_t = \frac{P_3}{A_t} = \frac{855}{.0334} = 25,600 \text{ PSI}$$

$$R_a = \frac{1.5 f_t}{F_u} = \frac{1.5(25,600)}{160,000} = .240$$

$$M.S. > \frac{1}{R_a + R_b} - 1 = \frac{1}{.240 + .451} - 1$$

(THREAD ROOT BENDING AND TENSION)

⇒ YIELD MARGIN OF SAFETY IS POSITIVE.

AFTER YIELDING, ADDITIONAL MOMENT SUPPORT WILL BE FURNISHED BY INTERFACE PRESSURE DISTRIBUTIONS NEAR UPPER AND LOWER HOLE EDGES OF BOTTOM PLATE. THE ABOVE ANALYSIS IS CONSERVATIVE.

HINGE CONNECTION AT POINT F_R

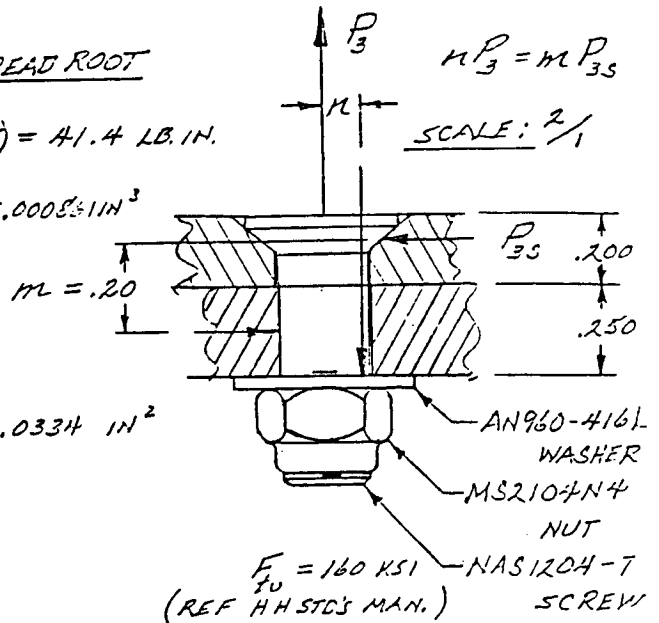
$$\text{BEARING AREA, } A_{br} = t d = (.31)(.250) = .0775 \text{ IN}^2$$

$$f_{br} = \frac{P_{FR}}{A_{br}} = \frac{825}{.0775} = 10,650 \text{ PSI}$$

$$\frac{e}{D} = \frac{.500}{.250} = 2.0 \Rightarrow F_{brU} = 115 \text{ KSI}$$

LUG FACTOR 1.15 IS APPLICABLE.

$$M.S. \text{ (BEARING/TEAR-OUT)} = \frac{F_{brU}}{1.15 \times 1.50 f_{br}} - 1 = \frac{115,000}{1.725(10,650)} - 1 = \underline{\underline{+ 5.3 \text{ M.S.}}}$$



$$> \underline{\underline{+ .45 \text{ M.S.}}}$$

TAIL ROTOR CONTROLS

SUPPORT, BELLCRANK, TAIL ROTOR

HHC STA 98.50

BOLT SHEARS:

ASSUME SHEAR LOADS FROM ΣF_{xcs} AND ΣF_{ycs} ARE SHARED EQUALLY AND LOADS FROM ΣM_{zcs} ARE PROPORTIONAL TO MOMENT ARM LENGTHS ABOUT C_s .

$$x_1 = (1.807 - 3.68) = -1.873 ; x_2 = (1.807 - 1.48) = .327 ; x_3 = (1.807 - .26) = 1.547$$

$$y_1 = (1.217 - 3.33) = -2.113 ; y_2 = (1.217 - .27) = .947 ; y_3 = (1.217 - .05) = 1.167$$

$$z_1 = z_2 = z_3 = 0 ; P_{cx} = P_{FRX} + P_{FLX} = 234 + (-474) = -240 \text{ LB} ; P_{cy} = P_{FRY} + P_{FLY} = (41.0 + 0) = 41. \text{ LB}$$

$$P_{1x} = \frac{P_{cx}}{3} + \frac{y_1 M_{zcs}}{\Sigma x_n^2 + \Sigma y_n^2} \quad P_{1y} = \frac{P_{cy}}{3} + \frac{x_1 M_{zcs}}{\Sigma x_n^2 + \Sigma y_n^2}$$

$$P_{2x} = \frac{P_{cx}}{3} + \frac{y_2 M_{zcs}}{\Sigma x_n^2 + \Sigma y_n^2} \quad P_{2y} = \frac{P_{cy}}{3} + \frac{x_2 M_{zcs}}{\Sigma x_n^2 + \Sigma y_n^2}$$

$$P_{3x} = \frac{P_{cx}}{3} + \frac{y_3 M_{zcs}}{\Sigma x_n^2 + \Sigma y_n^2} \quad P_{3y} = \frac{P_{cy}}{3} + \frac{x_3 M_{zcs}}{\Sigma x_n^2 + \Sigma y_n^2}$$

NAS1204-7
STEEL SCREWS
(R1157, HH STDS. MAX)

$$\frac{M_{zcs}}{\Sigma x_n^2 + \Sigma y_n^2} = \frac{-1028}{(-1.873)^2 + (.327)^2 + (1.547)^2 + (-2.113)^2 + (.947)^2 + (1.167)^2} = -80.7 \text{ LB/IN}$$

$$P_{1x} = -80.7 + (-2.113)(-80.7) = +90.5 \text{ LB} ; P_{1y} = +13.7 + (-1.873)(-80.7) = +164.9 \text{ LB}$$

$$P_{2x} = -80.7 + (.947)(-80.7) = -156.4 ; P_{2y} = +13.7 + (.327)(-80.7) = -12.7$$

$$P_{3x} = -80.7 + (1.167)(-80.7) = -174.2 ; P_{3y} = +13.7 + (1.547)(-80.7) = -111.1$$

$$\text{RESULTANTS: } P_{1s} = \sqrt{P_{1x}^2 + P_{1y}^2} = \sqrt{(+90.5)^2 + (+164.9)^2} = 188. \text{ LB}$$

$$P_{2s} = \sqrt{P_{2x}^2 + P_{2y}^2} = \sqrt{(-156.4)^2 + (-12.7)^2} = 157.$$

$$P_{3s} = \sqrt{P_{3x}^2 + P_{3y}^2} = \sqrt{(-174.2)^2 + (-111.1)^2} = 207.$$

$$\text{BEARING AREA AT SCREW SHANK, } A_{br} = \pi d l = \pi (.2462)(.075) = .058 \text{ IN}^2$$

$$f_{br} = \frac{P_{3s}}{A_{br}} = \frac{207}{.058} = 3570. \text{ PSI (100° CSK HEAD IGNORED)}$$

⇒ NOT CRITICAL FOR BEARING (OR SHEAR) UNDER SCREW HEAD. M.S. HIGH

TAIL ROTOR CONTROLS

SUPPORT, BELLCRANK, TAIL ROTOR

HHC STA 98.50

ORIGINAL PAGE IS
OF POOR QUALITY

BOLT TENSIONS

DIMENSIONAL DATA: $\Delta x = \bar{x}_T - \bar{x}_C = (1.855 - 1.807) = .048$ IN
 $\Delta y = \bar{y}_C - \bar{y}_T = (1.217 - .655) = .562$

$a_1 = 1.875 - .048 = 1.825$ $b_1 = 2.113 + .562 = 2.675$
 $a_2 = .327 + .048 = .375$ $b_2 = .947 - .562 = .385$
 $a_3 = 1.547 + .048 = 1.595$ $b_3 = 1.187 - .562 = .625$
 $a_4 = 2.000 - 1.855 = .145$ $b_4 = .655 + 1.03 = 1.685$

EQUILIBRIUM EQUATIONS:

① $\sum F_z = 0$: $P_1 + P_2 + P_3 + P_4 = P_{CT}$; $P_{CT} = P_{FR2} + P_{FL2} = (+791 - 327) = +464$ LB

② $\sum M_{y_T} = 0$: $-a_1 P_1 + a_2 P_2 + a_3 P_3 - a_4 P_4 = M_{y_{CT}} = +1053$ LB IN

③ $\sum M_{x_{CT}} = 0$: $b_1 P_1 - b_2 P_2 - b_3 P_3 - b_4 P_4 = M_{x_{CT}} = +774$ LB IN

ASSUME CONNECTORS #2 AND #3 ARE BOTH LOCATED AT THE CENTROID OF THE PAIR.
 $P_{23} = P_2 + P_3$; $a_{23} = \frac{1}{2}(.375 + 1.595) = .985$; $b_{23} = \frac{1}{2}(.385 + .625) = .505$

① $P_1 + P_{23} + P_4 = +464$ (BOLT TENSIONS TO BE INDICATED POSITIVE)

② $-a_1 P_1 + a_{23} P_{23} - a_4 P_4 = M_{y_{CT}}$
 $P_1 + \frac{.985}{-1.825} P_{23} - \frac{.145}{-1.825} P_4 = \frac{+1053}{-1.825}$
 $P_1 - .5397 P_{23} + .0795 P_4 = -577.0$

③ $-b_1 P_1 - b_{23} P_{23} - b_4 P_4 = M_{x_{CT}}$
 $P_1 - \frac{.495}{-2.675} P_{23} - \frac{1.685}{-2.675} P_4 = \frac{+774}{-2.675}$
 $P_1 + .1850 P_{23} + .6299 P_4 = -289.35$

④ = ② - ① $-1.5397 P_{23} - .9205 P_4 = -1041.0$

$P_{23} - \frac{.9205}{-1.5397} P_4 = \frac{-1041}{-1.5397}$

$P_{23} + .5978 P_4 = +676.11$

TAIL ROTOR CONTROLS

SUPPORT, BELLCRANK, TAIL ROTOR HHC STA 98.50

BOLT TENSIONS (CONT'D.)

$$\textcircled{5} = \textcircled{3} - \textcircled{1} \quad -.8150 P_{23} - .3701 P_4 = -753.35$$

$$P_{23} - \frac{.3701}{-.8150} P_4 = \frac{-753.35}{-.8150}$$

$$P_{23} + .4541 P_4 = +924.36$$

$$\textcircled{6} = \textcircled{5} - \textcircled{4} \quad -.1437 P_4 = +248.25$$

$$P_4 = \frac{248.25}{-.1437} = -1728 \text{ LB (INTERFACE PRESSURE)}$$

$$\textcircled{5} \quad P_{23} = 924.36 - .4541(-1728) = +1709 \text{ LB}$$

$$\textcircled{4} \quad P_{23} = 676.11 - .5978(-1728) = +1709 \checkmark$$

$$\textcircled{3} \quad P_1 = -289.35 - .1850(1709) - .6299(-1728) = +483 \text{ LB (TENSION)}$$

$$\textcircled{2} \quad P_1 = -577.0 + .5397(1709) - .0795(-1728) = +483 \checkmark$$

$$\textcircled{1} \quad +483 + 1709 - 1728 = +464 \checkmark \Rightarrow P_2 = P_3 = \frac{1709}{2} = 855 \text{ LB}$$

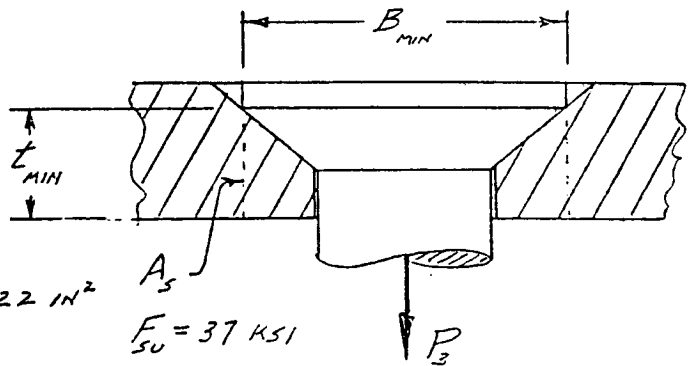
SCREW HEAD SHEAR-OUT:

NAS 1204-7 100° HD SCREW
 $B_{MIN} = .449 \text{ IN}$ (H.H. STD'S MAN, P1157)
 $t_{MIN} = .155 \text{ IN}$

$$A_s = \pi B_{MIN} t_{MIN} = \pi (.449)(.155) = .22 \text{ IN}^2$$

$$f_s = \frac{P_3}{A_s} = \frac{855}{.22} = 3900 \text{ PSI}$$

$$M.S. = \frac{F_{su}}{1.5 f_s} - 1 = \frac{37,000}{1.5(3900)} - 1 = \underline{\underline{+5.3 \text{ M.S.}}}$$



SCALE: $\frac{1}{4}$

REVERSED LOADING: (P_5 AT CORNER OF BASE DIAGONALLY OPPOSITE TO P_4)

$$P_1 = -212 \text{ LB (INTERFACE PRESSURE)}$$

$$P_2 = P_3 = +203 \text{ LB (TENSION)}$$

$$P_5 = -658 \text{ LB (INTERFACE PRESSURE)}$$

COMPUTED IN SAME WAY AS SHOWN ABOVE. \Rightarrow NOT CRITICAL

TAIL ROTOR CONTROLS

SUPPORT, BELLCRANK, TAIL ROTOR

HHC STA 981.50

SECTION A-A

ORTHOGONAL LOAD COMPONENTS APPLIED ON SUPPORT:

$$P_{1x} = 90.5 ; P_{1y} = 165. ; P_{1z} = -483. \text{ LB}$$

$$\left(\frac{I}{C}\right)_W = \frac{.75(.62)^2}{6} = .0481 \text{ IN}^3$$

$$\left(\frac{I}{C}\right)_z = \frac{.62(.75)^2}{6} = .0582 \text{ IN}^3$$

$$A_a = (.62)(.75) = .465 \text{ IN}^2$$

$$P_a = \frac{1}{2}\sqrt{2}(P_{1x} + P_{1y}) = .7071(90.5 + 165) = 181. \text{ LB}$$

$$M_{z-z} = 1.50 P_{1y} - 1.75 P_{1x} = 1.50(165) - 1.75(90.5) = 89.1 \text{ LB IN}$$

$$M_{W-W} = -2.30 P_{1z} + 2.00 \times \frac{1}{2}\sqrt{2}(P_{1x} + P_{1y}) = -2.30(-483) + 2.00(181) = 1473. \text{ LB IN}$$

$$T_{zw} = .7071(P_{1y} - P_{1x})(2.00) = 1.414(165 - 90.5) = 105. \text{ LB IN TORSION}$$

$$f_{b1} = \frac{M_W}{\left(\frac{I}{C}\right)_W} + \frac{M_z}{\left(\frac{I}{C}\right)_z} + \frac{P_a}{A_a} = \frac{1473}{.0481} + \frac{89.1}{.0582} + \frac{181}{.465} = (30,624 + 1531 + 389) = 32,544. \text{ PSI}$$

$$F_{bu} = f_m + f_o(k-1) = [62 + 57.5(1.5-1)] \frac{52+62}{2 \times 62} = 83.4 \text{ KSI (REF TABLE C3.2, BRUHN)}$$

$$M.S. = \frac{F_{bu}}{1.5 f_{b1}} - 1 = \frac{83400}{1.5(32544)} - 1 = +.71 \text{ M.S.}$$

COMBINED BENDING

COMBINED BENDING AND TORSION STRESS AT MIDDLE OF BOTTOM SIDE:

$$f_{b2} = (30,624 + 389) = 31,013 \text{ PSI} ; f_{bs} = \frac{3V}{2A_a} = \frac{3}{2} \frac{\frac{1}{2}\sqrt{2}(165-90.5)}{.465} = 170. \text{ PSI}$$

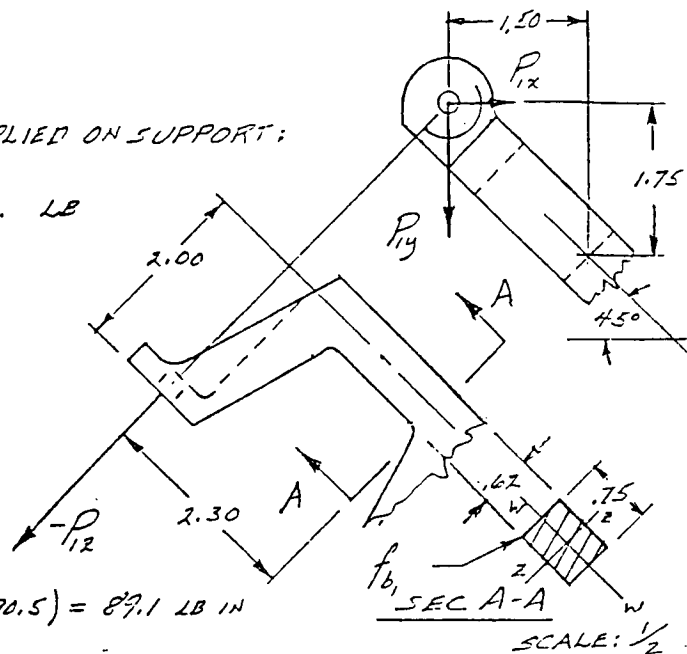
$$\text{TORSIONAL SHEAR STRESS, } \tau_s = K_1 \frac{T}{BD^2} ; \frac{D}{B} = \frac{.62}{.75} = .83 \Rightarrow K_1 = 4.5 \text{ (TABLE 21.2, SHANLEY, STR. OF MAT.)}$$

$$\tau_s = 4.5 \frac{105}{.75(.62)^2} = 1640 \text{ PSI} ; f_s = f_{bs} + \tau_s = (170 + 1640) = 1810. \text{ PSI}$$

$$R_s = \frac{1.5 f_s}{F_{bu}} = \frac{1.5(1810)}{83,400} = .0734 ; R_b = \frac{1.5 f_{b2}}{F_{bu}} = \frac{1.5(31,013)}{83,400} = .5578$$

$$M.S. = \frac{1}{\sqrt{R_b^2 + R_s^2}} - 1 = \frac{1}{\sqrt{(.5578)^2 + (.0734)^2}} - 1 = +.78 \text{ M.S.}$$

COMBINED TORSION AND BENDING



TAIL ROTOR CONTROLS

ROD ASSY, INTERMED. T/R CONTROL - HHC

LIMIT LOAD = 390 LB REF. REPORT 369-S-5202
P. 2.6-5

M/S 20470 AD 4 RIVET CHECK:

RIVET SHEAR STRENGTH = 388 LB REF. MIL-HDBK 5C
(SINGLE SHEAR) TABLE 8.12.6

BEARING ALLOW. ON .058 SHEET \approx 700 LB

ULT SHEAR ALLOW FOR 3 RIVETS = $6(388)$
= 2328 LB

M.S. (RIVET SHEAR) = $\frac{2328}{1.5(390)} - 1 = \underline{\underline{\text{HIGH M.S.}}}$

COLUMN ANALYSIS

TUBE $I_1 = 0.0193 \text{ in}^4$

ADAPTER $I_2 = \frac{\pi}{64} (.62)^4 = .0073 \text{ in}^4$

$\frac{EJ_2}{EJ_1} = 0.38$

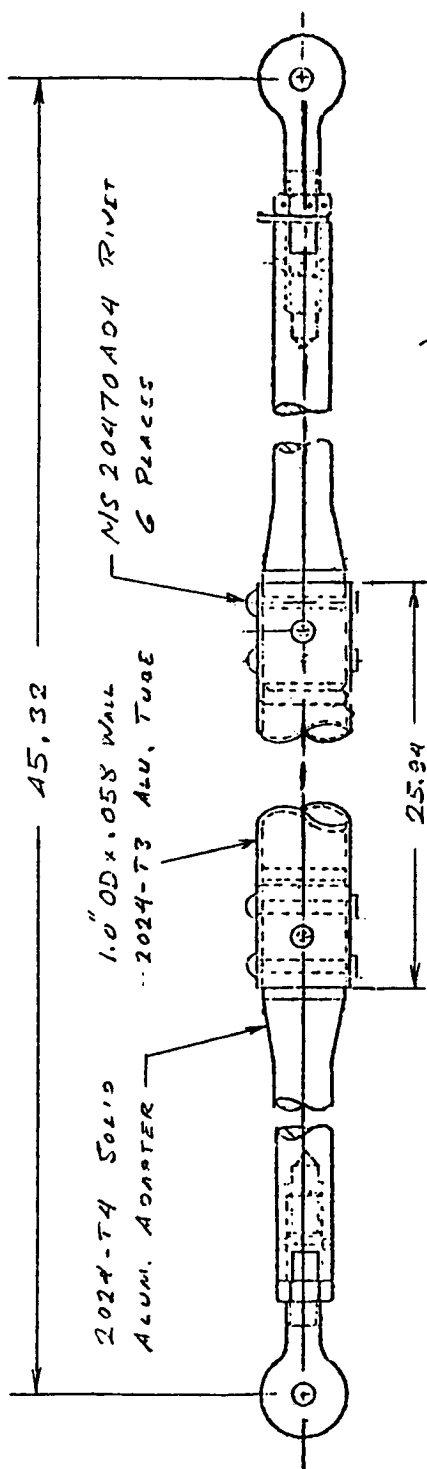
$\frac{a}{L} = \frac{23.56}{45.32} = .52$

$m = 7.7$ FIG. 302.6-3 HHI SDM

$P_{cr} = m \frac{EI_1}{L^2} = \frac{7.7(10.7 \times 10^6)(.0193)}{(45.32)^2}$

$P_{cr} = 774 \text{ LB}$

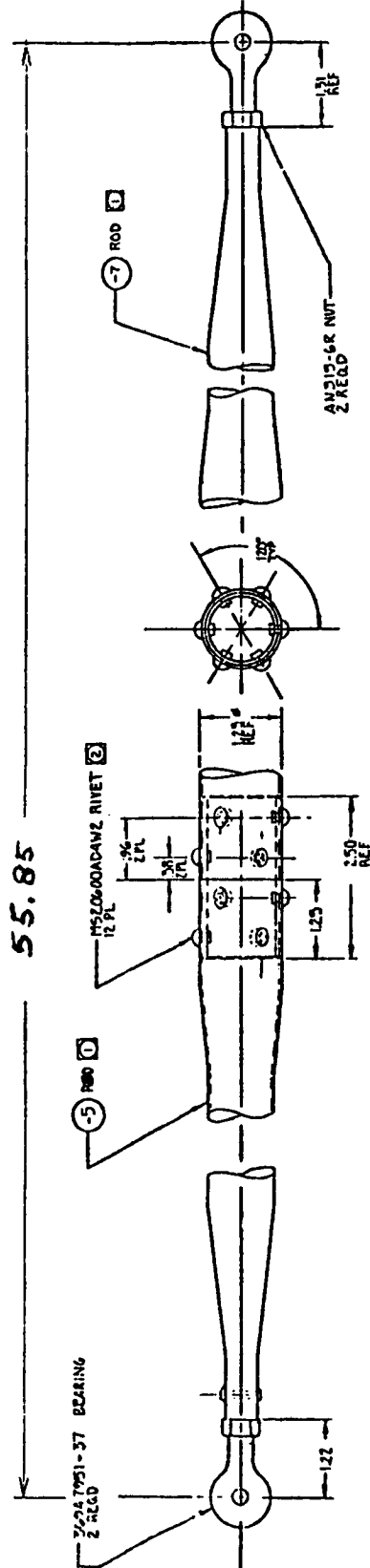
M.S. (COLUMN) = $\frac{774}{1.5(390)} - 1 = \underline{\underline{.32 \text{ M.S.}}}$



TAIL ROTOR CONTROLS

ORIGINAL PAGE IS
OF POOR QUALITY

ROD ASSY TAIL ROTOR CONTROL, HHC



THE 369 ASK 3188 ROD ASSY IS MADE FROM STANDARD OH-6A PUSH ROD 369A7007-3 BY MAKING IT 2.1" SHORTER. THE TUBE IS CUT IN THE CENTER AND A 1.25 OD x .028 WALL 2.56 IN. LONG SLEEVE IS INSERTED AND RIVETED IN PLACE AS SHOWN.

SINCE THE ROD IS MADE SHORTER THAN THE ORIGINAL AND THE LOAD REMAINS THE SAME, THE COLUMN STABILITY IS NOT REDUCED AND NO COLUMN ANALYSIS IS REQUIRED.

RIVETED JOINT ANALYSIS: LIMIT LOAD = 390 LB

6 MS20600 A04 W2 RIVETS IN SINGLE SHEAR

RIVET SHEAR STRENGTH = 388 LB

BEARING ON 6061-T6 .028 WALL TUBE:

6061-T6 $F_{tu} = 42 \text{ ksi}$
2024-T3 $F_{tu} = 64 \text{ ksi}$

BEARING ALLOW. ON .028 SHEET:

$$P_{bu} = \frac{42}{64} \left(\frac{.028}{.025} \right) (233) \quad \text{REF. TABLE 8.1.3.1.d MIL HDBK 5C}$$

$$P_{bu} = 171 \text{ LB}$$

FOR 6 RIVETS

$$\text{JOINT ALLOW} = 6(171) = 1026 \text{ LB}$$

$$M.S. (\text{BEARING}) = \frac{1026}{1.5(390)} - 1 = \underline{\underline{.75 MS}}$$

APPENDIX B: CONTROL SYSTEM LOAD DEFLECTION TEST

1. INTRODUCTION

On the following pages, the data for the control system deflection test is summarized. From this analysis, the stiffer primary control system is designed, as described in Section IV.C.2.1.

2. FORCE EQUILIBRIUM OF THE CONTROL MIXER ASSEMBLY

In Figures B-1, B-2, and B-3, the static loads of the collective, the lateral and the longitudinal systems respectively, are presented. In each case, a unit load P is inputted and the pitch link loads are computed.

For a complete view of the mixer assembly, see Figure B-4.

3. LOAD DEFLECTION CURVES

In Figures B-5 through B-7, the load deflection curves are presented for the old control mixer in the collective, in the lateral and in the longitudinal directions respectively. The free play in each directions is easily seen.

4. ADDED WEIGHT EFFECT ON PRIMARY BOOST STABILITY

4.1 LATERAL BELLCRANK

Total Solid Volume	27.6 cu. in.
4130 Steel weight density	0.283 lbs./cu in
Lateral Bellcrank weight in steel	7.80 lbs.
Lateral bellcrank and casting weight	1.05 lbs.
Solid steel weight penalty	6.75 lbs.

4.2 COLLECTIVE BELLCRANK

Total solid volume	26.81 cu. in.
4130 Steel weight density	0.283 lbs./cu.in.

Collective bellcrank weight in steel	7.59 lbs.
Collective bellcrank and casting weight	0.95 lbs.
Solid steel weight penalty	6.64 lbs.
4.3 TOTAL PENALTY	
Total weight penalty in steel system	13.40 lbs.

Since the servo stability analysis indicated that added weight up to 40 lbs would be acceptable, these new bellcranks will not harm the boost system.

5. FREE PLAY MEASUREMENT RESULTS

The free play measurements are summarized in Table B-1. The free play is the total width of the load deflection hysteresis curve.

6. STIFFNESS BREAKDOWN FOR MIXER ASSEMBLY

The stiffness test results are presented in Table B-2. In addition, the spring rates for the three loading directions are presented in Figures B-8 through B-10. This test determines the control system stiffness.

7. SUMMARY OF DATA

The following calculation determines the lost motion at the HHC actuators. Figure 32 displays the old and the new force displacement curves for the system. As shown, the control dead zone is significantly reduced with the modified parts.

7.1 LOST MOTION IN SYSTEM AT HHC ACTUATOR

Calculation of HHC Actuator Loads at Full Stroke $\pm 0.200"$ @ 32 Hz

$$P = \frac{8.43}{6.07} \times \frac{2.0}{0.22} \times 10.1 = \pm 127.53 \text{ lbs.}$$

Use ± 120 lbs., say.

Collective System:

Upper Stiffness:

$$\text{Avg.} = \frac{4196 + 5310}{2} = 4753 \text{ lbs./in.}$$

$$\frac{Ea1}{E_{mg}} = \frac{10 \times 10E6}{6 \times 10E6} = 1.67, \text{ say increase is mean (1.33)}$$

$$1.33 \times 4753 = 6321 \text{ lbs./in}$$

Use 6300 lbs./in. above as new spring rate.

Lower Stiffness:

$$\text{Avg.} = \frac{4512 + 7792}{2} = 6152 \text{ lbs./in.}$$

$$\frac{Est}{E_{mg}} = \frac{30 \times 10E6}{6 \times 10E6} = 5$$

Assume lateral and collective steel bellcranks yield threefold increase, and added inertia a twofold increase:

$$6 \times 6152 \text{ lbs./in.} = 36912 \text{ lbs./in.}$$

Use 36900 lbs./in. (Not critical)

Now consider worst measured case, left actuator in Lateral System:

$$\text{Upper Equiv. Stiffness} = 1.33 \times 4878 = 6488 \text{ lbs./in.}$$

$$\text{Lower Equiv. Stiffness} = 3530 \times 6 = 21180 \text{ lbs./in.}$$

Combine this with the worst free-play case for computation of lost motion, using the following data.

Spring Rate (above) at actuator before mod: $K = 5000 \text{ lbs./in.}$

After mod: $K = 6500 \text{ lbs./in.}$

Spring Rate (below) at actuator before mod: $K = 3500 \text{ lbs./in.}$

After mod: $K = 21000 \text{ lbs./in.}$

Consider worst free-play case: $\pm 40 \text{ mils}$

By proposed fixes can reduce to: $\pm 10 \text{ mils}$

Distribute as follows:

Kequiv before modification:

$$\frac{1}{K_e} = \frac{1}{5000} + \frac{1}{3500}$$

Ke = 2060 lbs./in. Use 2000 lbs./in.

Kequiv. after modification:

$$K_e = \frac{(6500)(21000)}{6500 + 21000} = 4964 \text{ lbs./in. Use } 5000 \text{ lbs./in.}$$

8. APPENDIX B TABLES AND FIGURES

	COLLECTIVE (#) (mils)	LATERAL (#) (mils)	LONGITUDINAL (@) (mils)
RESTRAINT	6.1 [2]	(1.5) [2]	(1.5) [2]
LONG. IDLER	N/A	N/A	6.5 [1]
IN. LONG. BC	N/A	N/A	42.0 [4]
OUT. LONG. BC	N/A	N/A	15.3 [1]
COLLECTIVE BC	27.2 [4]	7.1 [4]	13.5 [4]
LATERAL BC	7.7 [3]	12.0 [3]	2.4 [3]
S-PLATE UP	6.0 [3]	7.6 [3]	5.6 [3]
TOTAL	47.0 [12]	26.7 [12]	85.3 [18]

Loaded top down

@ Loaded bottom up

(..) Included in bottom loaded swashplate numbers

[..] Minimum achievable free play

N/A: Does not enter into load path

FREE PLAY SUMMARY
Referred to the Pitch Horn
TABLE B-1

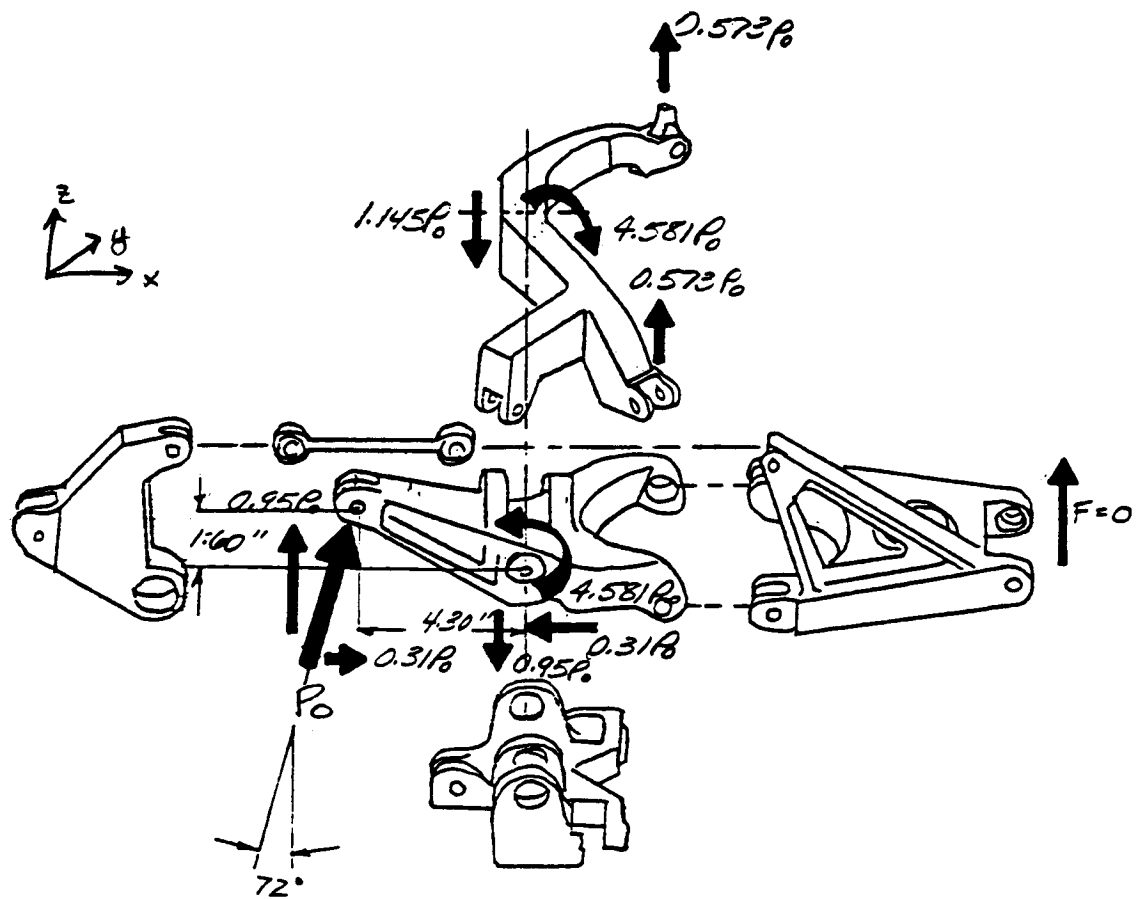
	COLLECTIVE (lbs./in.)	LATERAL (lbs./in.)	LONGITUDINAL (lbs./in.)
LOADS APPLIED BELOW CONTROLS (*)	4000	5882	4762
LOADS APPLIED ABOVE CONTROLS (**)	4267	6785	3870
RATIO OF LOADS BELOW TO LOADS LOADS ABOVE	0.937	0.867	1.23

* Measurements relate to input actuators with blade feathering locked.

** Test results referenced to input actuators by mechanical advantage

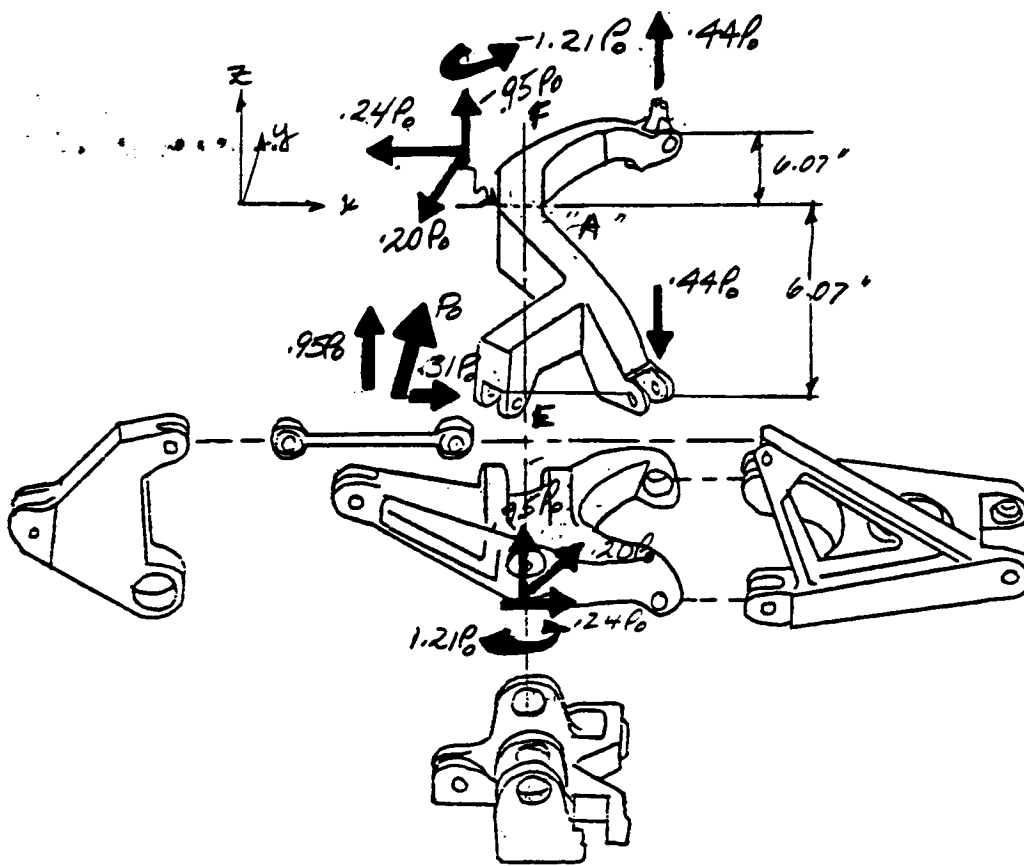
Note: All spring rates are determined outside the free play region.

SUMMARY OF STIFFNESS TEST RESULTS
TABLE B-2



$$\text{PITCH LINK LOADS} = \frac{1}{2} \cdot 0.573P_0 = \underline{0.286P_0}$$

COLLECTIVE SYSTEM LOADS
Figure B-1



ASSUME LOAD IS APPLIED IN THE PLANE OF THE LATERAL INPUT AXES
CLEVIS.

SUM MOMENTS ABOUT "A"

$$\begin{aligned} & .95P_0(6.07) - F_2(6.07) - F_1(6.07) - \cos 50^\circ(2.12)(.31P_0) = 0 \\ \hookrightarrow & 5.77P_0 - 6.07F_2 - 6.07F_1 - .42P_0 = 0 \end{aligned}$$

SUM VERTICAL SHEAR AT "A"

$$.95P_0 + F_1 - F_2 + F_3 = 0$$

SUM HORIZONTAL SHEARS

$$\cos 50^\circ(.31P_0) - F_4 = 0 \quad \rightarrow \quad F_4 = .20P_0$$

$$\sin 50^\circ(.31P_0) - F_5 = 0 \quad \rightarrow \quad F_5 = .24P_0$$

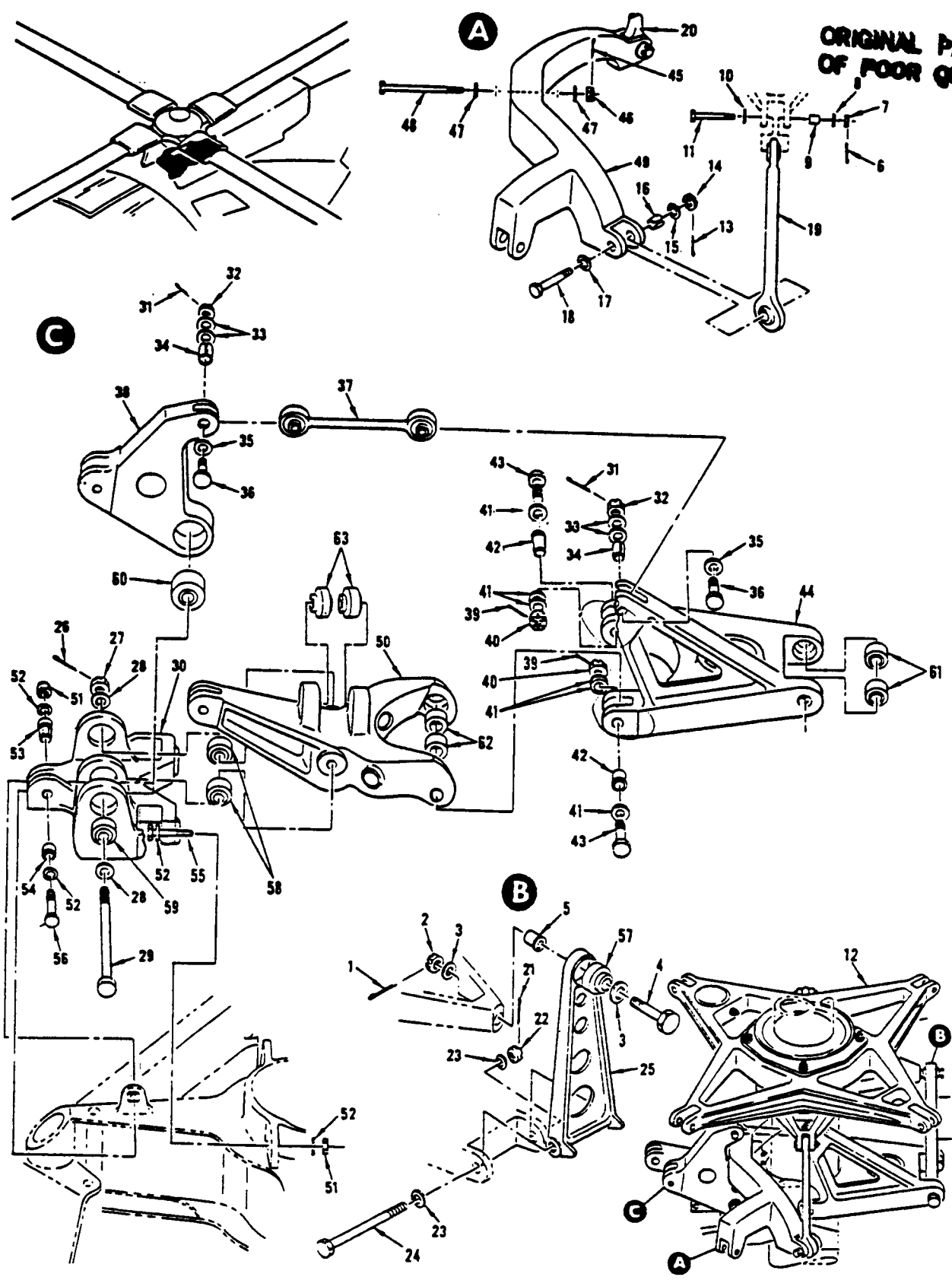
SUM VERTICAL MOMENTS ABOUT E-F

$$F_1(6.07) = F_2(6.07) \quad \rightarrow \quad F_1 = F_2 \text{ (DUE TO SLATE MOMENT EQUIL.)}$$

$$F_1 = .44P_0 \quad \text{PITCH LINK LOADS} = \pm .32P_0$$

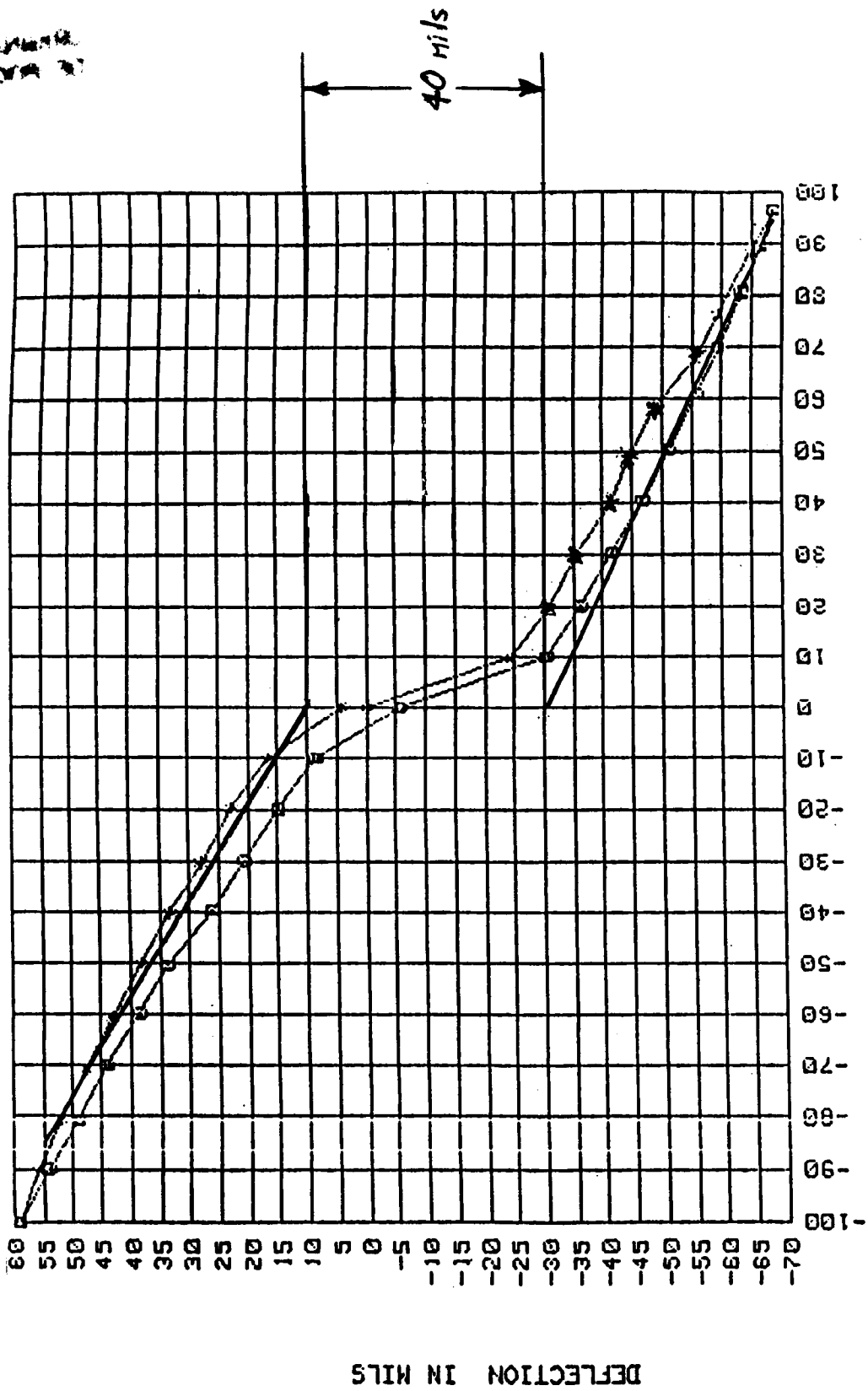
LATERAL SYSTEM LOADS
Figure B-2

ORIGINAL PAGE IS
OF POOR QUALITY

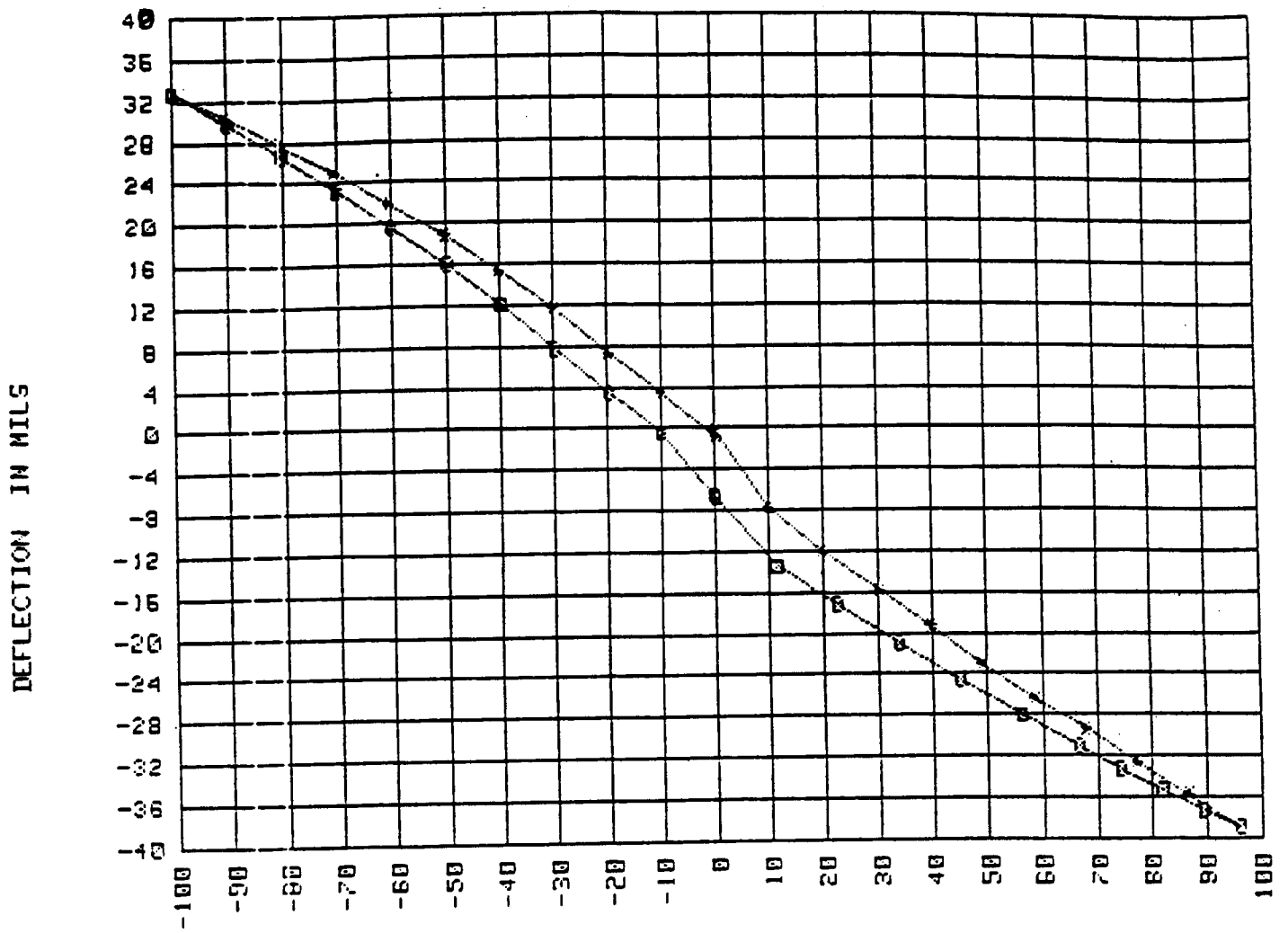


EXPLODED VIEW OF THE CONTROL MIXER ASSEMBLY
Figure B-4

SECRET

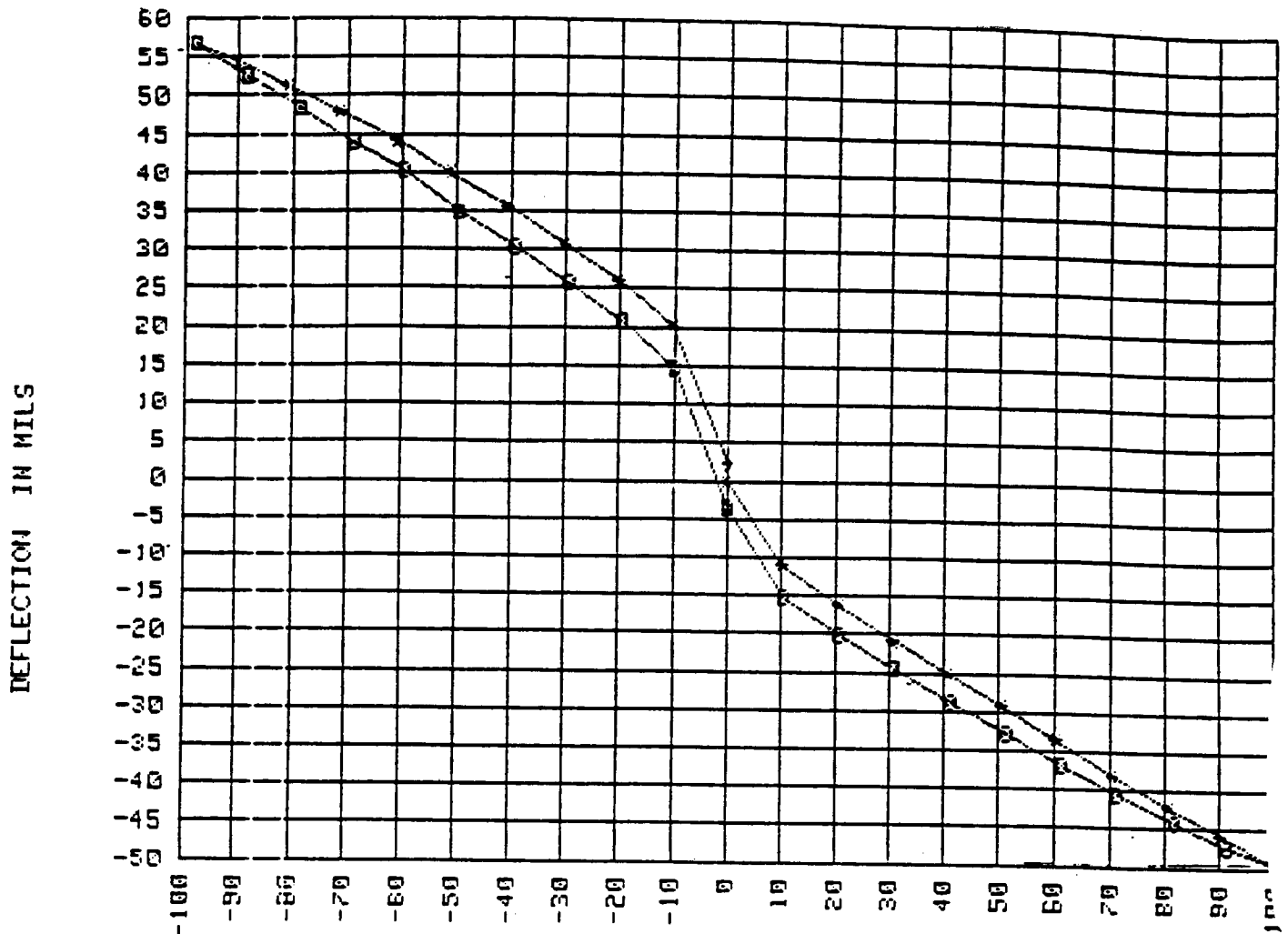


DEFLECTION CURVE FOR COLLECTIVE LOADING
Figure B-5



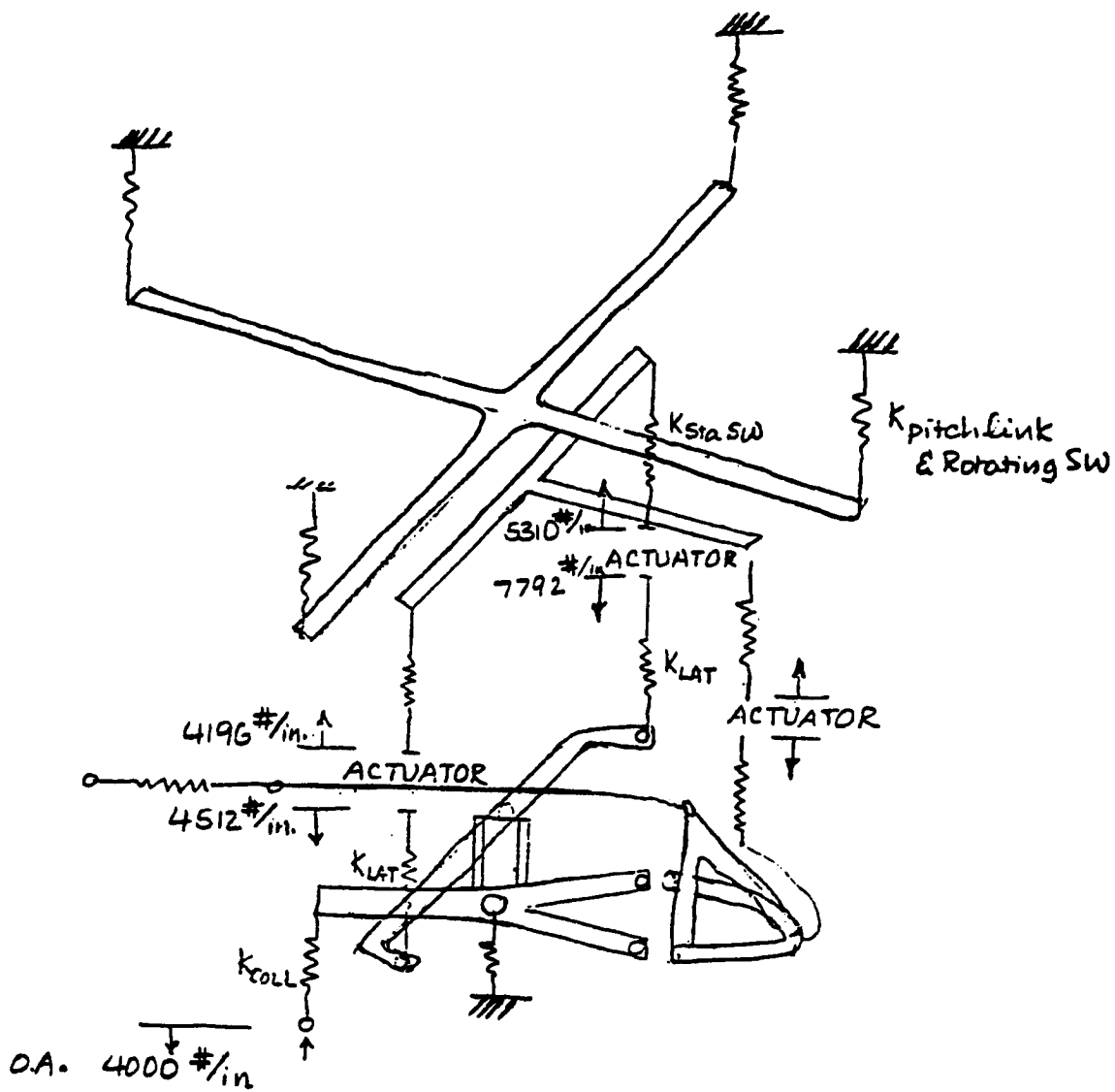
⊗ INPUT LOAD PEAK LOAD WAS -202.3 LBS.

DEFLECTION CURVE FOR LATERAL LOADING
Figure B-6

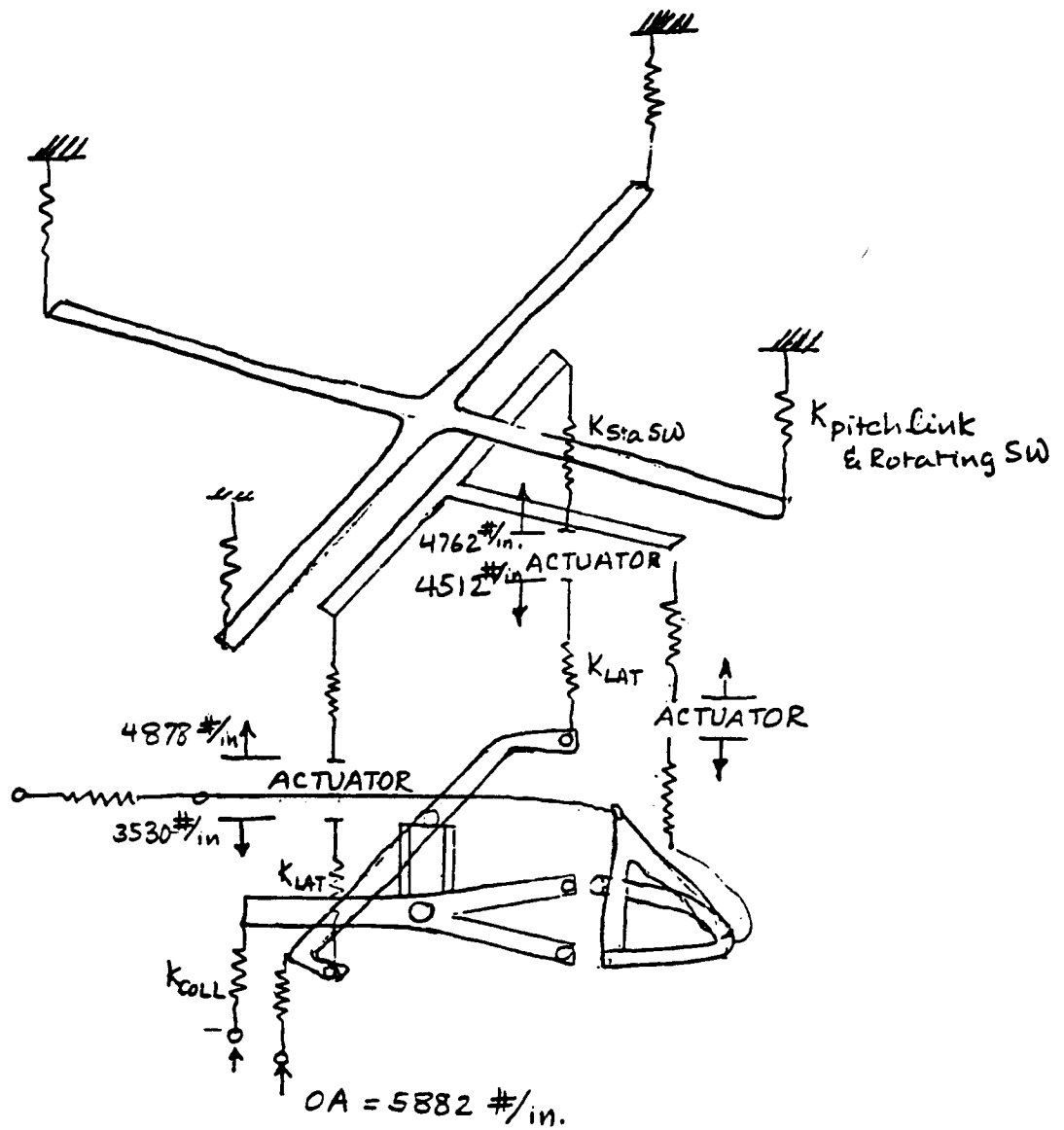


% INPUT LOAD PEAK LOAD WAS
 * - INCREASING LOAD 0 - DECREASING LOAD

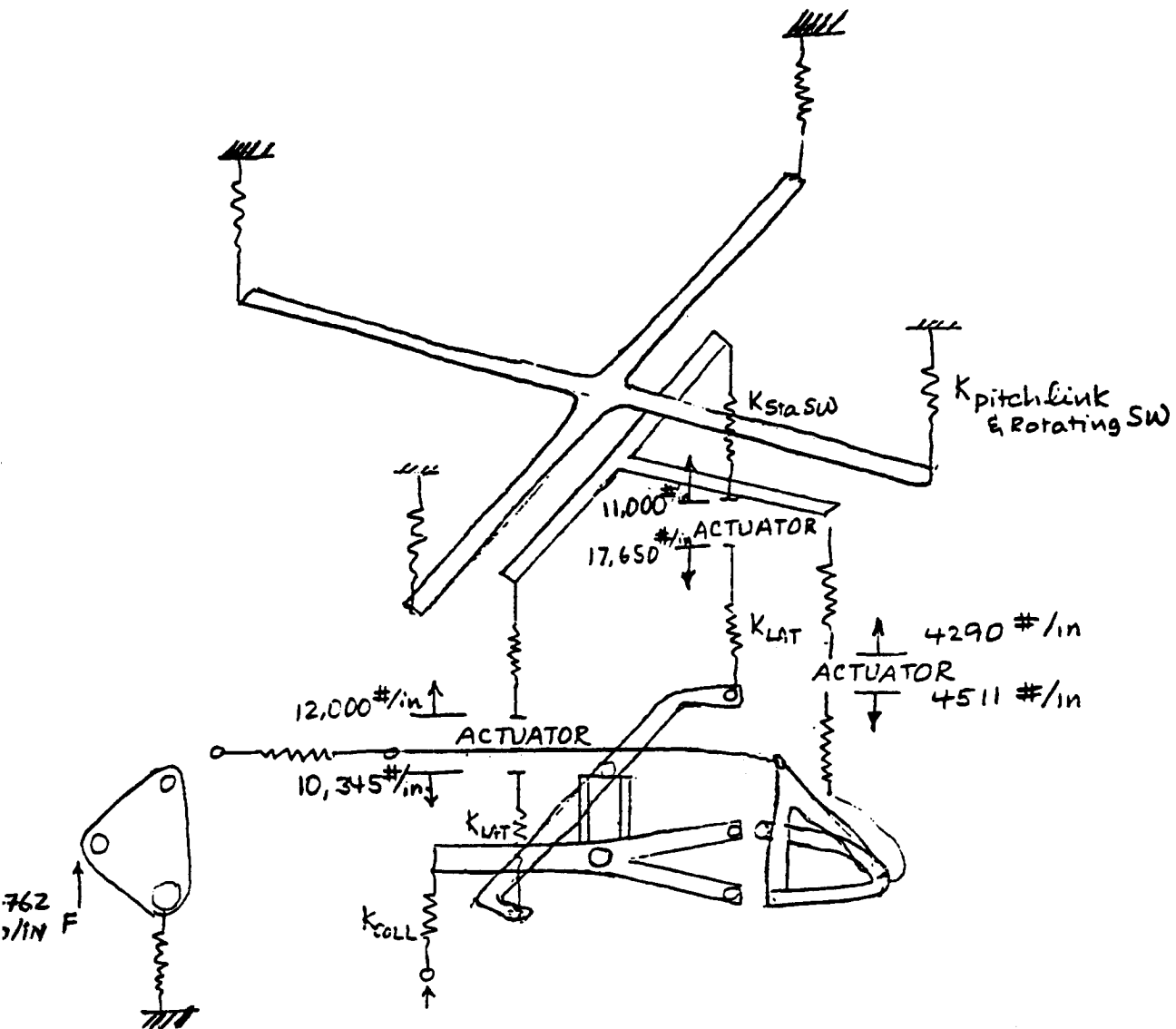
DEFLECTION CURVE FOR LONGITUDINAL LOADING
 Figure B-7



SPRING RATES FOR COLLECTIVE LOADING OUTSIDE THE FREE PLAY REGION
 Figure B-8



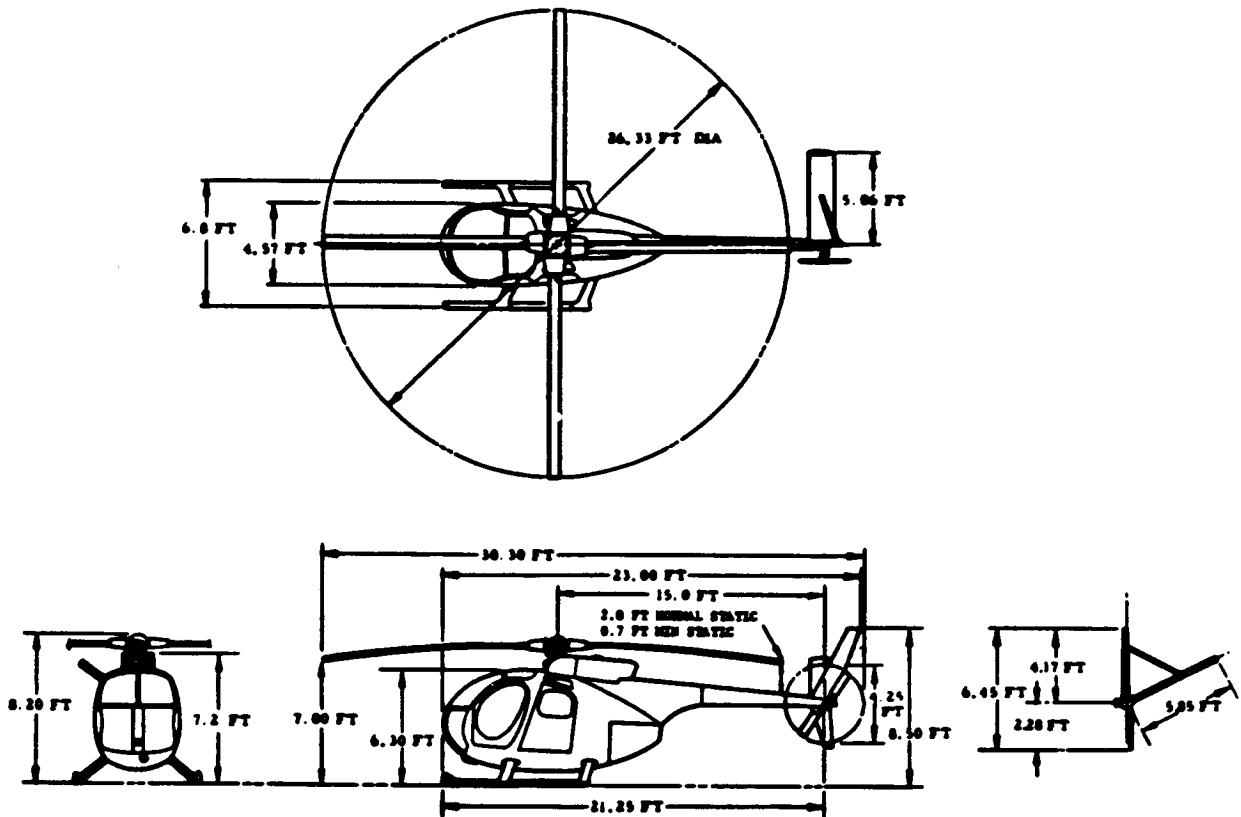
SPRING RATES FOR LATERAL LOADING LOADING OUTSIDE THE FREE PLAY REGION
 Figure B-9



SPRING RATES FOR LONGITUDINAL LOADING OUTSIDE THE FREE PLAY REGION
 Figure B-10

ORIGINAL PAGE IS
OF POOR QUALITY

APPENDIX C: OH-6A CHARACTERISTICS



OH-6A CHARACTERISTICS

AIRCRAFT

Gross Weight-----	2550 lb.
C_T , Sea Level Standard-----	.00442
C_T / σ , Sea Level Standard-----	.0814

MAIN ROTOR

Hub Type-----	Fully Articulated
Number of Blades-----	4
Rotor Diameter-----	26.33 ft
Total Blade Area-----	29.63 ft ²
Blade Chord-----	6.75 in
Blade Twist-----	-9 degrees
Solidity, Thrust Weighted-----	.0544
Pitch Flap Coupling, δ_3 -----	0 degree
Built in Pitch-----	8 degrees
Flap Hinge Offset-----	5.5 inches
Lag Hinge Offset-----	16.19 inches
RPM-----	483
Weight Moment Σmr -----	5.927 slug-ft
δ , Lock Number-----	4.919 (a-5.73)
Precone-----	0 degree
V_H -----	125 knots

Standard Bibliographic Page

1. Report No. NASA CR-4031		2. Government Accession No.		3. Recipient's Catalog No.	
4. Title and Subtitle Application of Higher Harmonic Blade Feathering on the OH-6A Helicopter for Vibration Reduction				5. Report Date December 1986	
				6. Performing Organization Code	
7. Author(s) F. K. Straub and E. V. Byrns, Jr.				8. Performing Organization Report No.	
				10. Work Unit No.	
9. Performing Organization Name and Address McDonnell Douglas Helicopter Company 5000 East McDowell Road Mesa, Arizona 85205				11. Contract or Grant No. NAS1-16266	
				13. Type of Report and Period Covered Contractor Report	
12. Sponsoring Agency Name and Address National Aeronautics and Space Administration Washington, DC 20546				14. Sponsoring Agency Code 505-61-51	
				15. Supplementary Notes Langley Technical Monitor: John H. Cline Final Report	
16. Abstract This report describes the design, implementation, and flight test results of higher harmonic blade feathering for vibration reduction on the OH-6A helicopter. The higher harmonic control (HHC) system superimposes fourth harmonic inputs upon the stationary swashplate. These inputs are transformed into 3P, 4P and 5P blade feathering angles in the rotating system. This results in modified blade loads and reduced fuselage vibrations. The primary elements of this adaptive vibration suppression system are: 1) acceleration transducers that sense the vibratory response of the fuselage; 2) a higher harmonic blade pitch actuator system; 3) a flightworthy micro-computer, which incorporates the algorithm for reducing vibrations; and 4) a signal conditioning system, which interfaces between the sensors, the microcomputer and the HHC actuators. The program consisted of three distinct phases. First, the HHC system was designed and implemented on the MDHC OH-6A helicopter. Then, the open loop, or manual controlled, flight tests were performed, and finally, the closed loop adaptive control system was tested. In 1983, one portion of the closed loop testing was performed, and in 1984, additional closed loop tests were conducted with improved software. With the HHC system engaged, the 4P pilot seat vibration levels were significantly lower than the baseline ON-6A levels. Moreover, the system did not adversely affect blade loads or helicopter performance. In conclusion, this successful proof of concept project indicated HHC as a viable vibration suppression mechanism.					
17. Key Words (Suggested by Authors(s)) Higher Harmonic Controls Helicopter Vibration Reduction Adaptive Controls			18. Distribution Statement Unclassified - Unlimited Subject Category 02		
19. Security Classif.(of this report) Unclassified		20. Security Classif.(of this page) Unclassified		21. No. of Pages 193	22. Price A09